UNIVERSIDAD DE GRANADA

CSIC
CONSEJO SUPERIOR DE INVESTIGACIONES CIENTÍFICAS

ipbln

DOCTORAL THESIS

University of Granada

Doctoral Programme in Biomedicine

Deciphering the role of cortistatin in neuro-immune dysregulation and blood-brain barrier breakdown underlying ischemic strokes

Julia Castillo-González

Thesis supervisor: Elena González-Rey

Institute of Parasitology and Biomedicine "López-Neyra"

Spanish National Research Council (IPBLN-CSIC)

Granada, 26th January 2024

UNIVERSIDAD DE GRANADA

TESIS DOCTORAL

Universidad de Granada

Programa de Doctorado en Biomedicina

Descifrando el papel de cortistatina en la desregulación neuroinmunológica y la disrupción de la barrera hematoencefálica subyacente al infarto cerebral isquémico

Julia Castillo González

Directora de tesis: Elena González Rey

Instituto de Parasitología y Biomedicina "López-Neyra"

Consejo Superior de Investigaciones Científicas

(IPBLN-CSIC)

Granada, 26 de enero de 2024

Editor: Universidad de Granada. Tesis Doctorales
Autor: Julia Castillo González
ISBN: 978-84-1195-204-0
URI: https://hdl.handle.net/10481/89851

El doctorando / The *doctoral candidate* **[Julia Castillo González]** y los directores de la tesis / and the thesis supervisor/s: **[Elena González Rey]**

Garantizamos, al firmar esta tesis doctoral, que el trabajo ha sido realizado por el doctorando bajo la dirección de los directores de la tesis y hasta donde nuestro conocimiento alcanza, en la realización del trabajo, se han respetado los derechos de otros autores a ser citados, cuando se han utilizado sus resultados o publicaciones.

/

Guarantee, by signing this doctoral thesis, that the work has been done by the doctoral candidate under the direction of the thesis supervisor/s and, as far as our knowledge reaches, in the performance of the work, the rights of other authors to be cited (when their results or publications have been used) have been respected.

Lugar y fecha / Place and date:

Granada, 27 de noviembre 2023

Director/es de la Tesis / *Thesis supervisor/s;* Doctorando / *Doctoral candidate*:

Firma / Signed Firma / Signed

A mis padres,

A mi hermana,

A Pepe,

Y a mi abuela Teresa,

que murió de las secuelas de un ictus

Agradecimientos

Siempre he pensado en como empezar estos agradecimientos y ahora que me enfrento a esta página en blanco no se ni cómo empezar. Aviso, son largos y un poco lacrimógenos, ¡pero no me quiero dejar a nadie! ¡Lo siento!

A mis compañeros,

En primer lugar, quería agradecer a Elena, mi jefa. Ha sido un placer trabajar contigo todos estos años, y si hemos llegado hasta aquí es gracias a ti. Gracias por darme apoyo, cariño y refuerzo positivo con todo lo que hacía. Por dar alas a mi curiosidad científica y por volar conmigo. Por ser más nuestra compañera que jefa, por darme libertad y confianza. Por darnos tu tiempo, pero también por saber crecer y evolucionar con nosotros. Solo espero que después de este maratón puedas disfrutar más de tu tiempo para ti y los tuyos. Cuídate.

A Mario, que siempre ha confiado en mí y me ha dado su apoyo profesional y personal cuando más lo necesitaba. Y gracias por ser también una fuente incansable de conocimiento para todos.

A los mejores compañeros de laboratorio que nunca haya podido desear. Ir a trabajar en un ambiente de amigos, sonrisas familiares, risas y bromas, es una suerte y un privilegio, de verdad. Esto se lo debo a las magníficas personas que lo han conformado a lo largo de los años. A Irene y Marta, por ser Pili y Mili, por haber sido mis manos derechas, izquierdas, mis ojos y mis pies en estos años de tesis. Porque sin su ayuda esta tesis profesionalmente no hubiera sido posible, pero anímicamente tampoco. Porque hay muchas formas de tratar a la gente, pero vosotras siempre dais lo mejor. Os estaré eternamente agradecida. Irene, ha sido un placer haberte conocido y saber que me llevo una amiga para toda la vida (la última del labo además jejej, que ya tenemos una edad). Gracias también de corazón por presentarme a tus amigos y a Pablo, Unai y Naira, espero que cuando sean mayores, los peques aún se acuerden de nuestros pilla-pilla. A Clara, por tener un corazón que no le cabe en el pecho, y por a pesar de todas las dificultades con su tesis, haberme ayudado tan cariñosamente siempre. Se te ha echado de menos en esta etapa final sin duda. A Nacho, mi querido compañero de tesis. Gracias por tus bromas y tus chistes y por ser el mejor compañero (aunque quizás algo desgraciado de más jeje), siempre dispuesto a ayudar a cambio de absolutamente nada. Siento las dificultades que tuvimos al principio para entendernos, fue también *my fault.* A Pablo, mi pequeño *padawan*, que ahora continúa solo el difícil camino del ictus Ha sido un placer enseñarte, ¡porque en realidad tú me has enseñado mucho a mí! Gracias por los ánimos

y los chocolatitos. A Álex, que, aunque llegó hace poco siempre lo recordaré en esta etapa final, gracias por tu cariño, apoyo y risas. Y a todos aquellos compañeros que pasaron por el laboratorio, a Irene, Dani, Elena y especialmente a Ana, por ser una compañera increíble.

A todos los compañeros que están o han pasado por el 202, que son nuestro grupo hermano y que tanto me han ayudado y apoyado. A Jenny, por sus consejos siempre tan acertados, a Gema por dedicarme siempre una sonrisa mañanera. A Raquel y Marga, que empezaron conmigo la tesis y con las que tantos cafés y finales de etapa compartí. A Marina, por ser la mejor compañera de Departamento que uno podría tener, y a Ana por compartir su exquisito gusto culinario.

A los compañeros del López-Neyra que han colaborado en el desarrollo de esta tesis con sus consejos, ayuda técnica o simplemente alegría y cariño. A mi querido personal del Servicio de Animalario, donde he pasado infinitas horas y donde casi me ponéis un colchón jaja, pero donde me he sentido siempre tan querida. A Clara, por ser un ejemplo a seguir de energía y cariño, a Paco, por ser un “mala-follá” con tan buen corazón, a Jorge, por su compromiso y amabilidad, a Bea, por su cariño y sus bromas, a Bego y a Lina, por ser siempre tan flexibles y estar pendientes de mí. Gracias a todos por cuidarme, por tanto cariño, buenos ratos, bromas y galletas compartidas. Y por aguantarme con mis cientos de ratones y cuidar de ellos con muchísimo respeto. Al Servicio de Microscopía, a Laura, por ser una de las mejores profesionales que tiene el López-Neyra, siempre dispuesta a ayudar y a buscar soluciones imposibles a mis problemas imposibles. Pero sobre todo por tu cariño. Al servicio de Bioinformática, a Edu, Pepe, Laura e Iván. Por vuestros miles de horas extras dedicadas, vuestra paciencia y cariño. Os debo una. Al Servicio de Genómica, por toda su ayuda técnica. Y por supuesto al servicio de Esterilización y Limpieza, Informática y Administración, en especial a la pareja del año, Carmen y Ángeles, por prestarnos siempre su ayuda con la mejor de las sonrisas.

A todo el resto de compañeros que siempre habéis estado acompañando con vuestros consejos y bromas. En especial a Kiko, por toda su ayuda y preocupación con el postdoc, a María de Citometría por su alegría, a Adri por su ternura, a Paco por su humor ácido, a Luz por su amistad, a Juan Carlos, por ser un gran compañero de rocódromo, a Macarena por su dulzura y a Estévez por esos panettones que levantan el ánimo a cualquiera. Por supuesto también gracias al personal de Conserjería, a Javi, Lola, Dani y

Yolanda. Por cuidarnos, por regalarnos siempre vuestras palabras afectuosas, aunque todos vayamos corriendo. Se ha hecho un poco más fácil gracias a vosotros.

A mis queridos doctorandos del López-Neyra, con los que hemos compartido tantas risas y lágrimas, tantas comidas y cenas, tantos viajes y celebraciones. La tesis no hubiera sido posible sin vosotros. Gracias Nacho, Pablo, Álex, Marina, Ana, Sandra, María, Ana Belén, Esteban, Vanessa, Blanca, Pablo, Alonso, Candela, Rafa, Bárbara, Marina, Javi, Gonzalo, Inma, Elio, Gonzalo, Alejandro, Paula, Manu, Marta, Iván, Marco… Y por supuesto a todos los compañeros que ya no estáis en el López, pero de los que guardo una de las etapas más felices de mi vida, vosotros ya sabéis quienes sois y porqué. A Clara, Elenita, Antonio, Cris, Ivanchu y Rubén.

To my dear lab in Lausanne. Thank you, Lorenz, Lara, and Melanie. Arriving for the first time in a place alone is very tough (even more so with COVID restrictions). However, I felt at home in Lausanne, and I'll always remember you as my dear friends. Thank you, Lorenz, for giving me the opportunity to stay in your lab for 3 months and then 3 more! Thanks for being the perfect boss generously giving us your freedom and trust at work, and being always so nice making yourself available for a coffee chat, a meeting, or a wonderful picnic even when you were on call the previous night. Looking forward to this new chapter (fingers crossed). Thanks to you and Melanie for inviting us to your place and sharing delicious meals, and thanks Melanie for your always kind words and affection. Thanks to Lara, you are the best lab mate one could have, my cheerleader (you'll probably hate that I said this, haha), and the cheerleader for my mice. Thank you for giving me advice and helping me despite all your obligations. For your care and support. Moltes gràcies. To all my colleagues from the DNF, thank you for your support, help, and warmth, especially to Eva, our wonderful lab mate and great climber, missing you here!

A los compañeros del Departamento de Biología Celular, que me han permitido dar clase estos años y con los que tan a gusto me he sentido. En especial, gracias a José Luis, con el que di mis primeros pasos científicos y que de forma muy sincera me ayudó a tomar una buena decisión con respecto a mi camino. Gracias de verdad. A mis compañeras Chari, Vero, María y Sandra, por acogerme y enseñarme con tanta dulzura.

A mis profesores del instituto y de la universidad, que me descubrieron el amor por la Ciencia. Especialmente a Luis Quesada, que me enseñó lo bonita que era la Biología.

Por último, agradecer a nivel profesional la ayuda de Belén, Ana y especialmente de Pepe en la redacción y corrección de esta tesis.

A mis amigos,

A tres personas que llevan siendo tres ángeles de la guarda desde que las conocí hace ya muchos muchos años, Bel, Aixa y Anita. Qué haría yo sin vosotras. A Bel, la mejor amiga y *roomie* que nunca podré tener, siempre dispuesta a escuchar horas de audios, a compartir paseos infinitos y vinos deliciosos en cualquier lugar del mundo. Por ser la mejor consejera *fashion* y por tu admiración y orgullo. A Aixita, por su enorme corazón, y por,a pesar de su cabeza un poco despistada, estar rauda y veloz siempre que la he necesitado. Gracias por hacerme partícipe en esta etapa maravillosa que comienza para ti. Deseando ser tu dama de honor. A Anita, aquella muchacha a la que le presté mis apuntes de segundo en el bus, ay, ¡qué decir! Gracias por tu amistad y por tu confianza, por decir siempre las cosas cuando nadie quiere escucharlas, siempre tan acertada y cabal, y por tu admiración y apoyo. Os quiero chicas, no hubiera sido posible esta tesis sin vosotras.

A Paquito y Carmen, por luchar cada uno a su manera contra sus propios fantasmas y sin embargo estar siempre a mi lado, cuando la que tenía que escuchar era realmente yo. Cómo os admiro chicos. Gracias Sayoncito por ser el mejor amigo sevillano (menos sevillano) que podría tener. Por haberme invitado a migas, a tu casa del camino de Beas, y a nuestros grandes paseos. ¡Ojalá esos bichitos nos unan profesionalmente algún día! A Carmencita, por entender perfectamente los tiempos de la tesis, y darme su gran apoyo. Gracias por ser la mejor compañera de tenis y lectora que uno puede desear tener.

A Sofi, Pedro y Fer, que sé que les hace una ilusión tremenda estar en esta tesis, pero a mí me hace más ilusión que estén ellos en mi vida. A Sofi, por estar siempre tan pendiente de mí (y de todos, en realidad) y apoyarme y cuidarme tanto. Qué haría yo sin ti. Gracias por abrirme las puertas de tus amigos, y descubrirme unas personas maravillosas en un momento en el que estaba un poco perdida. Gracias por ponernos siempre mensajes, videollamarnos y estar al otro lado cada una de las veces, siempre serás nuestra mejor entrenadora. A Pedro, mi querido Peter, cuánto te echamos de menos por aquí, a ti y a tu intensidad de poeta, a tus remates de enroque, y a tu dulzura. Ojalá la vida nos lleve pronto a tirarnos al río de Berna y a nuestras charlas intensas; ya sabes, ¡nada de compartimentalizar dramas! A Fer, ¡lo prometido es deuda! Gracias por nuestros viajes, charlas, bailes e intercambios. Gracias por tener un corazón tan enorme y compartirlo.

A mi familia suiza, a dos personas que quiero con locura, y que son mucho más que amigos, a Bernardo y Mariola, gracias no solo por acogerme en Suiza, sino por

apoyarme tantas veces y por incluirme en vuestra familia con Figarito y Ashoka. Gracias por vuestra boda, donde fui tan inmensamente feliz, por Benito, por las piedras del Catan, por las raquetas y las barbacoas. Os quiero con locura. A Tarik, quien nos iba a decir que Pimp Flaco y unas (muchas para algunos) tapas serían testigos de una amistad tan grande. Gracias por los viajes en tu coche bajo la tormenta, las sartenes de la pandemia y por descubrirme Suiza y a los suizos (¡aunque no sepas ya español!). A Victor y Bianca, porque un buen amigo me dijo que una vez que si te haces amigo de un catalán es para siempre. Pues tenía razón, la verdad. Gracias amigos. Por acogerme, por las tortillas, la nieve y el paddle surf. A Mauricio, por su enorme cariño, sus risas contagiosas y sus bailes salseros. Gracias por el apoyo y por tu ayuda con la vida científica.

A mi Evita, mi corresponsal al otro lado del armario. El día que me cambie de acera… ¡espero que estés esperándome! Gracias por escuchar mis audio-podcast, por los maimones, y por nuestras citas en las gasolineras. Se echan de menos los domingos de vóley y los huevos por la ventana (inválida… es que tiene tela).

Al deporte, y todos los amigos que me ha dado. A mi peña de vóley, donde hace unos años intenté unir a toda la gente *random* que conocía y que tocara un balón… y mira ahora. Gracias por soportar los momentos más difíciles de esta tesis, comprender mis ausencias y estar animándome tanto en este último año. Sé que el día de mi defensa estarán todos ahí apoyando a su *pupas*. Gracias a Lu, mi querida y endemoniada Frau, gracias por tu cariño y sensibilidad, y esa capacidad que tienes de superar siempre tus miedos, te admiro mucho (aunque seas tan hetero). A Álex, gracias por su encanto y cariño, que va a evitar (por muy poco) que lo echemos del equipo. A Pedrosa, mi compañero de escalada, gracias por enseñarnos el gran corazón que tienes. A Chino, por sus reglas imposibles pero su simpatía *cuacksi* infinita. A Antonio Castilla, por su gran cariño a pesar de su rodilla maltrecha. A José, que siempre está (él o el pollo) de guardia velando por todos. A Nacho, por ser nuestro fisio física y emocionalmente. A Jorge, por ser nuestra torre y darnos su (*joooder*) cariño. A Enrico, por su gran afecto y su dulce sonrisa, y a Javi, por ser nuestro mejor DJ. Y por supuesto a Sofi, Fer y Pepe, y a todos los que me han acompañado en estos años en este magnífico deporte, especialmente a mi antiguo entrenador y a mis compañeras de equipo.

A la escalada y a mi familia lagartija. Quién hubiera pensado en aquel Cube de Lausanne (el pobre Bernardo lo sufrió en sus propias carnes) que un deporte me llegaría a hacer tan feliz. Gracias a Bernardo y Mariola por ser mis mejores maestros. Gracias a todos mis amigos del R&B, por seguirme hacia el tango de la muerte, por animarme a

seguir subiendo (mental y físicamente), y por ser mi desconexión de la ciencia cuando más lo necesitaba. En especial quiero agradecer a mi querida María, que con su eterna sonrisa y su ánimo ha supuesto en este último año un apoyo científico y personal gigante, y con quien me he podido desahogar y animar. A mi querida Ana, la gran artista detrás de la portada de esta tesis, con un corazón, alegría y paciencia para escucharnos más grande que ella misma. *Merci* Ana. A Ángel, que, si algún día me perdona por su cicatriz de tiburón, será el mejor compañero de cuerda que se pueda tener. A todos los compañeros del roco, en especial a Inma, Pablo, Hannah, Anita, Antonio, Mari Ángeles, Antonio y Sacha, gracias. Y por último, a nuestro profe Manu, que nos ha sabido enseñar, animar y hacer qué consiguiéramos cosas que nos parecían imposibles, pero que él confiaba ciegamente que sí podíamos (y sino, *lo que no va a la libreta, ¡pa' la tableta*!). Gracias a todos amigos, subiría mil montañas más con vosotros.

A mis compañeros de universidad, en especial a Curro, con el que hemos compartido tantas prácticas, exámenes y ahora duras preocupaciones de la vida de adulta jaja. Gracias por tu cariño y simpatía.

To me dear friends of LISA. That summer in Hannover and that trip to Greece stay in my heart forever. Thanks to Liana, Jorge, Ioannis, Luca, Laura, Margarida; Gonzalo; Irakli, Martin; Melina, and Anastasiya. You are the best guys, looking forward to seeing you again! Special thanks to Liana; life randomly led us to the same country, where we shared so many trips and adventures. Thanks for the picnics, BBQs, croquetas, granadas, and your peaceful and always supportive words. Don't ever lose that beautiful smile that lights up and cheers every person you meet. Love you, my dear!

A mis amigos políticos, grandes amigos ahora también. A Jorge, Juanlu, Rafa, Marcos y Rafa que me han tratado como una más de su *crew*, con un cariño enorme. A Bea, Juanjo, Paco, Pastora, Virginia y David, Laura, Clara, Inés, Santi y Carlos, por acogerme en su pequeña gran familia, especialmente a Bea, que es un ser de luz y tiene un corazón enorme. Gracias chicos!

A mi familia,

A mis abuelos Teresa y Francisco, a quienes desgraciadamente conocí poco, pero de quienes guardo unos recuerdos maravillosos. Mi abuelo siempre con sus radios y mi abuela siempre con su punto y su gran sonrisa al ver a sus nietas. Gracias por los juegos en la casapuerta, el olor a papas con chocos, las violetas, y los pensamientos. A mis abuelos Ana y José, que afortunadamente conocieron a su nieta investigadora, de la que

estaban tan orgullosos, aunque apenas sabían leer. Gracias por los pestiños, las poesías, la lumbre y los higos. Se os echa de menos a todos.

A mi familia gaditana, de Camposoto y alegría, de salitre y República, de poniente y cariño. A Tere, por enseñarnos la belleza de la lectura y del francés, y por estar tan pendiente de nosotras, tratándonos siempre con tanto cariño. A Isa, por su humor maravilloso ante cualquier situación, por su generosidad y acogida. Por sus chicharrones y por muchos más carnavales juntas. A Antonio, por su eterna sonrisa y afecto y sus magníficas comidas. Y por supuesto a Paco, Tata y Mª Ángeles, por todo su cariño. A mis primos Ángela, Andrea, Marco y Paula. Gracias por unos veranos maravillosos.

A mi familia jienense, de olivos y huertos, pero también de gofio y papas. A Caro, por inculcarme su amor por la biología y por su enorme ternura, a Nono y Paco, por tratarnos siempre con cariño y afecto y por vuestros super arroces o migas. Y por supuesto a Salvador y Guiomar, mis queridos guanches.

A Pedro, Ana y Bea, por formar parte de esa familia que se elige y vuestro siempre apoyo incondicional.

A mi familia política de Sevilla, a Mª José, Enrique, Javi, Quique y Pilar. Gracias por acogerme en vuestra casa como si fuera una hija más, por vuestro cariño y apoyo. También especial gracias a May, Tete y a la abuela Maruja, que tanto me alegré de conocer, gracias por acogerme a través de tus periódicos y jazmines.

A Pepe, por ser el mejor compi de piso, de aventuras y de vida que podría desear. Por haberme ayudado en esta etapa final de la tesis, dándome apoyo moral, profesional y ocupándote de todo (sin esas patatas fritas no hubiera sobrevivido ese último día). Porque ves el mundo desde una sensibilidad que nadie tiene y que te convierte en una de las mejores personas que he conocido. Gracias por acompañarme en mis locuras, pero dejarme vivir las mías propias. Gracias por cuidarme y cuidar de casita y de Chopper. Por teletransportarte a miles de km de distancia con un brazo y dos corazones, por contarme historias para dormir, por llevarme flores y siempre tener preparada una sorpresa (aunque a veces tu propia emoción la estropee antes de tiempo). Por aprender y saber equivocarte, por tu ceñito fruncido. Por tus enormes gafas moradas. Por el orgullo con el que miras todas las cosas qué hago, y por ser siempre un lugar seguro, por ser casita. Por esta nueva etapa que comienza, donde estás dispuesto a seguirme al fin del mundo, con todo lo que ello implica. Gracias, por ser mi equipo, de corazón. Te quiero. Haruru.

A mi hermana Ana, mi pequeña Vincent, que tantas veces ha ejercido de hermana mayor. Gracias por estar ahí siempre, por tus mensajes de apoyo, tus memes, tus detallitos tan cuidados, y por tus grandes abrazos de frambuesa. Por transmitirme una ilusión y orgullo tan grande por este mundo que te es tan ajeno, que solo refleja la grandísima persona que eres. Por compartir conmigo gustos, aficiones o por inventarte sino nuevos. Por seguirme a cualquier aventura u observar a esta cabra loca desde la distancia con tu orgullosa mirada. Por tu seguridad en perseguir tus sueños y el enorme cariño con el que tratas a todo el mundo. Estoy muy orgullosa de ti, tenerte como hermana es un tesoro. Sin ti esta tesis tampoco sería posible. Te quiero Visenti. Gracias también a Álex, el mejor cuñado que podría tener, siempre tan atento y cariñoso, transmitiendo tu alegría almeriense y tus camisas hawaianas a cualquier persona que ve. Gracias de corazón.

A mis padres, por apoyarme y animarme en cada una de las etapas de mi vida. Por alimentar mi curiosidad y comprarme libros de setas, visitar todos los jardines botánicos del mundo o cualquier otra cosa que se le ocurriera a esa niña que solo quería ser bióloga. Por darme una infancia bonita y llena de cariño de la que solo tengo buenos recuerdos. Por viajar con nosotros por todo el mundo, enseñándonos a tratar bien a los demás y a cuidar de nosotras mismas. Por educarme en la igualdad y en la empatía. Por confiar en cada uno de mis pasos, aconsejarme pacientemente y dejarme que me equivoque. Por entender este mundo tan complicado sin pertenecer a él. Por darme libertad, pero ofrecerme siempre un refugio y un lugar seguro. Esta la mejor herencia que nos podríais dejar. Esta tesis no hubiera sido posible sin vosotros. Os quiero mucho.

Y finalmente, y sobre todo hoy 25 de noviembre, a todas las mujeres, científicas, profesoras, historiadoras, traductoras, amas de casa, deportistas, cocineras, informáticas, agricultoras, escritoras, médicas, psicólogas, políticas, bomberas, madres, hermanas, abuelas, tías, primas, amigas, novias que han luchado a lo largo de los años y siguen luchando por un mundo más justo e igualitario, donde no haya violencia contra las mujeres, y donde que una mujer pueda estar defendiendo hoy una tesis, sea posible. Gracias a todas las que me habéis ayudado a ponerme unas gafas moradas, que, aunque pesadas de llevar, prometo no quitarme nunca.

Index

Abbreviations

AA	Aminoacids
ABC	ATP-binding cassette
ABTS	2,2′-azino-bis(3-ethylbenzothiazoline-6-sulfonic acid)
ACA	Anterior cerebral artery
ACE-1	Angiotensin-converting enzyme-1
ACHA	Anterior choroidal artery
ACTH	Adrenocorticotropic hormone
AD	Alzheimer's disease
ADAMs	A disintegrin and metalloproteinases
ADAMTSs	Metalloproteinase with thrombospondin motifs
AE	Active efflux
AICA	Anterior inferior cerebellar artery
AJs	Adherens-junctions
Ang	Angiopoietin
APCs	Antigen-presenting cells
AQP4	Aquaporin-4 transporter
Aβ	Amyloid-β
BBB	Blood-brain barrier
BCRP	Breast cancer resistance protein
BDNF	Brain-derived neurotrophic factor
BECs	Brain endothelial cells
BM	Basement membrane
BP	Biological processes
BSA	Bovine serum albumin
cAMP	Cyclic adenosine monophosphate
CAT1/3	Cationic AA transporter 1 and 3
CBF	Cerebral blood flow
CC	Cellular components
CCA	Common carotid artery
CCL2	Chemokine (C-C motif) ligand 2
CD45	Cluster of differentiation 45
CHA	Convex hull area
CL	Contralateral side
Cldns	Claudins
CMT	Carrier-mediated transport
CNS	Central nervous system
CNT2	Sodium-independent concentrative nucleoside transporter-2
CNTF	Ciliary neurotrophic factor
CRH	corticotropin-releasing hormone
CSF	Cerebrospinal fluid
CST/Cort	Cortistatin
CTL1	Transporter like protein type 1
Cx	Connexin
D	Fractal dimension
DALYs	Disability-adjusted life-years
DAMPs	Danger-associated molecular pattern molecules
DCs	Dendritic cells

DEGs	Differentially expressed genes
DMEM	Dulbecco's modified Eagle's medium
DNF	Department of Fundamental Neurosciences (UNIL)
EAE	Experimental autoimmune encephalomyelitis
EB	Evans blue
EBA	Evans blue-albumin
ECA	External carotid artery
ECM	Extracellular matrix
ECs	Endothelial cells
EMT	Endothelial-mesenchymal transition
eNOS	Endothelial NO synthase
ENT1/2	Sodium-independent equilibrate nucleoside transporter-1 and 2
EPO	Erythropoietin
EVT	Endovascular therapy
FBS	Foetal bovine serum
FDA	American Food and Drug Administration
FDR	False discovery rate
FGF	Fibroblast growth factor
G-CSF	Granulocyte colony stimulating factor
GD	Glucose deprivation
GDNF	Glial cell-derived neurotrophic factor
GFAP	Glial fibrillary acidic protein
Ghsr	Ghrelin receptor
GJs	Gap junctions
GLUT-1	Glucose transporter 1
GO	Gene ontology
GUK	Guanyl kinase-like
hBLECs	Human brain-like endothelial cells
HIF-2α	Hypoxia-inducible factor-2α
HMGB1	High-mobility group protein B1
HPA	Hypothalamic-pituitary-adrenal
HPX	Hypoxia
HPX-R	Hypoxia-reperfusion
HRP	Horseradish peroxidase
HSP60	Heat shock protein 60
IBD	Inflammatory bowel disease
ICA	Internal carotid artery
ICAM-1	Intercellular adhesion molecule 1
IFN-γ	Interferon-gamma
IGF-1	Insulin-kike growth factor 1
IL	Interleukin
IPBLN	Institute of Parasitology and Biomedicine López-Neyra (CSIC)
IR	Insulin receptor
IT	Ion transport
JAMs	Junctional adhesion molecules
KO	Knock-out
KV1	Voltage-gated K+ channel
LAP	Latency-associated peptide

LAT1/2	Large neutral endothelial AA transporter 1 And 2
log_2FC	Log_2 fold change
LPS	Lipopolysaccharide
LRP1	Lipoprotein receptor 1
LSA	Lenticulostriate artery
MAGI	Membrane-associated guanylate kinase inverted
MAPK	Mitogen-activated protein kinase
MBP	Myelin basic protein
MCA	Middle cerebral artery
MCAO	Middle cerebral artery occlusion
MCT	Monocarboxylate transporter
MDMs	Monocyte-derived macrophages
MF	Molecular functions
MHC	Major histocompatibility complex
MMPs	Matrix metalloproteinases
MrgX2	Mas-related gene 2 receptor
MRP1-5	Multidrug resistance-associated proteins 1–5
MS	Multiple sclerosis
NADPH	Nicotinamide adenine dinucleotide phosphate
NaF	Sodium fluorescein
NETs	Neutrophil extracellular traps
NG	Normoglycemia
NG2	Neuron-glial antigen 2
NGF	Nerve growth factor
NK	Natural killer
NO	Nitric oxide
NS	Nervous system
NSCs	Neural stem cells
NSE	Neuron-specific enolase
NT-3	Neurotrophin-3
NVU	Neurovascular unit
NX	Normoxia
OATP1C1	Organic anion transporting polypeptide 1C1
OGD-R	Oxygen-glucose deprivation and reperfusion
OPCs	Oligodendrocyte progenitor cells
O/N	Overnight
PBS	Phosphate buffer solution
Pc	Permeability coefficient
PCA	Posterior cerebral artery
PCoA	Principal coordinates analysis
PDGFR-β	Platelet-derived growth factor receptor beta
PECAM-1	Platelet endothelial cell adhesion molecule-1
PFA	Paraformaldehyde
PHD2	Prolyl hydroxylase domain 2
PICA	Posterior inferior cerebellar artery
PK	Protein kinase
PMAT	Plasma membrane monoamine transporter
PNS	Peripheral nervous system
PPA	Pterygopalatine artery

PRRs	Pattern-recognition receptors
PU	Perfusion units
RA	Retinoic acid
RAGE	Receptor for advanced glycation end products
RAMPs	Receptor activity modifying proteins
rCBF	Regional cerebral blood flow
RGS5	Regulator of G-protein signaling-5
RIN	RNA integrity number
RMT	Receptor-mediated transport
ROI	Region of interest
ROS	Reactive oxygen species
RPKM	Reads per kilobase million
RT	Room temperature
rtPA	Recombinant tissue plasminogen activator
SCA	Superior cerebellar artery
sECM	Supplemented endothelial cell growth medium
Shh	Sonic hedgehog
SMCs	Smooth muscle cells
SMVT	Sodium-dependent multivitamin transporter
SNPc	Substantia nigra pars compacta
SR	Scavenger receptor
SST	Somatostatin
SSTR	Somatostatin receptor
SVZ	Subventricular zone
TCRs	T cell receptors
TEER	Transendothelial electrical resistance
TfR	Transferrin receptor
TGF- β	Transforming growth factor B
TIMPs	Tissue MMP inhibitors
TJs	Tight-junctions
TLR4	Toll-like receptor 4
TNF-α	Tumour necrosis factor-A
TRP	Transient receptor potential
VCAM-1	Vascular cell adhesion protein 1
VEGF	Vascular endothelial growth factor
VIP	Vasoactive intestinal peptide
WHO	World health organization
ZO	Zonula occludens
α-MSH	α-melanocyte-stimulating hormone
α-SMA	α-smooth muscle actin

Summary/Resumen

Summary

Ischemic stroke is the result of a permanent or transient occlusion of a major brain artery that provokes irreversible tissue injury and long-term sequelae. Beyond neurodegeneration, the subsequent energy/oxygen deprivation triggers a cascade of cellular and molecular events encompassing the nervous, immune, and vascular systems. Despite ongoing improvements, therapeutic failure remains notorious, and stroke carries and enormous global burden, being the second leading cause of death worldwide. Neuroinflammation, blood-brain barrier (BBB) breakdown, and immune deregulation are the major hallmarks of the pathogenesis and outcomes of brain ischemia. Importantly, these processes unfold over different spatiotemporal scales, including both responses to damage and the ensuing attempts at recovery. Understanding the interconnected and complex mechanisms that globally modulate these responses is essential for developing successful therapeutic strategies, and also emphasizes the need to comprehensively explore endogenous mediators. In this context, our study focuses on cortistatin, a neuropeptide widely distributed neuropeptide in the central nervous and immune systems. The anti-inflammatory, immunomodulatory, and neuroprotective properties of cortistatin make it an attractive endogenous target and a novel therapeutic agent for neuroinflammatory-vascular disorders including stroke. Therefore, our investigation explores the involvement of this neuropeptide in neuroinflammation, immune dysregulation, and BBB dysfunction associated with stroke, as well as its potential therapeutic application. For this purpose, we used the widely-known preclinical model of stroke MCAO (middle cerebral artery occlusion) in young (3 months old) and middle-aged (6 months old) wild-type and cortistatin-deficient mice. Our findings reveal that the absence of cortistatin increases susceptibility to stroke and worsens prognosis in cortistatin-deficient mice (*i.e.*, worsened neurological score, severe microglial activation, impaired astrocyte scar, disrupted BBB, dysregulated angiogenesis, and exacerbated immune infiltration and peripheral response). Furthermore, we found that the endogenous lack of cortistatin predisposes brain endothelium to weakening, leading to increased permeability, tight-junctions breakdown, dysregulated immune activity, and disrupted and/or deactivated genetic programming. These pathways, crucial for both basic physiology and repair after damage (*e.g.,* extracellular matrix remodeling, angiogenesis, response to oxygen, signaling, and metabolites transport), become dysfunctional, rendering cortistatin-deficient brain endothelium unresponsive to further injury. Our results also demonstrate that treatment with cortistatin at later stages in wild-type and cortistatin-deficient mice of both age groups reverses stroke outcomes. This is evidenced by improved neurological score,

smaller lesions, reduced/modulated glial response, regulation of the glial scar formation, BBB recovery, and decreased peripheral immune response. Importantly, we reported that cortistatin targets hyperpermeability, tight-junctions disruption, and the inflammatory response observed after ischemic conditions in the human and mouse brain endothelium. In conclusion, our results highlight the key role of cortistatin in regulating the intricate interplay between the nervous and the immune systems, modulating dysregulated cellular and molecular responses from both systems that could impact brain homeostasis. This also underscores the importance of shifting the focus of stroke therapies towards regulating and balancing neurotoxic processes to prevent chronic detrimental responses rather than entirely halting them. Moreover, our findings suggest that cortistatin-based therapies may represent a novel multifunctional treatment for ischemic stroke, holding significant promise compared to interventions targeting only a single aspect of stroke physiopathology. Finally, the efficient application of these multimodal therapies at later times and across different ages and phenotypes opens the door for extending the therapeutic window for many patients who unfortunately do not meet the current clinical criteria.

Resumen

El accidente cerebrovascular isquémico o ictus se produce debido a la obstrucción permanente o temporal de una arteria cerebral, generando daño irreversible en el tejido y secuelas a largo plazo. Más allá de la neurodegeneración, la subsiguiente privación de energía y oxígeno desencadena una cascada de eventos celulares y moleculares que afectan a los sistemas nervioso, inmunológico y vascular. A pesar de los continuos avances en investigación y clínica, el fallo terapéutico sigue siendo notorio y el ictus se mantiene como la segunda causa de muerte a nivel mundial. La neuroinflamación, la ruptura de la barrera hematoencefálica (BHE) y la desregulación inmunológica son los principales rasgos patogénicos de la isquemia cerebral. Estos procesos se desarrollan en diferentes etapas espacio-temporales, abarcando respuestas agudas al daño, pero siendo también partícipes en la recuperación posterior. Comprender los complejos e interconectados mecanismos que modulan estas respuestas es esencial para desarrollar estrategias terapéuticas exitosas, destacando especialmente la necesidad de explorar exhaustivamente los mediadores endógenos. En este contexto, nuestro estudio se centra en cortistatina, un neuropéptido ampliamente distribuido en los sistemas nervioso central e inmunológico. Las propiedades antiinflamatorias, inmunomoduladoras y neuroprotectoras de cortistatina le convierten en una atractiva diana endógena y en un nuevo agente potencialmente terapéutico para trastornos neuroinflamatorios-vasculares como el accidente cerebrovascular. Por lo tanto, nuestra investigación explora la participación de este neuropéptido en la neuroinflamación, la desregulación inmunológica y la disfunción de la BHE asociadas con el ictus, así como su potencial aplicación terapéutica. Para ello, utilizamos el modelo preclínico de ictus por oclusión de la arteria cerebral media (MCAO) en ratones jóvenes (3 meses) y de mediana edad (6 meses) salvajes (*wild-type)* y deficientes en cortistatina. Nuestros descubrimientos revelan que la ausencia de cortistatina aumenta la susceptibilidad al accidente cerebrovascular y agrava el pronóstico clínico en ratones deficientes en cortistatina (empeoramiento del daño neurológico, activación microglial severa, cicatriz astrocítica disfuncional, BHE disrumpida, angiogénesis desregulada e infiltración inmunológica y respuesta inmunológica periférica exacerbadas). Además, encontramos que la falta endógena de cortistatina predispone al endotelio cerebral a debilitarse, además de aumentar su permeabilidad, romper las llamadas uniones estrechas, desregular la actividad inmunológica y desactivar ciertas vías moleculares. Estas vías, cruciales tanto para la actividad fisiológica básica como para procesos de reparación después del daño (por ejemplo, remodelación de la matriz extracelular, angiogénesis, respuesta al oxígeno,

señalización y transporte de metabolitos), se vuelven disfuncionales, haciendo que el endotelio cerebral deficiente en cortistatina sea incapaz de responder a daños adicionales. Nuestros resultados también demuestran que el tratamiento con cortistatina en etapas tardías revierte los resultados del accidente cerebrovascular en ambos grupos de edad de ratones y tanto en *wild-type* como deficientes en cortistatina. Esto se evidencia por la mejora de la escala de daño neurológico, lesiones isquémicas reducidas, respuesta glial reducida/modulada, regulación de la formación de la cicatriz glial, recuperación de la BHE y disminución de la respuesta inmunológica periférica. Es importante destacar que cortistatina también modula la hiperpermeabilidad de la BHE, la disrupción de las uniones estrechas y la respuesta inflamatoria en condiciones isquémicas en el endotelio cerebral humano y de ratón. En conclusión, nuestros resultados destacan el papel clave de cortistatina endógena en la regulación de la compleja interacción entre los sistemas nervioso e inmunológico, modulando respuestas celulares y moleculares desreguladas de ambos sistemas que podrían afectar la homeostasis cerebral. Esto subraya la necesidad de cambiar el enfoque de las terapias del ictus, orientándolas hacia la regulación y el equilibrio de los procesos neurotóxicos para prevenir respuestas crónicas perjudiciales en lugar de detenerlas por completo. Además, nuestros hallazgos sugieren que las terapias basadas en cortistatina pueden representar un novedoso tratamiento multifuncional para el accidente cerebrovascular isquémico, con un gran potencial en comparación con las intervenciones que se solo centran en un aspecto de la fisiopatología del mismo. Finalmente, la aplicación eficiente de estas terapias multimodales en etapas tardías y en diferentes edades y fenotipos (considerando posibles cambios interindividuales en diferentes factores y mediadores endógenos) abre la puerta para ampliar la ventana terapéutica para la mayoría de pacientes que no cumplen con los criterios clínicos.

1. Introduction

1. Introduction

1.1. Stroke: definition, types, aetiology, and epidemiology

According to the World Health Organization (WHO), the term “stroke” refers to an acute brain injury derived from no other than a vascular cause, leading to neuronal damage and functional disability [1,2]. Stroke is commonly categorized into two subtypes: ischemic and haemorrhagic. Haemorrhagic strokes are caused by a vessel rupture and the subsequent entry of blood to the brain parenchyma, while ischemic strokes are the result of a permanent or transient occlusion in a major or minor brain artery (Figure 1) [3,4].

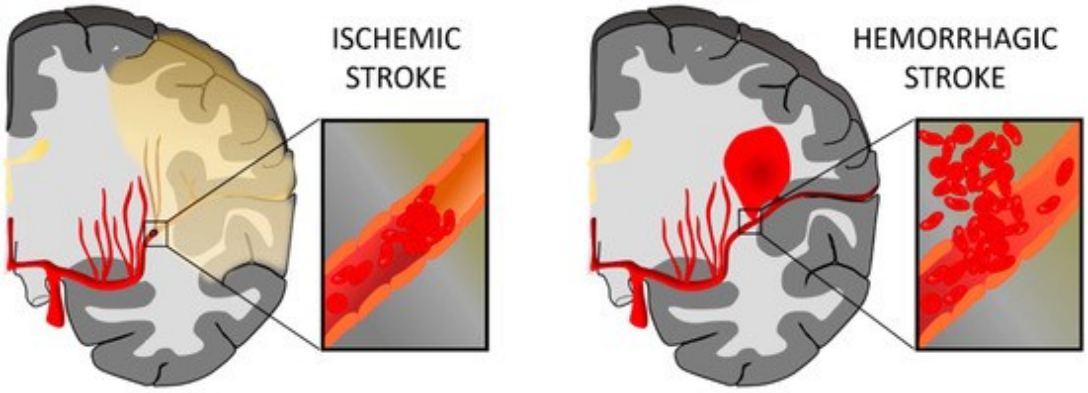

Figure 1. Graphic representation of an ischemic (vessel occlusion) and haemorrhagic (vessel rupture) stroke. Adapted from Correa-Paz et al. [5].

Based on the most recent Global Burden of Diseases report published in 2019 [1,6], strokes, including ischaemic and haemorrhagic strokes, affected up to 12.2 million people worldwide in 2019 (Figure 2). This made strokes the second leading cause of death, resulting in 6.55 million deaths in that year. Overall, 1 in 4 adults will experience a stroke in their lifetime [7]. Besides, strokes represent the third-leading cause of combined death and disability, as measured by disability-adjusted life-years (DALYs) [1,7]. It is estimated that there are over 101 million stroke survivors globally, which are unfortunately living with stroke aftermaths (Figure 2). Worryingly, this number has almost doubled in the last 30 years, conforming a high-risk group and being the current focus of secondary prevention strategies [7].

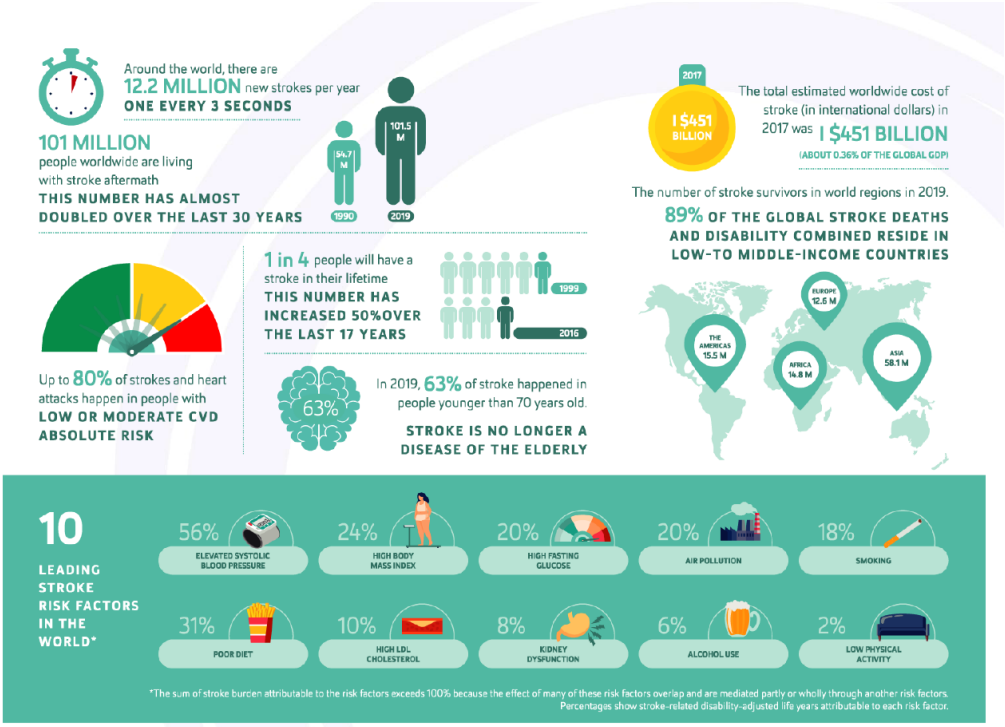

Figure 2. **Stroke infographic**. Data about incidence, prevalence, risk factors and disability after stroke are included. Extracted from Owolabi et al. [6].

In 2019, five primary specific risk factors were identified, namely high systolic/diastolic blood pressure (> 140/90 mmHg), high body mass index (> 25), high fasting plasma glucose (100-125 mg/dL), ambient particulate matter air pollution, and smoking (Figure 2). These risk factors are often linked to a sedentary lifestyle, (*i.e.,* low levels of physical activity) and diets rich in fats and red meats but low in fruits and vegetables. Additionally, factors, such as alcohol and drug consumption, psychosocial stress, depression, sleep deprivation, and certain medical conditions like diabetes, chronic kidney disease, or periodontal disease, can also contribute to an increased risk of stroke (Figure 2) [1,7]. Moreover, environmental factors besides air pollution, such as low/high ambient temperature or lead exposure also appear to play an important role in the stroke burden. Importantly, other non-modifiable risk factors including age, sex, and genetic factors must not be overlooked [1,7].

It is essential to note that there are substantial differences in the incidence rates of stroke among the different countries. The incidence is notably higher in low and upper-middle countries than in high-income countries (Figure 3), which could be attributed to factors, such as limited access to healthcare, lower awareness about stroke, and a higher prevalence or impact of various risk factors (including smoking, unhealthy diet, diabetes,

hypertension, and other health conditions) [1]. While the number of DALYs was higher among men compared to women, the prevalence of strokes was very similar between the two sexes in 2019. However, on a more worrying note, there was a significant rise in the incidence rates in people under the age of 70 (they account for 63 % of all strokes) between 1990 and 2019, with even faster trends from 2010 to 2019 [1].

Since ischemic strokes account for approximately 85 % of all strokes, this thesis will primarily focus on them.

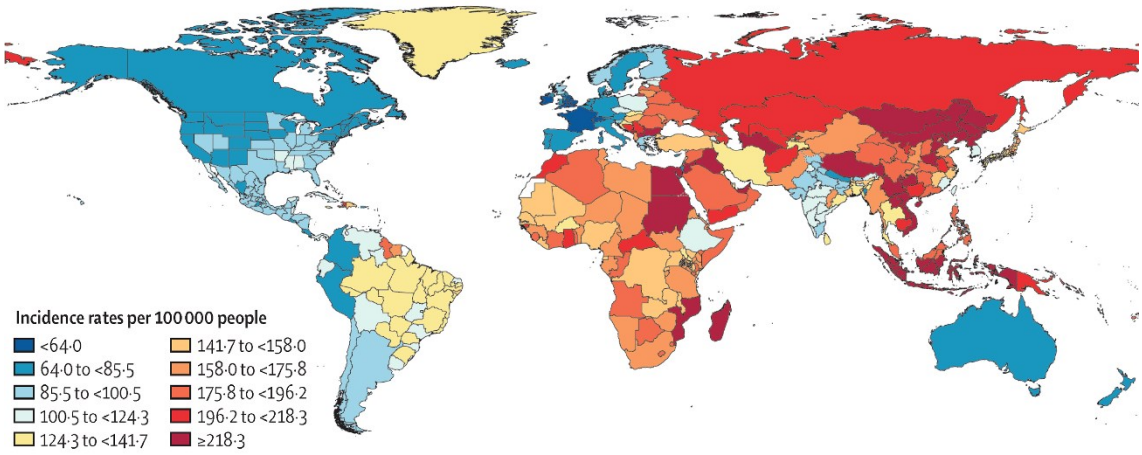

Figure 3. Stroke incidence rates per 100,000 people in all types of strokes for both sexes and by country (2019). Modified from Feigin et al. [1].

1.2. Pathophysiology of ischemic stroke. Cell populations involved in neurodegeneration and neuroinflammation

The majority of ischaemic strokes originate from thromboembolic events, being large artery atherosclerosis and atrial fibrillation the primary underlying causes. Small vessel disease, (particularly common in Asia and associated with high blood pressure and diabetes mellitus), arterial dissection, or vasculitis, represent a smaller proportion of cases [7]. Since brain function relies on the continuous supply of oxygen and glucose through the blood flow, any interruption in the cerebral blood supply may lead to irreversible brain damage. Hence, shortly after the occlusion of the artery, noticeable symptoms start to manifest, such as one-side arm and/or leg weakness, loss of balance or coordination (*i.e.,* ataxia), sudden loss of one or more senses, blurred vision, headache, facial weakness or speech difficulty. This emphasizes the urgent need for rapid detection to prevent the escalation of more severe symptoms that might result in arm/leg motor impairment, head/gaze deviation, facial palsy, aphasia, or agnosia [8].

The middle cerebral artery (MCA) is the most common artery involved in ischemic stroke. MCA originates from the internal carotid artery and through four branches (M1, M2, M3, and M4 arteries) provides the blood supply to a substantial portion of the frontal, temporal, and parietal lobes of the brain, as well as to part of the basal ganglia, thalamus and the internal capsule (Figure 4). This would explain the motor and sensory deficits affecting the face and upper extremities (*i.e.,* facial paralysis, contralateral hemiparesis, and sensory loss) [9].

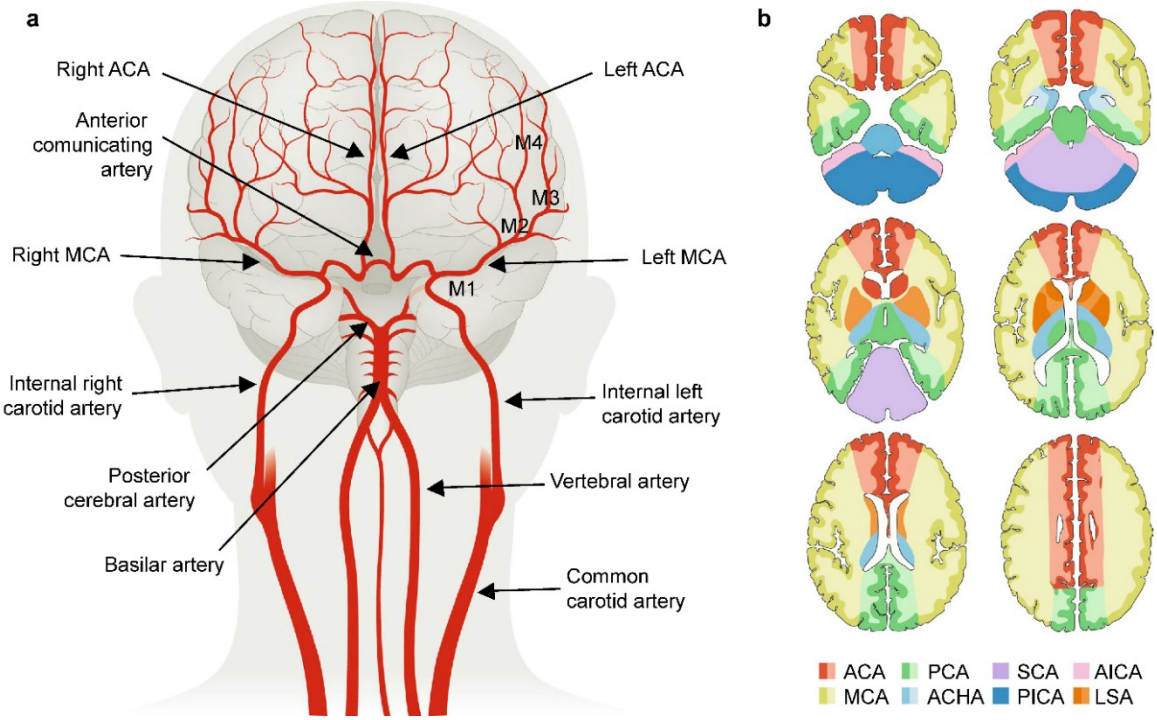

Figure 4. Human cerebral vascular tree and affected areas following arterial occlusion. **a-b.** Arteries susceptible to occlusion **(a)** and their vascular territories and brain regions affected **(b)**. ACA, anterior cerebral artery; MCA: middle cerebral artery (with M1, M2, M3, and M4 territories); PCA, posterior cerebral artery; ACHA, anterior choroidal artery; SCA, superior cerebellar artery; PICA, posterior inferior cerebellar artery; AICA, anterior inferior cerebellar artery; LSA, lenticulostriate artery. Modified from Campbell et al. [7].

The sudden lack of blood flow in these areas followed by the subsequent reperfusion triggers a cascade of cellular and molecular events that ultimately drive to ischemic damage [10]. Paradoxically, oxygen, calcium, and pH changes due to the reperfusion process after the ischemic event contribute to the production of free radicals and other toxic factors that generate oxidative stress [11]. These initiate a rapid and complex cascade of genomic, molecular, and cellular events that may evolve over hours to days and weeks after the onset [2]. These pathophysiology incidents are diverse and include energy failure, oxidative stress, loss of cell homeostasis, excitotoxicity, glial cell activation, inflammation, and disruption of the blood-brain barrier (BBB) with infiltration of

leukocytes [12] (Figure 5). Although they can be differentiated as stroke early and late processes, it is important to emphasize that some events are intricately and subsequently connected, often unfolding in parallel or simultaneously within a short time frame (Figure 5). To ensure a clear and comprehensive understanding of these phenomena, and enable a thorough explanation of all of them, this thesis will be focus on early processes (0-72 h post-stroke) and will be divided and explained based on the involvement of the different cell types and structures.

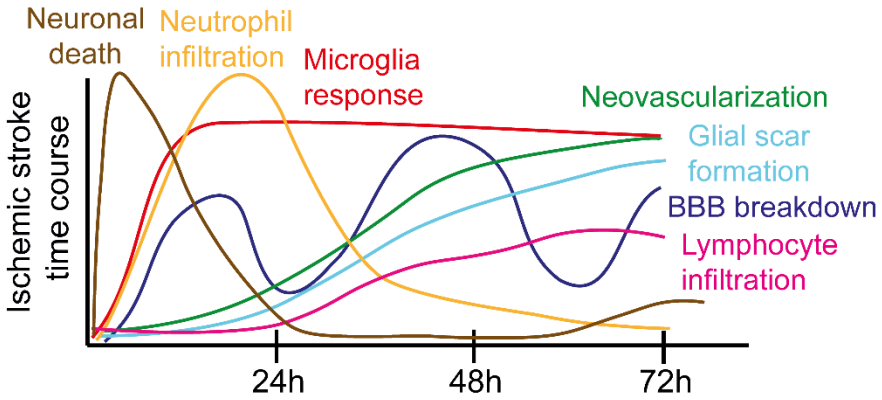

Figure 5. **Schematic representation of the time-coursed events underlying ischemic stroke during the first 72 h**. These events include neuronal death, neutrophil infiltration, microglia response, neovascularization, glial scar formation, BBB breakdown, and lymphocyte infiltration.

1.2.1. Neurons

The nervous system (NS) is a sophisticated network underlying any interaction of an organism with its surroundings. It comprises sensory components responsible for detecting environmental stimuli, as well as motor components that control skeletal, cardiac, and smooth muscle activities, together with glandular secretions. These elements work in coordination to generate appropriate motor responses to the sensory inputs. Signalling within these circuits enables thinking, language, learning, feeling, and memory [13].

The NS can be divided into the peripheral (PNS) and central nervous system (CNS). The PNS includes cranial, spinal, and peripheral nerves while the CNS arises from the encephalon and the spinal cord. The encephalon can be further categorized into four primary regions: (1) the brain stem (2) the cerebellum; (3) the diencephalon, housing the thalamus and hypothalamus; and (4) the cerebral hemispheres, comprised of the cerebral cortex, basal ganglia, white matter, hippocampi, and amygdalae. The CNS is responsible for processing sensing information and generating appropriate responses accordingly, whereas the PNS serves as a communication conduit transmitting information to and from

the CNS. The NS is made up of vast networks of neurons, *i.e.,* electrically excitable cells capable of generating signals called action potentials. Anatomically, neurons are composed of a cellular body (soma) and at least one extended branch called neurite. Neurites relaying signals away from the soma are axons, while those transmitting signals towards the soma are termed dendrites. This morphological arrangement enables the transmission of both electrical and chemical signals between neurons, establishing a complex network of cellular connections known as synapses. Neurons constitute approximately 10 % of all nervous cells, with the remaining 90% being glial cells [14].

Neurons are more vulnerable than glia and vascular cells, and they quickly experience dysfunction or death upon exposure to hypoxia-ischemia. In ischemic stroke, the damage is more severe and rapid in the central area of the ischemic territory, also known as the *ischemic core*, where the blood flow experiences the most dramatic depletion (blood flow < 10 ml/100 mg/min) (Figure 6). However, in the 1970s, a series of pioneering experiments found that much of the initial clinical deficit in stroke patients was related to a "hypo-perfused, hibernating, electrically non-functional" brain area in the periphery of the ischemic region, known as the *ischemic penumbra* (blood flow > 10, but less than 20 mL/100 mg/min) (Figure 6) [7]. Here, neuronal damage develops more gradually because collateral blood flow from adjacent vascular territories maintains slow and intermittent cerebral perfusion above the threshold of instant cell death [10,15].

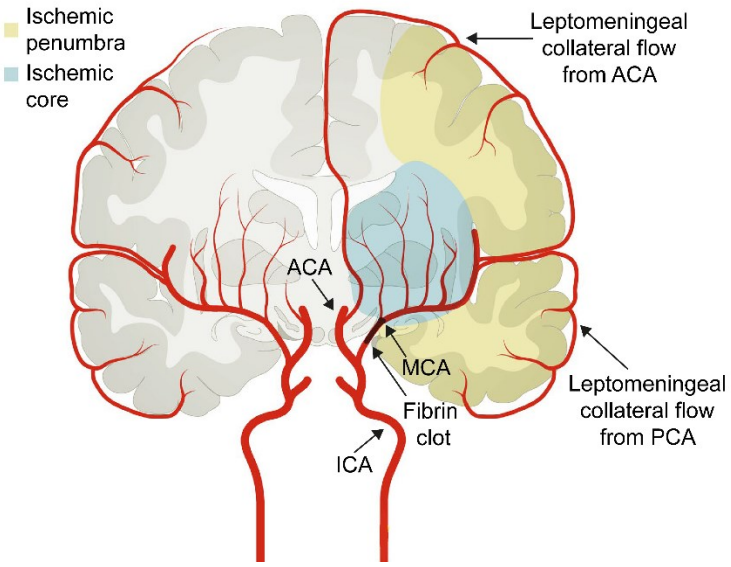

Figure 6. Schematic drawing illustrating the cerebrovascular tree after stroke. When a clot occludes the middle cerebral artery (MCA), blood circulation stops in this area, leading to neuronal cell death (ischemic core). However, branches from the anterior cerebral artery (ACA) and posterior cerebral artery (PCA) supply retrograde blood flow to a variable proportion of the MCA: this supply is sufficient for metabolic viability but not electrical activity (ischemic penumbra). Modified from Campbell et al. [7].

In the ischemic core, cell death primarily occurs due to energy failure. Neurons, deprived of enough oxygen and glucose, fail to generate the required ATP to fuel the ionic pumps that maintain the ionic gradient across the neuronal membrane, particularly the Na^+−K^+ ATPase. This leads to massive Na^+ and Ca^{2+} accumulation in the cytoplasm, resulting in swelling and degeneration of the organelles, loss of membrane integrity, and ultimate necrotic cell death. Conversely, in the ischemic penumbra, the reduced blood flow is not sufficient to cause energy failure, allowing neurons to remain metabolically viable for a prolonged period after the insult. However, these neurons are under stressed and highly susceptible to any pathogenic event that can disrupt their delicate metabolic balance [10]. In particular, excessive extracellular accumulation of glutamate plays a significant role in the death of neurons in the ischemic penumbra. This leads to an overactivation of the NMDA glutamate receptors, causing a cytoplasmic accumulation of Ca^{2+} into the cytoplasm. Subsequently, elevated Ca^{2+} levels activate multiple Ca^{2+}-dependent enzymes, including proteases (mainly calpains and caspases), as well as enzymes that produce free radicals, nitric oxide (NO), and arachidonic acid metabolites. Together, these events can promote programmed cell death (*i.e.,* cytoplasm shrinkage, chromatin compaction, nuclear condensation, pyknosis, and apoptotic body formation). This may occur even in post-ischemic states, releasing danger signals that activate the immune system and contribute to the subsequent inflammatory response [10]. However, it is important to note that, compared with necrotic cell death within minutes after ischemia, apoptotic cell death is delayed by several hours or even days, which may provide a therapeutical window for neuroprotection [2]. Targeting the mechanisms involved in the apoptotic cascade could potentially prevent or mitigate the death of vulnerable neurons. By protecting these neurons, it may be possible to salvage the remainder neurons ischemic penumbra and reduce the overall extent of brain damage.

Finally, it is important to remark that in the later stages of stroke, the process of neurogenesis becomes activated. The activity in the subgranular and subventricular zone (SVZ) is increased, and neural stem cells (NSCs) begin to proliferate in response to stroke. These are multipotent cells capable of differentiating into neurons, oligodendrocytes, and astrocytes. Thanks to the influence of chemokines and cytokines secreted by resident and activated microglia and astrocytes, neuroblasts and immature neurons migrate into the infarct and peri-infarct region. There, they undergo final differentiation into mature neurons, aiding synaptogenesis and the stabilization of the synapses [16]. Despite ongoing research, the underlying mechanisms of NSC neurogenesis are not fully understood yet. Studies have reported the presence of neuroblasts in the ischemic striatum from 1 week

up to 16 weeks after a stroke, while newborn neurons have been detected as early as 26 days after the ischemic insult in experimental stroke models. However, these time frames might differ in humans and call for further investigation to inform effective treatment strategies. This critical period must be urgently targeted to design new neuroprotective factors that promote neuronal survival [16,17].

1.2.2. Oligodendrocytes

Oligodendrocytes are the myelinating cells of the CNS, essential for axonal integrity. They comprise 5-10 % of the total glial population and were first identified by Virchow, Deiters, and Golgi in the 19th century (revised in [18]). In the adult brain, they originate from oligodendrocyte progenitor cells (OPCs) through a well-coordinated process involving migration, proliferation, and differentiation. OPCs play a crucial role in maintaining CNS homeostasis and facilitating myelin regeneration following injury [19]. The primary function of oligodendrocytes is to generate myelin, a protective membrane that ensheaths axons. Myelin sheaths are crucial to enable the propagation of action potential through different neurons, which enables brain-efficient connectivity. Independently from a myelination role, oligodendrocytes contribute to immune-surveilling and trophic factor secretion (*i.e.,* insulin-like growth factor 1, IGF-1, and glial cell-derived neurotrophic factor, GDNF) [18]. Similar to neurons and due to their high energy requirements, oligodendrocytes are greatly susceptible to the effects of ischemia. Remarkably, within just 30 min of artery occlusion, microglia-induced swelling of oligodendrocytes occurs, and within 3 h post-occlusion, a significant portion of oligodendrocytes undergo cell death [20]. Interestingly, this oligodendrocyte death appears to precede neuronal death in the ischemic area. The damage of oligodendrocytes in the white matter induces axonal instability and it is closely associated with early functional ischemia impairment (*i.e.,* sensorimotor impairments, cognitive dysfunction, and mood disorders). Of note, a single oligodendrocyte can myelinate up to 50 axons and create up to 150 layers of myelin membrane, illustrating the profound impact of the dysfunction of a solitary oligodendrocyte, let alone a population [18].

However, after ischemic damage, a rapid oligodendrogenesis response is triggered. In response to signals of demyelination, OPCs derived from NSCs in the SVZ proliferate, and migrate to the periphery of the ischemic region, where they further mature into oligodendrocytes to establish and restore myelin sheaths [21,22]. Yet, the precise mechanisms and origin of these newly generated oligodendrocytes remain unknown. Furthermore, oligodendrocytes behaviour is intricately connected with the surrounding

cells of the neurovascular unit, which can promote either their survival or damage according to microenvironment cues [18].

1.2.3. Microglia

- **Ontology and functions**

Microglia are specialized cells of myeloid origin, normally described as the resident macrophages and the first line of defence against injury in the CNS. Microglia were first described by Franz Nissl as *Staebchenzellen* or “rod cells”, due to their rod-shaped nuclei. Later, in 1913, Ramón y Cajal referred to them as a “third element”, distinguishing them from neurons and astrocytes [20]. A couple of years later, Pío Del Río-Hortega building on Cajal’s work, further phenotypically characterized and officially named these cells as microglia, recognizing them as the only immune cells in the brain parenchyma (reviewed in [23]).

In the adult mouse brain, microglia constitute 5–12 % of all glial cells, with varying distributions in different brain regions. There are approximately 3.5×10^6 microglia in the adult mouse brain, with more located in the grey matter than in the white matter. In the human brain, the distribution of microglia varies significantly, accounting for approximately 0.5 % to 16 6 % of all brain cells. Unlike in mice, more microglia are found in the white matter than in the grey matter in humans, providing valuable insights into the likely differential response of microglia in both organisms under pathological conditions [20].

In the context of CNS injury, microglia play a crucial role in phagocytosis and removal of microbes, dead cells, soluble antigens, protein aggregates, or any other harmful particle that may threaten the CNS. Additionally, microglia secrete various soluble factors, such as cytokines, chemoattractants, and neurotropic factors which contribute to immune responses and tissue repair in the CNS [24]. However, due to the historical misconception that the brain was an immune-privileged site, microglia have been mistakenly considered bystanders in the healthy CNS, with minimal homeostatic roles beyond the above-mentioned phagocytic scavenging and immune surveillance [23]. On the contrary, numerous studies have now unveiled that microglia serve critical physiological roles in the healthy prenatal and postnatal brain, including supporting the development of brain connectivity and vascular growth, monitoring and supporting neuronal activity, synaptic maturation and remodelling, and maintaining CNS homeostasis throughout adulthood [23,25].

To perform such diverse functions, microglia must sense different signals in their microenvironment and adapt their morphology accordingly, resulting in a wide variety of cellular shapes (Figure 7). The morphological plasticity of microglial cells was already acknowledged by Río-Hortega in his 1919 series of papers about microglia. He proposed that microglia exist in two different states: i) “resting” microglia, characterized by a highly ramified morphology, small cell soma, fine processes, and limited phagocytic and migratory activity, and ii) “activated” microglia, characterized by an amoeboid shape, cell body hypertrophy, process thickening and retraction, high motility, and phagocytic and proliferative capacities [20,25]. For much of the last century this “two-state paradigm” dominated the understanding of these cells, driving to the misconception that microglia in the healthy brain were functionally quiescent or dormant and that only the ameboid microglia phenotype was related to activation, which was believed to be always detrimental for brain activity. This oversimplified view categorized microglia for a long time as either “resting-ramified/good” or “activated-ameboid/bad” microglia [25]. However, the current knowledge has evolved, revealing that “resting” microglia are not truly inactive but rather actively surveilling their microenvironment [26]. Additionally, the concept of “activated-ameboid” microglia being the only phenotype related to activation has been extensively challenged, and it has been demonstrated that microglia activation is necessary to promote further recovery [24]. It is important to note that microglia activation is a complex and dynamic process that encompasses a broad spectrum of phenotypes and functions (Figure 7), ranging from hyper-ramified forms to activated short-ramified forms, or even bushy or ameboid microglia. Importantly, all these changes are reversible at every stage [27].

Therefore, considering the diversity in microglia morphotypes, activated microglia have been characterized as “classical” (M1 pro-inflammatory and neurotoxic) or “alternative” (M2, anti-inflammatory and healing) following the paradigm used for macrophages. “M1 activation” has been characterized by the production of tumour necrosis factor-α (TNF-α), interleukin (IL) 6 (IL-6), IL-1β, IL-12, chemokine (C-C motif) ligand 2 (CCL2), major histocompatibility complex (MHC) class II, and the expression of nicotinamide adenine dinucleotide phosphate (NADPH) oxidase, which generates superoxide and reactive oxygen species (ROS), among others. Conversely, “M2 activation” has been associated with the production of anti-inflammatory cytokines, including IL-10, transforming growth factor β (TGF-β), growth factors (*e.g.,* IGF-1, fibroblast growth factor (FGF), nerve growth factor (NGF), or brain-derived neurotrophic factor (BDNF)), as well as other pro-survival factors [24]. Nevertheless, it has become increasingly clear that the M1/M2 paradigm is neither inadequate to fully describe microglia

and macrophage activation *in vivo*, since microglia rarely display a significant bias towards either the M1 or M2 phenotype [24]. They can display overlapping functions and can either or both promote injury and facilitate repair, depending on the activation signals [25]. This paradigm shift emphasizes the complexity and plasticity of microglial responses, highlighting their vital roles in maintaining CNS homeostasis and their contributions to brain health and disease. In this thesis, we aim to describe the complexity of these cells to the full extent in the context of stroke development and the cortistatin-deficient environment.

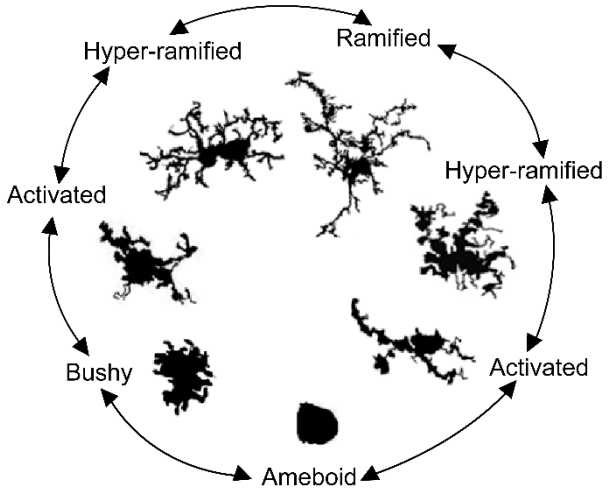

Figure 7. Microglia morphology in the adult human brain. Ramified surveilling microglia can rapidly transition towards an activated phenotype. This activated phenotype, in turn, can display multiple phenotypes depending on the insult and the brain region, ranging from hyper-ramified microglia to an activated short-ramified form or a bushy or ameboid microglia. Importantly, all these changes are reversible at every point. Modified from Karperien et al. [27].

- **Microglia in stroke**

Microglia activation is the first step of the inflammatory response in the ischemic brain, followed by infiltration of immune cells, such as neutrophils, macrophages/monocytes, natural killer cells, T cells, and other glial cell activation [20], as we will later describe.

Microglia are the first responder to the damage, rapidly undergoing dynamic morphological and molecular changes upon activation. Similar to other neurodegenerative disorders, microglia play a dual role during ischemic pathology. Initially, they display predominantly beneficial anti-inflammatory states in the early stages, followed by a subsequent transition to primarily detrimental pro-inflammatory states in the later stages [12,28]. The role of activated microglia is complex and can be influenced by various factors, including the severity of initial ischemia, the different ischemic pathological phases, and the location within the lesion, among others [12].

Therefore, activated microglia can exhibit early beneficial effects by phagocytosing cell debris and restraining the inflammatory response, overall aiming to promote neuronal repair. Besides, microglia regulate processes such as angiogenesis, myelin regeneration, synaptic remodelling, and neurogenesis [12]. However, activated microglia may not always be beneficial, as they secrete a plethora of cytokines and chemokines that can induce excitotoxicity, phagoptosis, and BBB disruption. Additionally, they upregulate endothelial adhesion molecules and further promote leukocyte infiltration [28,29]. Microglia play such an important role, that several studies have shown that the removal of microglia provokes a significant increase in infarct size and it is associated with elevated neuronal apoptosis [28]. Accordingly, modulating and maintaining a balanced and controlled microglial response, especially preventing chronic uncontrolled microglial activation, seems to be essential for ensuring a favourable outcome after ischemic injury.

Regarding experimental models of stroke, such as the middle cerebral artery occlusion (MCAO) model, activated microglia are detected in the boundary zone of the ischemic lesion as early as thirty minutes after the damage onset [30]. The immunoreactivity of Iba1, a marker for microglia, increases from one hour within the lesion and gradually intensifies up to one week. During the early stages of ischemia (3 h), microglial processes, which are long, thin, and highly ramified, start to retract in the ischemic core. By 24 h, microglia become hypertrophic, characterized by enlarged cell bodies and extended long, wide processes. After 48 h, cells adopt a more globose, amoeboid-like shape, with extending short processes that swallow up nearby structures. One week after ischemia, the ischemic core becomes more populated with an increased number of Iba1-labelled immune cells, which exhibit a more elongated shape compared to 48 h (Figure 8). Importantly, their distribution respects the architecture of the striatum, avoiding the white matter bundles that are characteristic of this brain structure. Despite the most prominent microglial activation occurring within the lesion, there are also important changes in the peri-lesioned area [3]. Within the first 48 h, the number of highly ramified microglia present in the surrounding penumbra starts to increase, experimenting relevant molecular and morphological changes. These suggest that microglia migrate from the penumbra to the ischaemic core post-stroke [3,31]. The major changes in microglial morphology in the peri-lesion seem to happen at 48 h post-injury, although at one week after ischemia; strong activation in the penumbra is still evident (Figure 8).

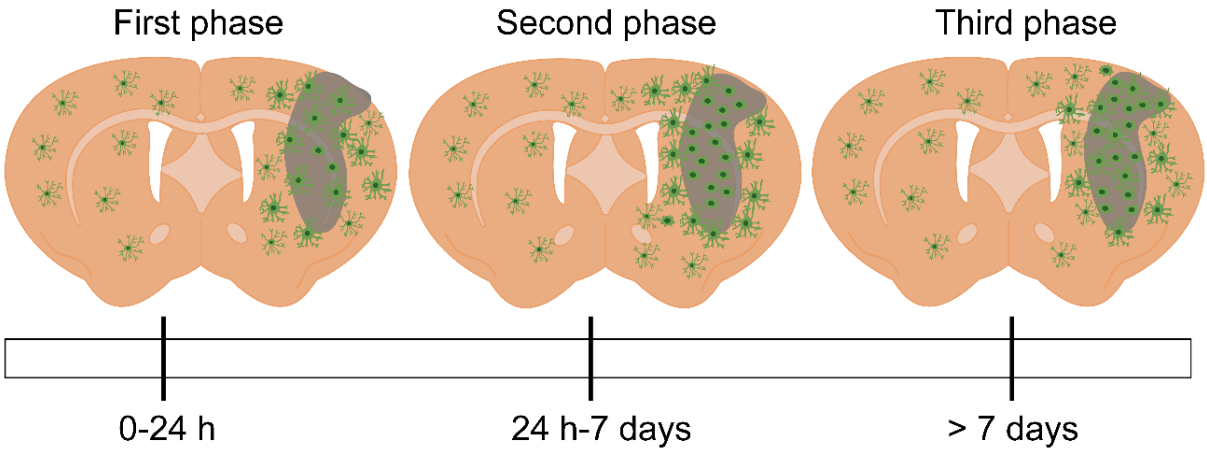

Figure 8. Spatio-temporal representation of microglia dynamics following a stroke. In the initial stages (0-24 h), microglia undergo rapid activation, with their processes transitioning from initially long and highly ramified to hypertrophic by 24 h. After 48h, microglia adopt a phagocytic amoeboid-like shape. Additionally, microglia in the penumbra begin the activation process and become hypertrophic. One week after ischemia, the ischemic core becomes more populated with cells, displaying a reduced level of hypertrophy.

The dynamic and mutable inflammatory environment plays a pivotal role in orchestrating microglial polarization. While a complete understanding of these dynamics remains elusive, recent studies suggest that microglial polarization tends to shift towards an anti-inflammatory phenotype within the initial hours, reaching its peak at 3-5 days after stroke. However, this anti-inflammatory state gradually decreases over time, transitioning towards a pro-inflammatory-like phenotype. This pro-inflammatory microglia peaks at 14 days after MCAO, which may cause further neuronal damage and BBB breakdown [32]. In fact, the inhibition of pro-inflammatory shift in microglia has been found to reduce neurological deficits in later stages [32–34]. Conversely, fostering the polarization of anti-inflammatory microglia appears to contribute to tissue remodelling and repair [32,35,36]. Nonetheless, the activation of microglia and its effects are far more complicated. Importantly, pro-inflammatory microglia have beneficial effects that should not be simply eliminated, and maintaining anti-inflammatory phenotypes for a long time may have detrimental consequences, such as increased susceptibility to tumour growth [32]. Future research should delve into regulating the balance between both phenotypes maintaining inflammatory defence, as well as promoting neuroprotection, rather than merely focusing on reducing the damage caused by pro-inflammatory microglia.

1.2.4. Astrocytes

- **Biology and functions**

Astrocytes are specialized glial cells that constitute the most abundant type of cell in the brain -and also the largest one-, accounting for approximately 20-40 % of the total cell population [37,38]. They are named based on their distinctive star-shaped appearance. Similar to microglia, astrocytes exhibit heterogeneous morphology and distinct spatial organization, being classically divided into three categories: fibrous astrocytes located in white matter, protoplasmic astrocytes in grey matter, and radial astrocytes surrounding ventricles. Nonetheless, for the purpose of this thesis, and due to their complex morphological and functional diversity, we will use the umbrella term “astrocytes” to encompass all these categories [39].

During postnatal development, astrocytes play a crucial role in guiding the formation of excitatory and inhibitory synapses, contributing to axon myelination, and facilitating the development and establishment of neural circuits. They achieve these relevant functions by releasing soluble factors, such as tenascin C and proteoglycans, as well as through physical cell contact [40,41]. Throughout adulthood, astrocytes closely interact with neurons, providing structural support, and taking part in metabolic coupling, acting as a nutrient source and storage for neurons [41]. In particular, astrocytes release growth factors (TNF-α, BDNF, NGF, GDNF, and CNTF, ciliary neurotrophic factor), transmitters precursors (glutamine), and energy substrates (lactate, ATP) all through exocytosis and ion channels [41,42]. For example, the lactate shuttle between astrocytes and neurons is particularly important for modulating normal brain function, providing vital support to neurons, and mediating long-term memory while enhancing neuronal excitability and plasticity [43]. Besides, astrocytes can release synaptically active molecules known as “gliotransmitters”, which can directly influence synaptic activity [40]. Astrocytes are also responsible for maintaining appropriate levels of pH, ions, neurotransmitters, and fluid in the microenvironment around neurons [40]. Specifically, they handle the clearance of transmitters and other extracellular factors, protecting neighbouring cells by ingesting excessive glutamate, GABA, and glycine, which could otherwise cause neurotoxic damage. Moreover, astrocytes are involved in pH regulation by transporting water through the aquaporin 4 transporter (AQP4) and utilizing transporters for K^+, bicarbonate, and monocarboxylic acid [37].

Importantly, astrocytes are also capable of regulating blood flow in the brain. Particularly, neuron signals trigger calcium waves in astrocytes that, in response, release

mediators, such as prostaglandin E, NO, or arachidonic acid. These are substances that can have vasodilator or vasoconstrictor effects [39,40]. Finally, astrocytes are important players in the formation, maintenance, and dynamics of the BBB. This last function will be extensively reviewed in section 1.3.1.

- **Astrocytes in stroke**

In addition to the important functions related to the healthy CNS depicted above, astrocytes play a crucial role in sensing and responding to CNS insults through a multistep, delicate, and complex process called astrogliosis [41,44]. Astrogliosis involves a combination of extracellular danger signals, including cytokines, chemokines, growth factors, and hormones, which induce transcriptional and morphological remodelling of astrocytes. As a result, astrocytes undergo cellular hypertrophy, swelling, proliferation, and there is an increase of associated proteins, such as glial fibrillary acidic protein (GFAP), S100β, and vimentin. Additionally, astrocytes secrete inflammatory mediators [39,41]. The severity and permanence of these changes depend on the type and intensity of the insult, ranging from reversible alterations to severe astrogliosis and the formation of thick glial scars [41]. Notably, under normal physiological conditions, astrocytes cover the entire CNS in a continuous and non-overlapping manner, and many astrocytes do not express detectable levels of GFAP. However, in response to damage, the expression of GFAP is upregulated and becomes detectable. In the initial stages, the astrocytic bodies and processes become slightly hypertrophic, but the boundaries of each astrocyte remain clearly non-overlapping, and minimal proliferation occurs [39]. The more severe the injury becomes the more upregulated GFAP expression, resulting in obvious hypertrophic astrocytes with numerous processes that extensively overlap and intertwine. This allows the formation of compact borders that surround and demarcate areas of severe tissue damage, necrosis, infection, or autoimmune-triggered inflammatory infiltration [39,45].

Similar to the repair process in skin injuries, the response of the CNS to acute damage can be time-coursed divided into three overlapping but different phases: (1) cell death and inflammation, (2) cell proliferation for tissue replacement, and (3) tissue remodelling [46,47].

In the first phase, within 24 h after ischemic damage, a rapid cascade of events occurs as extensively reviewed above. Astrocytes remain *in situ* and do not migrate to or away from the injured location, unlike other cells that promptly respond and migrate to the damaged tissue, such as OPCs and microglia. Depending on the severity of the injury,

astrocytes may either die in the centre of severe lesions, or undergo proliferation, activation, and hypertrophy in less severe lesions (Figure 9) [46,47].

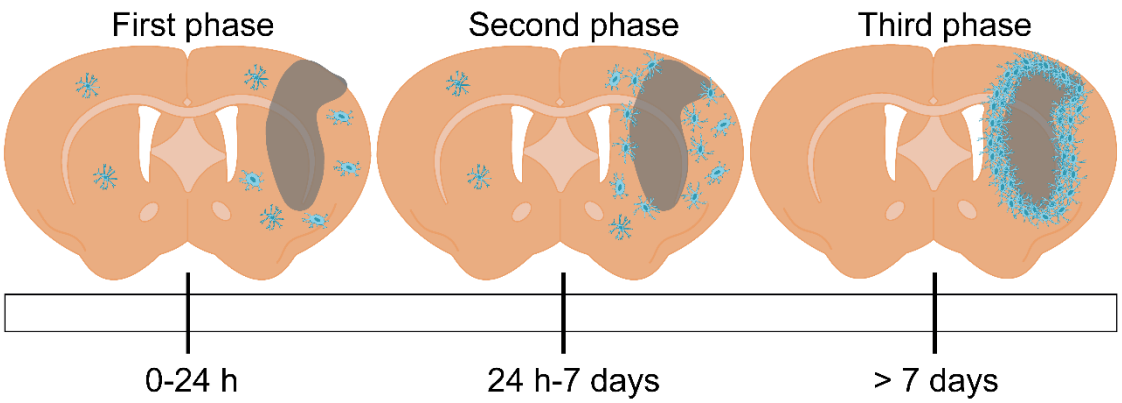

Figure 9. Spatio-temporal representation of astrocyte dynamics in stroke. In the initial stages (0-24 h) astrocytes undergo slight activation without migrating to the ischemic core. During the second stage (1-7 days after stroke), astrocytes proliferate and migrate to the damaged area. This leads to the formation of the glial scar, that separates the non-functional damaged tissue from the immediately adjacent healthy neural tissue. Finally, in the third stage (from 7 days onward), a remodelling process initiates within the damaged area.

The second phase of the response to tissue damage takes place approximately 2 to 10 days after the insult. During this phase, astrocytes proliferate and migrate (through FGF, EGF, or endothelin-1), leading to the formation of the glial scar [39]. The dense astrocytic scar is primarily shaped by newly proliferating elongated astrocytes derived from local astroglial progenitors. These new astrocytes gather around the edges of severely damaged tissue, creating a barrier that separates areas of non-functional damaged tissue (ischemic core) from the immediately adjacent and potentially functional neural tissue (Figure 9). This would prevent damage spread, while maintaining nutritional support and ion homeostasis within the non-lesioned area (*i.e.,* ischemic penumbra). The molecular and cellular mechanisms that underlie the formation of the glial scar are not completely understood. Nonetheless, they likely involve a complex and balanced interplay of molecular signals that can simultaneously boost phagocytosis and debris clearance, which would be essential for the protection and conservation of the still-healthy tissue [39,46,47].

The third phase is characterized by tissue remodelling. It typically starts towards the end of the first week but can comprise events that last within the following weeks. During this phase, a well-organized, interdigitated scar forms around the lesion core (Wanner et al., 2013). This compact scar acts as a protective barrier, preventing the migration of inflammatory cells from the lesion core into the surrounding viable neural tissue. The remodelling period lasts long, but as the tissue remodelling progresses, a

gradual reduction and contraction of lesion cores and astrocyte scars are typically observed (Figure 9). [46,47].

Despite being far less studied, it has been reported that when ischemia occurs, fibroblasts also become activated along with astrocytes. They migrate towards the site of injury, undergo proliferation, and contribute to the production of extracellular matrix (ECM) proteins. Importantly, during the later stages of ischemia, unlike astrocytes, fibroblasts and ECM do not experience replacement by regenerated tissues. Instead, they accumulate within the lesion area and can form fibrous scars that can persist for a long time. While such a response would be beneficial in other tissues, in the brain it can impair axon growth due to the inhibitory properties of collagens and proteoglycans [39,46].

Historically, astrogliosis and scar formation have been viewed as harmful responses that should be inhibited. However, recent research has firmly established the essential and beneficial functions of these processes in CNS repair and recovery. These roles include wound closure, BBB repair, neuronal protection, and restriction of CNS inflammation. Nevertheless, it is important to note that ultimately, uncontrolled astrogliosis and excessive scar formation over time may potentially be harmful (*e.g.,* exacerbating inflammation or interfering with synapse sprouting or axon growth during the recovery phase) [46–49].

1.3. Pathophysiology of ischemic stroke: blood-brain barrier breakdown

1.3.1. Components of the blood-brain barrier

The BBB is a highly dynamic interface between the CNS and the peripheral circulation [50], which harbours a unique microenvironment necessary for maintaining brain function and homeostasis [51,52]. BBB is comprised of brain endothelial cells (BECs) surrounded by the basement membrane (BM) and pericytes, all of them ensheathed by astrocyte endfeet [53] (Figure 10). Collectively, this structure, together with neurons, microglia, and smooth muscle cells (SMCs) in the surrounding microenvironment, is also known as the neurovascular unit (NVU) [54]. The BBB tightly regulates the transport of ions and nutrient influx, restricts the transport of harmful agents, and selectively limits the traffic of immune cells and inflammatory mediators, preserving neuronal homeostasis and shielding the CNS from injury and disease [55].

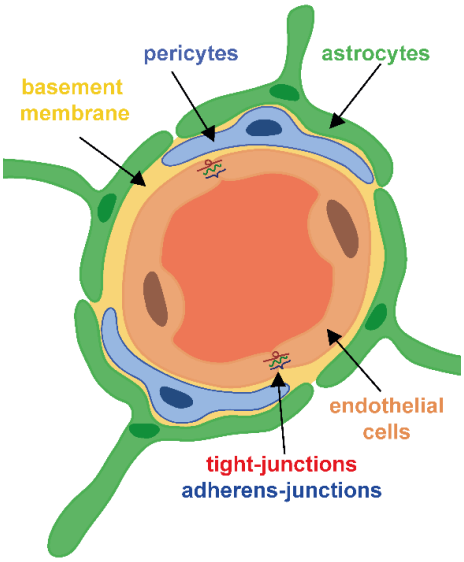

Figure 10. Schematic illustration of the blood-brain barrier. It comprises BECs forming brain vessels, surrounded by a basal lamina, wrapped by pericytes, pericytes-basal lamina and finally ensheathed by astrocytes endfeet.

The BBB was first identified at the beginning of the 20th century by the Nobel Prize-laureates Paul Ehrlich and his pupil Max Lewandowsky, when they discovered that an intravenous administration of bile acids and ferrocyanide had no pharmacological effects in the CNS (reviewed in [56,57]). The concept of the barrier between blood and brain was further supported by Edwin Goldmann when he demonstrated the penetration of dyes into the brain only from cerebrospinal fluid but not from blood (Figure 11) [56,57]. Finally, Lina Stern coined the term *barrière hémato-encéphalique* or *blood-brain barrier,* describing it as a "complex cerebral mechanism protecting cerebral function" [56,57]. However, our understanding has evolved since those seminal studies, as the BBB is no longer considered a physical barrier between blood and brain, but rather a lively boundary between the CNS and the rest of the body.

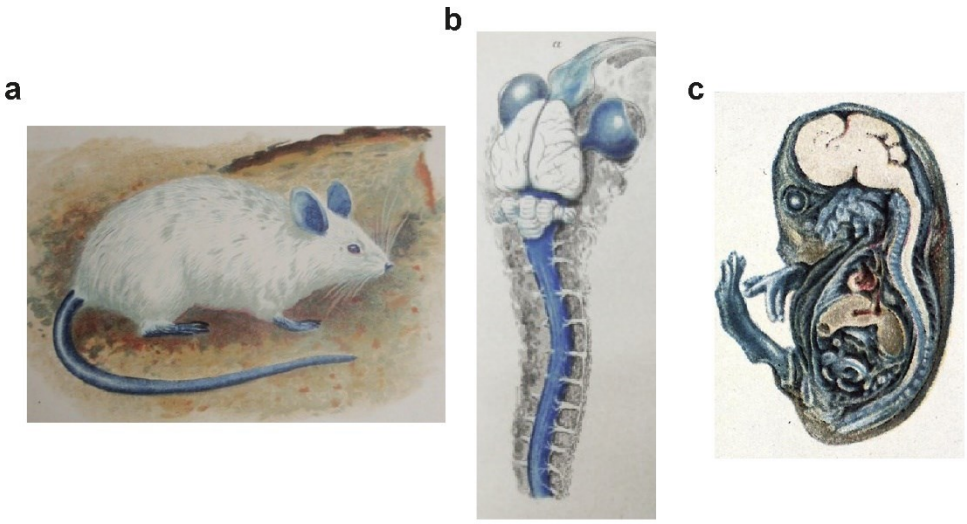

Figure 11. **First experimental demonstration of the blood-brain barrier. a.** Goldmann's "1st experiment": illustration of a rat that received a systemic injection of trypan blue. **b.** Goldmann's "2nd experiment": illustration from the rat brain and spinal cord after lumbar subarachnoid injection of trypan blue. **c.** Illustration demonstrating the presence of BBB in a mid-gestation guinea pig embryo injected with trypan blue. Note that only the brain and spinal cord remain unstained, while other organs are dyed. Adapted from Saunders et al. [57].

Next, we will thoroughly describe each one of the main components of the BBB listed from blood to brain (*i.e.,* BECs, BM, pericytes, and astrocytes) and their implication in the ischemia process.

- **Brain endothelial cells**

BECs have a mesodermal origin and develop from squamous epithelial cells that line the blood vessel walls. The diameter of large brain arteries and veins can consist of numerous endothelial cells (ECs), whereas the tiniest capillaries are formed by a single cell folding upon itself to create the vessel lumen [58]. In the human brain, the total length of cerebral blood vessels is approximately 650 km, with capillaries accounting for 85 % of this length [59]. Due to the extensive density of the capillary network, it has been estimated that every neuron is supplied by its own individual capillary, underscoring the essentiality of tightly controlled vascular support within the brain [58].

BECs are the central element of the microvasculature that forms the BBB (Figure 10) and have unique structural and biological properties compared to peripheral ECs. These allow them to precisely regulate the movement of ions, molecules, and cells between the blood and the brain, and to maintain CNS homeostasis [58,60]. This way, BECs exclusively have (1) tight-junctions (TJs) and adherens-junctions (AJs), (2) low rate of pinocytosis and transcytosis, (3) no fenestrations, (4) abundant transporters to facilitate nutrient uptake and waste elimination, (5) low levels of leukocyte adhesion molecules, (6)

high mitochondrial activity, and (7) a complex set of enzymes to degrade toxic compounds [58,61,62].

Thanks to these special properties of BECs, BBB plays a dual-balanced role, acting simultaneously as a “barrier” but also as a “carrier”, as well as a “fence” and also as a “gate” [62]. In more detail, the BBB can play a “barrier” role because (1) it efficiently separates the CNS from the peripheral circulation through a complex network of TJs and AJs, and (2) it strictly selects brain traffic with low levels of endocytosis and transcytosis. At the same time, BBB can function as a “carrier” (3), ensuring nutrient supply to the brain through specific influx transporters, while at the same time (4) guaranteeing waste elimination through efflux transporters and detoxification enzymes (*i.e.,* endopeptidases, aminopeptidases, cholinesterases, and monoamine oxidases) [28,62]. Beyond “barrier-carrier” characteristics, TJs and AJs not only separate CNS and blood compartments but also define the apical and basolateral membrane domains, contributing to the establishment of cell polarity and hence to the “fence” function. On the other hand, TJs and AJs modulate the paracellular transport, thereby contributing to the “gate” function [62].

- *Tight-junctions and adherens junctions*

TJs and AJs comprise essential junctional complexes between adjacent endothelial cells (Figure 12). They were first described in epithelial cells in the 1960s [63]. Using electron microscopy Farquhar and colleagues described some regions where the membrane appeared to fuse at several spots or “kisses” [64,65]. These so-called “kisses” are multiprotein complexes consisting of cytosolic and transmembrane proteins, which are responsible for the extremely low paracellular permeability and the high transendothelial electrical resistance (TEER) of the BBB [28]. The TEER in the BBB is normally above 1,000 ohm/cm^2, whereas it only reaches 2–20 ohm/cm^2 in peripheral capillaries [66].

Both of these types of junctions are associated with the actin cytoskeleton, being involved in the formation and maturation of cell-cell contacts, while also contributing to the rearrangement of the actin cytoskeleton. However, while AJs promote cell-cell contacts, and modulate their maturation and maintenance over time, TJs regulate the paracellular pathway through which solutes and ions can move between cells [67]. Unlike in epithelial cells, where they have well-defined locations, TJs and AJs are intermingled in endothelial cells, showing no distinctive spatial location [68].

TJ transmembrane proteins include a series of proteins embedded in the membrane, such as claudins, junctional adhesion molecules, occludin, and tricellulin

(Figure 12). The cytoplasmic terminals of the transmembrane TJ proteins bind to several cytoplasmic proteins including zonula occludens (ZO) ZO-1, ZO-2, ZO-3, and cingulin [69,70]. These proteins not only form a scaffold within the TJ but also regulate its function. Additionally, they link TJs to primary cytoskeleton proteins, such as actin, which is important for maintaining the structural and functional integrity of the endothelium [53].

Claudins (Cldns) were first purified and identified by Furuse and colleagues in 1998. The term "claudin" derives from the Latin word *claudere* which means "to close". The family of claudins comprises small proteins from 20–34 kDa, containing four transmembrane domains, N- and C-terminal cytoplasmic domains, and two extracellular loops. In particular, the C-terminal tail is essential for stability and intracellular transport. Phosphorylation of this domain can regulate barrier function, either enhancing or decreasing TJ assembly and function (reviewed in [64]).

To date, there are 27 claudin genes described in mammals, and 26 in humans. So far, Cldns are categorized based on their amino acid sequence similarity, namely "classic" (Cldn-1–10, -14, -15, -17, and -19) or "non-classic" (Cldn-11, -12, -13, -16, -18, and -20–27) (Cldn-13 is not present in humans) [61].

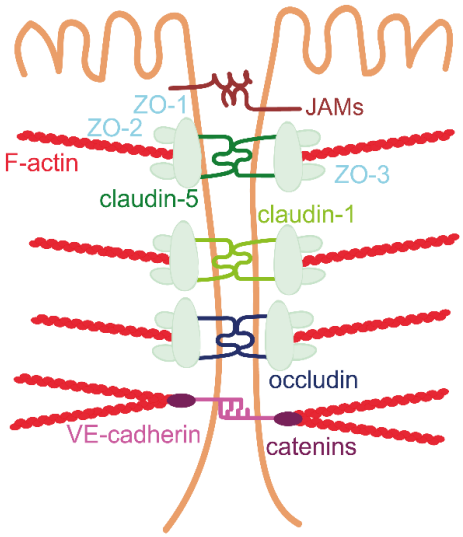

Figure 12. Schematic diagram illustrating JAMs, tight-junctions, and adherens-junction proteins. Tight-junctions include claudin-5, claudin-1, and occludin (transmembrane proteins) with their corresponding zonula-occlude proteins (intracellular proteins), ZO-1, ZO-2, ZO-3. The adherens junctions include the transmembrane protein VE-cadherin and the cytoplasmic catenins. Actin filaments anchor all the junctional proteins.

Cytoplasmic proteins are crucial for the formation of TJ. Examples include ZO proteins (*e.g.,* ZO-1, ZO-2, and ZO-3) (Figure 12), 7H6, and cingulin, among others. Zonula occludens proteins feature three PDZ domains (PDZ1, PDZ2, and PDZ3), an SH3

domain, and one guanyl kinase-like (GUK) domain. Together, they serve as binding-organizing proteins at the membrane. Specifically, the PDZ1 domain has been found to directly interact with the COOH-terminal of cldns. Notably, actin can also bind to the COOH-terminal of, ZO proteins, forming a complex that cross-links transmembrane components and providing structural stability [53]. The TJ module also comprises an array of additional adaptor proteins, that often interact with one another, forming a highly dimensional protein network. The multi-PDZ domain proteins MUPP1 or the membrane-associated guanylate kinase inverted (MAGI) proteins are examples [70].

Similar to TJs, AJs also involve transmembrane proteins, known as cadherins, and being the vascular endothelial (VE)-cadherin the most important in BECs. The cytoplasmic domain of cadherins binds to the submembrane proteins β-/γ-catenin and p120, which in turn connects the actin cytoskeleton via α-catenin [53]. Notably, TJ and AJ components, particularly ZO-1 and catenins, exhibit interactions that influence the assembly of TJs [28,53,71].

Furthermore, there are other families of transmembrane proteins, such as the junctional adhesion molecules (JAMs) that belong to the immunoglobulin superfamily and have a single transmembrane domain. Despite being less studied than TJs and AJs, they are known to participate in cell-cell adhesion and leukocyte transmigration processes [28].

Apart from TJs, AJs, and JAMs, BECs also present gap junctions (GJs), formed by proteins of the connexin (Cx) family. In particular, BECs express Cx37, Cx40 and Cx43. GJs are known to play a crucial role in the transduction of signals between neighbouring cells, promoting cell proliferation and migration. Moreover, they facilitate the transport of small molecules and ions through GJ plaques [69]. Importantly, some connexins can also modulate the expression of other junctional molecules, such as N-cadherin through Cx43 interaction [72,73] .

Interestingly, apart from the well-known roles of TJs and AJs in organizing cell architecture, polarity, and cell-cell contacts, other non-canonical functions have recently been described. These include cell differentiation, proliferation, regulation of gene expression, and involvement in processes such as angiogenesis and inflammation [59,70,74].

Regarding their role in barrier integrity, numerous studies have demonstrated that disturbances in the cellular distribution, content, and/or post-translational modifications of TJs and AJs enhance BBB dysfunction, playing a role in the onset of neurodegenerative diseases [55,75].

- *Transporters*

Another unique feature of BECs is the abundance of transporters to facilitate nutrient uptake and waste elimination. Except for water, small water-soluble agents (*i.e.,* O_2 and CO_2), or small lipophilic molecules (< 400 Da / or < 8 hydrogen bonds), which can freely diffuse across the endothelium, TJs and AJs network strictly restrict the transport of small and large molecules between the cells (paracellular transport). Hence, except for the above-mentioned, the molecular exchanges between the blood and the brain and *vice versa* (*i.e.,* transcellular transport), are regulated by brain endothelial transport systems [59,76]. These transporters play a pivotal role in efficiently delivering essential nutrients, such as glucose, amino acids (AA), vitamins, and ions from the blood into the brain, thereby supporting its metabolic functions. Moreover, they facilitate the removal of metabolic waste products and toxins from the brain, allowing their elimination through the bloodstream.

These transport systems can be categorized as follows (Figure 13) [59]:

1) Carrier-mediated transport (CMT): This mechanism enables the crossing of the BBB for specific solutes, such as AA, carbohydrates, monocarboxylic acids, fatty acids, hormones, nucleotides, vitamins, inorganic ions, amines, and choline.
2) Endothelial receptor-mediated transport (RMT): While most circulating large proteins and macromolecules are generally unable to cross the BBB (*e.g.,* growth factors, immunoglobulins, albumin, fibrinogen, thrombin, or plasminogen), some proteins and peptides can access the brain via RMT. To note, this transport rate of circulating proteins is slower compared to nutrient transport across the BBB. These receptors normally follow transcytosis-mediated pathways.
3) Endothelial ion transport (IT): Given the critical need to regulate ion concentration in the CNS, endothelial cells are equipped with essential ion transporters.
4) Endothelial active efflux (AE): To prevent the accumulation of drugs, toxic substances, and xenobiotics within the brain, the luminal side of endothelial cells presents active efflux transporters known as ATP-binding cassette (ABC) transporters. These transporters use ATP as a source of energy and eliminate such substances through the bloodstream.

Examples of each category are summarized in Table 1 [59].

Alterations in the expression and activity of BBB transporters contribute to the permeability changes and pathophysiological processes (*i.e.,* edema) underlying ischemia

[77]. Hypoxia has been shown to alter ion transporters, disrupting ion homeostasis. For example, hypoxia increases the activity of Na^+-K^+-Cl^- cotransporter, leading to the formation of ischemia-induced brain edema [77,78]. Likewise, it has been reported that reduced ATP availability results in the failure of ATPases (*e.g.,* Na^+/K^+-ATPase), triggering the massive entry of extracellular Na^+ that causes endothelial swelling and cytotoxic edema in stroke patients [28,77]. However, hypoxia also enhances GLUT-1 and SGLT transporters, aiding in the maintenance of glucose levels during both short and long-term ischemia conditions [77,79].

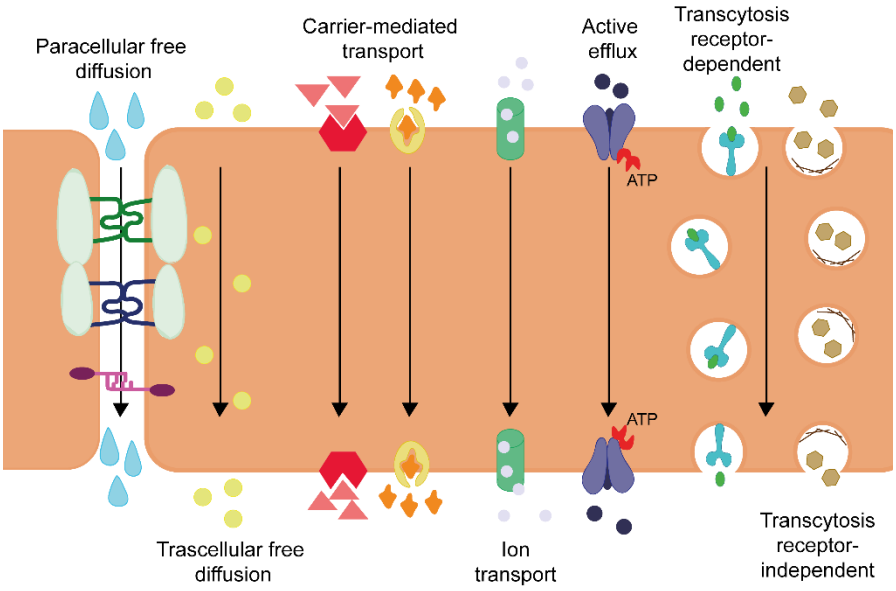

Figure 13. Schematic drawing of BECs transport. This includes paracellular and transcellular free diffusion, carrier-mediated transport, ion transport, active efflux (ATP-dependent), and transcytosis receptor-dependent/independent.

Finally, it is important to note that the selective permeability of the BBB also restricts the transport of drugs and neurotherapeutics. It is estimated that 100 % of large and 98 % of small drug molecules cannot cross the BBB. Several attempts have been made to deliver drugs across the BBB, including (1) opening of the BBB with ultrasounds or other techniques, (2) use of molecular Trojan horses, such as TfR or IR, (3) biosynthesis of molecules that can target specific receptors, or (4) encapsulation of therapeutics in nanoparticle biocompatible carriers that can cross the BBB [59,62]. Finally, the paracellular pathway seems a promising alternative for rapid and reversible opening of the BBB [62].

Type of transport	Solute	Transporter	Description
Carrier-mediated transport	Carbohydrates	Glucose transporter 1 (GLUT-1/SLC2A1)	Only located in endothelial cells (not in neurons), transport glucose, providing the key energy metabolite for the CNS
	Amino acids	Large neutral endothelial AA transporter 1 and 2 (LAT1/2)	Bidirectionally transport of large neutral AA, such as tyrosine and tryptophan
		Cationic AA transporter 1 and 3 (CAT1/3)	Transport cationic AA, such as arginine or lysine
	Monocarboxylate	Monocarboxylate transporter 1 (MCT1/SLC16A1)	Transport lactate or ketone bodies from muscles and liver respectively as an alternative energy metabolite for the brain.
	Hormones	Monocarboxylate transporter 8 (MCT8)	Triiodothyronine T_3 hormone transporter
		Organic anion transporting polypeptide 1C1 (OATP1C1)	Thyroxine T_4 hormone transporter
	Nucleotides	Sodium-independent concentrative nucleoside transporter-2 (CNT2/SLC28A2)	Suppliers of nucleotides and nucleobases for DNA and RNA synthesis
		Sodium-independent equilibrate nucleoside transporter-1 and 2 (ENT1/2/ SLC29A1/2)	
	Vitamins	Sodium-dependent multivitamin transporter (SMVT)	Translocate vitamins and cofactors, such as biotin, pantothenic acid and lipoic acid [80]
	Amines	Plasma membrane monoamine transporter (PMAT/ SLC29A4)	Transport of amines and xenobiotics. It represents the major uptake transporter of monoamine neurotransmitters. Also responsible for the removal of neurotoxins and drugs [81].

	Choline	Transporter like protein type 1 (CTL1/SLC44A1)	Transporter of choline, basic in the synthesis of membrane phospholipids and the neurotransmitter ACh [82]
Receptor-mediated transport	Iron	Transferrin receptor (TfR)	Mediates the uptake of iron from the plasma glycoprotein transferrin [83]
	Insulin	Insulin receptor (IR)	Mediates the transport of insulin to the brain and mediates IGF-1 signalling
	Amyloid-β (Aβ) deposits	Lipoprotein receptor 1 (LRP1)	Mainly located in the abluminal side binds Aβ deposits aiding its clearance. Also mediates APOE2 and APOE3 efflux
		Receptor for advanced glycation end products (RAGE)	RAGE facilitates the transport of circulating Aβ deposits into the brain, which is related to neuroinflammatory damage, and BBB breakdown
Ion transport	Sodium	Abluminal sodium pump (Na^+-K^+-ATPase)	Regulates Na^+ influx into the brain and K^+ efflux from the brain, essential for the electrical activity of neurons and ensuring the Na^+ gradient at the BBB, which drives sodium-dependent transport processes
	Calcium	Na^+-Ca^{2+} exchanger cotransporter	Mediates Ca^{2+} efflux which maintains low intracellular concentration of Ca^{2+}
		Abluminal transient receptor potential (TRP)	Modulates Ca^{2+} influx into brain endothelium which in turn releases vasodilating soluble factors, such as NO, prostaglandins, and endothelial-derived hyperpolarizing factor

	Potassium	Voltage-gated K^+ channel (K_V1)	Responsible for blood flow regulation by generating outward K^+ currents, which in turn provoke endothelial cell hyperpolarization and the propagation of vasodilatory signals upstream to arterioles
Active efflux (ATP-binding Cassette transporters)	Aβ deposits	ABCB1/P-gp	Alzheimer's Aβ toxin clearance from brain-to-blood
	Xenobiotics and drugs	Breast cancer resistance protein (BCRP/ABCG2)	Efflux of xenobiotic and drugs
		Multidrug resistance-associated proteins 1–5 (MRP1-5/ABCC1-5)	Transport out a wide range of substrates to the blood, especially lipid xenobiotic compounds [28]

Table 1. Transport systems in BECs. Examples of transporters that can be found in BECs, classified by the type of transport and the cargo. Extracted from Sweeney et al. [59]

- *Low transcytosis rate*

Another distinctive feature of BECs is the presence of a small number of caveolae and an inherently low rate of transcytosis compared to other ECs in peripherical tissues. Notably, ECs present 80–84 % fewer endocytic vesicles than their counterparts in peripheral endothelial cells (< 100 / μm^3) [28,84]. Interestingly, this feature becomes upregulated in response to injury and brain damage [28,58]. Specifically, it has been reported an increased transcytosis during the early stages of ischemia (3-6 h), despite TJs and ECM still remaining intact [28].

The transcytosis process can be receptor-dependent or receptor-independent (adsorptive transcytosis). In receptor-dependent transcytosis, a ligand binds to its receptor (*e.g.*, insulin, transferrin, or leptin receptors), whereas in adsorptive transcytosis, a charge interaction between a molecule and the luminal membrane triggers endocytosis [28]. Adsorptive transcytosis is primarily mediated via caveolin-1-coated vesicles, being responsible for the uptake of several macromolecules into the brain. Specifically, caveolin-1 is crucial in the invagination of the membrane to create caveolae. However, the role of caveolin-1-mediated transcytosis in BBB dysfunction after ischemic stroke remains largely elusive, since depletion of caveolin-1 decreases endothelial transcytosis, but does not

appear to modulate BBB-enhanced permeability [85,86]. In fact, caveolin-1 KO mice present larger infarct volumes and BBB disruption compared to wild-type mice [28,87]. These results suggest that caveolin-1 in stroke may not only play a role in caveolae formation but also modulate other mechanisms underlying BBB integrity, such as differentiation, cell growth, endocytosis, cellular senescence, and cholesterol trafficking [88]. One of the most important proteins transported via caveolae is albumin, as well as other plasma proteins, that can be carried by receptor-dependent or receptor-independent pathways.

- *Leukocyte adhesion molecules*

In the healthy brain, the presence of neutrophils and lymphocytes within the brain parenchyma is extremely low. Compared to ECs found in peripheral tissues, BECs possess low levels of leukocyte adhesion molecules (*i.e.,* E-selectin or P-selectin) and a reduced number of proteins from the immunoglobin family. These molecules are responsible for rolling and firm adhesion, respectively. The expression of these proteins is upregulated during neuroinflammatory disorders, such as multiple sclerosis (MS) or stroke [58]. Consequently, the brain parenchyma remains relatively isolated from circulating peripheral immune cells under healthy conditions. Instead, brain immune surveillance by lymphocytes is developed at the blood-cerebrospinal fluid (CSF) interfaces of the meninges and choroid plexus in healthy conditions [89,90].

- **Basement membrane**

The basement membrane (BM) is a special configuration of ECM found underneath endothelial and epithelial cells. In the brain, there are two types of BM, 1) the one surrounding endothelial cells (endothelial BM), and 2) the one surrounding pericytes (parenchymal BM) [91] (Figure 10). Apart from structural support, the BM modulates signalling transduction and participates in cell anchoring. From a structural point of view, BM is formed by different ECM proteins, mainly laminin, fibronectin, collagen IV, agrin, perlecan, and nidogen, which are secreted by BECs, astrocytes and pericytes [91,92].

Laminins are glycoproteins, that include a combination of α, β, and γ chains, displaying several isoforms. At the BBB, the four main laminin isoforms are laminin 8 / α4β1γ1, laminin 10 / α5β1γ1 (mainly in the endothelial BM), laminin 1 / α1β1γ1 and laminin 2 / α2β1γ1 (mainly in the parenchymal BM), which is specific of the brain microvasculature [92]. The majority of knock-out (KO) mice of these proteins are inviable, and even conditional KOs suffer severe BBB breakdown and haemorrhages. Collagen IV and fibronectin are also crucial for BM assembly as they uphold laminin, perlecan, and nidogen.

Notably, mutations in the *Col4a1* gene are associated with fragile vessels and an increased predisposition to stroke [92]. Alternatively, nidogen is responsible for the stabilisation of collagen IV and laminin networks. KO mice for nidogen suffer BM alterations in brain capillaries. Lastly, agrin and perlecan (also known as HSPG2) are heparan sulphate proteoglycans. Interestingly, agrin is only present in barrier endothelium and is also linked to BBB formation. On its side, mice lacking perlecan in ECs BM present gaps in its membrane and microvessels bleeds [91,92].

Regarding cell–cell and cell–matrix interactions, there are two main types of receptor proteins involved: dystroglycan and integrins. Structurally, dystroglycan is composed of a highly glycosylated extracellular α subunit and a transmembrane β subunit (Moore and Winder, 2010). In turn, integrins are transmembrane glycoproteins formed by heterodimers of α and β chains. While integrins are expressed in all cells forming the NVU, dystroglycan is only expressed in BECs, astrocytes, and neurons [92]. These receptors are involved in regulating signalling pathways, which sense microenvironment changes, and in cell anchoring since they are the physical link between the cytoskeleton and the ECM. Specifically, collagen IV, fibronectin, and nidogen normally bind to different types of integrins while agrin and perlecan binds to dystroglycan. Laminins could bind both receptors.

BM proteins are degraded and remodelled by proteolysis, mainly by metalloproteases encompassing three enzymatic families: matrix metalloproteinases (MMPs), A disintegrin and metalloproteinases (ADAMs), and A disintegrin and metalloproteinase with thrombospondin motifs (ADAMTSs). MMPs are the most common in ischemic stroke [93] and their expression and activation are tightly controlled and complex processes. MMPs are secreted as inactive zymogen forms, and their activation is controlled by transcriptional regulation and several tissue MMP inhibitors (TIMPs). Remarkably, ECM dynamics not only involve ECM protein expression or degradation but also post-translational and localization modifications [51,93].

The degradation of the BMs after stroke occurs within 12–48 h after MCAO, in parallel with the disintegration of the ECM components [92]. Specifically, the reduction of collagen IV becomes evident between 24 to 72 h after the injury [94]. Similarly, other key BM proteins like laminin, fibronectin, agrin, and perlecan also undergo a decline in their levels. Notably, perlecan, in particular, exhibits a significant 50 % reduction as early as 2 h following ischemic stroke [95,96].

- **Pericytes**

- *Biology, ontology, and functions*

Pericytes are perivascular multipotent cells found in almost all tissues [97,98]. These cells were first described and named “Rouget’s cell” by Rouget in 1873. In 1923, Zimmermann renamed them as “pericytes” (reviewed in [97–99]). Pericyte biology and origin are far from completely understood, but a series of seminal bird chimerism studies reported that pericytes in the forebrain might derive from the neural crests, whereas those in the brainstem, midbrain, and spinal cord would derive from mesenchymal stem cells (MSCs) [100].

Pericytes typically display an elongated, stellate morphology with numerous branches wrapping the endothelium [99]. As previously mentioned, pericytes within the BBB share the endothelial BM with BECs, being simultaneously enveloped by the parenchymal BM (Figure 10). In regions where a direct connection is not present, pericytes and endothelial cell membranes form invagination areas called peg-and-socket contacts, which house TJs, AJs, and GJs [101]. This complex arrangement enables sophisticated interactions between these two cell types.

The classification and precise function of pericytes are currently subjects of intense debate in the field. The similarities shared by precapillary SMCs and pericytes in terms of morphology, location, and molecular markers, make this a challenging issue. Indeed, it is not fully understood whether they represent two distinct cell types or a single cell type with different phenotypes [100]. Both cells express several contractile and cytoskeletal proteins including, α-smooth muscle actin (α-SMA), vimentin, and desmin, as well as cell surface antigens, including, platelet-derived growth factor receptor beta (PDGFR-β), neuron-glial antigen 2 (NG2), or regulator of G-protein signaling-5 (RGS5), among others. However,3 this repertoire of proteins ultimately depends on their location and phenotype [102]. Furthermore, while there is a sort of general consensus regarding the location of SMCs in large arteries, veins, smaller arterioles, and venules, the classification and nomenclature of pericytes have been heavily contested, largely due to the inherent heterogeneity of pericytes [102]. Therefore, identifying novel markers to differentiate SMCs from pericytes in the cerebral vascular tree seems to be essential to elucidate the exact roles of these two cell populations in the healthy brain and under pathological conditions [11]. Despite this enormous complexity, the following up-to-date classification is generally accepted.

When considering the vascular brain tree, arterioles branch from larger arterioles and penetrate the brain parenchyma (Figure 14). As they traverse the brain parenchyma,

arterioles further divide into smaller arterioles known as precapillary arterioles, which eventually lead to capillaries. Capillaries then increase in diameter as they transition into post-capillary venules, which subsequently join to form collecting venules that converge into larger veins [98,102]. Arterioles are surrounded by arterial SMCs that form concentric rings around them. However, as we move towards smaller diameters, precapillary arterioles are enveloped by a unique cell type known as a smooth muscle-pericyte hybrid cell (also known as transitional pericyte or pre-capillary pericyte). These cells interlock with mesh pericytes at the arteriole-capillary interface, particularly where arterioles branch into the capillary network. These pericytes are involved in cerebral blood flow (CBF) regulation through the contraction or relaxation of their longitudinal processes. They express high levels of α-SMA. On the contrary, pericytes in the capillary bed express less α-SMA and present long, thin, meandering processes that transverse the microvasculature. These capillaries pericytes are also called thin-strand pericytes or helical pericytes referring to the complex morphology of their processes. They are likely involved in maintaining the integrity of the BBB. Interestingly, brain capillaries exhibit increased pericyte number compared to peripheral capillaries, having pericyte-to-endothelial cell ratios ranging from 1:1 to 1:3. In fact, approximately 70-80 % of the brain capillary surface area is covered by the processes of pericytes. Next, mesh pericytes become more prevalent as capillaries transition into postcapillary venules. While their precise role is not yet fully understood, they are thought to be involved in regulating immune cell infiltration. Finally, stellate-shaped SMCs are found within the walls of parenchymal venules (Attwell et al., 2016; Hartmann et al., 2015; Uemura et al.,2020).

Pericytes perform multiple and varied functions in the CNS. One of their essential roles is regulating the maintenance of the BBB. Specifically, they modulate BBB permeability by regulating transcytosis and inducing the expression and arrangement of endothelial TJs and AJs. Additionally, during CNS development and vascular remodelling, pericytes play a crucial function in regulating angiogenesis, microvascular stability, and angioarchitecture (see section 1.3.3). As mentioned above, pericytes also interact with BM, where they regulate the secretion and remodelling of the extracellular matrix through MMPs and TIMP-3 secretion. They also interact with astrocytes, mediating AQP4 anchoring and polarization [11].

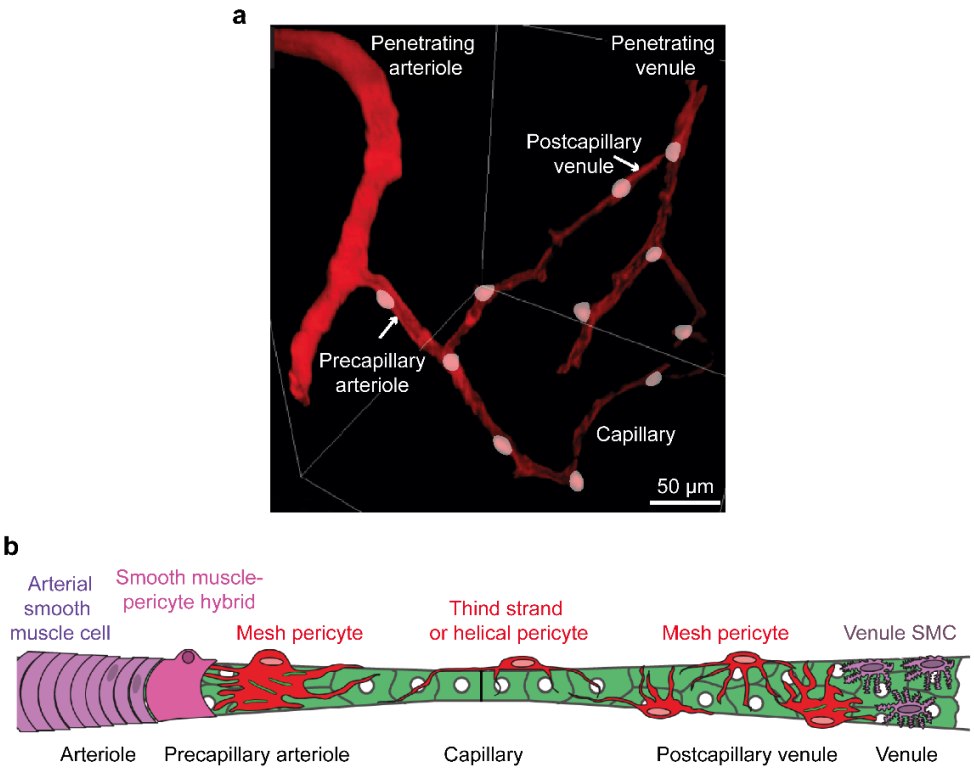

Figure 14. **Pericytes localization in the brain a.** Brain tree vasculature distribution. **b.** Graphic drawing showing the distribution of SMCs/pericytes along the cerebral vasculature. First, SMCs form concentric rings on arterioles. Next, hybrid smooth muscle-pericyte cells surround precapillary arterioles and interlock with mesh pericytes at the arteriole–capillary interface. Within the capillary bed pericytes exhibit long processes that traverse the microvasculature in single strands or pairs that twist in a helical manner. Next, as capillaries turn into postcapillary venules mesh pericytes become prevalent again. Finally, stellate-shaped SMCs cover the walls of parenchymal venules. Extracted from Hartmann et al. [104].

Moreover, pericytes can control blood flow, by controlling dilation and constriction in terminal vessels where SMCs are no longer present. Their contractile properties are attributed to contraction-related proteins (*i.e.,* α-SMA, tropomyosin, or desmin, among others). In physiological conditions, pericytes dilate or contract vessels in response to the energy demand of the tissue. While there is increasing evidence supporting this role, their exact function in regulating CBF and whether SMCs can also perform this function, are still under debate [11].

Pericytes also exhibit active immune properties, playing both pro-inflammatory and anti-inflammatory functions. They continuously express low levels of adhesion molecules, such as the intercellular adhesion molecule 1 (ICAM-1) or the vascular cell adhesion protein 1 (VCAM-1), which enable them to sense danger and modulate leukocyte adhesion and transmigration into the CNS. Furthermore, some studies have reported that retinal

pericytes can inhibit cytokine production of activated T cells during inflammation, protecting ECs from inflammation-mediated apoptosis [11,105]. Additionally, pericytes can also act as perivascular macrophages, clearing cell debris, toxins, and Aβ deposits in models of Alzheimer's disease (AD). Pericytes also express various pattern recognition receptors (PRRs) including toll-like receptor 4 (TLR4), scavenger receptor (SR), and Fc receptors, enabling them to recognize invading or abnormal antigens. Moreover, they can function as antigen-presenting cells (APCs), contributing to immune-promoting activities [11,99]. Conversely, under physiological conditions, pericytes secrete immunoactive molecules, including IL-9, IL-12, IL-13, IL-17, TNF-α, and interferon-gamma (IFN-γ). In response to immune challenges, pericytes can produce large amounts of ROS, NO, and other inflammatory cytokines. The bidirectional anti-inflammatory and pro-inflammatory effects of pericytes suggest that this dual role could help prevent unnecessary immune reactions in physiological conditions while being prepared to react to any damage [11,99].

Finally, pericytes have been shown to present stem cell properties. Under physiological conditions, they present a minimal rate of turnover, which significantly increases in response to tissue damage. Importantly, they are not only capable of self-renewal but also can differentiate into other types of CNS cells (*i.e.,* BECs, astrocytes, microglia, oligodendrocytes, SMCs, fibroblasts, and even neurons)**.** This remarkable versatility in differentiation potential highlights the similarities between pericytes and MSCs and further opens new therapeutic opportunities in the management of neurodegenerative and neuroinflammatory disorders [11,98]**.**

- *Pathological alterations under stroke*

After an ischemic event, pericytes are among the first cell types to react to brain hypoxia, as they are even more sensitive to it than BECs. In response, they undergo a transformation from a quiescent flat form into an ameboid morphology, expressing RGS-5, an activation marker of these cells [11]. In the acute phase of ischemic stroke, pericytes primarily exhibit a constricting function on blood vessels. Oxygen, calcium, and pH changes in the ischemia-reperfusion process contribute to the production of free radicals and the development of oxidative stress, which act as potent constriction inducers of pericytes. Importantly, pericytes may remain in a contracted state even after reperfusion. As a result, despite the occlusion disappearing, the microcirculatory is not fully restored. This impaired reperfusion is known as the "no-reflow" phenomenon and severely impacts the survival of tissues post-stroke [106].

Shortly after performing the vasoconstrictive function, pericytes are observed to die or undergo detachment from the blood vessel basal lamina as early as 1 h after stroke in a permanent MCAO model in rats [11,99,107]. This event result in reduced pericyte coverage and increased BBB permeability during the acute phase. Following detachment, some pericytes migrate towards the lesion, starting as early as 2 h and peaking at 7 days after ischemic damage. Detachment and migration of pericytes are associated with the secretion of MMPs, particularly MMP-9, stimulated by TNF-α, a crucial mediator of stroke. The migration of pericytes serves a double-edged function. By migrating, pericytes destabilize BBB while at the same time escaping from injury and initiating neuroprotective and angiogenic functions in the ischemic lesion [11]. In the long run, these play an important role in stroke outcome [106].

The regenerative functions of pericytes are indeed progressively enhanced in the late recovery phase, from 1 week after the onset of the ischemia [99]. Specifically, migrated pericytes play a role in clearing up neural debris in the lesion area. Moreover, they can differentiate to microglia. Both phagocytic microglia and microglia derived from pericytes can eliminate dead cells in ischemic areas, which helps alleviate local inflammation and reduces secondary tissue damage. This regenerative capacity is enhanced under conditions of oxygen-glucose deprivation (OGD), which makes pericytes a crucial mechanism of neuroprotection after ischemic stroke [106].

Beyond regeneration, pericytes exert protective effects providing neurotrophic factors to the surviving neurons, as well as other types of cells of the NVU. Specifically, pericytes secrete GDNF, BDNF, and NGF, which are neuroprotective and facilitate axonal regeneration. Moreover, pericytes express neurotrophin-3 (NT-3), which activates astrocytes, and increases astrocytic secretion of NGF. This indirectly contributes to enhancing neuroprotection in the peri-ischemic area [11]. As mentioned before, pericytes also enhance and protect TJ proteins, indispensable for maintaining BBB integrity. In particular, after ischemic damage, angiopoietin-1 (Ang-1) and GDNF secreted by pericytes are found to be responsible for TJ protection. Additionally, VEGF is another pericyte-derived factor that helps to preserve endothelial function in the brain [11].

Finally, a crucial process to compensate for vascular occlusion and return blood flow to the ischemic core is the formation of new vessels, named angiogenesis (see section 1.3.3). The angiogenic process includes the proliferation of ECs, recruitment and coverage of pericytes to the new endothelial tube, and the final maturation of neovessels thanks to

pericyte guidance. VEGF signalling, Ang/Tie system, PDGF-β/PDGFR-β system, and RGS-5 signalling in pericytes seems essential for this process [11].

- **Astrocytes in the BBB**

The functions and biology of astrocytes, as well as the processes of glial scar formation and astrogliosis during brain injury, have been extensively described in point 1.2.4. Hence, in this section, we will focus solely on their role in the formation and regulation of BBB homeostasis. As mentioned above, astrocytes extend their large processes to ensheath neurons and blood vessels [58]. This close association was first observed by Virchow (1858), Golgi (1894), and Ramón y Cajal (1895) in the 19th century, with the latter being the first to propose that astrocytes might play a role in regulating CBF (Figure 15) (reviewed in [108]). Interestingly, astrocytes provide almost complete coverage of the vessel (including BECs and pericytes). In the rare instance of a gap between the endfeet, microglial or neuropil processes can be observed in contact with the BM [92]. Thus, astrocytes serve as a critical cellular link between the neuronal circuitry and blood vessels, enabling them to regulate CBF in response to neuronal activity signalling. This regulatory role encompasses the control of contraction/dilation of vascular SMCs/pericytes surrounding vessels [58].

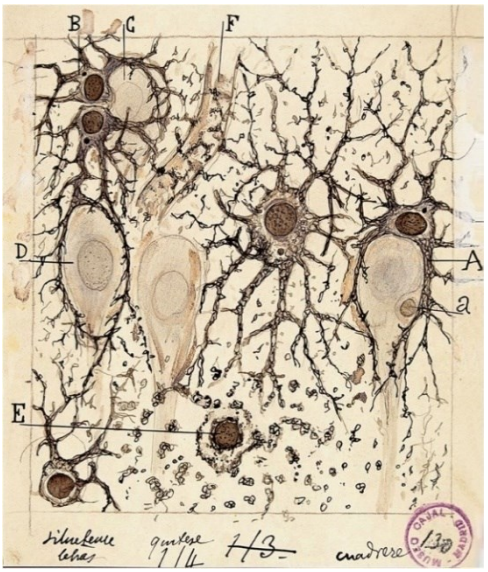

Figure 15. Original drawing of brain astrocytes, neurons, and ECs by Santiago Ramón y Cajal. Astrocytes (depicted with A and B) contact with neurons (depicted with C and D) and blood vessels (depicted with F). According to Ramón y Cajal insights, astrocytes are strategically positioned to mediate the connection from neurons to blood vessels, potentially influencing blood flow in response to neuronal activity. Adapted from MacVicar & Newman [108]**.**

The physical proximity of astrocytes and brain microvessels is so that several proteins essential for BBB water homeostasis, including AQP4 and the potassium channel Kir4.1, are localized in astrocytes endfeet [109]. Furthermore, astrocytes are the major source of Wnts and Norrin, crucial factors in maintaining BBB homeostasis. Examples of these factors are sonic hedgehog (Shh), angiotensin-converting enzyme-1 (ACE-1), retinoic acid (RA), TGF-β, and Ang-1 [58,109]. For instance, ACE-1 converts angiotensin I into angiotensin II, a molecule that induces the formation of TJs by its recruitment into lipid rafts. Conversely, the binding of RA to its receptor RAR-β, enhances TEER and increases ZO-1, VE-cadherin, and P-gp expression. Interestingly, RA participates in the modulation of Shh, TGF-β, and Wnt, suggesting its potential as a master regulator of BBB homeostasis.

Interestingly, despite some *in vitro* studies indicating the ability of astrocytes to induce BBB properties in non-BECs [58], recent studies in rodent embryos have demonstrated that BBB is established before astrocytes formation and their ensheathment of the vasculature [110]. Therefore, the factors secreted by astrocytes mentioned above may primarily regulate BBB function once it is already well-established in adulthood [58]. Accordingly, astrocytes cannot be the unique regulator of BBB formation during embryogenesis [92]. Finally, it is important to highlight that BECs-astrocytes interactions are not only crucial for BBB maintenance but also for astrocyte differentiation.

1.3.2. BBB formation and regulation

The development of the BBB is a multistep process that starts when endothelial progenitor cells invade the embryonic neuroectoderm and give rise to new vessels. First, VEGF and Wnt gradients released by neural progenitors guide the migration of ECs into the embryonic neural tissue. Interestingly, these early vascular sprouts already exhibit some BBB properties, including the expression of TJs and nutrient transporters, though they still retain a high number of leukocyte adhesion molecules, and there is a significant presence of transcytotic vesicles.

In a second step, pericytes and astrocytes are recruited to ensheath the developing vessels and promote barrier properties (*i.e.,* TJs formation, downregulation of leukocyte adhesion molecules, or decreased transcytosis, among others). Notably, ECs release PDGF-β, which acts as a chemoattractant for pericytes expressing the PDGFR-β receptor. Once pericytes and astrocytes are positioned, they secrete a wide range of compounds including Ang-1, which through endothelial Tie-2 receptors binding, limit BBB permeability by promoting the development of advanced TJs. The final sealing of TJs

occurs during maturation through the upregulation and redistribution of TJ proteins, a process that must be maintained throughout adulthood. Astrocytes play a role in this process by releasing Wnt ligands, which interact with Fzd receptors expressed by BECs and modulate TJ formation. Moreover, continuous crosstalk between BECs and pericytes, mediated by TGF-β–TGF-βR and Ang-1–Tie-2 signalling pathways, contributes to the ongoing formation and maintenance of the BBB. While the exact roles of pericytes and astrocytes in BBB development and maintenance are still debated, recent research suggests that pericytes are more heavily involved in the embryonic development of the barrier, whereas astrocytes are likely to play a greater role in its maintenance throughout adulthood [111].

1.3.3. BBB dysfunction in ischemic stroke

After thoroughly exploring the functionality of the components and dynamics of the BBB, as well as its contribution in the context of stroke, in this section we will address the chronological sequence of events occurring during BBB dysfunction after the ischemic-reperfusion process. As mentioned before, one of the prominent events that takes place during a stroke is the breakdown of the BBB. It occurs shortly after the artery occlusion and can persist for several weeks after the onset of the stroke [112]. The term “BBB breakdown” may evoke the wrecking of a physical wall, enabling the unconstrained entry of all types of molecules, cells, or harmful agents from the bloodstream into the brain. However, it is important to note that BBB disruption may solely refer to a change in one of its physiological important properties (*e.g.,* transport, polarity, transcytosis) that significantly alters the neural environment [89].

The disruption of the BBB is generally linked to endothelial damage and disrupted TJs and AJs, often triggered by reperfusion, leading to increased permeability of the affected vessels. However, BBB breakdown is not only a consequence of the damage, as it also plays a role in the injury process itself, being often correlated with poor clinical prognosis [112]. The increased permeability of the barrier sets off a complex pathophysiological cascade that is not yet fully comprehended, but it is known to include the initial injury, secondary injury, tissue repair, and subsequent regenerative processes. Traditionally, the behaviour of the BBB was thought to follow a biphasic “open–close–open” pattern, but recent studies have revealed that the process is considerably more complex than initially believed. In particular, several biphasic peaks would occur along four different stages without a complete BBB closing between them (Figure 16).

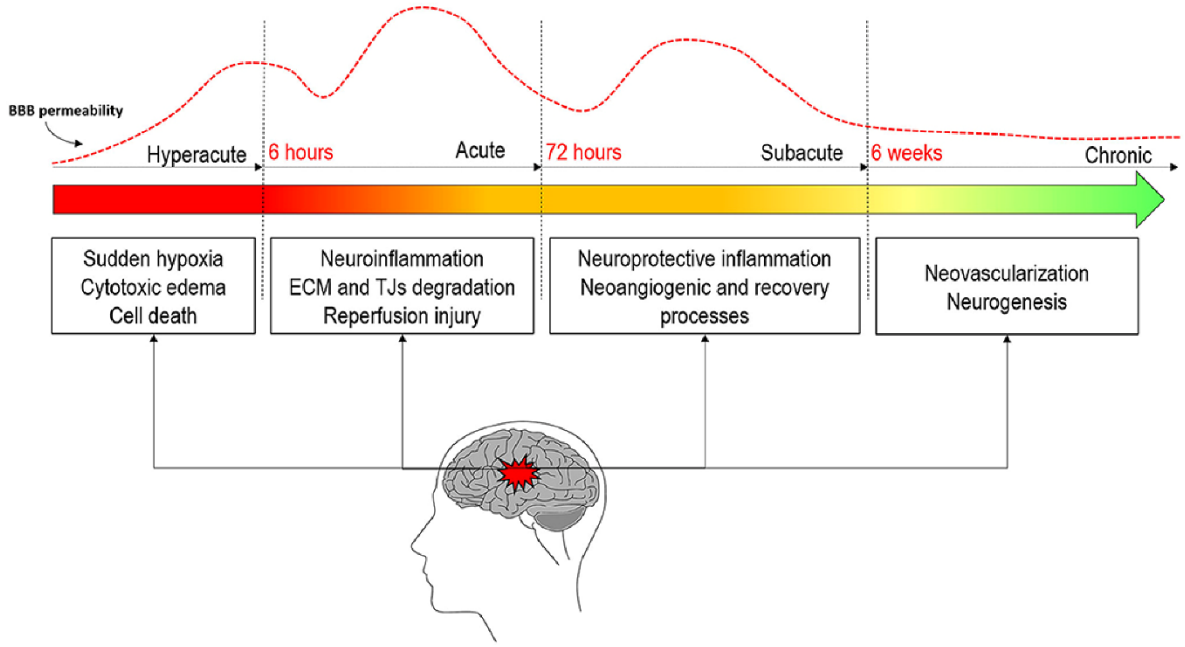

Figure 16. Stages of blood-brain barrier disruption following stroke. These four stages can be categorized as hyperacute (0-6 h), acute (6-72 h), subacute (72 h-6 weeks), and chronic (> 6 weeks). Extracted from Bernardo-Castro et al. [112].

These four stages can be categorized as hyperacute, acute, subacute and chronic.

- *Hyperacute phase (< 6 h)*

As explained before, when artery occlusion occurs and causes a deficiency in oxygen and glucose supply, ATP levels decrease and essential ion pumps like Na^+-K^+-ATPase and Ca^{2+}-ATPase lack the required energy for normal functioning. As a result, Na^+ accumulates in the cytosol resulting in cytotoxic edema. This is accompanied by an increase in Ca^{2+} which disrupts cellular mechanisms and contributes to cell death. Glutamate excitotoxicity and cellular depolarization contribute to the stimulation of glutamate receptors, (*i.e.,* AMPA and NMDA receptors), exacerbating the disruption of calcium homeostasis. Moreover, the disruption in Ca^{2+} homeostasis provokes mitochondria dysfunction and ROS formation [112]. In addition to cell mechanisms, other mediators such as MMPs further contribute to the disruption of BBB integrity, for example directly degrading TJs and ECM. In fact, several studies reported decreased expression of claudin-5 and occludin just 1 h after focal ischemia [112,113]. As a consequence, larger macromolecules pass through the vessel wall and enter the extracellular space of the brain. This event sets off an osmotic gradient that draws water into the brain tissue, leading to the development of vasogenic edema. Vasogenic edema is a serious and potentially life-threatening complication of stroke. The accumulation of a substantial volume of water within the brain provokes brain swelling and can elevate intracranial pressure, which may generate additional ischemic injuries due to

an imbalance between the pressure within the brain and the capillaries. Finally, other mediators, such as aquaporins, VEGF, nitric oxide synthase, or ultimately inflammatory cells, may contribute to BBB early disruption [112].

- *Acute phase (6–72 h)*

The next stage occurs within a relatively brief time frame, approximately 72 to 96 h after the onset of the stroke. During this critical period, a cascade of events unfolds in response to cell death, the accumulation of cell debris, and the elevated levels of ischemia-induced ROS. These factors collectively trigger the local neuroinflammatory response, being microglia, the first responders as extensively reviewed in section 1.5. Microglia release pro-inflammatory compounds, including IL-6, IL-1β, IL-1α, TNF-α, and NO, which contribute to the disruption of the BBB and an increase in its permeability. For example, TNF-α can activate apoptotic factors and MMPs, while also diminishing claudin-5, and ZO-1 expression, thereby compromising the stability of TJs. Similarly, IL-6 and IL-1β can induce endothelial activation, and stimulate the production of cytokines, chemokines, and MMP-9. In particular, MMP-9, plays a crucial role in the proteolytic degradation of ECM components (*i.e.*, collagens, laminin, or fibronectin) and the digestion of TJ proteins, such as occludin and claudin, also contributing to BBB disruption and permeability increase. The expression of MMP-9 rapidly escalates in response to ischemic injury, reaching its peak activity around 24–48 h after the event. Indeed, the elevated activity of MMP-9 within the acute phase of ischemic stroke has been linked to an increased risk of secondary bleeding, and its presence in the serum of stroke patients correlates with worse clinical outcomes. Another significant contributor to the progression of ischemic damage is cyclooxygenase COX-2, which plays a role in BBB impairment as part of a secondary inflammatory response. Collectively, all these processes render the BBB more permeable and pave the way for immune cell infiltration (see section 1.4.1). Importantly, the BBB becomes extremely fragile at this point, and thus more susceptible to a complete rupture. In such cases, a substantial volume of blood extravasates into the brain, leading to one of the most frequent and unpredictable outcomes of ischemic stroke: the so-called haemorrhagic transformation [112].

- *Subacute phase (> 72 h)*

The subacute phase typically starts approximately one week after the stroke onset, being essential for brain recovery. During this phase, astrocytes and microglia release neurotrophic factors and anti-inflammatory cytokines (*e.g.*, IL-4, IL-10, TGF-β), which contribute to tissue repair and wound healing. These factors also aid in the stabilization of

the BBB, although it is worth noting that numerous studies suggest that BBB may remain permeable during this stage. Remarkably, the duration and characteristics of this permeability time window are extremely diverse and contingent upon the severity of the stroke [112].

The regenerative response after stroke also includes angiogenesis and the modification of the vascular tree. Angiogenesis is a complex, multi-step process that entails the formation of new blood vessels from pre-existing ones (Figure 17). In the healthy adult brain, BECs are equipped with oxygen sensors and hypoxia-inducible factors, such as hypoxia-inducible factor-2α (HIF-2α) and prolyl hydroxylase domain 2 (PHD2), which enable BECs to adjust their size in accordance with CBF. Following ischemia/reperfusion events, a combination of pro-inflammatory cytokines, chemokines, and hypoxia-derived factors, such as VEGF, angiopoietin-2 (Ang-2), or FGFs serve as angiogenic signals for quiescent vessels. As explained above, pericytes are among the first components to detach from the vessel wall. Through the action of MMPs, they undergo proteolytic degradation, detaching from the BM, and initiating the early-stage disruption of the BBB. Next, BECs begin to loosen their junctions, resulting in dilation of the newly formed vessel. In this step, VEGF enhances the permeability of the endothelial cell layer, causing plasma proteins to extravasate and accumulate within the new provisional ECM [114].

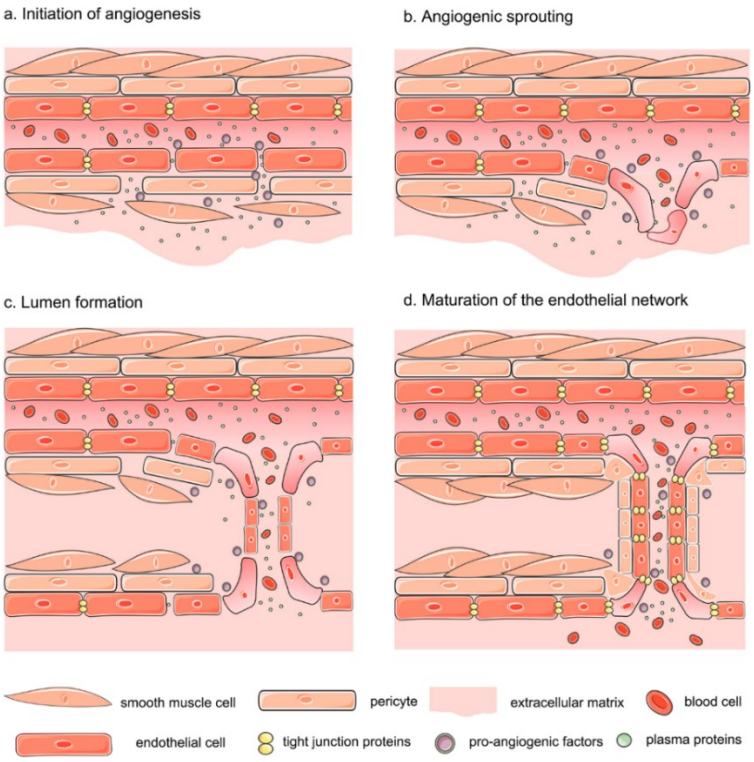

Figure 17. Angiogenesis process after ischemic stroke. This process is characterized by first angiogenic sprouting, subsequent lumen formation, and the final maturation of the endothelial network Adapted from Carmeliet and Jain [114].

Afterwards, in response to integrin signalling derived from the ECM, BECs begin to migrate onto this ECM surface. Notably, only one endothelial cell, the *tip cell*, takes the migration lead, and moves towards the angiogenic signals (VEGF receptors, neuropilins, and Notch ligands). This coordinated migration of tip cells prevents a massive movement of BECs. The neighbouring cells migrate towards tip cells adopting the role of *stalk cells*. These stalk cells, driven by signals, such as Notch, Wnts, and growth factors, undergo division to elongate the stalk and establish the lumen of the newly forming blood vessel. Myeloid bridge cells assist with the fusion of the new vessel branch with another, enabling the initiation of the blood flow. However, the vessel is not fully functional until maturation is completed. During maturation, pericytes cover the vessel and secrete signals, such as PDGF-β, TGF-β, Ang-1, ephrin-B2, and Notch. This signalling supports the final stages of vessel development. Subsequently, TIMPs and plasminogen activator inhibitor-1 contribute to the deposition of the BM, and TJs are re-established to ensure optimal flow distribution within the mature vessel [114].

Notably, the same signals that promote BBB destabilization in early stages, enhance and modulate brain angiogenesis during later stages. This dual role highlights the complex interplay between vascular remodelling and BBB integrity after a stroke. Therefore, while angiogenesis modulation holds great potential as a therapeutic approach, it should be addressed with caution. In stroke animal models, there is evidence of endothelial proliferation within the first 12–24 h after the stroke event. However, the full maturation and stabilization of these newly formed blood vessels do not take place until 3–4 days after the injury [112]. Interestingly, survival in patients is directly associated with the number of new vessels in the ischemic penumbra [115].

- *Chronic phase (> 6 weeks)*

Finally, the chronic phase begins approximately six weeks after the stroke onset. The BBB is still disrupted but its permeability is significantly lower compared to the previous stages. During this phase, sealing processes to restore the BBB begin. Specifically, there is a reorganization and enhanced expression of TJs and AJs. At the same time, many factors responsible for hyperpermeability slowly decrease, whereas others that contribute to the restoration of the BBB become enhanced [112]. Examples include Ang-1, which stabilizes cell–cell and cell–ECM interactions, or activated protein C and sphingosine-1- phosphate, which settles TJs and cytoskeleton coupling. Additionally, neurotrophic factors secreted by

astrocytes, such as VEGF, GDNF, BDNF, NGF, or FGF contribute to the migration of neuronal progenitor cells favouring neural repair and survival, axonal sprouting, and neuroplasticity [112].

Nevertheless, a certain degree of BBB dysfunction may persist long-term after the onset of stroke. Specifically, it has been reported that partial or improper organization of the novel TJ complex, along with the enhanced expression of claudin-1, or reduced levels of claudin-5, might cause long-lasting leaky vessels in stroke patients. In fact, there is a significant risk of intracranial haemorrhage within the first 30 days following an ischemic stroke [112]. Unfortunately, the heightened risk persists elevated beyond this initial period and remains higher than the one observed in the general population. However, this partial closing of the BBB may offer a unique window of opportunity for therapeutic interventions, as the increased permeability of the BBB could potentially facilitate the delivery of cell therapy and drugs into the brain [112].

1.4. The pathophysiology of ischemic stroke: The immune response.

1.4.1. The initiation of the inflammatory cascade

In parallel with the aforementioned events, immediately after occlusion and triggered by ischemia and reperfusion, the inflammatory process initiates in a well-orchestrated sequence involving the brain, its vasculature, the circulating blood, and lymphoid organs [10] to resolve the damage and protect the brain (Figure 18). Brain ischemia engages both innate and adaptive immunity, both of which play crucial roles in the acute and chronic phases of the damage. Initially, innate immunity is rapidly activated, relying on low-affinity and versatile receptors on innate immune cells. This enables the recognition of the so-called danger-associated molecular pattern molecules (DAMPs), released by injured and dead cells. These molecules include heat shock protein 60 (HSP60), ATP, UTP, high-mobility group protein B1 (HMGB1), and Aβ, among others. Innate immune cell response not only encompasses neutrophils, monocytes, and macrophages, but also a diverse variety of T lymphocytes, and NK cells, among others. The immediate response aims to eliminate potential threats through a broad and indiscriminate humoral and cellular inflammatory reaction. In contrast, adaptive immunity takes several days to develop and retains a memory of antigen exposure. In this case, adaptive immunity relies on high-affinity receptors, including T cell receptors and immunoglobulins [10].

Innate and adaptive immunity are intricately intertwined. In particular, dendritic cells (DCs), the typical innate immune cells, are responsible for presenting antigens to lymphocytes (the typical adaptive immune cells), thereby initiating the adaptive immune

response. Subsequently, lymphocytes undergo clonal expansion within lymphoid organs, re-entering the circulation and engaging the antigen throughout the body. The ensuing humoral and cellular responses aim to neutralize the harmful antigen in a selective and specific way [116].

In detail, the inflammatory cascade begins with the sudden interruption of blood flow and the subsequent hypoxia, which leads to the production of ROS and endothelial shear stress within minutes after the ischemic insult. In response, BECs express selectins, which are translocated to the surface membrane. This boosts the rapid adhering of leukocytes and platelets to the endothelium, which instigates a rapid pro-inflammatory signalling. However, leukocytes cannot transmigrate until BBB is disrupted a few hours later, and until DAMPs and chemokine gradients are established. Even so, this adhering may clog vessels and could be implicated in the “no-reflow” phenomenon explained before, which prevents reperfusion even after occlusion release. Furthermore, oxidative stress produces the constriction of pericytes which may enhance these microvascular occlusions. Oxidative stress also alters BBB permeability by enhancing the number of pinocytic vesicles and thereby promoting transendothelial transport [10]. Additionally, the increased levels of thrombin, a coagulation factor and major player in thrombogenesis [117], also induce the expression of adhesion molecules on BECs, disrupt the BBB, and activate the C3 and C5 components of the complement system.

Meanwhile, at the perivascular space, ischemia and reperfusion activate perivascular macrophages and mast cells. Macrophages secrete pro-inflammatory cytokines and mast cells undergo degranulation, thanks to the chemotactic complement subunits, releasing vasoactive mediators, such as histamine, proteases, and TNF-α. These mediators collectively aid in the increase of endothelial adhesion molecules, which will promote the posterior infiltration of leukocytes (neutrophils, lymphocytes, and monocytes) [10]. Moreover, the proteases released by vascular cells and leukocytes, contribute to the degradation of junctional proteins of the BBB and components of the ECM, facilitating the extravasation of proteins and cells.

- **The innate immune response**

The complex intravascular inflammation sets the stage for BBB breakdown and leukocyte invasion of the ischemic lesion. Simultaneously with the opening of the BBB described in section 1.3.3, numerous peripheral immune cells infiltrate into the ischemic area at different time intervals and with variable cadences (Figure 18).

- *Neutrophils*

The first peripheral immune cells to enter the brain are neutrophils, which begin infiltrating within the first 3 h, reaching a peak in approximately 24 h, and then gradually decreasing over the following 7 days [118,119]. The early infiltration of neutrophils is driven by potent levels of chemoattractants (*e.g.,* CXCL1, CXCL2, CXCL5, MCP-1/CCL2, CCL3, CCL5). The entry of neutrophils enhances BBB disruption and brain damage through the production of ROS, proteases, IL-1β, lipocalin-2, and neutrophil extracellular traps (NETs) [116,119]. In particular, the excessive production of ROS alters ZO-1, claudin-5, and the cadherin-catenin complex. Additionally, they induce cytoskeleton re-organization via signalling pathways associated with hyperpermeability including mitogen-activated protein kinase (MAPK), protein kinase C (PKC), and Rho GTPases. Besides, the secretion of proteases, including MMPs, elastase, and proteinase 3, negatively impacts in the integrity of TJs, AJs, and extracellular matrix components [119]. However, neutrophils can also exhibit neuroprotective effects. For instance, they secrete MMP-9, which can harm the BBB, but also degrades DAMP signalling. Additionally, neutrophils produce VEGF, promoting angiogenesis [118].

- *Monocyte-derived macrophages*

In turn, the monocyte-derived macrophages (MDMs) influx from the spleen to the brain starts 1 day after the onset, peaks between 3 to 7 days, and then returns to basal levels by day 14 (Figure 18) [116,119]. Monocyte recruitment is significantly influenced by the chemokine receptor CCR2. However, the precise role of MDMs in stroke pathophysiology remains largely unknown. While some studies associate high levels of MDMs with larger lesions, others argue for the opposite. For example, blocking CCR2 has been shown to significantly protect against cerebral edema but negatively impact long-term recovery. This controversial effect is likely related to distinct populations of monocytes and/or their functional switch to an anti-inflammatory phenotype influenced by the neural microenvironment [119]. In fact, it has been shown that MDMs may express in early stages markers associated with a protective role, including CD206, Arg1, and chitinase-like protein 3 (YM1/Chil3). However, in later stages, they may exhibit a pro-inflammatory phenotype contributing to chronic inflammation [116].

- *Natural-killer cells*

Natural killer (NK) cells infiltrate the ischemic region as early as 3 h after stroke, peaking at 12 h, and remaining elevated for at least 4 days. The chemoattraction of NK cells is mediated through the IP-10/CXCR3 and CX3CL1/CX3CR1 axes [119]. NK cells can

contribute to local inflammation by secreting pro-inflammatory cytokines such as TNF-α, IL-1β, IFN-γ, IL-17a, IL-6, and IL-12 after MCAO [118].

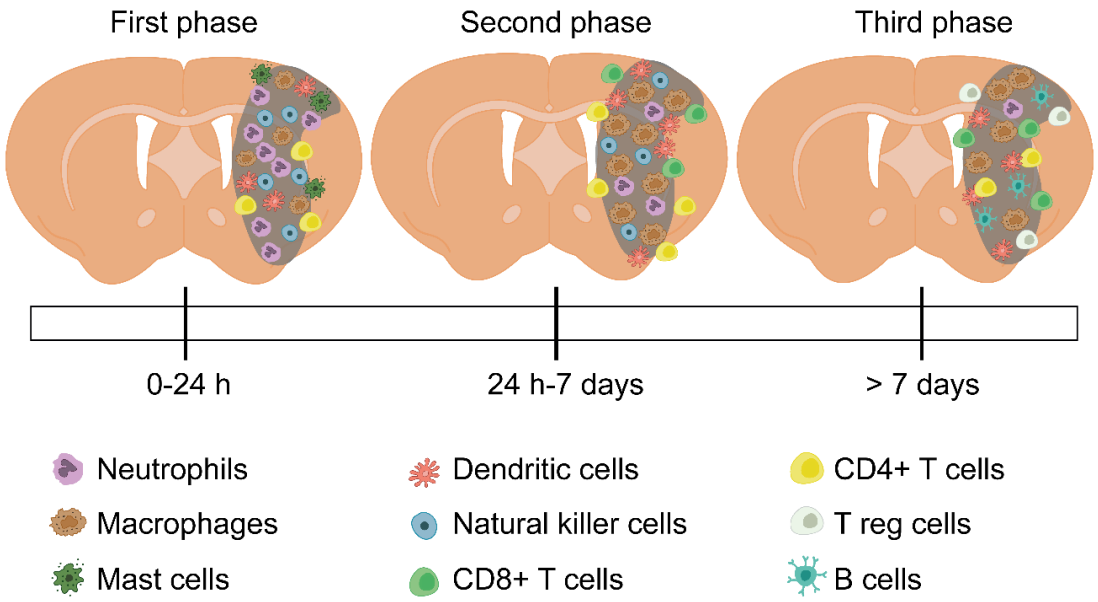

Figure 18. **Spatio-temporal representation of the dynamics of the different immune cell populations in brain ischemia.** In the early acute phase (0-24 h), neutrophils are the first immune cells to arrive at the ischemic core, followed by macrophages, mast cells, dendritic cells, and the first T cells. At later stages (24 h to 7 days) there is a peak of macrophages and T cells. Chronic stages are characterized by the presence of T reg and B cells.

- *Dendritic cells*

DCs appear in the ischemic brain within the early stages of stroke, remaining for around 7 days in animal experimental models and up to a month in humans. The specific role of DCs is not fully stablished but it is recognized that they function as APCs with high migratory capacity. Besides, they have been reported to secrete IL-23, which triggers IL-17 expression in γδ T cells and promotes neutrophil infiltration [116].

- **The adaptive immune response**

Starting immediately after stroke, there is a release of novel brain antigens, including myelin basic protein (MBP), GFAP, S100β, or neuron-specific enolase (NSE). These antigens, previously concealed by the BBB or released due to the breakdown of cell membranes, become exposed and reach the circulation. As a result, B and T lymphocytes from the spleen and lymph nodes become activated, thereby initiating the humoral and cellular immune response [10]. Concurrently, myeloid cells in the brain become APCs after phagocytosing dead cells. They upregulate the MHC class II and migrate to the lymph nodes and spleen. It has also been reported that autoreactive $CD4^+$ and $CD8^+$ T cells and

B cells increase 4 days after stroke [116]. Remarkably, the peak of lymphocytes coincides with the peak of APCs, which become reduced in the periphery [10,119]. In fact, peripheral blood lymphocytes tested in survivors two weeks after stroke, demonstrate more activity against myelin than those in controls or even people with MS [116,120]. However, the precise nature of this autoimmunity during stroke, similar to antigen-independent responses, remains elusive. Its impact on long-term injury can be both exacerbating and ameliorating, depending on factors, such as the lymphocyte population, their polarization, their location, and the timing of their activation. Location and timing are of particular importance, as the recovery of lost function in stroke patients hinges on the functional plasticity of areas beyond the infarcted lesion [121].

- *T cells*

As previously mentioned, T cells are involved in the inflammatory cascade through both antigen-independent and antigen-dependent mechanisms. In the early phase of ischemic stroke, T cells are involved in an antigen-independent manner and are closely related to the development of the infarct lesion. However, the underlying mechanisms and the specific time frame are not yet well understood. Antigen-dependent responses of T cells require the binding of T cell receptors (TCRs) to specific antigens, which must be processed and presented by APCs, along with costimulatory signals [122]. This typically takes 3 to 7 days [123], aligning with the observed increase in the diversity of TCRs around 7 days after MCAO [124]. The temporal gap between T cell-dependent effects in the early phase and the T cell-dependent effects in the later adaptive immune response suggests that the detrimental impacts of T cells in, at least, the initial 3 days, are not reliant on an antigen-dependent response [122].

Regarding T cell infiltration dynamics, it has been reported that the number of lymphocytes increases within the first 24 h following a stroke, reaching its peak at 3 days and subsequently declining, although others have indicated that the initial infiltration may occur between days 3 and 7 or even only during the chronic phase (Figure 18). These variations in findings could be attributed to differences in stroke models and testing techniques [119,125]. However, it is worth noting that regardless of the timing and despite extravasating in smaller quantities, lymphocytes persist longer in the ischemic area than neutrophils and monocytes, sometimes lasting up to a month [119].

Despite numerous studies reporting the infiltration of various lymphocyte subtypes (*i.e.,* $CD4^+$, $CD8^+$ T cells, non-Treg T cells, Tregs, and γδ T cells) into the brain parenchyma after ischemic stroke [126,127], their specific roles remain controversial. However, the

consensus seems to be that the depletion of $CD4^+$, $CD8^+$, and γδ T cells reduces ischemic lesions and improves behavioural outcomes in mouse stroke models [128], suggesting a deleterious role of these cells, at least at early stages. Approximately 40 % of the T cells that infiltrate the ischemic brain tissue are $CD4^+$ helper T cells, while about 30 % are $CD8^+$ cytotoxic T cells. Remarkably, it has been reported that $CD8^+$ cytotoxic T cells are the first T cell subset to infiltrate, showing an increase within the first 3 to 24 h following the ischemic event (Figure 18). These $CD8^+$ cytotoxic T cells contribute to brain injury and neuron death by releasing perforin and granzyme, which induce cell death pathways [129]. In contrast, $CD4^+$ T infiltration becomes apparent only around 24 h post-stroke, peaking at 72 h (Figure 18). $CD4^+$ T cell functions are closely linked to the activated and infiltrated microglia/macrophages, which ultimately differentiate $CD4^+$ T cells into either Th1 or Th2 cells in response to brain injury [129]. Hence, while IFN-γ, IL-2, and IL-12 released from Th1 cells appear to be associated with worsened outcomes, the anti-inflammatory cytokines released by Th2 cells (*i.e.,* IL-4, IL-5, IL-10, and IL-13) exert neuroprotective effects, mitigating the inflammatory response [125,129].

Conversely, it has been reported that γδT cells and Th17 cells caused damage to the surrounding tissues by secreting IL-17. The levels of IL-17 have been shown to peak on the third day after the onset of the stroke, being associated with detrimental effects on the stroke outcome. However, in contrast to the deleterious effects in the acute phase, IL-17 expression during the chronic phase (approximately 1 month after the onset and potentially mediated by astrocytes), has been linked to the promotion of neurogenesis. This dual inflammatory and regenerative function depending on the time point underscores the complexity of the adaptive immune response after stroke [129].

Despite being controversial, regulatory T cells also appear to play a crucial role in modulating the inflammatory response in the chronic phase of ischemic stroke, with a window spanning up to several months (Figure 18). It has been reported that regulatory T cells exert a protective effect through the release of IL-10 and TGF-β, which enhance neural stem cell proliferation. Moreover, osteopontin derived from regulatory T cells has been shown to enhance microglia anti-inflammatory activity, thereby supporting oligodendrocyte regeneration. Lastly, amphiregulin released by regulatory T cells suppresses neurotoxic astrogliosis and promotes neural recovery [125].

- *B cells*

Finally, B cells, despite being present in a small number in the brain, play an important role in humoral immunity, contributing through functions such as antigen presentation, antibody

production, and cytokine secretion. However, the precise role of B cells in stroke pathogenesis remains unclear. While certain studies have not identified significant effects of B cells, others have suggested potential benefits [116,125]. For instance, it has been reported that B cells produce BDNF and NGF, exerting a neuroprotective function. Moreover, during the chronic phase of stroke, B cells have been observed to infiltrate regions distant from the injury site, potentially aiding neuronal viability and promoting dendritic arborization (Figure 18) [121,125]. Interestingly, some studies also reported that the number of T and B lymphocytes in the periphery inversely correlates with stroke outcomes [128,130].

1.4.2. The systemic immune response linked to stroke

At the same time that the inflammatory response derived from the ischemic stroke progresses in the brain, systemic immune response unfolds in the blood, spleen, bone marrow, and other lymphoid organs. Cytokines and DAMPs generated by the brain injury escape into the systemic circulation through BBB disruption or CSF lymphatic pathways, reaching lymphoid organs and triggering the inflammatory response. In experimental stroke models, the systemic immune response is characterized by an increase in pro-inflammatory cytokines in the serum (*e.g.*, IFN-γ, IL-6, CXCL1) and an elevated production of inflammatory mediators in splenic and circulating immune cells (IL-2, IL-6, TNF-α, CCL2, and CXCL2) within the first hours [10,116]. However, this elevated immune response only lasts for the initial 24 h, followed by an acute immunodepression, especially in individuals with large strokes. This response is characterized by peripheral lymphopenia, decreased functional activity of monocytes and T cells, lymphocyte apoptosis, and splenic atrophy [10,116]. This phenomenon increases the incidence of respiratory and urinary tract infections [131] (~ 30 % of patients), which are major causes of morbidity and mortality [116]. The precise underlying mechanism is not entirely understood, but it has been suggested that the autonomous nervous system and the hypothalamic-pituitary-adrenal (HPA) axis are involved, enhancing the release of glucocorticoids, norepinephrine, and acetylcholine [116]. Furthermore, in the past few years, it has been proposed that these infections may result from the disruption of the gut-epithelial barrier after stroke [132].

At this point, it is crucial to emphasize the continuous crosstalk between the immune system, the nervous system, and the gut microbiota, which is the most abundant symbiotic compartment in the body. The microbiota is involved in various aspects such as intestinal development and gut permeability, energy harvest and storage, as well as metabolic functions like fermenting and absorbing undigested carbohydrates [133]. Besides, the gut

microbiota dynamically interacts with the immune system, releasing signals that promote the maturation of immune cells and maintain immune homeostasis. Finally, the microbiota plays a key role in bidirectional gut-brain interactions. Specifically, it regulates BBB permeability, synaptogenesis, and the release of neurotransmitters and neurotrophic factors [134]. In recent years, studies have highlighted the significant role that the microbiota-gut-brain axis plays in the occurrence and development of ischemic stroke [135]. Both animal models and stroke patients experience alterations in microbiota composition, called gut dysbiosis, which may potentially impact the pathophysiology of stroke, leading to neuroinflammation, immune dysregulation, and BBB dysfunction. For instance, recent findings have demonstrated that gut microbiota regulates intestinal immune cell trafficking after stroke, influencing immune infiltration into the brain parenchyma [135].

Finally, it is important to remember that the crosstalk between cerebral immune cells and peripheral immune cells represents a delicate and complex network, whose integrity is essential for avoiding BBB disruption and further brain damage. In this sense, as mentioned before, astrocytes, microglia, and pericytes upregulate and release diverse chemokines to stimulate neutrophils, monocytes, and lymphocytes in the affected ischemic region. In particular, astrocytes secrete TNF-α and IL-17α, which in turn stimulate neutrophils to secrete CXCL1. Moreover, CNS cells secrete VEGF and IL-1β and stimulate the expression of VCAM-1 and ICAM-1 in BECs, promoting the attachment and infiltration of immune cells. Once immune cells adhere to the endothelium, both pericytes and astrocytes directly guide immune cell extravasation through chemoattractants like MIF and ICAM-1. Pericytes undergo changes in their cytoskeleton upon the interaction with neutrophils, enlarging the gaps between pericytes and ECM, and facilitating leukocyte extravasation. On its own, astrocytes provide guidance for infiltrated monocytes and macrophages through the interaction of fractalkine and CX3CR1. Finally, microglia have a significant impact on T cell polarization, influencing their final phenotype. In particular, IL-15 produced by microglia and astrocytes increases the levels and activation of $CD8^+$ T cells and NK cells. *In vitro* studies have also demonstrated that astrocytes can polarize $CD4^+$ T cells into Th1 cells. Finally, pericytes have been found to inhibit the proliferation and secretion of pro-inflammatory factors in activated T cells in the retina, although direct evidence of this in experimental stroke is yet to be fully established [119].

In conclusion, the pathogenesis of stroke is a highly intricate process in which various types of nervous, circulating, and cerebral immune cells exert profound dual roles depending on their cell context, spatial location, and timing. Consequently, therapeutic

interventions focused solely on one cell type may lead to unintended negative consequences or counteract the benefits from another type of immune cell, resulting in an unsatisfied stroke prognosis. Moreover, a critical timing for treating the different phases of the stroke may be relevant. Therefore, therapeutical approaches that comprehensively consider fine-tuned modulation of the different components in a time-depend manner may yield more satisfactory outcomes.

1.5. Neuropeptides: key mediators in the nervous-immune crosstalk

Considering the significant neuroinflammatory nature of stroke pathophysiology, and the intricate interaction between the functions of resident (*i.e.,* microglia and astrocytes) and peripheral immune cells, there is an increasing need to better elucidate the crosstalk between the nervous and the immune system in this cerebrovascular injury. Though for many years they were considered to be two autonomous systems without apparent connection between them, it has now become evident their coordinated action in most biological responses.

In general, the immune system acts as a sixth sense [136], signalling the brain when damage occurs and triggering the corresponding behavioural responses. Similarly, the immune system is regulated by the CNS in response to various stressors. The immune system-CNS bidirectional communication is tightly controlled to maintain a balance in the response of both systems to toxic insults, ensuring that it is neither excessive, causing neuronal damage, nor too mild, preventing the proper repair of the damaged area. This crosstalk is possible because both systems share a common biochemical language, namely neuropeptides, hormones, and cytokines, as well as their respective receptors [136].

Neuropeptides are molecules released in response to various stimuli by the peripheral terminations of efferent and sensitive nerves adjacent to immune cells, as well as by immune cells such as lymphocytes, macrophages, or neutrophils, among other organs and tissues [137]. Over the last two decades, distinct neuropeptides with immunomodulatory properties and therapeutic potential have been utilized in different animal models of inflammatory diseases, such as sepsis [138,139], rheumatoid arthritis [140,141], experimental autoimmune encephalomyelitis (EAE) [142–144], atherosclerosis [145,146], autoimmune myocarditis [147], or inflammatory bowel disease (IBD) [148,149]. Among relevant immunomodulatory neuropeptides examples are vasoactive intestinal peptide (VIP), urocortin, α-melanocyte-stimulating hormone (α-MSH), adrenomedullin, ghrelin, somatostatin, and cortistatin, which stand out for their pleiotropic

immunomodulatory actions. Despite being released by different types of cells and displaying distinctive molecular structures, they all share features that make them potential regulators of the immune response. Particularly, the therapeutic effect of these neuropeptides is based on suppressing early events that trigger the autoimmune response, addressing late stages typically associated with an exacerbated inflammatory response, aiming to restore immune tolerance, and exerting neuroprotective effects in certain cases [136]. Additionally, the antimicrobial and antiparasitic effects of some of these neuropeptides have also been described, being based on their structural similarities to host defence peptides [150–152]. For instance, VIP, αMSH, ghrelin, adrenomedullin, and cortistatin are capable of modulating autoreactive responses by inhibiting the activation of Th1/Th17 lymphocytes, and promoting Th2-type responses [137,153,154]. Alternatively, VIP and α-MSH inhibit the phagocytic capacity of macrophages and microglia [155], while adrenomedullin and ghrelin reduce the inflammatory glial response therefore preventing oxidative stress-induced death in OPCs and mature oligodendrocytes [156,157]. Some of these neuropeptides are even currently in clinical trials, for example, VIP treatment for human sarcoidosis [158] or recent studies with this neuropeptide for the treatment of cytokine storm in COVID-19 patients [159].

Regarding their safety, neuropeptides are inherently non-toxic physiological compounds that have been administered in humans without apparent complications or side effects. They are small and hydrophilic molecules that quickly reach the site of inflammation and are rapidly eliminated from circulation through natural hepatic detoxification mechanisms [144]. Although many neuropeptides have been proven to be effective and safe in the many preclinical models of disease described above, even in the treatment of human disorders [160,161], certain obstacles must be always taken into account for their therapeutic application [162]. Specifically, due to their peptidic nature, these molecules have a short-life in body fluids and tissues because of their rapid degradation by endopeptidases [162]. Moreover, neuropeptides are produced in multiple body locations and can have several binding sites, which raises the risk of generating undesired side effects. In this regard, various approaches have been proposed to enhance their stability, such as amino acid sequence modifications, encapsulation into nanoparticles, or other engineering structures that increase their protection, stability and bioavailability [162].

In this thesis and in the context of the pathophysiology of ischemic stroke, we will particularly focus on the role of the neuropeptide cortistatin in the CNS-immune system crosstalk.

1.6. Stroke therapies. Time is brain

Prior to the 1990s, treatment options for ischemic stroke were severely limited, primarily focusing on managing symptoms, implementing secondary prevention measures, and providing rehabilitation-based approaches. However, this landscape underwent a transformative shift due to two significant breakthroughs. The first ground-breaking innovation occurred in 1995 with the approval of the intravenous recombinant tissue plasminogen activator (rtPA), commonly known as alteplase, by the American Food and Drug Administration (FDA). The rtPA has remained the fundamental treatment for nearly 2 decades, until 2015, when the introduction of more advanced clinical trials led to the emergence of the endovascular therapy (EVT) [8]. Despite extensive research efforts, rtPA and the EVT are still the two only FDA-approved treatments available.

Regarding the mechanisms of action, rtPA and EVT aim to dissolve or mechanically remove the clot, respectively, with the common goal of restoring the blood flow and reperfusing the ischemic region. However, the eligibility for rtPA treatment is limited to a very small percentage of stroke patients (5-10 %) due to the narrow therapeutic time window (< 4.5 h after suffering stroke), and the safety concerns, involving increased intracerebral haemorrhage, thrombus migration, and neurotoxicity [7,119]. For EVT, also known as mechanical thrombectomy, the time window can extend up to 24 h. Unfortunately, it only applies to carefully selected patients with proximal large vessel occlusions, also depending on the availability of imaging techniques to diagnose (Figure 19). Both therapies are time-critical, and optimizing health system engineering to accelerate treatment and reduce door-to-needle times remains an urgent challenge. Time is so critical in stroke management that 1.9 million neurons are lost per minute as the stroke progresses, so *time is brain* [163].

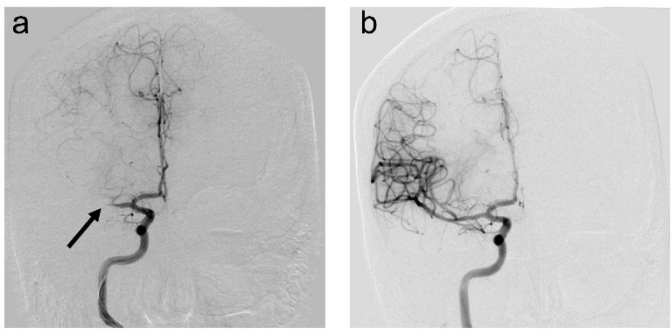

Figure 19. **Real images of a thrombectomy after an acute ischemic stroke due to large vessel occlusion**. **a.** Angiogram of the right internal carotid artery showing an occluded right MCA (arrow). **b**. Angiogram of the same region after a thrombectomy and complete revascularization. Adapted from Xiong et al. [164].

Despite the need to restore blood flow to prevent further brain damage, not all the effects of the restoration of blood flow are beneficial, as detrimental processes may have been already initiated during the ischemic period. After reperfusion, the generation of reactive oxygen molecules and activation of the immune system, including the recruitment of inflammatory cells and activation of the microglia, may lead to further injury despite reperfusion. Unfortunately, both rtPA and EVT treatments can contribute to reperfusion injury themselves. For example, rtPA upregulates MMPs, increasing the risk of BBB disruption, while EVT can cause injury to the endothelial lining. Both processes can initiate haemorrhagic transformation and provoke intracerebral haemorrhage. In fact, stroke-induced breakdown of the BBB is the most significant factor restricting the therapeutic time window for rtPA administration. Thus, novel therapeutic strategies focused on preventing BBB damage after ischemic stroke, hold immense potential for revolutionizing the clinical care of stroke patients, as for example more patients would benefit from rtPA without the risk of suffering internal haemorrhages [7,119]. Besides, another relevant therapeutic approach has been attempting to impede the ischemic cascade. Traditionally, this approach has been referred to as neuroprotection, but the term cytoprotection seems to be more appropriate according to recent studies. This is because all cells of the NVU in the ischemic region are at risk of damage, including neurons, astrocytes, microglia, pericytes, and BECs (Fisher and Savitz, 2022; Xiong et al., 2022). Nevertheless, despite the plethora of therapeutic approaches targeting the cellular consequences of ischemic brain injury, the results have been largely unsuccessful over the past 40 years. Many pharmaceuticals that target different components of the ischaemic cascade have been shown to be promising in animal models of stroke. However, when it comes to primary clinical endpoints in human trials, none of these agents have demonstrated clear and reproducible efficacy. The reasons behind the lack of translational success have been thoroughly discussed for more than 20 years, and are summarized in Table 2 [164,165].

Preclinical reasons	Clinical reasons
Drugs were not evaluated in animals with risk factors, such as aging, hypertension, atherosclerosis or diabetes	Drugs were tested in patients who were unlikely to benefit
Drugs were limited to only male animals, while females may respond differently	Studies had an insufficient number of patients, making it challenging to detect a treatment effect

Treatments were only tested at the stroke onset or shortly thereafter but not in the long-term	The use of neuroprotective agents in isolation without previous thrombolysis
Only infarct volume was evaluated, overlooking behavioural or glial/immune responses	A considerable number of patients with mild or severe stroke were included, in whom a clinical benefit is difficult to detect
Treatments were applied into temporary occlusion models but seemed to be ineffective in permanent models, or *vice versa*	Trials included a substantial number of patients with lacunar stroke with white matter infarction, despite no evidence suggesting that the studied drug affects white matter injury
The sample sizes evaluated were inadequate to draw meaningful conclusions	Trials in later time windows did not utilize advanced imaging to confirm whether the infarct size precluded beneficial treatment
Lack of reproducibility between models and laboratories	Only one dose was evaluated in comparison to placebo
Outcome assessments lacked randomization and blinding, potentially influencing the results	Patients were assigned to treatment too late after stroke onset, limiting the potential for substantial salvage of ischemic tissue
Lack of randomized and blinded outcome assessment.	The treatment only targeted one component of the complex ischemic cascade.
Lack of monitoring of physiological measurements, such as blood pressure and temperature	
The treatment only targeted one component of the complex ischemic cascade.	
Lack of dose-response and therapeutic time windows	

Table 2. Preclinical and clinical reasons for translational failure in clinical trials for stroke treatment. Extracted from Fisher & Shavit and Xiong et al. [164,165].

In summary, most preclinical trials did not include in their studies risk factors or comorbidities, such as aging and hypertension, or did not properly address the optimal time-dose or time window for their treatments. Similarly, in most clinical trials, the majority of enrolled patients did not receive concomitant thrombolysis or the treatment was not

adequate to their specific stroke timepoint or severity. Table 3 summarizes some of the most promising treatments over the last decade and their failure in clinical trials.

Trial name and description	Drug	Mechanism of action	Clinical trial stage	Findings/reasons for failure	Safety concerns
NeuMAST: Neuroprotection with Minocycline Therapy for Acute Stroke Recovery Trial	Minocycline	Anti-inflammatory agent. Suppression of free-radicals, microglia activation, and MMPs induction	Phase IV	Trial stopped because did not show a significant benefit in terms of its intended neuroprotective effects	N/A
ESS: Multicentre Efficacy Study of Recombinant Human Erythropoietin in Acute Ischaemic Stroke	Erythropoietin	Promotion of neuronal survival after hypoxia and other metabolic insults	Phase II/III	No significant differences in primary outcome (day 90) or secondary outcomes between treatment and control groups.	Treated patients suffered thrombolysis
ALIAS: High-dose albumin treatment for acute ischaemic stroke	Albumin	Neuroprotective and anti-inflammatory and effects	Phase III	No significant differences in primary outcome (day 90) or secondary outcomes between treatment and control groups	N/A
SAINT II: Stroke -Acute Ischaemic- NXY-059 Treatment II	NXY-059	Nitrone-based free radical trapping agent	Phase III	No significant difference in primary outcome (day 90) or secondary outcomes between control and treatment groups	N/A
AXIS 2: AX200 for the Treatment of	Granulocyte colony	Trophic factor with neuroprotective and	Phase IIb	G-CSF treatment did not meet the primary and the secondary end	N/A

Ischaemic Stroke	stimulating factor (G-CSF)	neurogenesis properties		points at day 90, although there was a trend towards a reduced infarct growth in the G-CSF group	
Effect of Natalizumab on Infarct Volume in Acute Ischemic Stroke (ACTION)	Natalizumab	Blockade of the α4-β1 integrin	Phase II	No reduction in focal infarct from day 1-5. Functional outcome improvement sustained over 90 days	N/A
Enlimomab acute stroke trial (EAST)	Enlimomab	Monoclonal antibody against cellular adhesion molecule ICAM-1. Block leukocyte attachment and migration through the BBB	Phase III	No significantly positive effects with Enlimomab. Terminated	Mortality higher in enlimomab -treated patients

Table 3. Most promising but failed trials in the last decade. It is described the drug involved in the trial, the mechanism of action, the clinical trial stage, the findings/reasons for failure, and the safety concerns. N/A: not applicable. Extracted from Smith et al. and Veltkamp & Grill [166,167].

It is interesting to note that in the past many drug candidates primarily targeted individual aspects of the ischemic cascade, often focusing on neuro-centric mechanisms. On the contrary, drugs with multiple targets were seen as flawed or less desirable. However, such single-target therapeutics were shown to display crucial limitations in addressing the intricate and interconnected network of pathophysiological events triggered by cerebral ischemia. Currently, based on the up-to-date understanding in the field of the complexity of the ischemic cascade, the use of cytoprotective approaches that modulate multiple aspects of the ischaemic cascade is far more attractive (*i.e.,* addressing neuronal damage, excitotoxicity, BBB disruption, inflammatory cascade, or microglia glial activation). Nonetheless, rather than attempting to completely halt specific processes, the focus should be shifted towards regulating and balancing them. Indeed, stopping certain neurotoxic processes might inadvertently hinder neuroprotective mechanisms (*e.g.*, microglia pro-inflammatory factors inducing angiogenesis and neurogenesis). Of particular

note, therapeutic strategies should gear towards controlling exacerbated uncontrolled processes that occur at later stages of ischemic injury and may be more detrimental. These include addressing chronic inflammatory responses that persist beyond the acute phase, which would allow managing the ongoing disruption of the BBB, while enhancing processes like neurogenesis and angiogenesis that are crucial for recovery.

1.7. Cortistatin

- **Discovery, structure, and receptors**

Cortistatin (CST) is a cyclic neuropeptide that was first discovered in the rat brain cortex and hippocampus by Luis de Lecea in 1996 [168]. The name cortistatin was chosen due to its expression in the cortex and its ability to suppress cortical activity [169]. Cortistatin is encoded by the *Cort* gene localized on chromosome 1 in *Homo sapiens* (EntrezID: 1325) and chromosome 4 in *Mus musculus* (EntrezID: 12854). It is first synthetized as pre-pro-cortistatin consisting of 114 AA in humans and 108 in mice [170]. After proteolytic processes, the secretion signal sequence associated with preprocortistatin is cleaved, leading to the formation of procortistatin. This molecule also presents certain basic AAs (KR, RK, KK, RR), that serve as potential sites for prohormone convertases. Depending on the specific AA that these convertases target, various sizes of mature cortistatin peptides may be produced. Although multiple cleaved variants are generated, some of their functions remain unknown. The most biologically relevant forms are CST-14 (1.7 kDa) and CST-29 (3.44 kDa) (14 and 29 AA respectively) in rodents, and CST-17 (2.1 kDa) and CST-29 (17 and 29 AA respectively) in humans [169,170].

Recently, it has been demonstrated that cortistatin is found not only in cortex and hippocampus, but in other brain structures such as the olfactory bulb, the striatum, and the hypothalamus, although to a lesser extent [171,172]. Moreover, its expression has been widely described in other peripheral organs, such as the lungs, prostate, testis, heart, pancreas, and kidney, among others, as well as in many tumours. In fact, several studies by our group and others described cortistatin specific expression in (i) other brain cells apart from neurons (*i.e.*, microglia, astrocytes, BECs, pericytes), (ii) immune cells (B and T lymphocytes, monocytes, macrophages, dendritic cells), (iii) ECs and muscular cells from the periphery, and (iv) endocrine cells from adrenergic glands, thyroid, parathyroid, stomach, and kidneys (Table 4) [136,168,173]. Importantly, cortistatin shows a remarkable structural homology to the neuropeptide somatostatin (SST), with cortistatin in humans sharing 11 out of its 17 AA with the 14 AA of somatostatin (Figure 20). These shared residues include two homologously placed cysteines linked by a disulfide bridge, along

with a FWKT (phenylalanine-tryptophan-lysine-threonine) tetramer. This is crucial for the peptide binding to all five of the so-called somatostatin receptors (as they were first described for somatostatin) that have been identified thus far (Sstr1-Sstr5) (Figure 20). This allows cortistatin to perform similar functions to somatostatin, such as the depression of neural activity or the inhibition of cell proliferation [170,174].

Despite the considerable homology and shared functions and receptors between cortistatin and somatostatin, their expression patterns diverge and do not overlap across various organs and tissues. Additionally, they are differentially regulated. This way, cortistatin also exerts several novel and distinct functions compared to somatostatin, such as slow-wave sleep induction, reduction of locomotor activity, and an important immunomodulator role [168,170,174]. Notably, the capacity of cortistatin to elicit these novel functions appears to be dependent on the two adjacent AA near the disulfide bridge (Figure 20). These two specific residues allow cortistatin, but not somatostatin, to bind to the ghrelin receptor (Ghsr), with the same affinity than the endogenous ghrelin.

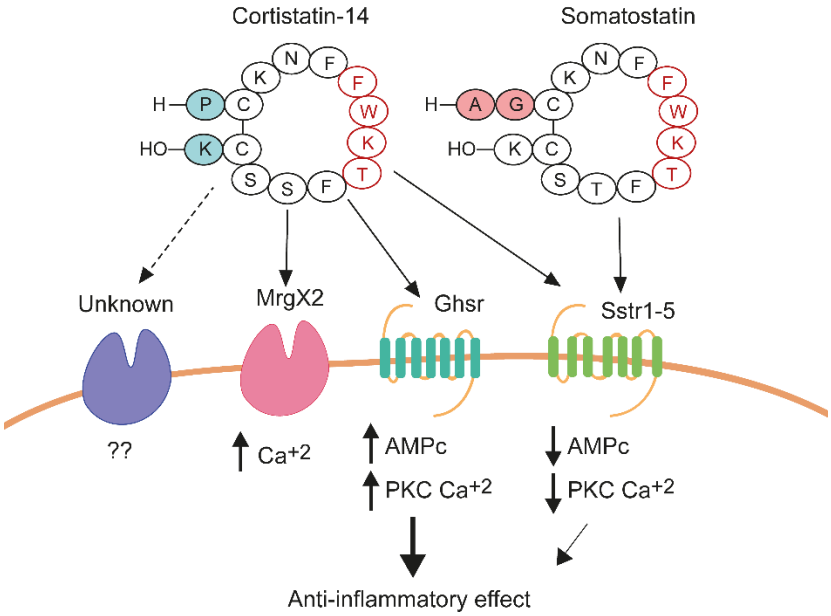

Figure 20. Schematic drawing of cortistatin sequence and receptors. To note, cortistatin and somatostatin exhibit similar structures and share the binding site (red) to somatostatin receptors (Sstr1-5). Importantly, while somatostatin only binds to Sstr1-5, cortistatin also binds the ghrelin receptor, the MrgX2 in humans, and an unknown yet receptor, probably specific for cortistatin. The binding to Sstr1-5 reduces the AMPc / PKA pathway, activating K^+ channels. This phenomenon induces the outward movement of K^+ into the extracellular space, hyperpolarizing the cell. Consequently, intracellular Ca^{2+} levels decrease, as well as PKC activity. Conversely, binding to the ghrelin receptor promotes the AMPc / PKA pathway, triggering the cell signalling and exerting opposite effects to those of binding to somatostatin receptors. The exact role of cortistatin-MrgX2 interaction remains incompletely understood, but it has been associated with an increase in cytosolic Ca^{2+}.

Furthermore, cortistatin interacts with the orphan Mas-related gene 2 receptor (MrgX2) in humans, which is related to the Mas1 oncogene family sequences. This receptor is still only described in humans, and it was first discovered in sensory neurons within the dorsal root ganglia. The exact role of cortistatin-MrgX2 interaction remains incompletely understood, but it has been associated with an increase in cytosolic calcium ions, potentially associated with nociception modulation [175].

Binding to these receptors, as well as interactions with yet-unidentified receptors, or truncated receptor variants (*e.g.,* Sstr5 truncated receptor) could collectively explain the distinct functions of this neuropeptide. Moreover, it has been described that somatostatin receptors can form homo/heterodimers or interact with receptor activity modifying proteins (RAMPs), which might also contribute to the divergence in functions exhibited by cortistatin and somatostatin [176,177]. Consequently, depending on the context, cell type, or activated receptor, cortistatin may trigger different signalling pathways, resulting in diverse functions.

Thus, the interaction of cortistatin with Sstr reduces the activity of the enzyme adenylate-cyclase, with the subsequent decrease in the cytosolic levels of cyclic adenosine monophosphate (cAMP), a critical messenger in intracellular signalling. Additionally, this interaction results in an activation of K^+ channels, prompting the outward movement of potassium ions into the extracellular space. This phenomenon hyperpolarizes the cell, consequently reducing intracellular Ca^{2+} levels and dampening PKC activity [170] (Figure 20). On the other hand, cortistatin binding to Ghsr favours the AMPc / protein kinase A (PKA) pathway, stimulating the activity of the adenyl cyclase, triggering the cell signalling, and exerting opposite effects to those of binding to somatostatin receptors [178] (Figure 20).

- **Role in the nervous system**

Multiple studies have described the expression of cortistatin in the NS. As mentioned before, cortistatin is known to be expressed in the cortex, hippocampus, olfactory bulbs, amygdala, corpus callosum, and striatum (GABAergic neurons). Apart from the above-mentioned slow-wave sleep induction and locomotor activity reduction, cortistatin has the capacity to regulate learning and memory in the hippocampus by reducing the activity of excitatory neurons [169]. Moreover, it has been described the role of cortistatin in the establishment of synaptic connection within the neocortex and the hippocampus during embryonic development through BDNF modulation [169].

In addition, several works have reported that cortistatin treatment exerts immunomodulatory and neuroprotective effects in models of neuroinflammatory/neuroimmune injury, such as excitotoxicity [138], sepsis/meningoencephalitis [179,180], MS [144], Parkinson's disease [181], or neuropathic pain [182]. In particular, cortistatin-induced neurotrophic factors (BDNF and ADNP), modulated the glial response and reduced inflammatory mediators (TNFα, IL-6, NO) [136,138,144,173,181,183] and regulated oligodendrogenesis and myelination [183]. Therefore, cortistatin reduces the inflammatory response as the same time that induces an active program of neuroprotection and regeneration.

Moreover, beyond its anti-inflammatory function, cortistatin serves as a natural analgesic component in both central and peripheral nociceptive systems, which respond to injury by secreting this neuropeptide. In fact, cortistatin and its receptors are highly expressed in human nociceptive pathways, including spinal cord neurons, neurons of the dorsal root ganglia, and GABAergic inhibitory interneurons of the brain cortex and hippocampus [184]. In particular, cortistatin has demonstrated analgesic effects by reducing tactile allodynia and heat hyperalgesia induced by two models of inflammatory and arthritic pain [141]. Additionally, it ameliorated neuropathic pain following the transaction of the sciatic nerve, enhancing the production of neurotrophic factors both at the peripheral and central levels [182]. Moreover, cortistatin has also been shown to decrease the severity of neurogenic skin inflammation triggered by mustard oil and carrageenan [185], as well as to reduce sensitivity to noxious heat in rats [186]. These analgesic effects of cortistatin appear to be mediated through the binding to Sstr2 and Ghsr [141].

- **Immune functions**

Although cortistatin was first discovered in the CNS, its expression has been widely described in other tissues and peripheral systems, such as the immune system. Thus, cortistatin, but not the homolog somatostatin, and its receptors are expressed in both innate and adaptative immune cells, such as macrophages, neutrophils, dendritic cells, and lymphocytes [187]. Moreover, the levels of cortistatin correlate with the state of activation of these cells, suggesting a role of this neuropeptide in the regulation of the immune system [187]. In fact, cortistatin has been described as a potent anti-inflammatory molecule. Our group has described in the last two decades the molecular and cell mechanisms of the anti-inflammatory function of cortistatin in both *in vitro* and *in vivo* models of inflammation and autoimmunity. For example, cortistatin modulates *in vitro*

innate immune response by reducing pro-inflammatory cytokines, such as TNFα, IL-6, IL-1β and IL-22, chemokines, including RANTES/MIP1α and NO in activated macrophages by LPS [138]. *In vivo*, cortistatin demonstrated therapeutic efficacy in sepsis models by decreasing inflammatory mediators both locally (pulmonary infection) [188] and systemically [138]. This anti-inflammatory effect, combined with an immunoregulatory role (an increase of Treg cells), was also reported in IBD and rheumatoid arthritis [149,189]. Similarly, Th1/Th17 lymphocyte balance was modulated and anti-inflammatory-like macrophages were induced in atherosclerosis [145] and myocarditis models [147]. Additionally, in recent years cortistatin has been disclosed as an endogenous inhibitor of pulmonary, dermal, and hepatic inflammation and fibrosis, especially modulating the activation and differentiation of stellate cells and fibroblasts in the latter [190–192]. Finally, cortistatin exerts beneficial effects in the context of EAE, a preclinical model of MS, reducing the severity and incidence of the disease in the mice, lowering the immune infiltration into the spinal cord and modulating the neuroinflammatory processes [144].

- **Effects on the peripheral and brain vascular systems**

Apart from its expression in the nervous and immune system, our group and others have previously described the important role of cortistatin in peripheral vascular function [145,145,146]. In particular, it has been reported that heart, arterial endothelium, and arterial SMCs express cortistatin and its receptors, especially in response to injury [146,175,193]. Notably, cortistatin expression is augmented in human atherosclerotic plaques, mouse arteries subjected to blood-flow alterations, the plasma of patients with coronary heart disease, and the hearts of mice suffering autoimmune myocarditis [145,146]. Interestingly, cortistatin-deficient mice exerted exacerbated vascular responses in response to neointimal lesions [146].

Crucially, treatment with cortistatin has been demonstrated to improve vasculopathies associated with vascular remodelling and reduce experimental arterial stenosis and vascular calcification [146]. Besides, cortistatin treatment in a mouse model of atherosclerosis (apolipoprotein E-deficient mice fed with a high-lipid diet), reduced the number and size of atherosclerotic plaques, lowered the Th1/Th17-driven inflammatory response, increased the regulatory T cell response, and decreased the binding of immune cells to the peripheral endothelium [145].

In contrast to the well-described role of cortistatin in the peripheral vascular system, the precise function of cortistatin in the brain endothelium remained elusive up to this day. In fact, the expression of somatostatin and its receptors (especially Sstr2 and Sstr4) in

BECs has been scarcely reported [194–196]. Despite different studies have described a protective effect of somatostatin ghrelin, and receptors-agonists over the disrupted endothelium [194–198], other works have presented controversial pro- and anti-angiogenic properties of ghrelin [196,199], and even somatostatin-induced hyperpermeability [200]. Additionally, Basivireddy and colleagues [194] described that decreased levels of somatostatin contribute to BBB dysfunction in MS.

Of note, only one recently published study has reported some preliminary data describing that cortistatin reduced BBB disruption induced by sepsis [180]. Specifically in the context of strokes, only a pioneering study conducted over 20 years ago first described that both cortistatin and somatostatin treatment reduced the infarct volume after 7 days in a permanent MCAO model in rats [201]. Nonetheless, the mechanism underlying this effect, the role of cortistatin in stroke pathophysiology, and/or over the brain endothelium following ischemic damage was not assessed, and no further works have addressed this issue thus far.

- **Deficiency of cortistatin**

Mice lacking cortistatin have proven to be valuable models for investigating the intrinsic role of this neuropeptide. They exhibit alterations in the HPA axis, which produces high levels of glucocorticoids [202] and a chronic state of anxiety [144]. Moreover, they present reduced levels of prolactin and an altered glucose-insulin homeostasis [202]. In addition, from an immune point of view, cortistatin-deficient mice display exacerbated inflammatory responses both in basal and after damage conditions. For instance, LPS-induced damage triggers an exacerbated pro-inflammatory response in macrophages and T cells [138]. However, in certain autoimmune disease models like EAE, cortistatin-deficient mice show paradoxical effects, with delayed disease onset and reduced clinical symptoms [144]. This unexpected outcome could be attributed to the immunosuppressive properties of the elevated glucocorticoid levels observed in these mice. In any case, models of pain, local inflammatory or neurological damage in cortistatin-deficient mice [147,154,182,190,192] correlate with greater severity and higher production of inflammatory mediators, underscoring the complexity of cortistatin-mediated responses.

Additionally, it is important to note that cortistatin levels are impaired in the temporal lobule of AD patients [203], in the hippocampus of AD mouse models expressing the human β-amyloid precursor protein [204], in the retina of diabetic retinopathy patients [205], and in the ipsilateral and contralateral ischemic brain mouse cortex [206]. This

suggests a close relationship between cortistatin deficiency, neurodegeneration, and glial activation.

Source	Functions	Receptors	Preclinical model
	↓Locomotor activity ↑Slow-wave sleep ↓Growth factor hormone ↓Cell proliferation		
SNC Kidneys Stomach Liver Testis Retina Heart Skin Lungs Lymphocytes T Macrophages Monocytes Dendritic cells	↓ Inflammatory factors ↓Chemokines ↑Anti-inflammatory factors (IL-10/TGF-β) ↓Th1/Th17 response ↑Treg response ↓Lymphocytes proliferation ↑Neuroprotective and neurotrophic factors ↑Protection of oligodendrocytes ↑Myelination ↓Inflammatory glial response ↑BBB protection (this thesis)	Sstr1-5 Mrgx2 Ghsr Unknown	Sepsis Meningoencephalitis IBD Hepatic, lung and dermic fibrosis Atherosclerosis Rheumatoid Arthritis Autoimmune myocarditis EAE Pain Ischemic stroke (this thesis) Parkinson

Table 4. General characteristics of cortistatin. Source, receptors, and preclinical models where it was demonstrated to have protective effects are included.

2. Hypotheses and objectives

2. Hypotheses and objectives

The current understanding of the intricate relationship between the central nervous system (CNS) and the immune system, both in baseline conditions and pathological scenarios, has significantly reshaped the point of view in the context of diseases categorized as neurodegenerative. This transformation encompasses the characterization of cellular mechanisms, identification of related molecular disorders, development of novel therapeutic interventions, and exploration of biomarkers for the diagnosis and monitoring of these pathologies. For an extended period, ischemic stroke was predominantly attributed to vascular changes leading to neurodegenerative condition. Indeed, ischemic stroke is the result of a permanent or transient occlusion of a major brain artery followed by subsequent reperfusion that triggers a cascade of cellular and molecular events leading to irreversible tissue injury and long-term sequelae. However, currently, the influence of the immunological component influence on the susceptibility and progression of damage and repair processes associated with stroke is acknowledged. This component is intricate, involving temporal and spatial successions of molecular and immune factors regulating the behavior of immunological populations at systemic and central levels, as well as their interactions. Considering the pivotal role of the local and peripheral immune response in the initiation of the ischemic process, evolution of primary and recurrent lesions, recovery, repair, and post-stroke progression, it should be better identified and targeted when developing stroke therapies. In fact, experimental data obtained from therapeutic strategies targeting the immune system and inflammatory response, though yielding contradictory results, suggest that this is a plausible therapeutic target for stroke.

Stroke represents the second leading cause of death worldwide. Despite continuous improvements, therapeutic failure remains notorious, and rtPA and endovascular therapy (EVT), are the only approved treatments for stroke. Therapeutic shortcomings primarily arise from the simplistic use of preclinical animal models (excluding risk factors), utilization of drugs with a single spectrum of action (in a process with multiple simultaneous factors), and reliance on immunosuppressants rather than immunomodulators (which influence both deleterious and beneficial aspects of inflammation, potentially negatively impacting autoimmune processes or infections in stroke patients).

Therefore, there is an urgent need to comprehend the immunological context at different stages of ischemic pathology and the involved factors to facilitate appropriate and successful therapeutic approaches. Neuroinflammation, orchestrated by glia and

peripheral immune cells, and the breakdown of the blood-brain barrier (BBB), especially related to brain endothelial cell dysfunction, are two of the major hallmarks of the pathogenesis and further outcomes of brain ischemia. Hence, investigating multifactorial endogenous mediators that modulate neurodegeneration, BBB disruption, and immune responses, rather than approaching these pathogenic mechanisms independently, seems essential for better management of these disorders. The ideal treatment would entail modulation of the inflammatory and neuroinflammatory response, regulating the local and peripheral immune response while permitting immune activity associated with cleaning and repair processes.

Cortistatin is a neuroimmune mediator. It is a neuropeptide widely distributed in the central nervous system and the immune system, exhibiting anti-inflammatory, immunomodulatory, and neuroprotective properties in experimental models of neuroinflammatory/neuroimmune injury, such as excitotoxicity, meningoencephalitis, MS, or neuropathic pain. In all of them, cortistatin reduced inflammatory mediators and modulated glial cell function while maintaining their tissue-surveillance activities. Moreover, cortistatin plays a key role in regulating peripheral vascular function, particularly in response to injury. Conversely, the absence of cortistatin has been associated with an exacerbated pro-inflammatory state in the CNS and periphery, accompanied by decreased expression of neurotrophic factors and altered neuroinflammatory responses.

However, the intrinsic function of cortistatin in modulating the immune response in neurodegenerative disorders characterized by an immunological component remains unexplored. Additionally, its role in processes arising from the interaction between immune cells in both the peripheral and CNS, along with its participation in stimulating endogenous repair mechanisms, is not well-understood. Based on its neuroprotective, anti-inflammatory, and immunomodulatory properties, as well as its role in peripheral vascular endothelium, we hypothesize that cortistatin may be a key endogenous factor in the dynamics of ischemic stroke damage and recovery mechanisms, making it a promising therapeutic agent, especially in the context of glial responses, vascular and barrier changes, and peripheral immune activation. Additionally, we suggest that investigating events occurring in the absence of cortistatin (utilizing mice deficient in this neuropeptide) could yield valuable insights into these processes and the regulation of associated factors during stroke.

Thus, the general goal of this thesis is to study the involvement of cortistatin in the processes of neurological damage, neuroinflammation, BBB dysfunction, and immune

dysregulation associated with stroke in wild-type and cortistatin-deficient mice, along with exploring its potential therapeutic application.

Herein, the specific objectives of this thesis are:

1. To investigate the potential therapeutic effect of cortistatin in a pre-clinical model of stroke, the middle cerebral artery occlusion model (MCAO), in young and middle-aged mice:

i. To establish the MCAO model.

ii. To determine the potential therapeutic window of cortistatin by administering the neuropeptide at different time points after stroke: immediate (0 h+ 24 h), early (4 h + 24 h), or later (24 h) treatment.

iii. To assess the potential therapeutic role of the neuropeptide in reducing neurological deficits and improving motor functions.

iv. To evaluate the role of the neuropeptide in the infarct volume and neurodegeneration.

v. To evaluate its impact on microglial activation dynamics and glial scar formation after stroke.

vi. To investigate the capacity of cortistatin to modulate BBB breakdown and promote barrier-recovery mechanisms.

vii. To address its ability to regulate immune cell infiltration of peripheral immune responses.

2. To explore the endogenous role of cortistatin in stroke pathobiology of young and middle-aged mice deficient in this neuropeptide:

   i. To characterize the role of endogenous cortistatin in functional and neurological stroke outcomes

   ii. To assess the importance of cortistatin in the modulation of neuroinflammation after stroke

   iii. To examine the effect of cortistatin in vascular responses and BBB permeability dynamics after stroke

   iv. To characterize the role of cortistatin in peripheral immune activation after stroke

v. To determine the role of exogenous cortistatin administration in modulating the stroke-induced phenotype of cortistatin-deficient mice

3. To investigate the specific endogenous role of cortistatin on the dynamics of brain endothelium, and explore its possible therapeutic role in modulating brain endothelium breakdown after ischemic injury:

i. To set up an *in vitro* BBB model simulating stroke conditions (oxygen-glucose deprivation).

ii. To characterize the role of cortistatin in the permeability and integrity of the brain endothelium barrier after ischemic conditions.

iii. To assess the function of cortistatin in the inflammatory response and immune cell extravasation across the barrier.

iv. To thoroughly analyse the impact of cortistatin on the molecular pathways associated with essential responses of the brain endothelium after ischemic injury.

3. Materials and methods

3. Materials and methods

3.1. Peptides

Mouse cortistatin-29 and human cortistatin-17 were acquired from Bachem. The lyophilized peptides were dissolved into distilled water (for *in vivo* studies) or into phosphate buffer 20 mM (pH 7.4, for *in vitro* studies), and stored at -80 ºC until use (final concentration 10^{-4} M). For *in vitro* studies, 100 nM was used, while 3.45 µg/mouse (115 µg/kg) µg/kg was used for the mouse models.

3.2. Buffers and solutions

- Stock solution for storage of free-floating sections: 30 % glycerol, 30 % ethylene glycol, 10 % PB 0.2 M, and 30 % ddH_2O
- PB 0.2 M: 50 ml of solution A+ 50 ml of solution B
- Solution A: NaH_2PO_4 0.2 M in H_2O
- Solution B: Na_2HPO_4 0.2 M in H_2O
- Washing buffer for ELISA: 0.1 % Tween-20 in PBS
- Blocking buffer for ELISA: 0.1 % FBS in PBS
- Binding buffer pH 6 (0.1 M) for ELISA: 8.77 ml of solution A + 1.23 ml of solution B + 10 ml of ddH_2O
- Binding buffer pH 9 (0.1 M) for ELISA: 10 ml of solution B + 9 ml of ddH_2O
- Lysis buffer for erythrocytes (Ack buffer): 150 mM NH_4Cl, 10 mM $KHCO_3$, 0.1 mM Na_2EDTA
- Permeability buffer: 141 mM NaCl, 2.8 mM $CaCl_2$, 1 mM $MgSO_4$, 4 mM KCl, 1 mM NaH_2PO_4, 10 mM glucose, and 10 mM Hepes pH 7.4

3.3. Culture media

- **b.End5 medium:** Dulbecco's modified Eagle's medium (DMEM, Sigma) supplemented with 10 % foetal bovine serum (FBS), 1 % penicillin/streptomycin (P/S), 1 % MEM Non-Essential Amino Acids Solution, 2 mM L-glutamine, and 1 mM sodium pyruvate (all from Gibco)
- **BECs medium:** DMEM F12 (Biowest) supplemented with 10 % FBS, 1 % P/S, 2 mM L-glutamine (all from Gibco), 1 % endothelial growth factor supplement, 0.5 % heparin, and 0.5 % ascorbic acid (all from Sigma-Aldrich)

- **Human pericytes medium:** DMEM supplemented with 20 % FBS (Life Technologies), 2 mM L-glutamine, and 50 µg/mL gentamycin (both from Sigma)
- **Human ECs medium**: Endothelial cell growth medium (sECM, Innoprot) supplemented with 5 % FBS (Life Technologies) and 50 µg/ml gentamycin (Sigma)
- **Macrophages medium:** DMEM supplemented with 10 % FBS, 1 % P/S, and 2 mM L-glutamine
- **T cells medium:** RPMI medium (Gibco) supplemented with 10 % FBS, 1 % P/S, 2 mM L-glutamine, and 50 µM 2-mercaptoethanol (Gibco)

3.4. Animals

The animal procedures were conducted at both the Institute of Parasitology and Biomedicine, IPBLN (Granada, Spain) and in the Department of Fundamental Neurosciences, DNF (Lausanne, Switzerland). All procedures were approved by the Animal Care and Use Board and the Ethical Committee of the Spanish National Research Council (Animal Care Unit Committee IPBLN-CSIC # protocol CEEA OCT/2017.EGR) and the Vaud Cantonal Veterinary Office (Switzerland), in accordance with the guidelines from Directive 2010/63/EU of the European Parliament and the Swiss laws on the protection of animals used for scientific purposes.

For the experiments conducted in the IPBLN, transgenic mice lacking the cortistatin gene (*Cort*$^{-/-}$) were generated and maintained within a C57BL/6J background in collaboration with Dr. Luis de Lecea (Stanford University, United States) and Dr. Justo Castaño (University of Córdoba, Spain), following the methods previously described [202]. Additionally, *Cort*$^{+/-}$ mice were produced by mating C57BL/6J *Cort*$^{-/-}$ females with C57BL/6J *Cort*$^{+/+}$ males. Subsequently, the breeding of *Cort*$^{+/-}$ pairs resulted in an offspring with three distinct genotypes (*Cort*$^{+/+}$, *Cort*$^{+/-}$, and *Cort*$^{-/-}$ mice). For the *in vitro* studies, all three genotypes were employed, while for the *in vivo* studies only *Cort*$^{+/+}$ and *Cort*$^{-/-}$ mice were included, given the previously established similarity between heterozygotes and hemizygotes. For the experiments performed in Switzerland, male C57BL/6J wild-type mice (8 weeks old) were purchased from Charles River.

Animals were housed in groups of ten mice per cage in a regulated environment (22 ± 1ºC, 60–70 % relative humidity), and subjected to a 12 h light/dark cycle (lights on at 7:00 a.m.). Food and water were provided *ad libitum*. For the *in vitro* experiments animals of 8-10 weeks old were used, while 12-week-old, 6-month-old, or 1-year-old male mice were used for the *in vivo* models.

3.5. Transient middle cerebral artery occlusion model

Young (12 weeks old) and middle-aged adult (6 months old) *Cort*$^{+/+}$ and *Cort*$^{-/-}$ mice, or C57BL/6J (10-week-old) mice were subjected to transient middle cerebral artery occlusion (MCAO) model, employing a modified protocol from Dr. Hirt's lab [3,207]. This procedure was performed in both the IPBLN and the DNF. The goal of this model is to induce a transient focal ischemia by introducing a silicon-coated nylon suture through the left common carotid artery (CCA) until reaching the origin of the middle cerebral artery (MCA). In detail, mice were anesthetized under isoflurane (Fatro Iberica) (1.5–2 % in 70 % N_2O / 30 % O_2) using a facemask (Anaesthesia workstation McKinley 2) (Figure 21a). Before surgery, analgesic treatment was applied: buprenorphine (0.03 mg/kg, intraperitoneally, Temgesic, Schering-Plough) (DNF) or meloxicam (2 mg/kg, subcutaneously, Norbrook) (IPBLN). Body temperature was maintained constant throughout the surgery using a heating pad (ThermoStar Homeothermic Monitoring System). The regional cerebral blood flow (rCBF) by laser-Doppler flowmetry (moorVMS-LDF1, Moor Instruments) was monitored. To this aim, under a dissecting microscope (Leica S9E), mice were placed in prone position and a small incision was made at the left side of the skull skin (Figure 21a). The temporal muscle was then gently dissected and the temporal bone was cleaned with a scalpel (VWR) until the MCA was visible. The fibre-optic probe was then fixed to the skull (surgery glue, Wurth) over the core area supplied by the MCA (approximately 1 mm posterior and 6 mm lateral from the bregma) (Figure 21a). Once, the rCBF was correctly detected (approximately 100-200 conventional perfusion units, PU), the mouse was turned around, placed in supine position, and fixed to the surgical table using adhesive tape. Consequently, fur and skin were disinfected with 70 % alcohol, and a midline neck incision was made. Next, the salivary glands and other soft tissues were gently pulled apart using tweezers (Dumont #BA-332-05) (Figure 21b). Pretracheal and sternocleidomastoid muscles were retracted and diverted to the right and left side, respectively, until the carotid artery was exposed using retractors (custom-made fabrication). First, the left CCA was dissected with fine forceps (Dumont #11254-20) from the surrounding structures and tightly knotted as distal as possible (5-6 mm approx. from the bifurcation) (Figure 21c, 1) using a 7-0 polypropylene-polyethylene monofilament (Optilene, Braun). Second, the next suture (Figure 21c, 2) was placed in the left external carotid artery (ECA) after being carefully dissected from the bifurcation. Third, a less tight suture (Figure 21d, 3) was placed in the internal carotid artery (ICA) to prevent the backflow of blood. Once the flow was restricted in this area, a tiny incision was made in the CCA (Figure 21d, 4) using micro-scissors (Fine Science Tools, # 15000-00). If successful, the procedure should only involve a small blood drip. Finally, a 7-0 silicone rubber-coated monofilament (filament size 7-0,

diameter 0.06-0.09 mm, length 20 mm; diameter with coating 0.17 +/- 0.01 mm, 701756PK5Re, Doccol corporation) was introduced through the incision (Figure 21e, 5). At this point, great care and expertise were required, as the less tight suture from the ICA should be loosened (Figure 21e, 6) simultaneously with the filament pushing.

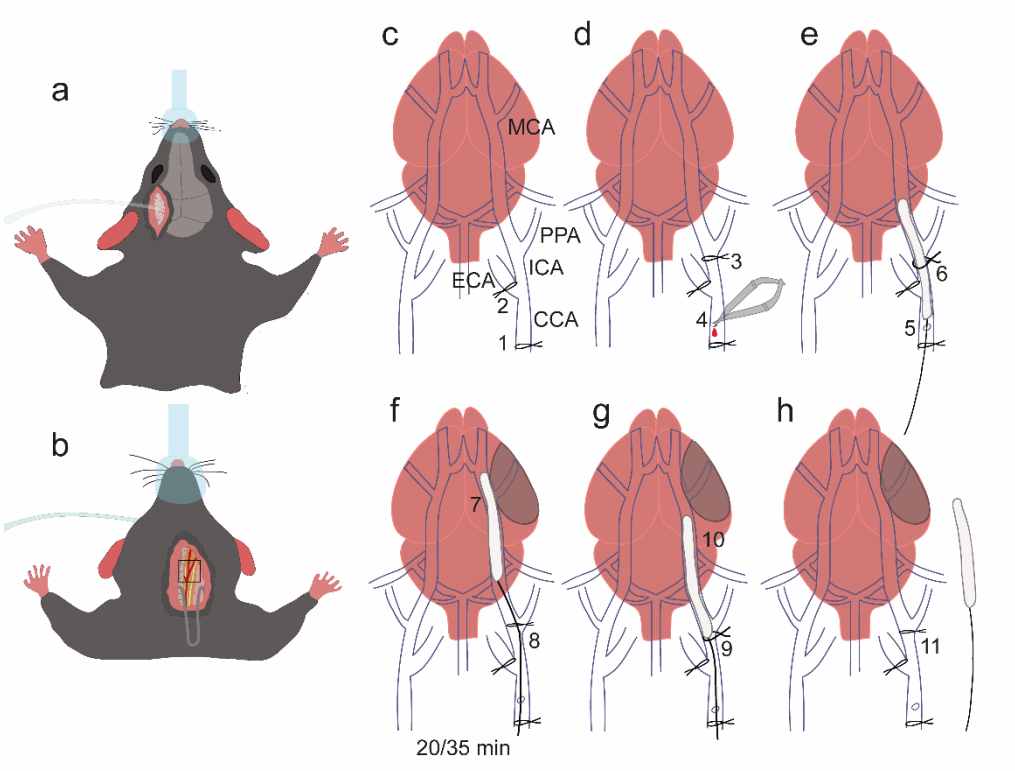

Figure 21: Schematic representation of MCAO procedure. **a.** First, mice were placed in prone position and an incision was made on the skull skin. After gently dissecting the temporal muscle, laser-Doppler was stuck to the skull. **b.** Then, mice were turned over and a midline neck incision was made to expose the carotid area. **c-h.** Detailed images illustrating key steps during the surgery from 1-11. The CCA **(1)**, the ECA **(2)**, and the ICA **(3)** were ligated. Next, a small incision **(4)** was made in the CCA and a 7-0 silicone rubber-coated monofilament was carefully introduced towards the ICA **(5)** while releasing the 3rd suture **(6)**. The filament was placed occluding the MCA for 20 and 35 min (3-month- and 6-month-old mice, respectively) **(7)** and the 3rd suture was closed again **(8).** After this time, the suture was loosened **(9)**, the filament was gently withdrawn **(10)** and the suture was tightly closed again **(11)**. The filament was placed correctly when the rCBF dropped down to < 20 % of the baseline, and the reperfusion was deemed successful when the flow was > 50 % of the baseline after reperfusion (10 min max.). CCA: common carotid artery, ECA, external carotid artery, ICA, internal carotid artery, PPA, pterygopalatine artery, and MCA middle cerebral artery.

The filament should be pushed until approximately half of the total filament is inside and little resistance is felt. The threshold for considering the filament correctly placed was rCBF dropping down to < 20 % of the baseline (Figure 21f, 7). Caution is advised, as the filament can be introduced in the pterygopalatine artery (PPA). In this case, the drop of the rCBF cannot be observed and blood drop normally occurs. Once the filament was

occluding the MCA, the third suture was rapidly closed again (Figure 21f, 8). The filament was placed at the MCA for 20 or 35 min for young and middle-aged mice, respectively. Times of occlusion were chosen based on bibliography and personal experience evaluating survival and ischemic injury for each age. After this time, the third suture was slightly opened (Figure 21g, 9), and the filament was rapidly withdrawn to enable reperfusion (Figure 21g, 10). Immediately, the third suture was tightly closed again (Figure 21h, 11). Reperfusion was considered to be successful when the flow was > 50 % of the baseline after reperfusion (10 min max.). Finally, the wound was closed with a 5-0 silk suture (Braun), laser Doppler was removed and 500 µl of saline solution was injected subcutaneously for volume replenishment after the surgery. Mice were housed in their cage until sacrifice, with *ad libitum* access to food and water. Each cage was equipped with water-softened chow and recovery gel. For sham surgeries, the same procedure was followed, but filament was not introduced. All procedures were finished within 15-20 min, excluding the occlusion and reperfusion periods. [208,209].

Cortistatin (3.45 µg/mouse) dissolved in a final volume of 100 µl of PBS, was administered at different time points (0 h, 4 h, or 24 h) after MCAO. Controls were injected with the same amount of saline solution. Neurological score, behavioural tests, ischemic volume determination, morphometric characterization of glial populations, and inflammatory response, were determined 48 h after surgery.

3.6. Functional outcome assessment

- **Neurological score**

The functional outcome of each mouse was assessed by a neurological score evaluation each 24 h after MCAO and before sacrifice. Severity was graded from 0 to 3 evaluating motor, sensory, reflex, and balance using a compendium of previously published scales [207,210] (Table 5).

Degree of deficit	Neurobehavioral alterations
0	No observable deficit
0.5	Hypomobility (slight) Passivity Normal walk
1	Hypomobility (moderate) Flattened posture

	Hunched back Piloerection (slight) Decreased body tone (slight) Decreased muscular strength (slight) Motor incoordination (slight) Inability to walk straight
1.5	Piloerection (moderate) Motor incoordination (moderate) Intermittent circling Ataxic gait
2	Persistent circling Tremor twitches Forelimb flexion Decreased body tone (moderate) Motor incoordination (severe)
2.5	Hypomobility severe Motor incoordination (severe) Loss of right reflex Respiratory distress Seizures
3	Death

Table 5. Neurological deficit score. It is ranged from 0 to 3 according to motor, sensory, reflex, and balance alterations.

- **Behavioural tests**

- *Rotarod test*

This procedure is designed to assess motor function and ataxia in mice. The set-up includes a rotating cylinder with a rubber surface (to provide grip) of an approximate diameter of 3 cm, equipped with an attachment featuring multiple compartments separated by thin walls, allowing for testing multiple mice simultaneously [211] (Figure 22). When placed on the rotating rod, mice naturally attempt to walk on it and maintain their balance to avoid falling to a platform located below. To ensure the reliability of the test results and to exclude motivational factors, such as mice that might fall off very early [211], a training

phase was conducted. Mice were subjected to three consecutive daily training trials (within a gap of 10 min between them) for two days pre-surgery and three daily test trials at 24 h and 48 h after MCAO [207]. Mice were placed on the rotating cylinder (Ugo Basile, Gemonio, Italy) with a gradual acceleration protocol (from 4 rpm to 40 rpm over a span of 216 s, and left at a constant 40 rpm speed until reaching 300 s from the start). Mice were allowed to run on the rod until they either fell off, completed two consecutive full turns gripping the rod, or reached the 300-second time limit. The longest latency to fall from the rod over the three trials was scored for each mouse.

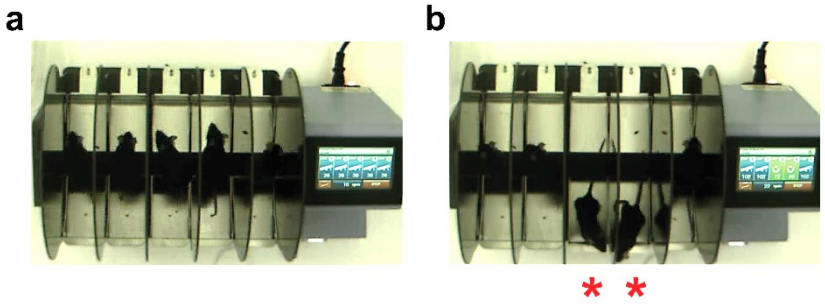

Figure 22. Frames of the rotarod test recording. Mice were placed in the cylinder with gradual acceleration (**a**) and allowed to run until reaching the 300-second time limit towards or falling (**b,** asterisks).

- *Wire-hanging test*

This test is employed to assess the degree of muscle coordination and endurance in mice [212]. Mice were suspended in a single wire (60 cm) stretched between two posts (31 cm high) above a soft ground (custom-made fabrication) and allowed to escape towards the posts (Figure 23). Mice were trained 1 day before surgery and scored for the times they escaped (touching and reaching either left or right post) or fell 24 h and 48 h after MCAO [207]. Escaping time or falling time was also evaluated. The test concluded after either 180 s or a mouse had fallen off the wire ten times.

Figure 23. Frames of the wire-hanging test recording. Mice were suspended in the wire (**a**) and allowed to escape towards one of the posts (**b**) until reaching it (**c**).

- *Pole test*

This procedure is employed to assess the motor skills of mice in terms of their ability to grip and manoeuvre their way down a pole until they reach a safe surface [213]. The set-up comprises a metal pole (45 cm high, 1 cm diameter) wrapped with autoclave tape to prevent slipping and a soft mat base (custom-made fabrication) to protect mice from a fall injury (Figure 24). Mice were acclimatised to the set-up for some minutes and then placed faced down in the pole. Three consecutive training trials were conducted 24 h before surgery. Post-surgery mice were evaluated again at 24 h and 48 h after MCAO. Mice were scored for escaping or falling (reaching or falling to the mat respectively). Total time to reach the mat (with at least two limbs) was scored as well as the number of turns that mice required to get down. The test was over after three trials, if the trials exceeded a duration of 120 s, or after 3 falls.

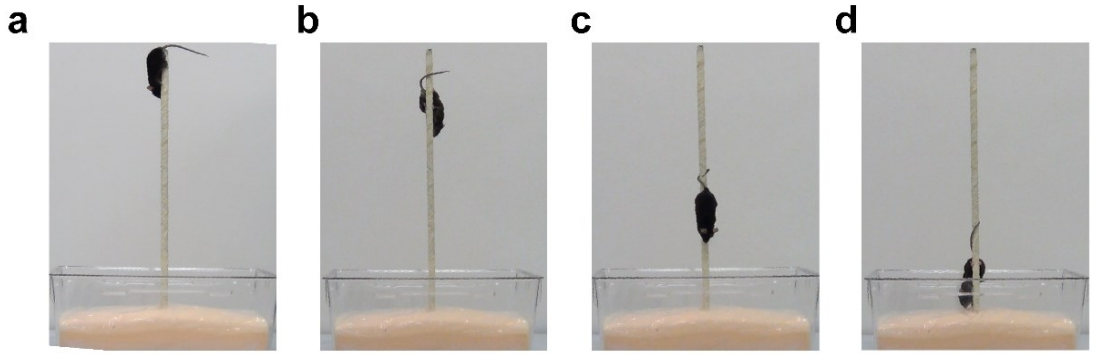

Figure 24. Frames of the pole test recording. Mice were placed faced down in the pole (**a**) and total time to reach the mat (**d**) was recorded. Mice were scored for escaping or falling, as well as for the number of turns (**b,c**).

Note: Wire-hanging was performed in both the IPBLN and DNF, while rotarod test was only performed in the DNF and pole test only in the IPBLN. All data was recorded manually by a camera (Handycam, Sony). The Observer XT 14.0 software (Noldus, Wageningen, The Netherlands) was used for data extraction in the DNF and was extracted manually in the IPBLN.

3.7. Ischemic Lesion Volume Determination

48 h after MCAO surgery, mice were sacrificed by an overdose of intraperitoneal injection of ketamine (100 mg/kg, Ritcher Pharma) and xylazine (10 mg/kg, Fatro Iberica) and intracardially perfused with 4 % paraformaldehyde (PFA). Brains were dissected and fixed in 4 % PFA for 24 h at 4 ºC and cryoprotected in 30 % sucrose for 48 h at 4 ºC. Brains were then frozen in isopentane (VWR) in dry ice at -25 ºC and stored at -80 ºC until use.

Brains were cut into 20 µm coronal sections with a cryostat (LEICA CM 1850 UV) using M1-embedding matrix (Epredia) to fix the brain to the disc chuck. One section out of each 25 (500 µm apart) (total of 8-10 sections) was collected into polysine adhesion frost slides (Epredia) in order to determine the ischemic lesion volume. The rest of floating sections were maintained in cryoprotection buffer at 4º C until use.

For cresyl violet (CV) staining, slides were dried at RT for one hour. Next, they were gradually hydrated in EtOH 100 % for 2 min, EtOH 85 % for 2 min, EtOH 70 % for 2 min, and finally in distilled water for 2 min. Next, slides were stained with CV-acetate (1 mg/mL of CV (Sigma) in distilled water and 0.3 % of glacial acetic acid (Carlo Erba)) for 6 min, rinsed in distilled water for 2 min, dehydrated in graded alcohols (EtOH 70 % for 2 min, EtOH 85 % for 2 min, EtOH 100 % for 2 min) and clear in xylene (Applichem) for 10 min. Finally, they were mounted in Entellan (Merk).

Images were captured with a stereomicroscope (Leica DM2000 Transmit, IPBLN, and Nikon SMZ 25, DNF) at 2.5x and 5x magnification respectively. The infarct volume was calculated by multiplying the sum of the infarcted areas on each section by the spacing distance (Figure 25). Each area was calculated using the ImageJ Fiji free software (https://fiji.sc) [214].

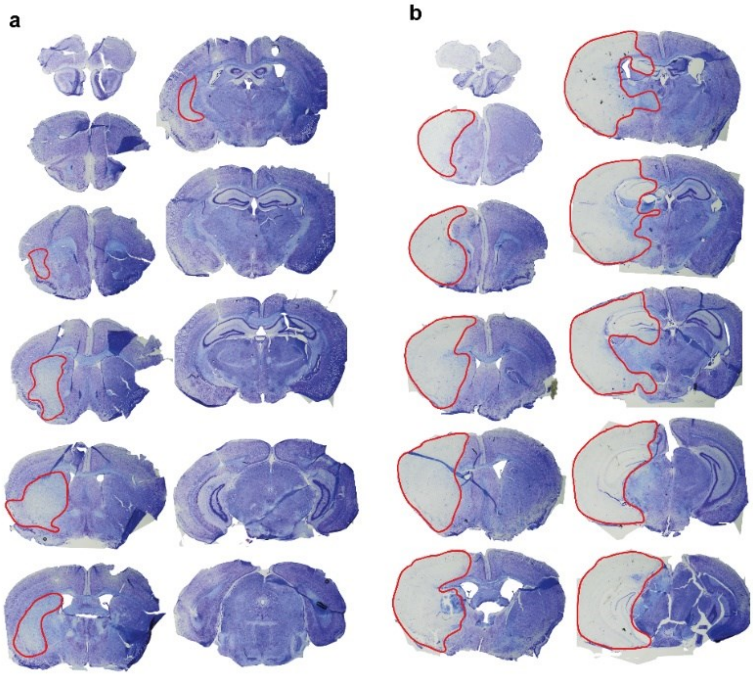

Figure 25. **Examples of CV coronal sections from the whole brain used for quantifying ischemic damage in mice with mild (a) and severe damage (b)**. Note that in the first one (**a**), ischemic lesion occupies the striatum and part of the cortex, while in the second one (**b**), it extends up to the hippocampus.

3.8. Immunofluorescence staining (brain sections)

For immunofluorescence labelling, 20 µm free-floating sections were washed with PBS (3 times, 5 min each), and blocked and permeabilized with PBS 1x, 1 % BSA, 0.1 % Triton X-100, and 5 % goat serum for 60 min at RT. Then, sections were incubated with primary antibodies anti-MAP2 (microtubule-associated protein 2, neurons), anti-Iba1 (ionized calcium-binding adaptor molecule 1, microglia), anti-GFAP (glial fibrillar protein, astrocytes), anti-CD31/PECAM-1 (platelet endothelial cell adhesion molecule-1, ECs), anti-αSMA (alpha-smooth muscle actin, pericytes, and smooth muscle cells), anti-ZO-1 (tight-junction protein, ECs) or APC-labelled anti-CD45 (cluster of differentiation 45, immune cells) (Table 6) in PBS 1x, 1 % BSA, 0.1 % Triton X-100 and 5 % goat-serum overnight (O/N) at 4º C. Next, sections were washed with PBS (3 times, 5 min each) and incubated with secondary Alexa Fluor™ 488/568/594/647-conjugated donkey/goat anti-rabbit/rat/mouse IgG antibody, and DAPI in PBS 1x, 1 % BSA, 0.1 % Triton X-100 and 2 % goat-serum for 60 min. After being washed again, sections were allowed to dry and mounted with Mowiol (Sigma). For IgG staining, the procedure remained the same, but no primary antibody was used. Instead, an Alexa Fluor™ 594-conjugated goat anti-mouse IgG antibody was directly used (1:1000 O/N 4 ºC). Images were taken with a LEICA DMi8 S Platform Life-cell microscope at 20x and with a confocal Leica TCS SP8 STED microscope at 63x in the IPBLN: In the DNF, images were taken using a slide-scanner Zeiss AxioScan Z1 microscope at 10x magnification.

Antibodies	Company	Catalogue number	Stock dilution	Use	Work dilution
Anti-MAP2	Sigma	MAB3418	0.2 mg/ml	Brain sections IPBLN Brain sections DNF	0.2 µg/ml
Anti-Iba1	Wako Abcam	19-19741 ab5076	0.5 mg/ml 0.5 mg/ml	Brain sections IPBLN Brain sections DNF	0.25 µg/ml 1 µg/ml
Anti-GFAP	Dako Millipore	20334 AB5804	2.9 mg/ml 1,000 mg/ml	Brain sections IPBLN Brain sections DNF	0.58 µg/ml 0.5 µg/ml
Anti CD45 APC-labelled	BD	559864	0.2 mg/ml	Brain sections IPBLN	1 µg/ml

Anti-CD31	BD	550274	15,63 µg/l	Brain sections IPBLN	0.05 µg/ml
Anti-αSMA	Sigma	A5228	2 mg/ml	Brain sections IPBLN	5 µg/ml
Anti-ZO-1	Fisher	40-2200	0.25 mg/ml	Brain sections IPBLN Transwells	1.25 µg/ml 2.5 µg/ml
Anti-Claudin-1	Fisher	71-7800	0.25 mg/ml	Transwells	2.5 µg/ml
Anti-Claudin-5	Fisher	34-1600	0.25 mg/ml	Transwells	2.5 µg/ml
Anti-VE-cadherin	Fisher	Ab-33168	1 mg/ml	Transwells	10 µg/ml
Rhodamine phalloidin-conjugated (F-actin)	Invitrogen	1034052	0.25 mg/ml	Transwells	1.25 µg/ml
Alexa Fluor 488	Invitrogen ThermoFisher	A21206 A11055	2 mg/ml	Brain sections IPBLN Brain sections DNF	2 µg/ml
Alexa Fluor 594	Invitrogen	A21206	2 mg/ml	Brain sections IPBLN	2 µg/ml
Alexa Fluor 568	ThermoFisher	A10037	2 mg/ml	Brain sections DNF	6.6 µg/ml
Alexa Fluor 647	ThermoFisher	A31573	2 mg/ml	Brain sections DNF	6.6 µg/ml
DAPI	Sigma	32670 D9542	1 mg/ml	Brain sections IPBLN Brain sections DNF	0.1 µg/ml

Table 6. Immunodetection antibodies. List of antibodies for *ex vivo* brain sections used in IPBLN and DNF and for cell transwells in the *in vitro* assays, specifying company, catalogue number, stock concentration, and working dilution

3.9. Morphometric characterization

To comprehensively describe the complex and diverse morphology of microglia, astrocytes, and BECs, along with all changes displayed after a stroke in these cells and structures, we employed ImageJ Fiji to perform the different morphometric analyses.

These analyses involved several preliminary steps to preprocess the images and ensure accurate and unbiased results.

- **Image processing**

First, we randomly selected a crop of the region of interest (ROI) (periinfarct area for studying glial scar and microglia, or infarct core for assessing microglia density and angiogenesis). We took great care to ensure that there was no overlap between cells, that the entire nucleus and branches were included, and to prevent tissue tears. In total, we analysed 15-30 cells from each mouse (*n* = 15-30) from a total of 3-6 mice (*N* = 3-6).

To analyse various morphological parameters, we followed a systematic protocol developed during this thesis and adapted from others [181,215,216]. First, the image was transformed to 8-bit grayscale (*Image* > *type* > *8-bit*) and pre-processed to reduce background noise and enhance contrast (*Image* > *Adjust* > *Bright/Contrast* and *Process* > *Math* >*Subtract,* respectively*)*. Second, images were binarized by applying a pre-established threshold (*Image* > *Adjust* > *Threshold* > *Dark background*). To obtain a cell image consisting of a single, continuous set of pixels, we used several tools to eliminate extraneous pixels that did not correspond to cells (*Process* > *Noise* > *Remove outliers* and *Process* > *Noise* > *Despeckle*). In cases where the original image contained a significant amount of background noise, we performed manual edits. We cleared some pixels to separate branches belonging to neighbouring cells and added pixels to connect processes from the selected cell. This precise step was carefully carried out under the view of the original image of the cell, with careful attention to avoid bias. Finally, individual cells were cropped and saved to be analysed.

- **Morphometric analyses**

Once the images were processed, Skeleton Analysis, Fractal Analysis, and Particles Analysis were conducted.

- *Skeleton Analysis*

This tool is used to study the complexity of the cell skeleton. This plugin [217] “tags all pixels/voxels in a skeleton image and then counts all its junctions, triple and quadruple points, and branches, while measuring their average and maximum length” (extract from user manual). From its several measurements, we evaluated the number of branches, number of junctions, and maximum branch length (Figure 26a,b). First, images were skeletonized (*Process* > *Binary* > *Skeletonize)* and the skeletonized image was run

through the plugin AnalyzeSkeleton(2D/3D) (*Analyse* > *Skeleton* > *Analyse Skeleton (2D/3D)).*

Soma size was measured manually (Figure 26c).

- *Fractal Analysis*

Fractal Analysis [218] is “a modern approach that applies non-traditional mathematical concepts to describe patterns that cannot be easily understood using traditional Euclidean geometry” (extract from the user manual). This method is particularly useful for characterizing complex patterns or features that cannot be simply described with size or shape, as these traditional metrics often oversimplify the details. To perform Fractal Analysis, the Fraclac plugin was employed (*Plugins* > *Fractal Analysis* > *Fraclac).* The box-counting analysis was set up with the following steps: (1) we selected *BC* window on the Fraclac toolbar and (2) set number of positions to 4 in the *Grid Design* option. In the same window, (3) we navigated to *Graphics Options,* disabled *colour code* option, and (4) enabled *bounding circle* and *convex hull* options. Finally, (5) we pressed *OK* to save the configuration. Then, for each independent cell under analysis, (6) we used the *rectangle selection* from the tool main bar to create a rectangle around the cell. Finally, (7) we clicked the *scan* button on the Fraclac toolbar to run the box-counting scan. The scan generated three windows with data outputs: *Hull and Circle Results*, *Box Count Summary File*, and *Scan Types*. For the purposes of this thesis, we discarded the *Scan Types* window and selected the following parameters from the other two:

- Perimeter: the total length of the boundary of the shape (Figure 26d).

- Area: the extent of the surface of the cell (Figure 26e).

- Circularity: it measures how closely the shape of an object resembles a circle. It is calculated as $(4\pi \times \text{cell area}) / (\text{cell perimeter})^2$. The circularity value of a perfect circle is 1 (Figure 26f).

- Convex hull span ratio: it measures the ratio of the axes of the convex hull from major to minor, providing insight into the elongation or elongation of the enclosed shape (Figure 26g).

- Convex hull area (CHA): refers to the area containing the entire cell shape enclosed by the smallest convex polygon (one in which all interior angles are smaller than 180°) (Figure 26h).

- Fractal dimension (D): Without getting too technical, fractal dimension (D) is a statistical index of complexity that assesses the inherent scaling properties in biological forms or events. Rather than measuring traditional attributes like length, width, height, or density, it quantifies the scale-invariant details within a pattern. To note, a simple straight line yields a D of 1.00, and the greater the complexity of the pattern, the higher the D. In our context we use D to identify and quantify the complexity of microglial forms, ranging from simple rounded shapes to more intricate branched structures (Figure 26i) [215].

- Lacunarity (Λ): This parameter is used to measure the heterogeneity or the degree of translational and rotational invariance within a shape. A low Λ value indicates homogeneity, suggesting that various parts of an image exhibit similar variances. Conversely, high Λ measurements infer heterogeneity, indicating that the image contains numerous gaps or lacunas of varying sizes (Figure 26j) [215].

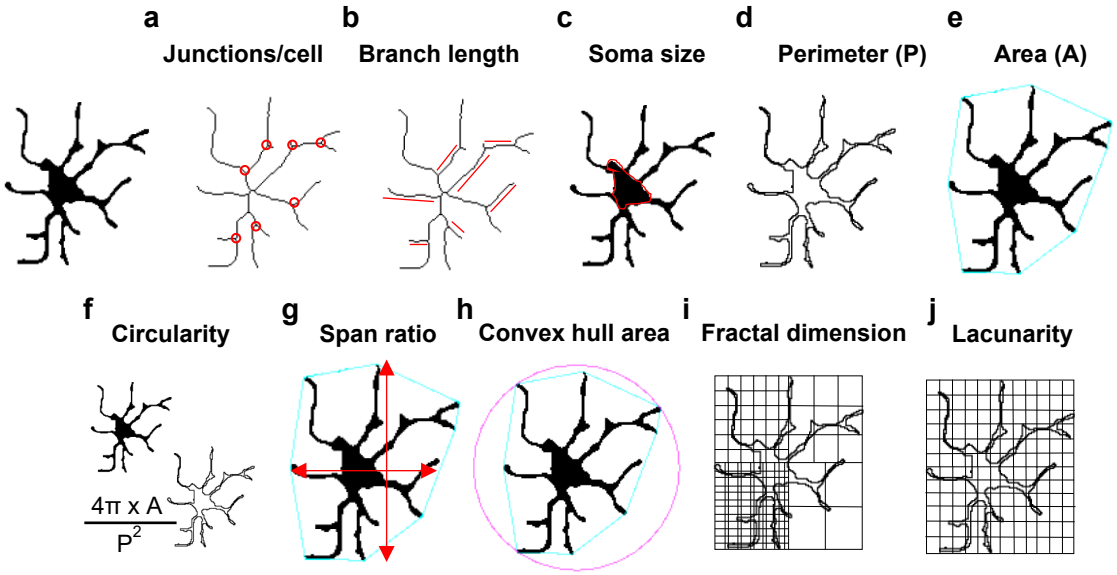

Figure 26: Schematic representation of the parameters used to analyse the morphology of the microglia and astrocytes. Junctions/cell (**a**) and branch length (**b**) were analysed with Skeleton Analysis. Soma size (**c**), perimeter (**d**), area (**e**), circularity (**f**) -using the area and perimeter calculated before-, span ratio (**g**), convex hull area (**h**), fractal dimension (**i**), and lacunarity (**j**) were analysed with Fractal Analysis.

- *Other analysis*

The cell counter plugin was used to quantify the number of cells of a selected ROI *(Plugins > Analyse > Cell counter).* To quantify area or vascular density we used the Analyse Particles tool (*Analyse > Analyse Particles*) selecting the *Summarize* option.

Finally, to assess ZO-1 coverage we followed these steps: (1) pre-processing and (2) binarizing the images as described above, (3) selecting the Colocalization Highlighter Plugin (*Plugins* > *Additional Plugins* > *Colocalization Highlighter*) and the *Colocalized points 8-bits* option. Then, to measure the % of the area covered by ZO-1, (4) the % of area occupied in the image corresponding to CD31, (5) ZO-1, and (6) the colocalized points 8-bits image was measured. Finally, (7) the percentage obtained from the colocalized points 8-bits image was divided by the percentage of the area occupied by ZO-1. The resulting percentage represents the proportion of the total vessel area covered by ZO-1.

3.10. Blood sampling

To determine inflammatory factors, blood was collected by cardiac puncture just before the sacrifice. To do so, a 23 g needle was gently introduced into the ventricle and blood was slowly withdrawn to prevent heart collapse. Approximately 0.5-1 ml of blood can be obtained through this method in a standard mouse of 25 g. Then, blood was allowed to clot for 2 h at room temperature (RT) and then centrifuged at 2,000 rpm for 10 min. After centrifugation, the serum was carefully pipetted off from the top. Particular care was taken to avoid disturbing the clot at the bottom of the tube and to prevent aspiration of any blood cells. The serum samples were stored at -20 ºC until ELISA was performed.

3.11. Determination of inflammatory factors

The concentration of inflammatory mediators from mouse serum or cells supernatants (see section 3.15) was determined by sandwich ELISA assay. Briefly, maxisorb plates (Millipore) were coated O/N at 4 ºC with the capture antibody anti-IL-6, anti-TNF-α, anti-IL-12 (BD Pharmigen) or anti-MCP-1 (PeproTech) dissolved in their specific buffer (Table 7). Next day, plates were washed twice with washing buffer and blocked with blocking buffer for 2 h at RT, and then incubated with the samples (70 µl) and the recombinant standards (10 ng/ml serially diluted in blocking buffer, Table 8) at 4 ºC O/N. Plates were then washed and biotinylated detection antibodies (Serotec) (Table 9) were added for 1 h at RT. After extensive washing, plates were incubated with avidin-streptavidin horseradish peroxidase (HRP) (Sigma) (1:500 in blocking buffer) for 1 h. Finally, plates were extensively washed again and developed with 0.1 M of 2,2′-azino-bis(3-ethylbenzothiazoline-6-sulfonic acid) (ABTS) (Sigma) and 0.03 % of H_2O_2 at RT in darkness. Absorbance was measured after some minutes at 405 nm with a VersaMax spectrophotometer (Molecular Devices). Concentrations were determined according to the standard curve generated at the same time. For nitrite quantification, equal volumes of

serum/culture supernatants and Griess reagents (0.1 % N-[naphthyl]ethylenediamine dihydrochloride in water and 1 % sulphanilamide in 5 % H_3PO_4) were loaded into a 96-well plate. Absorbance was measured at 540 nm in a spectrophotometer and the amount of nitrite was calculated from a $NaNO_2$ standard curve.

Cortistatin levels in serum/culture supernatants were determined using a competitive Elisa kit (Phoenix Pharmaceutics) following the manufacturer's instructions.

Capture antibodies	Company	Catalogue number	Stock concentration	Working dilution	Buffer
Anti-IL-6	BD Pharmigen	554400	0.5 mg/ml	2 µg/ml	pH 9
Anti-TNF-α	BD Pharmigen	551225	0.5 mg/ml	2 µg/ml	pH 6
Anti-MCP1	PeproTech	500-P113	0.5 mg/ml	2 µg/ml	pH 6
Anti-IL-12	BD	551219	1 mg/ml	4 µg/ml	pH 9

Table 7. Capture antibodies for ELISA. Table specifies company, catalogue number, stock concentration, working dilution, and their specific dissolving buffer.

Recombinant proteins	Company	Catalogue number
Anti-IL-6	BD Pharmigen	554582
Anti-TNF-α	PeproTech	315-01A
Anti-MCP1	PeproTech	PEP250-
Anti-IL-12	BD	554592

Table 8. Recombinant proteins for ELISA standard curve. Table specifies company and catalogue number. Stock concentration 5 ng/µl, working concentration 10 ng/ml.

Biotinylated antibodies	Company	Catalogue number	Stock dilution	Working dilution
Anti-IL-6	BD Pharmigen	554402	0.5 mg/ml	2 µg/ml

Anti-TNF-α	BD Pharmigen	554415	0.5 mg/ml	2 µg/ml
Anti-MCP1	PeproTech	500-P113Bt	0.5 mg/ml	1 µg/ml
Anti-IL-12	BD	554476	0.5 mg/ml	2 µg/ml

Table 9. Biotinylated antibodies for ELISA. Table specifies company, catalogue number, stock concentration, and working dilution.

3.12. Cell culture

To assess the role of cortistatin in brain endothelium barrier dynamics, we established an *in vitro* BBB model using different mouse and human cell lines, along with primary cells isolated from cortistatin-deficient mice. This section provides a detailed explanation of their culture or isolation processes. Cell culture media details are provided in section 3.3.

- **b.End5 cells**

The mouse brain endothelioma cell line b.End5 (Sigma-Aldrich, #96091930) was used to set up the conditions for the BBB *in vitro* model. For all experiments, b.End5 cells were seeded in b.End5 medium and used between passages 20 and 24, with changes of the medium every 2-3 days. Before procedures, adherent cells were rinsed in 1× PBS and detached by adding 0.1 % trypsin-EDTA, followed by the addition of an equal volume of fresh medium. The cell suspensions were centrifuged for 5 min at 150 rcf. The supernatant was then removed and cells were resuspended in fresh medium, counted, and allowed to grow at 37 ºC and 5 % CO_2 in a humidified incubator.

- **Isolation of mouse brain endothelial cells**

To isolate BECs from mouse brain microvasculature, we followed a dissociation protocol with some modifications [219] (Figure 27). Briefly, *Cort*$^{+/+}$, *Cort*$^{+/-}$, and *Cort*$^{-/-}$ 8-week-old mice were sacrificed by CO_2 inhalation. Brains were collected on ice under a laminar flow cabinet (olfactory bulbs and cerebellum were discarded), and gently dissected into smaller pieces using sterile chilled blades (VWR). The diced tissue of each brain was pelleted in ice-cold D-PBS solution (Gibco) at 290 rcf for 5 min at 4 ºC, and enzymatically dissociated for 70 min at 37 ºC using a solution containing 633.3 µl of buffer Z, 16.65 µl of enzyme P, 6.65 µl of buffer Y and 3.32 µl of enzyme A from the Adult Brain Dissociation Kit (Miltenyi Biotec), combined with DNAase I (42.5 µg/ml) (Roche). The homogenate was then mechanically dissociated through 19- and 21-gauge needles. Next, to remove myelin, the homogenate was gently mixed with 23 % BSA (ratio 1:1) and centrifuged at 1360 rcf 10 min at 4 ºC. Subsequently, cells from the pellet were washed by adding BECs medium,

centrifugated (290 rcf, 5 min, 4 ºC), and finally resuspended in fresh medium. Cells were counted and distributed onto rat tail collagen I-coated plates (BD Biosciences) (50 µg/ml), extensively washed after 19 h of culture to remove red blood cells and debris, and then incubated for 5 h with BECs medium. Next, fresh medium supplemented with puromycin (8 µg/ml) (Gibco) was added for 60 h (with changes every 24 h) to prevent the growth of non-endothelial cells. Finally, cells were allowed to reach confluency at 37 ºC and 5 % CO_2 in a humidified incubator, and BECs medium (w/o puromycin) was replaced every 2 days. Prior to cell seeding for experiments, adherent BECs were trypsinized (0.05 % trypsin-EDTA), centrifuged for 5 min at 290 rcf, and brought to suspension as described above for b.End5 cells.

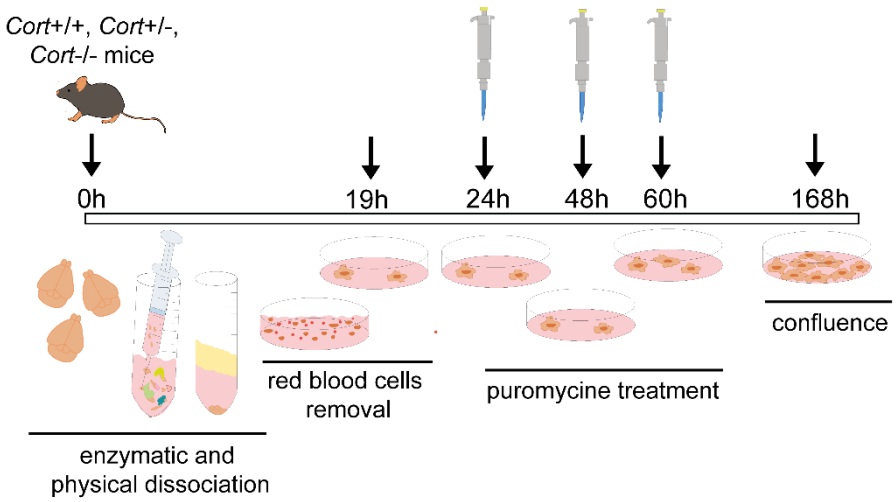

Figure 27. **Graphical representation of the isolation and culture of primary BECs from mouse brain microvasculature.** In brief, *Cort*$^{+/+}$, *Cort*$^{+/-}$, and *Cort*$^{-/-}$ 8-week-old mice were sacrificed by CO_2 inhalation. Brains were collected and enzymatically and physically dissociated. Next, myelin was removed and cells from the pellet were washed and resuspended in fresh medium. Following this, cells were distributed onto rat tail collagen I-coated plates. After 19 h, cells were extensively washed and incubated for 5 h with BECs medium. Next, fresh medium supplemented with puromycin was added for 60 h (with changes every 24 h) to prevent the growth of non-endothelial cells. Finally, cells were allowed to reach confluency over approximately 1 week.

- **Human brain endothelial cells (hBLECs)**

Human brain endothelial cells were generated by differentiating cord blood-derived hematopoietic cells into ECs, followed by the induction of BBB properties by co-culturing them with pericytes. Briefly, $CD34^+$-derived ECs and bovine pericytes (both kindly provided by Prof. Cecchelli) were defrosted in gelatin-coated Petri dishes (Corning). After 48 h, pericytes were plated in gelatin-coated 12-well plates (5 x 10^4 cells/well). Subsequently, ECs (8 x 10^4 cells/well) were seeded in 12-well transwell polycarbonate inserts (1.13 cm^2, 0.4 µm pore size, Corning) previously coated with matrigel (Corning), and placed above

the pericytes-seeded plates. In the co-culture, sECM supplemented with 5 % FBS was used for both cell lines and changed every 2-3 days. After 6-8 days of co-culture, ECs acquired BBB properties (renamed accordingly as human brain-like endothelial cells, hBLECs), and were used in permeability assays.

3.13. Brain endothelium barrier model

To establish the brain endothelium barrier model, mouse ECs (b.End5, BECs) (5 x 10^4 cells/well) were seeded onto the top of a PET transwell insert (0.33 cm^2, 8 µm pore size, Corning) previously coated with rat collagen-I (50 µg/ml) and fibronectin (20 µg/ml, Invitrogen) (Figure 28). For hBLECs, inserts containing cells from co-cultures were placed into new wells without pericytes. Cells were grown in their respective culture media until they reached confluence. To assure the establishment of endothelial integrity, we measured the TEER using an EVOM2 Epithelial Voltohmmeter (World Precision Instruments). Briefly, the chop electrode was carefully introduced into the transwell so that the largest chop was in contact with the medium below, and the shorter one with the endothelial monolayer. TEER measurements were conducted in at least three random transwells in each assay before any experimental procedures. We considered that barrier integrity was established when TEER readings were above 200 Ω/cm^2. In particular, TEER measurements were 550 ± 25.17 Ω x cm^2 for b.End5, 585.7 ± 22.15 Ω x cm^2 for BECs isolated from *Cort*$^{+/+}$ mice, 505.5 ± 27.78 Ω x cm^2 for *Cort*$^{+/-}$ BECs, and 525 ± 25.28 Ω x cm^2 for *Cort*$^{-/-}$ BECs. Conversely, human barrier integrity was evaluated before procedures by measuring the permeability coefficient (Pc, described in section 3.15) of Lucifer yellow. 500 µL of Lucifer yellow (25 µM) in Ringer HEPES (Thermo Fisher Scientific) was added to the donor compartment, while 1,500 µL of Ringer HEPES was introduced into the acceptor compartment. The amount of extravasated protein was quantified using a fluorimeter (λex: 428 nm, λem: 536 nm). We considered that barrier integrity was established when Pc was below 15x10^{-6} cm/s.

3.14. Establishment of brain injury-like conditions

To investigate the role of cortistatin in different neuroinflammatory insults related to brain ischemia (*i.e.,* neuroinflammation, or oxygen or nutrients deficiency), mouse ECs were exposed to bacterial lipopolysaccharide (LPS) inflammation, glucose deprivation (GD), or oxygen-glucose deprivation and reoxygenation (OGD-R), while hBLECs were incubated in a hypoxic environment as well as in OGD-R conditions (Figure 28). For inflammatory damage, LPS from *E. coli* 055:B5 (10 µg/ml, Sigma) was added to the cells for 24 h. For GD conditions, b.End5 were washed twice and placed in glucose and serum-free b.End5

culture medium for 24 h. For OGD-R, mouse cells were placed in their respective glucose and serum-free culture media and incubated in a sealed hypoxic workstation (1 % O_2, 99 % N_2, 5 % CO_2, 37 ºC; In vivO$_2$, Ruskin Technologies) for 4 h. Immediately after OGD, cultures were returned to normoxic (NX) and normoglycemic (NG) conditions (21 % O_2, 5.5 mM glucose), and incubated in 10% FBS medium for 20 h to mimic reperfusion. hBLECs were incubated under hypoxic conditions (HPX, 1 % O_2) for 4 h in normal sECM/5 % FBS medium and then returned to control conditions for 20 h (HPX-R). When needed, mouse cortistatin-29 or human cortistatin-17 (CST, Bachem) (100 nM) was added for 24 h immediately after LPS and GD, or for 20 h during reoxygenation in OGD-R or HPX-R conditions. For each cell type, controls were incubated simultaneously in normal medium in a NX/NG environment (95 % O_2 and 5 % CO_2 at 37 ºC).

3.15. Endothelial permeability *in vitro* models

After LPS, GD, OGD-R, or HPX-R incubations, the influx of Evans Blue-Albumin (Sigma, EBA, 67 kDa) and sodium fluorescein (Sigma, NaF, 376 Da) was determined as previously described [220]. Briefly, luminal culture medium from mouse/human ECs was collected to perform sandwich and competitive ELISA, and inserts were washed with permeability buffer and transferred to new 24 o 12-well plates (for mouse or human cells, respectively) with fresh buffer in the abluminal compartments (600 µl or 1,250 µl, mouse or human cells, respectively). In the inserts, luminal culture medium was replaced by 100 µl or 300 µl (mouse or human transwells, respectively) of buffer containing 4% bovine serum albumin mixed with 0.67 mg/ml Evans blue (EB) dye and 100 µg/ml NaF. After 60 min, the samples were collected from the abluminal side. NaF concentrations were determined by measuring fluorescence intensity with a microplate reader (TECAN) at 485 nm-Ex(λ); 535 nm-Em(λ). EBA concentration was measured with a spectrophotometer (VERSAmax Microplate Reader) at 630 nm and quantified according to a standard curve (Figure 28).

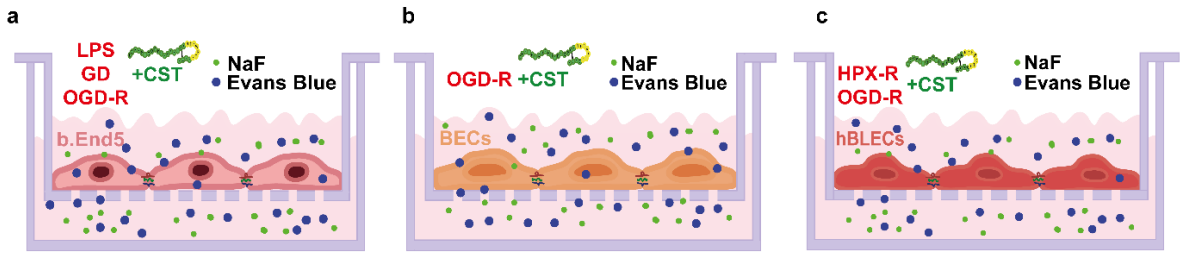

Figure 28. Schematic drawing of the *in vitro* model and description of the brain injury-like conditions. The mouse brain endothelial cell line b.End5 (**a**) were exposed to bacterial lipopolysaccharide (LPS) inflammation, glucose deprivation (GD), or oxygen-glucose deprivation and reoxygenation (OGD-R) while primary BECs (**b**) were only exposed to OGD-R. Human brain

endothelial cells (hBLECs) (**c**) were incubated in a hypoxic-reperfusion (HPX-R) environment as well as in OGD-R conditions. For inflammatory damage, LPS (10 µg/ml) was added for 24 h. For GD conditions, b.End5 were placed in glucose and serum-free b.End5 culture medium for 24 h. For OGD-R, cells were placed in their respective glucose and serum-free culture media and incubated in hypoxia (1% O_2) for 4 h. For reperfusion, cultures were returned to normoxic (NX) and normoglycemic (NG) conditions (21 % O_2, 5.5 mM glucose) for 20 h. For hypoxia (1 % O_2) cells were incubated for 4 h in normal sECM/5 % FBS medium and then returned to control conditions for 20 h. Mouse cortistatin-29 or human cortistatin-17 (CST) (100 nM) was added for 24 h immediately after LPS and GD, or for 20 h during reoxygenation in OGD-R or HPX-R conditions. For each cell type, controls were incubated simultaneously in normal medium in a NX/NG environment. After LPS, GD, OGD-R, or HPX-R incubations, the influx of EBA and NaF was evaluated.

The permeability coefficient (Pc) of the tracer was calculated as cm/min of the tracer diffusing from the luminal to the abluminal side as $Pc=(C_A/t)*(1/A)*(V/C_L)$. C_A is the tracer concentration in the abluminal side, t is the time (60 min), A is the total surface of the insert membrane, V is the final volume, and C_L is the initial known tracer concentration in the luminal side. To avoid inter-variability between assays, permeability was finally represented as the index (%) between the Pc of each well and the Pc of the control transwell (maximal influx of each tracer in an ECs-free coated insert).

3.16. Immunocytochemistry (transwells)

After exposure to insults, transwells were extensively washed with PBS to remove any leftover tracer. Then, transwells were fixed with 4 % paraformaldehyde (Sigma) for 10 min at RT. After washing with PBS, cells were incubated with 30 mM glycine (Sigma) for 5 min, washed again, and permeabilized with PBS containing 0.1 % Triton X-100 (Aplichem) for 15 min at RT. Cells were then blocked with 10 % goat serum, 3 % BSA and 0.1 % Triton X-100 in PBS for 60 min at RT, and O/N incubated (4 ºC) with primary polyclonal antibodies (1:100) rabbit anti-mouse ZO-1, claudin-1, claudin-5 (tight-junctions) (all from Thermo Fisher Scientific), and VE-cadherin (adherens-junction). For F-actin, rhodamine-phalloidin-conjugated antibody (Invitrogen) was used (1:250) (Table 6). Next, cells were washed with PBS followed by 60 min incubation at RT with secondary Alexa Fluor™ 488/594-conjugated donkey/goat anti-rabbit IgG antibody (1:1,000, Invitrogen). After repeated washes, nuclei were DAPI-counterstained (1 µg/ml) for 5 min RT, rinsed with PBS, and mounted with Mowiol (Sigma). Cells were imaged at 63x magnification in a LEICA DMi8 S Platform Life-cell microscope, selecting different ROIs with the same exposure parameters in at least three independent experiments. Image fluorescence analyses (mean grey value) were performed with ImageJ Fiji free software.

3.17. Transendothelial migration assay

To determine the immune cell extravasation across the brain endothelium, a transendothelial migration assay was performed. Macrophages and T cells were isolated from 8-week-old *Cort*$^{+/+}$ mice. Cell culture medium is detailed in section 3.3.

- **Macrophages isolation:**

Macrophages were obtained by peritoneal lavage. First, mice were euthanized by CO_2 inhalation. The outer skin of the peritoneum was cut using sterile surgical scissors and forceps, and it was pulled back to expose the inner skin. Next, peritoneum was gently grasped and lifted so 10 ml of macrophage medium was carefully injected into the peritoneal cavity. The abdominal cavity was massaged for 1 min to dislodge peritoneal cells. Great care was taken to avoid puncturing the intestine or other abdominal organs to prevent contamination. Finally, medium was drawn back up and collected with a new syringe. The collected medium, containing peritoneal macrophages and peritoneal cells [221,222] was spun down at 1,500 rpm for 10 min at 4 ºC, counted and directly added to the transwells in contact with BECs.

- **T cells isolation**

For T cells, the spleen was collected from the same mice in ice and carefully ground with the frosted sides of two slides onto a 100 mm culture dish. After 5 min on ice, cell suspension was taken (pellet was discarded) and centrifuged at 400 rcf for 10 min at 4 ºC. Next, pellet was treated with Ack buffer for 10 min at RT to lyse red blood cells. RPMI-T cells medium was then added, and cells were centrifuged again at 400 rcf for 10 min at RT. Finally, cells were passed through a 40 µm cell strainer (Corning) and seeded for 2 h in a 100 mm culture dish to separate adherent cells. Finally, the supernatant was taken and T cells were counted and added to the upper compartment of the transwells in contact with BECs.

- **Transendothelial migration assay**

Immune migration was evaluated in a BECs monolayer grown onto coated transwells (Figure 29), as described above. 24 h before the assay, cells were activated with TNF-α (10 ng/ml, BD Pharmigen). On the day of the experiment, transwells were transferred to a new 24-well culture plate containing 1 % FBS medium in the bottom side supplemented with MCP-1 (50 µg/ml, Bionova) or IP-10 (50 µg/ml, Bionova) for macrophages and T cells, respectively. Immediately, immune cells (2 x 10^5 / transwell) were added to the upper side of the transwell in contact with BECs and mouse cortistatin-29 (100 nM) was added to both sides. After 24 h, migrated T cells were counted on the bottom side using a Neubauer

chamber (VWR). Macrophages were identified at the bottom of the well after plate fixation and DAPI staining. As a positive control of migration, macrophages/T cells were incubated in a BECs-free coated transwell. The number of migrated cells was represented as the percentage of immune migrated cells *vs* the positive control.

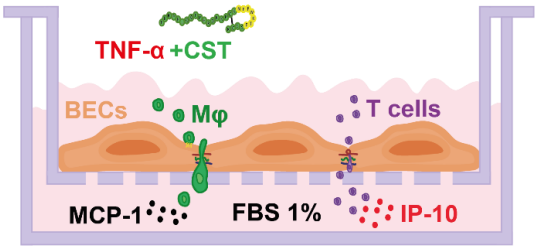

Figure 29. Graphical representation of the transendothelial migration assay. Macrophages/T cells were incubated for 24 h at the top of BECs covered inserts, previously activated with TNF-α (10 ng/ml, 24 h). The migration assay was performed using MCP-1 (50 µg/ml) or IP-10 (50 µg/ml), as macrophages and T-cell chemoattractants, respectively. CST (100 nM) was applied when indicated.

3.18. *In vivo* blood-brain barrier permeability assay

To further analyse BBB integrity in wild-type and cortistatin-deficient mice, we conducted a mild-neuroinflammation model by intraperitoneally injecting LPS from *E.coli* 055:B5 (6 mg/kg, Sigma). Immediately following LPS injection, 1 nmol of CST-29 (in PBS, Bachem) was intraperitoneally administered. 5 h after LPS or LPS + CST administration, EB (2 % in saline, 4 ml/kg) was injected through the tail vein for 1 h. PBS was administered in control mice. Mice were sacrificed by pentobarbital intraperitoneal injection and intracardially perfused with PBS. Brains were then collected, weighted, and minced in 700 µl of N,N-dimethylformamide (#) at 55 ºC for 24 h, following previously published studies [223]. Subsequently, brains were centrifuged (12,000 rpm, 30 min) and supernatants were collected. EB absorbance was measured in a spectrophotometer at 620 nm. The quantitative evaluation of the dye was performed by quantifying the concentration of EB based on a standard curve of the dye in formamide. Data were expressed as micrograms of the EB per mg or brain tissue.

3.19. RNA extraction and determination of gene expression

For RNA extraction and determination of gene expression, mouse b.End5 and BECs were incubated under the same conditions as described previously, but in 6-well plates. For human cells, RNA was extracted directly from the transwells. TriPure reagent (Roche) was added to the cells (approximately 500 µl for each 34 mm^2). The obtained cell lysate was passed through a pipette several times and transferred to a new tube. Next, samples were

incubated in ice for at least 15 min. Following that, they were vigorously mixed with chloroform and incubated for 7 min on ice. Samples were then centrifugated at 12,000 g for 15 min at 4 ºC, and the upper aqueous phase was carefully transferred to a new tube. The transferred material was incubated with isopropanol for 15 min at RT, and subsequently left at -20 ºC O/N. The next day, samples were centrifuged again at 12,000 g for 10 min at 4 ºC, and the supernatant was discarded. Precipitated RNA was washed with 70 % ethanol and centrifuged at 7500 g for 5 min at 4 ºC. The washing procedure was repeated until all residual ethanol was removed. Finally, samples were dried on ice, resuspended in RNAse-free water (previously heated to 60 ºC) (Biorad, and stored at -80 ºC until use. RNA quantification was carried out by measuring absorbance using a Nanodrop 100 spectrophotometer (Thermo Scientific).

- **Reverse transcription**

To perform reverse transcription (*i.e.,* generating cDNA from RNA via reverse transcriptase), we employed the RevertAid First Strand cDNA Synthesis Kit (ThermoFisher), following the manufacturer's instructions. First, to remove any genomic DNA leftover from the samples, 1 µg of RNA was incubated with 1 µl of DNAse (1 U/µl) along with 1 µl of reaction buffer 10x and nuclease-free water up to 10 µl, for 15 min at RT. The reaction was subsequently inactivated using 1 µl of stop solution (50mM EDTA) for 5 min at 65 ºC.

Following this, the reverse transcription reaction was conducted. Specifically, the resulting samples were incubated with 1 µl of random hexamer primers (100 µM), 2 µl of deoxynucleotide (dNTP) mix (10 mM), 4 µl of buffer reaction 5x, 1 µl of RevertAid RT enzyme (200 U/µl) and 1 µl of the Ribolock RNAse inhibitor (200 U/µl), in a final volume of 20 µl. Reverse transcription process was carried out in a CFX Connect PCR System (Biorad) under the following conditions: incubation at 25 ºC/5 min, reverse transcription at 42 ºC/60 min, inactivation at 70 ºC/5 min. The resulting product, cDNA, was diluted with RNAse-free water to obtain a final concentration of 15 ng/µl of RNA and stored at -20 ºC before use.

- **Real-time qPCR**

To assess the expression of cortistatin-somatostatin system and to validate a set of differentially expressed genes that were selected from our transcriptomic studies, we employed real-time qPCR. Specific primers for mouse/human transcripts for each technique are listed in Table 10.

First, the cDNA corresponding to 20 ng of RNA was added to the SensiFast Sybr No-Rox kit 1x (Bioscience), as well as the forward and reverse primers for each gene (Table 10), and nuclease-free water until a final volume of 20 µl. The reaction was performed on the thermocycler CFX96 (BioRad) using the following conditions: 94 ºC/5 min (polymerase activation) followed by 40 cycles at 94 ºC/30 s (denaturalization), 60 ºC/30 s (primer annealing), and 72 ºC/30 s (extension). For quantification analysis, the comparative threshold cycle (Ct) method was used. The Ct values of each gene were normalized to the Ct value of the housekeeping gene *rplp0* in each PCR reaction. Fold change was estimated with the ΔΔCt method.

Gene	Primer sequence (5'-3')
Rplp0 (NM_007475.5)	Fw: TGCACTCTCGCTTTCTGGAG Rv: CTGACTTGGTTGCTTTGGCG
Ghsr (NM_177330.4)	Fw: TCAGGGACCAGAACCACAAA Rv: CCAGCAGAGGATGAAAGCAA
Cort (NM_001420759.1)	Fw: GCCTTCTGACTTTCCTTGCC Rv: GAAAGCTCCCCGCTGATTGA
Sst (NM_009215.2)	Fw: TCTGCATCGTCCTGGCTTT Rv: CTTGGCCAGTTCCTGTTTCC
Sstr1 (NM_001411890.1)	Fw:TGCCCTTTCTGGTCACTTCC Rv:AGCGGTCCACACTAAGCACA
Sstr2 (NM_009217.5)	Fw:TGATCCTCACCTATGCCAACA Rv:CTGCCTTGACCAAGCAAAGA
Sstr3 (NM_001411768.1)	Fw:GCCTTCTTCGGCCTCTACTT Rv:GAATGCGACGTGATGGTCTT
Sstr4 (NM_009219.3)	Fw:AGGCTCGTGCTAATGGTGGT Rv:GGATGAGGGACACATGGTTG
Sstr5 (NM_011425.3)	Fw:ACCCCCTGCTCTATGGCTTT Rv:GCTCTATGGCATCTGCATCCT
Pdgfb (NM_001411619.1)	Fw: CCTGCAGTGAACTTTGGAGC Rv: AGCTTTCCAACTCGACTCCG

Slco4a1 (NM_001355218.1)	Fw: CCGGGTTCGTGGGAAGATAG Rv: ACACATACTGCACCTCACGG
Cldn1 (NM_016674.4)	Fw: GACTGTGGATGTCCTGCGTT Rv: TCATGCCAATGGTGGACACA
Col1a2 (NM_007743.3)	Fw: TCTCCTGGAAATGTTGGCCCATCT Rv: AATCCGATGTTGCCAGCTTCACCT
Pdpn (NM_010329.3)	Fw: TGGTGCCCCCAGGTATAGAA Rv: GTTGTCTGCGTTTCATCCCC
Rab6b (NM_173781.4)	Fw: GGAGATTTTGGGAACCCGCT Rv: TCGGATGTAGCTGGGGATCA
Krt8 (NM_031170.2)	Fw: CAAGGTGGAACTAGAGTCCCG Rv: CTCGTACTGGGCACGAACTTC
Cdh1 (NM_009864.3)	Fw: GAAGGCTTGAGCACAACAGG Rv: ACTGCTGGTCAGGATCGTTG
Klra4 (NM_001252577.2)	Fw: ACCCACCTCACTTCAGAAATCACT Rv: CAGGCTTCCGTGTCTCCTTG
hCort (NM_001302.5)	Fw: CTCCAGTCAGCCCACAAGAT Rv: CAAGCGAGGAAAGTCAGGA
hSst (NM_001048.4)	Fw: AACCCAACCAGACGGAGAA Rv: TAGCCGGGTTTGAGTTAGCA
hRplp0 (NM_053275.4)	Fw: CCTGTCTCTCCTCAGTGACA Rv: GCTTGGAGCCCACATTGTCT

Table 10. Sequence of primers used for real-time PCR quantifications. Rv: reverse; Fw: forward. *Rplp0*, ribosomal protein lateral stalk subunit P0; *Ghsr,* growth hormone secretagogue receptor; *Cort*, cortistatin; *Sst*, somatostatin; *Sstr1***,** somatostatin receptor 1**;** *Sstr2*, somatostatin receptor 2**;** *Sstr3*, somatostatin receptor 3**;** *Sstr4*, somatostatin receptor type 4**;** *Sstr5*, somatostatin receptor 5**;** *Pdgfb*, platelet-derived growth factor subunit b; *Slco4a1*, solute carrier organic anion transporter family member 4a1; *Cldn1*, claudin1; *Col1a2*, collagen type I alpha 2 chain; *Pdpn*, podoplanin; *Rab6b*, ras-related protein Rab-6b; *Krt8*, keratin 8; *Cdh1*, E-cadherin; *Klra4*, killer cell lectin-like receptor, subfamily A, member 4. All the primers are for mouse transcripts except for *hCort*, *hSst*, and *hRplp0* (for human sequences).

3.20. Next-generation transcriptome sequencing (RNA-seq)

To study the molecular pathways underlying the endogenous role of cortistatin in BECs, we conducted a next-generation transcriptome sequencing assay (RNA-seq).

- **Library preparation and sequencing**

For this experiment, RNA was extracted as previously described from primary *Cort*$^{+/+}$ and *Cort*$^{-/-}$ BECs cultures exposed to NX/NG or OGD-R conditions for 24 h. Three replicates were used in each case. Samples were sent to the Genomics Core Service (IPBLN), where library preparation and sequencing was conducted. First, RNA was quantified by Nanodrop 1,000 and RNA quality was assessed by electrophoresis in a Bioanalyzer RNA 6,000 Nano-chip (Agilent Technologies). Quality, expressed as the RNA Integrity Number (RIN), was > 9.9 in all samples.

Next, to prepare mRNA libraries, 200 ng of mRNA were utilized using the Illumina stranded mRNA Prep Ligation kit (Illumina), following the manufacturer's instructions. Quality and size distribution of mRNA libraries were validated by a Bioanalyzer High Sensitivity DNA assay (Agilent Technologies) and concentration was measured on the Qubit fluorometer (ThermoFisher). Final libraries were pooled in equimolecular ratios and then diluted/denatured as recommended by the Illumina NextSeq 500 library preparation guide. The sequencing was conducted on a NextSeq 500 sequencer, generating 75x2nt paired end reads. The average number of sequencing reads with a quality threshold of Q> 30 was 91.5 %. Our results included a mean GC content of 51.3 %, comprising 40,407,022 paired end reads, and > 28,000 transcripts on average.

- **Bioinformatics analyses**

The sequencing reads obtained were sent to the Bioinformatics Core Service (IPBLN). Data were analysed using the software reanalyzerGSE [224] to apply the RNA-seq analysis pipeline to obtain differentially expressed genes (DEGs). and to specifically prevent the exclusion of low expressed genes with potential biological relevance, such as cortistatin. The software reanalyzerGSE is based on the miARma-Seq pipeline [225] to perform the quality control, alignment and quantification steps, together with the edgeR R package [226] to obtain DEGs. Default parameters were used, except for the "bin" threshold when filtering low expressed genes. *Mus musculus* primary assembly GRCm39 was provided as the reference genome, and Gencode annotation version M28 was used. An average score of 86.7% unique mapped reads were obtained and the expression per gene in each sample was computed (reads per kilobase million, RPKM). To assess the replicability of the data, an approach based on both multidimensional scaling (Principal Coordinates Analysis, PCoA) and unsupervised hierarchical clustering of normalized data

was implemented. Both the different percentage of variability explained by each dimension and the grouping of samples may point to whether in a particular comparison the biological heterogeneity would cause the potential replicates to be in different group, which may obscure the differential expression. Therefore, only clear biological replicates in each of the independent comparisons were included. Two or more biological replicates were still available in all cases. DEGs with a False Discovery Rate (FDR) ≤ 0.05 were calculated by comparing: i) *Cort*$^{-/-}$ *vs* *Cort*$^{+/+}$ samples for each condition (NX/NG and OGD-R); ii) NX/NG *vs* OGD-R for each genotype (*Cort*$^{-/-}$ and *Cort*$^{+/+}$). The fold change (log_2FC) was used to evaluate the degree of expression change of each gene.

To investigate the potential effects and relevance of DEGs, functional enrichment analyses based on the Gene Ontology (GO) database were performed using the R packages ViSEAGO [227] and topGO [228], and the gene2go EntrezGene database [229,230]. The “elim” algorithm and the “fisher” statistic were performed. The terms corresponding to biological processes (BP), molecular functions (MF), and cellular components (CC) that were significantly overrepresented (P-value < 0.01) in each relevant group of DEGs were identified. The background used in all cases was the whole universe of transcripts with quantified expression. Unless otherwise specified, statistical tests and plots were performed in R using base [231] and Bioconductor [232] packages, mainly ggplot2 [233,234] and extensions, together with iheatmapr [235].

3.21. Statistical analysis

Data are expressed as the mean ± SEM. All experiments were randomized and blinded for researchers. The number of independent animals or cell cultures is shown (N) as well as the number of sections, cells, or structures analysed in each case (n). Statistical analysis was conducted using these independent values. Statistical differences comparing two groups were performed by using the unpaired Student's t test (for parametric data, and normal distribution) or the non-parametric Mann–Whitney U-test. For three or more groups with normal distribution and parametric data, one-way ANOVA with appropriate *post-hoc* tests for multiple comparisons were utilized (with a small number of data Bonferroni *post-hoc* test was preferentially used vs Tukey post-hoc test). Non-parametric data from three or more groups was analysed by Kruskal-Wallis test and Dunn *post-hoc* test. When standard deviations were assumed to be different, Brown-Forsythe and Welch ANOVA test were applied with Dunnett T3 *post-hoc* test. Spearman´s Rho non-parametric test was used for correlation studies. All analyses were performed using GraphPad Prism v8.3.0 software. We considered P-values < 0.05 (two-tailed) as significant.

3.22. Data availability

RNA-seq data is available in the GEO repository under accession number GSE207405 https://www.ncbi.nlm.nih.gov/geo/query/acc.cgi?acc=GSE207405.

4. Results

4. Results

Cortistatin has demonstrated immunomodulatory and neuroprotective properties playing a crucial role in modulating the glial neuroinflammatory response and regulating peripheral endothelium dynamics [144,146,179,182,236]. However, the role of cortistatin in the neuroimmune context of stroke pathophysiology is yet to be elucidated. To investigate the role of cortistatin in neurological damage, neuroinflammation, BBB dysfunction, and immune dysregulation associated with stroke, we conducted an *in vivo* stroke preclinical model (MCAO) in young and middle-aged wild-type and cortistatin-deficient mice. Additionally, we explored the potential therapeutic application of cortistatin and identified its most efficient therapeutic window. Furthermore, we studied the importance of cortistatin in brain endothelium using a BBB *in vitro* model subjected to OGD conditions. Of note, the study of the potential therapeutic role of cortistatin and its optimal time window was conducted at the Department of Fundamental Neurosciences at the University of Lausanne, Switzerland, while the remaining experiments were performed at the Institute of Parasitology and Biomedicine (IPBLN-CSIC).

4.1. Identification of the beneficial effect of cortistatin on an acute stroke model and determination of an efficient therapeutic window

To evaluate the potential therapeutic effect of cortistatin in ischemic stroke, we used a preclinical model based on the occlusion of the middle cerebral artery (MCAO), which is one of the best mirrors for this human condition. Regarding the time-dependent interactions involving glial dynamics, BBB disruption, and immune activation, the development of new therapies should carefully consider the distinct phases of ischemic stroke and determine the most effective timing for application. Taking into consideration the restricted time window for administering alteplase (< 4.5 h), the only FDA approved drug for stroke [7], we investigated whether cortistatin could exert beneficial effects beyond this limited timeframe. Therefore, we aimed to explore the potential therapeutic effect of cortistatin when administered 24h after reperfusion in an acute stroke model (late treatment, Figure 30a). Furthermore, we examined the impact of cortistatin in other temporal contexts during stroke development: immediate treatment post-MCAO, with cortistatin administered at 0 and 24 h post-reperfusion, affecting the neurodegenerative and neuroinflammatory responses immediately after reperfusion; or early treatment post-MCAO, with cortistatin administered at 4 and 24 h post-reperfusion, not affecting the early pathological processes associated with the first hours after hypoxia-reperfusion but regulating the progression of the pathology 4 h after reperfusion. For this, C57BL/6J mice

(10-12 weeks old) were subjected to the MCAO procedure and cortistatin was administered at the specified time points after reperfusion. Untreated MCAO control groups received injections of a saline solution at the same time points.

4.1.1. Cortistatin alleviates neurodegeneration in an acute stroke model only when administered at late time points

Stroke is characterized by neurological deficits particularly affecting motor function and coordination (assessed at 24-48 h after MCAO in the acute animal model) and cognition (memory and learning, evaluated from 7 days to weeks after MCAO). In our model, animals were sacrificed at an early timeframe (48 h post-MCAO). First, neurological score was determined, which analyses motor, sensory, reflex, and balance functions on a scale from 0 to 3 (modified from [207]). As depicted in Figure 30b, MCAO mice (saline-treated) showed a mean score between 0.5-1 (*i.e.,* slight motor incoordination, piloerection, and slight hypomobility). Surprisingly, the immediate treatment with cortistatin significantly worsened the score deficits, resulting in a mean score 1-2 (*i.e.,* moderate motor incoordination, intermittent circling, and tremor twitches). Conversely, early and late treatments did not demonstrate any impact on neurological deficits, exhibiting scores similar to those of the MCAO mice treated with saline (Figure 30b).

To further evaluate the neurological deficits in these animals, we conducted two behavioural tests: rotarod and wire-hanging test, to assess motor function, and muscle coordination and endurance, respectively (Figure 30c-h). In the rotarod test, mice latency to fall from the rod was measured 24 h before the surgery (baseline, BL), and 24 and 48 h post-surgery. As expected for MCAO mice, both rotarod and wire-hanging tests demonstrated a trend towards worsened performance at 24 h, with slight recovery in motor abilities at 48h post-MCAO (Figure 30c-h). Specifically in the rotarod, no significant differences were found when comparing cortistatin-treated and untreated mice at either 24 or 48 h post-MCAO (Figure 30c-e). In the wire-hanging test, MCAO mice exhibited a reduction in the number of scaping times while increasing the time for scaping and fall occurrences compared to healthy animals. Our results showed a similar trend for cortistatin-treated mice in the immediate (0 h + 24 h) and early treatment (4 h + 24 h) regarding the number of escaping times, the average time taken to escape, and the number of falls. (Figure 30f,g).

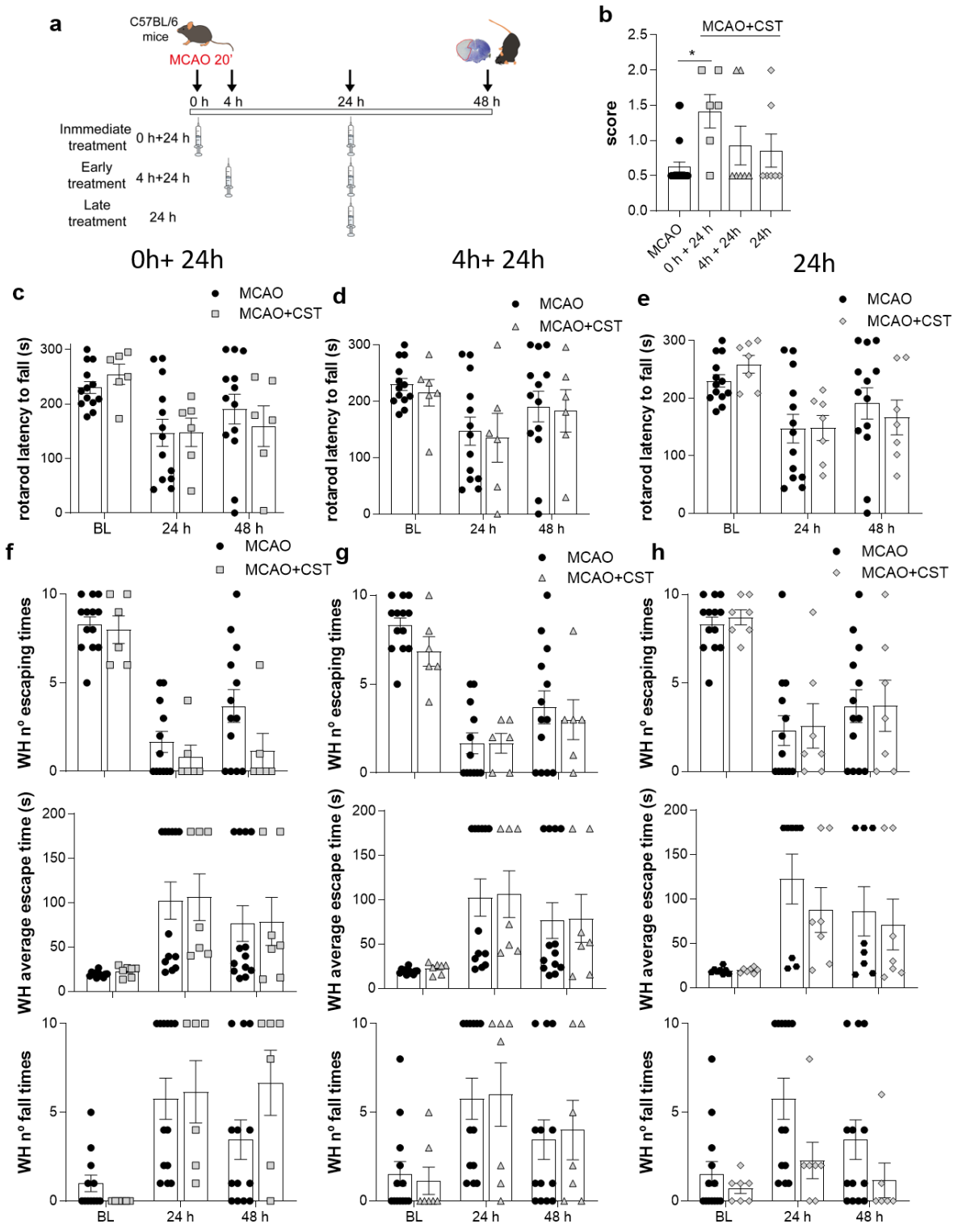

Figure 30. **Determination of the optimal time window for cortistatin administration. a.** Schematic representation of the timeline of the experiment. C57BL/6J mice were subjected to MCAO and treated with either saline solution (controls) or cortistatin (115 µg/kg) at 3 different time points: immediately after reperfusion (0 h + 24 h) (**c,f**), early after reperfusion (4 h + 24 h) (**d,g**), and at a later time (24 h) (**e,h**). **b**. Neurological score ranging from 0 to 3 was determined Behavioural performances were evaluated using the rotarod and the wire-hanging test. In rotarod test (**c-e**), latency to fall from the rod was recorded. In the wire-hanging test (**f-h**), the number of

escapes toward one of the posts, the average time taken to reach one of the posts, and the number of falls onto the pad, were measured. Data are the mean ± SEM. N = 6-13 mice/group from 3 independent experiments. *vs saline, *$p \leq 0.05$.

However, when cortistatin was administered 24 h post-MCAO, this treatment seemed to reduce the number of falling times and the time required to escape, despite not enhancing the number of successful escapes (Figure 30h). Interestingly, although not statistically significant, 48 h after MCAO, the group that received late treatment showed that the majority of mice (around 58%) lasted less than 50 s for escaping, with none falling more than 10 times. In contrast, 50% of the MCAO-mice needed more 50 s (with 40% of them needing more than 180 s to escape from the hanging-wire) and almost 24% fell 10 or more times. These results suggest that administering cortistatin early and in a double dose within the first 24 h post-MCAO appears to be detrimental, whereas a single dose of cortistatin 24 h after surgery (although promising) does not have a significant effect. This finding was surprising and contradicted our initial hypothesis. However, considering that cortistatin can induce a depressive effect on locomotor activity, potentially masking the results of early behavioural tests used to assess stroke, we decided to analyse stroke-induced neurodegeneration and the correlation between different administration times of cortistatin by identifying brain neuronal damage.

For this purpose, we determined neuronal lesion volumes using CV staining, a method that highlights intact neuronal cytoplasm in a robust purple colour, while dead neurons in the infarct area appear as faded light purple [237]. According to neurological scores, mice treated with cortistatin immediately after MCAO exhibited increased infarct volumes compared to MCAO controls (Figure 31a). Notably, while the majority of control mice displayed larger lesions in the striatum and smaller ones in the cortex, the immediate treatment with cortistatin resulted in considerable damage in both the striatum and cortex, even extending to the hippocampus (data not shown). Alternatively, cortistatin treatment at 4 + 24 h, led to lesions smaller and similar to those in control mice though to a lesser extent than immediate treatment (Figure 31a). Finally, late treatment with cortistatin at 24 h post-surgery appeared to decrease the infarct volume. Interestingly, while all these mice displayed infarct volumes below 50 mm^3, 30 % of MCAO mice, 83 % of immediately treated mice (0 + 24h), and 25 % of mice with early treatment (4 + 24h) showed higher infarct volumes (Figure 31a).

As an alternative approach, we also quantified dendritic and axonal damage by measuring the MAP-2 negative area. While both methods outlined the lesion, MAP-2 staining provided a superior definition of lesion borders and a better identification of the

penumbra area [238]. In our study, we observed similar lesion area depicted by lack of MAP-2 staining between control and cortistatin immediate and early treatments, while late cortistatin administration resulted in reduced lack of MAP-2 immunoreactivity, in concordance with CV approach (Figure 31b).

Together, our results show that the immediate treatment with cortistatin worsens neurodegeneration and motor behaviour while early treatment has no effect on MCAO neurological signs. This suggests that cortistatin administration within the first 4 h after stroke is detrimental, potentially impacting the initial biological interactions in this phase of the acute stroke. However, administering cortistatin 24 h after ischemic condition seems to diminish neuronal damage by reducing the infarct size and increasing the penumbra area in the MCAO model which may be relevant for further interventions. Although late cortistatin administration did not show a significant effect on locomotor deficits associated with stroke, the positive effect of cortistatin within an extended therapeutic window of 24 h is highly relevant.

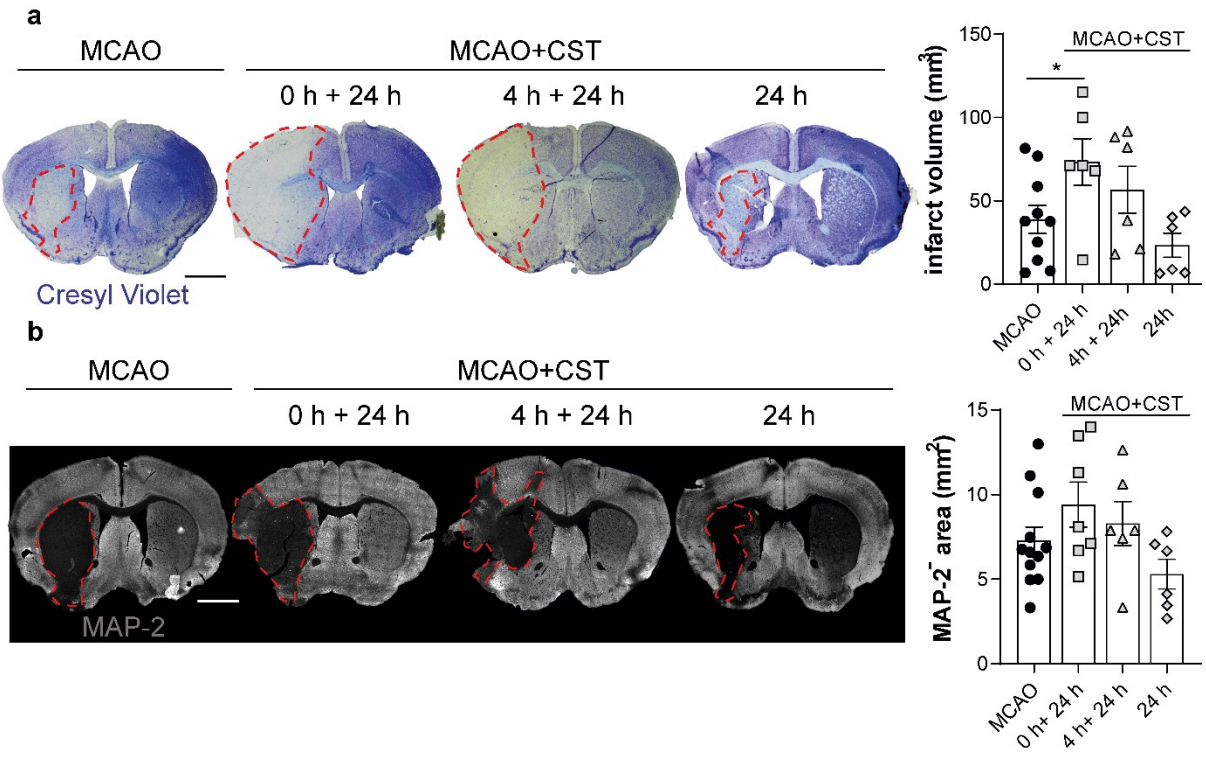

Figure 31. The neuroprotective effects of cortistatin are observed only when administered at later time points. a-b. Representative brain coronal sections of C57BL/6J mice subjected to MCAO and treated with saline solution (controls) or with cortistatin (115 µg/kg) at three different time points: immediately after reperfusion (0 h + 24 h), shortly after reperfusion (4 h + 24 h), and at a later time (24 h). **a.** Ischemic volume across the brain was calculated by measuring ten CV-stained slices at 2 mm intervals. **b.** Ischemic lesion area was assessed by measuring MAP-2 negative area in a representative selected coronal section. Scale bar 1,500 µm. Data are the mean ± SEM. N=6-10 mice/group from 3 independent experiments. **vs* saline, **$p \leq 0.05$.

4.1.2. Differential time-course administration of cortistatin impacts stroke-derived glial responses

To elucidate the underlying mechanisms of action of cortistatin when administered at the different time points and to investigate the observed disparities in ischemic lesions and neurological locomotor deficits, we conducted an analysis of the local neuroinflammatory response. To this purpose, immunodetection of microglia (Iba1), and astrocytes (GFAP) populations was employed. As mentioned above, microglia rapidly migrate to the infarct core, where they proliferate and adopt a globose, ameboid phenotype to engulf dead neurons [30]. Parallely, astrocytes initiate the formation of a glial scar around the lesion, confining the damage and preventing its spread to still-viable areas [41]. It is noteworthy that under normal conditions, fibrous $GFAP^+$ astrocytes are typically strongly labelled in the corpus callosum and the glia limitans, whereas the majority of astrocytes in the rest of the brain do not express GFAP [39]. However, following a stroke, astrocytes become activated, overexpressing GFAP and forming the glial scar.

Remarkably, in our study, the formation of astrocytic glial scars was impaired with the immediate cortistatin treatment, resulting in reduced glial scar depth compared to the presence of scars in MCAO mice (Figure 32a). However, a notable increase in glial scar formation was observed with early but especially late treatments. The deficient glial scar formation in the immediate treatment coincided with a reduction in microglia density in the ischemic core (Figure 32b). Conversely, there was a significant increase in microglia density during the later treatment, with no differences found between saline and early. These findings suggest that the initial glial response during the hyperacute phase of the ischemic stroke may be completely or partially deactivated by the potent anti-inflammatory properties of cortistatin when administered at immediately or early times. Consequently, diminished protection of the damaged area, and exacerbation of neuronal lesions and motor deficits are observed. In contrast, cortistatin administered at later stages appears to modulate the neuroinflammatory response by regulating activation and/or proliferation of glial cells in a different manner, leading to a beneficial outcome and contributing to the reduction of neuronal lesions.

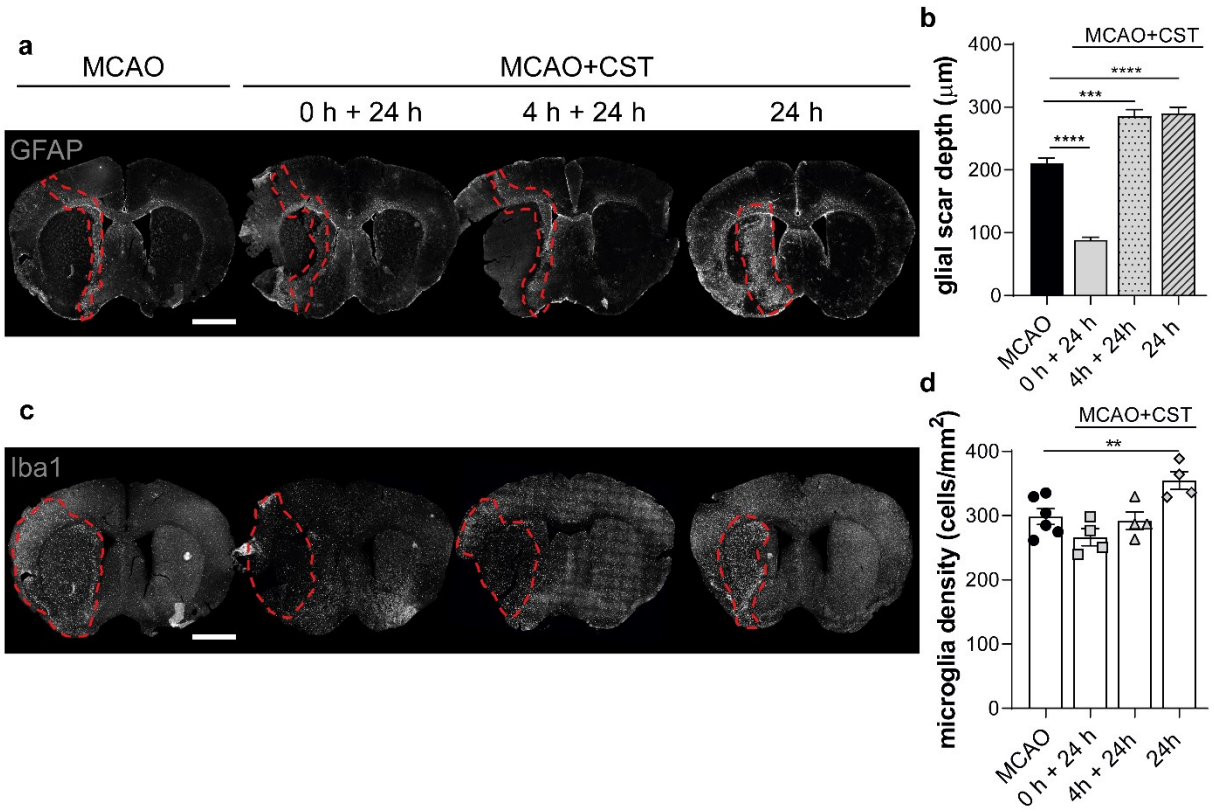

Figure 32. Later treatment with cortistatin reinforces glial scar formation and enhances glial response following stroke. a-b. Representative brain coronal sections of C57BL/6J mice subjected to MCAO and treated with saline solution (controls) or with cortistatin (115 µg/kg) at three different time points: immediately after reperfusion (0 h + 24 h), shortly after reperfusion (4 h + 24 h), and at a later time (24 h). **a.** Sections were stained with GFAP to detect astrocytes and glial scar depth. **b.** Iba 1 immunostaining was used to detect microglia and quantified microglia density in the striatum. Scale bar 1,500 µm. Data are the mean ± SEM. N=4-6 mice/group from 3 independent experiments. **vs* saline, **$p \leq 0.01$, ***$p \leq 0.001$, ****$p \leq 0.0001$.

4.2. Study of the therapeutic efficacy of cortistatin in mitigating acute stroke in young and middle-aged mice

Based on these observations, we aimed to further characterize the potential impact of cortistatin within an extended 24 h therapeutic window in preclinical studies incorporating the age-related risk factor (Figure 33a). To achieve this, we conducted experiments involving young (3 months old) and middle-aged (6 months old) mice subjected to MCAO, either treated or untreated with cortistatin at 24 h post-stroke (Figure 33a). Evaluation of neurodegeneration, glial population dynamics, BBB breakdown and brain vasculature alterations, and immune response were performed 48 h following MCAO.

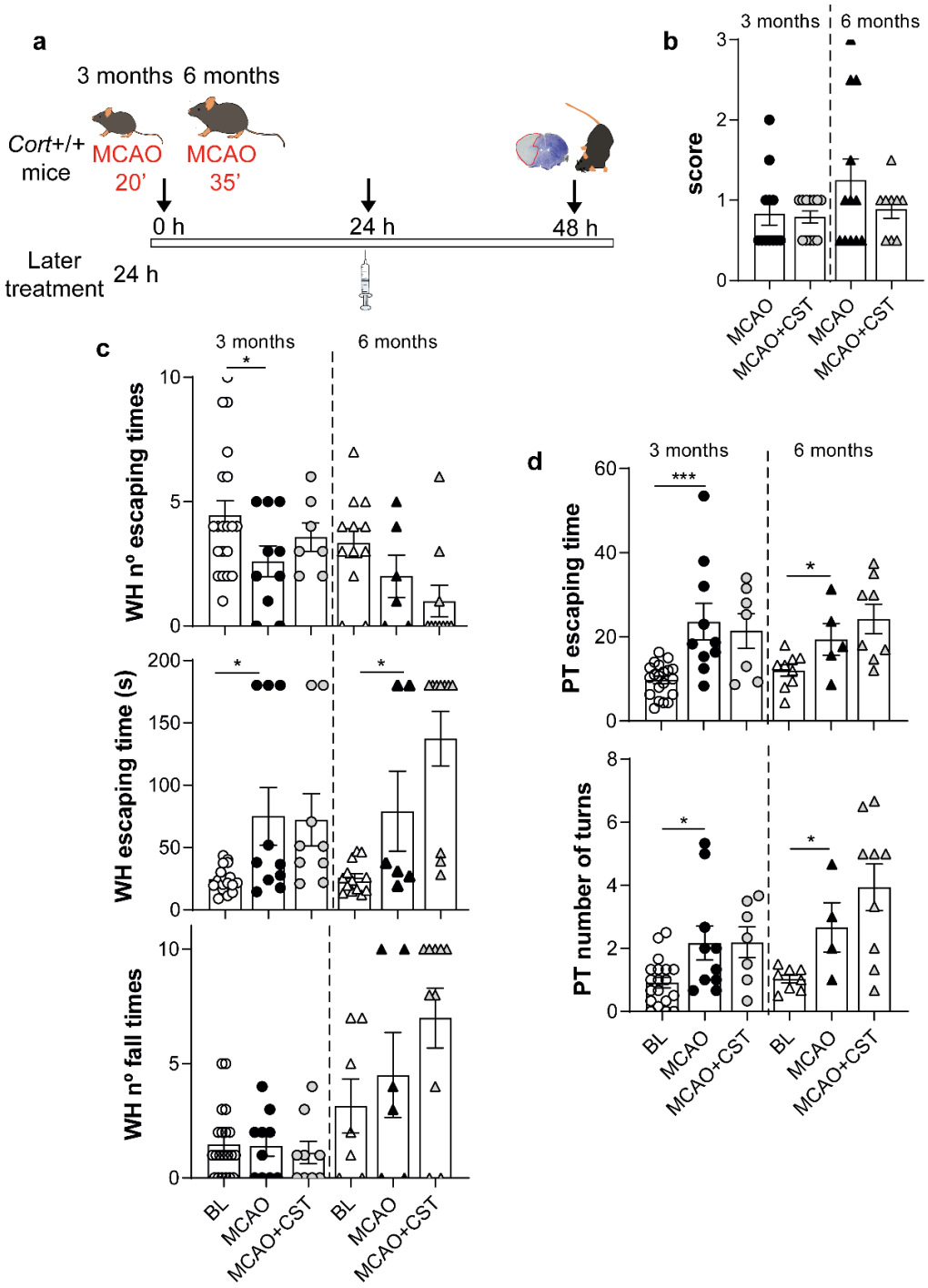

Figure 33. **Cortistatin treatment does not impact neurological scores or behavioural deficits.** **a**. Schematic representation of the timeline of the experiment. *Cort*$^{+/+}$ (wild-type) young (3 months old) and middle-aged (6 months old) mice subjected to MCAO and treated with saline solution (MCAO) or with cortistatin (115 µg/kg) (MCAO+CST) at 24 h. At 48 h, score, behavioural outcomes, and ischemic lesion determination were assessed. **b.** Neurological score was graded from 0 to 3 evaluating motor, sensory, reflex, and balance. **c-d.** Behavioural assessment in wire-hanging and pole tests. In wire-hanging test (**c**), the number of escaping times towards one of the posts, the average time taken to reach one of the posts, and the number of falls onto the pad, were recorded. In the pole test (**d**), the time taken to escape and the number of turns while descending were recorded. In both cases, data of the performance 24 h before the procedure (baseline, BL) are shown. Data are the mean ± SEM. N =6-12 mice/group from 3 independent experiments.

4.2.1. No significant differences in the neurological deficits or the motor performance after cortistatin treatment in young and middle-aged mice

According to our previous results with C57BL/6J animals (conducted in the DNF), treatment with cortistatin to young animals housed in the IPBLN did not significantly affect neurological score, although there was a tendency toward exacerbated deficits in older animals, with subsequent improvement following cortistatin administration (Figure 33b).

Next, based in our previous experience investigating the neurological deficits, we conducted again the wire-hanging test to assess muscle coordination and incorporated the pole test, to evaluate endurance/motor skills. As expected, MCAO procedure led to reduce the number of escaping times, prolonged the time taken to escape, and increased the number of falls in the wire-hanging test in young animals. Cortistatin treatment seemed to improve the number of escaping times and reduce falls, although differences were not significant (Figure 33c). However, this trend was not observed in middle-aged mice, and in turn, they seemed to display worse performances after cortistatin treatment, although differences did not reach the required level of significance either (Figure 33c). Regarding pole test, young mice subjected to MCAO exhibited prolonged escape times and increased turns, being these features very similar to the treated mice (Figure 33d). On the other hand, cortistatin-treated middle-aged mice, again appeared to display worse performances than their MCAO counterparts, although differences were not significant (Figure 33d).

Subsequently, we studied the neurological damage associated with the reported neurological deficits. We observed reduced infarct volumes in 3 and 6- month-old mice, as evidenced by CV staining after cortistatin treatment, particularly within the striatum (Figure 34a). A similar trend could be observed in MAP-2 staining, with improved detection of penumbra areas and initial ischemic lesions (Figure 34b).

Collectively, our results show that treatment with cortistatin significantly diminished neurodegeneration in both young and middle-aged animals although the functional consequences in motor abilities were not observed. The side effect of cortistatin on locomotor properties was even enhanced in 6-month-old mice.

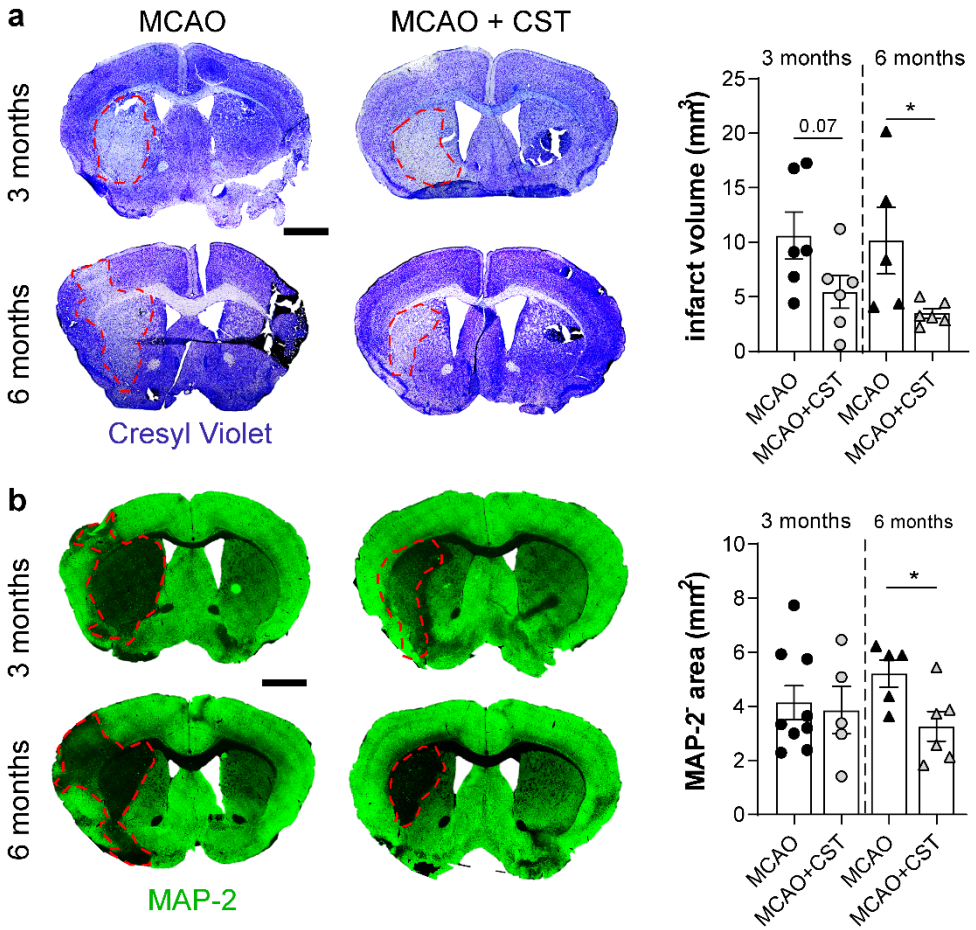

Figure 34. Cortistatin treatment reduced neuronal lesions in both young and middle-aged mice following acute stroke. a-b. Representative brain coronal sections of *Cort*$^{+/+}$ young (3 months old) and middle-aged (6 months old) mice subjected to MCAO and treated with saline solution (MCAO) or with cortistatin (115 µg/kg) (MCAO+CST) at 24 h. **a.** Sections were stained with CV (Nissl bodies). The ischemic volume across the brain was calculated by measuring ten CV-stained slices at 2 mm intervals. **b.** MAP-2 immunostaining identified dendrites and axonal processes. Ischemic area was assessed by measuring MAP-2^{-} area in a representative selected coronal section. Scale bar 1,500 µm. Data are the mean ± SEM. N =4-8 mice/group from 3 independent experiments. **vs Cort*$^{+/+}$ MCAO, **p* ≤ 0.05.

4.2.2. Cortistatin regulates the neuroinflammatory response displayed by glial cells from middle-aged mice suffering stroke

To further explore the role of cortistatin in stroke pathophysiology and neuronal injury, we investigated in more detail the local neuroinflammatory response in both middle-aged and young mice. To this aim, microglia response was analysed (Figure 35a). As previously found in C57BL/6J mice, microglia exhibited increased proliferation in the ischemic core, and this effect was augmented after cortistatin treatment irrespective of age (Figure 35b). While microglia play a clearly defined role in the ischemic core (*i.e.,* phagocytosing dead neurons and secreting neurotrophic factors), microglia in the ischemic penumbra

experiment intricate morphological and functional changes [12]. This area holds viable neurons, making the cellular and molecular environment pivotal for their preservation, and pointing to the penumbra the region as the one with the highest therapeutic potential. Hence, studying microglia activation process within this area proves particularly compelling [12]. Given that the morphological alterations in microglia are closely linked to their activation states and serve as indicators of the severity of brain injury [27,215], we conducted Skeleton and Fractal Analysis (details found in the Methods section) to analyse the microglia morphotype in the penumbra region in the mentioned mice.

As expected, both young and middle-aged animals showed a similar activated microglial phenotype in comparison to their corresponding ramified contralateral microglia (Figure 35c). This activated phenotype was marked by several characteristics, in one or both age groups, including a reduced number of junctions, branches with shorter lengths (Figure 35d), larger soma, and a smaller territory area (Figure 35e). Moreover, microglia from both age groups exhibited increased complexity (as reflected by fractal dimension) and span ratio, as well as reduced lacunarity and circularity (Figure 35f). However, treatment with cortistatin appeared to modulate the activation of these cells, inducing a shift towards a more ramified microglia morphology (Figure 35c), similar to the contralateral one. However, the modulation differed between young and middle-aged mice. In middle-aged animals, microglia exhibited an enhanced number of junctions, longer branches (Figure 35d), larger territory area (Figure 35e), reduced complexity, decreased span ratio, and increased lacunarity and circularity, compared to MCAO mice (Figure 35f). Conversely, treatment with cortistatin only impacted soma size in young mice (Figure 35e).

Given the observed impact of cortistatin on microglia activation, we extended our investigation to its modulation of the neuroinflammatory response of astrocytes (Figure 36a), as both cell types collaborate to limit the damage and prevent its spread [41]. We observed thicker glial scars in both age groups following cortistatin treatment, with a particularly pronounced effect in young animals (Figure 36a). This result aligned with our earlier observations in C57BL/6J mice (Figure 32a).

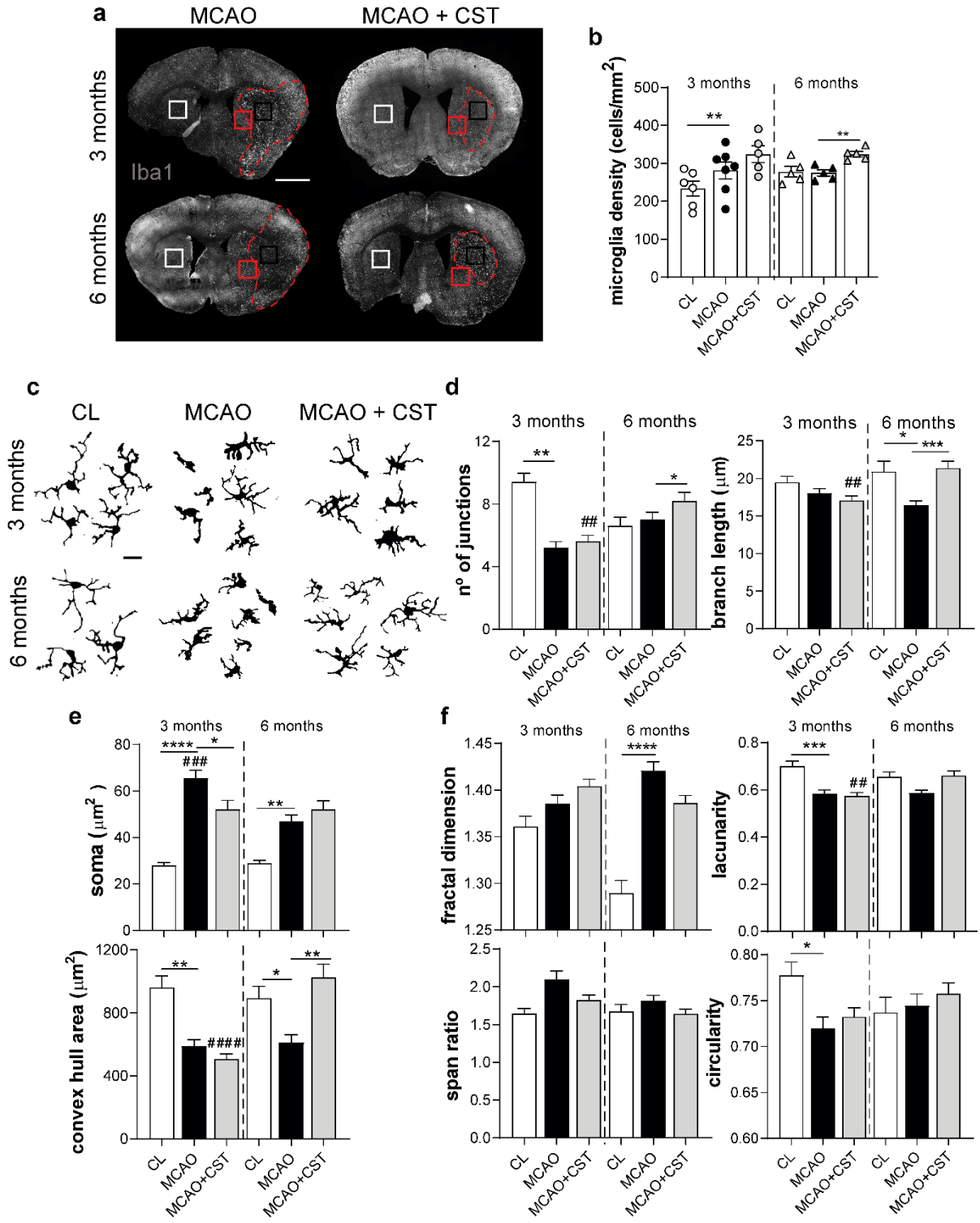

Figure 35. Cortistatin modulates microglia response. a. Representative brain coronal sections of *Cort*$^{+/+}$ young (3 months old) and middle-aged (6 months old) mice subjected to MCAO and treated with saline solution (MCAO) or with cortistatin (115 µg/kg) (MCAO+CST) at 24 h. Sections were stained with Iba1 antibody to identify microglia. Dashed red lines represent ischemic core. Scale bar 1,500 µm. **b.** Microglia density (number of cells/mm^2) was calculated in the ischemic core (striatum, black square) and the contralateral side (CL) (striatum, white square). **c.** Binary images of representative microglia were extracted from the ischemic penumbra (red square) and the CL (white square) from the different experimental groups. Scale bar 30 µm. **d-f.** Morphological parameters evaluated in microglia. Skeleton Analysis was used to assess the number of junctions

and their branch length (**d**). Soma size (**e**) was manually measured. Fractal Analysis was used to measure convex hull area (**e**), and fractal dimension/complexity, span ratio, lacunarity, and circularity (**f**). Data are the mean ± SEM. Analyses were conducted on 15-20 cells (n=15-20) from at least three independent mice (N=3). **vs Cort*$^{+/+}$ MCAO, *#vs* same experimental group at 6 months, $^{*/\#}p \leq 0.05$, $^{**/\#\#}p \leq 0.01$, $^{***/\#\#\#}p \leq 0.001$, $^{****/\#\#\#\#}p \leq 0.0001$.

To further study the phenotype and function of these astrocytes in the formation of the glial scar, we also studied their morphology using Skeleton and Fractal Analysis. Importantly, we identified more activated phenotypes in both age groups after cortistatin treatment (Figure 36c). These activated astrocytes exhibited in one or both age groups fewer junctions, shorter branch lengths (Figure 36d), increased soma, and reduced convex hull area (Figure 36e). These changes were accompanied by a decreased complexity index (fractal dimension), greater span ratio, and reduced circularity and lacunarity (Figure 36f). This activation likely contributes to the development of thicker glial scars after cortistatin treatment, and may be associated with the observed reduction in neuronal damage.

These findings highlight the role of cortistatin as a crucial regulator of glial responses. Treatment of both young and middle-aged animals 24 h after stroke does not deactivate glial cells, but rather modulates their functional properties likely associated with protecting and rescuing from neurodegeneration.

4.2.3. Regardless of age, administration of cortistatin demonstrates an improvement in stroke-associated BBB permeability, attenuation of brain endothelium breakdown, and an impact on vascular remodelling

As explained above, one of the most prominent events in stroke is the breakdown of the BBB. It occurs shortly after the artery occlusion and can persist for several weeks after the onset of the stroke. Hypoxic conditions particularly affect BECs, disrupting TJs and AJs, leading to increased permeability and contributing to the development of vasogenic edema [239]. To comprehensively investigate the extent of BBB breakdown after stroke in these animals and whether cortistatin could modulate this important structure, we examined IgG leakage as a measurement of the cerebral extravasation of endogenous blood proteins. Importantly, IgG leakage was only observable in the infarct hemisphere, being reduced after cortistatin treatment in both age groups (Figure 37a), although these differences did not reach statistical significance (Figure 37b).

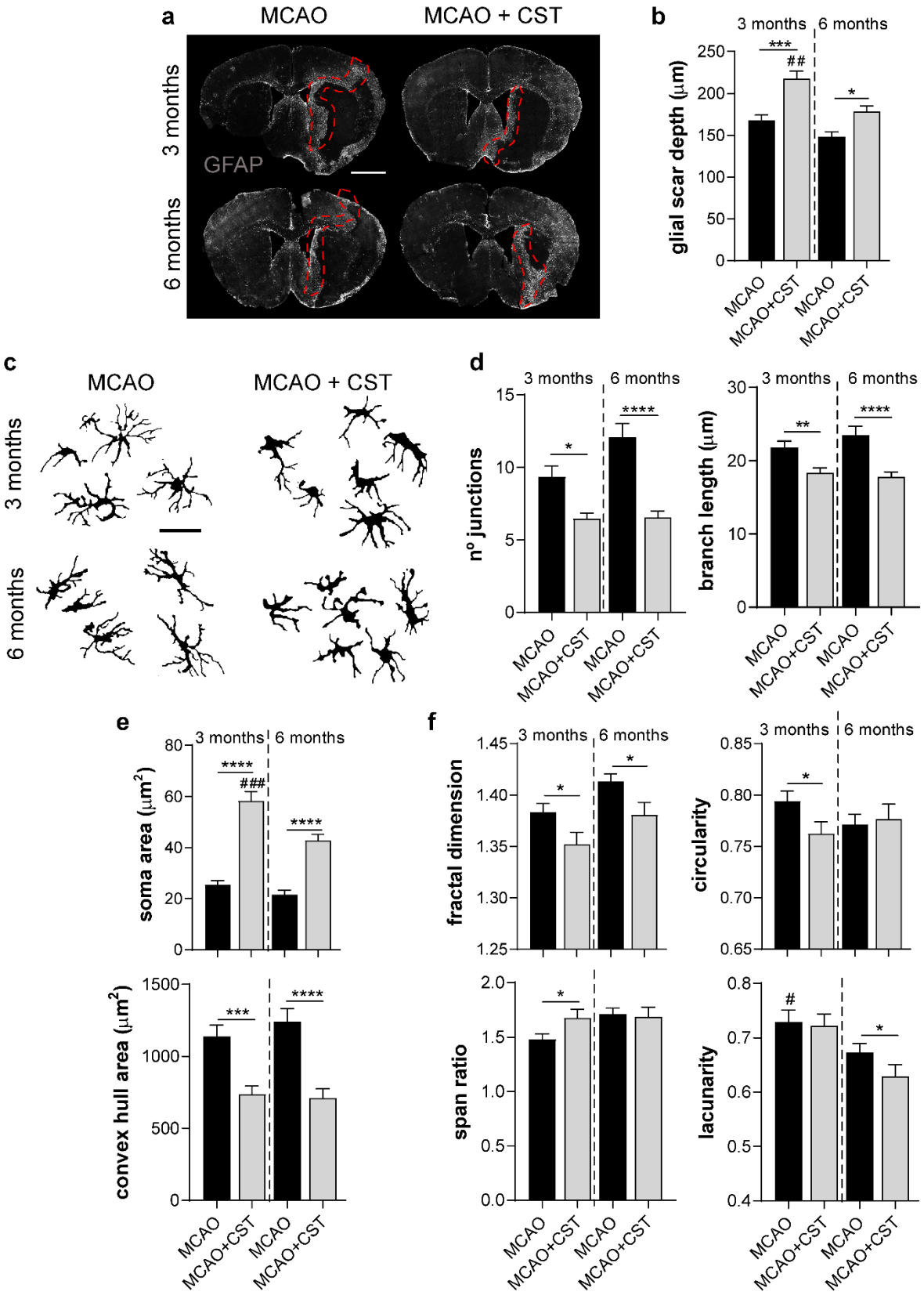

Figure 36. Cortistatin regulates glial scar formation and astrocytic functions. a. Representative brain coronal sections of *Cort*$^{+/+}$ young (3 months old) and middle-aged (6 months old) mice subjected to MCAO and treated with saline solution (MCAO) or with cortistatin (115 μg/kg) (MCAO+CST) at 24 h. Sections were stained with GFAP antibody to identify astrocytes. Scale bar

1,500 µm. Dashed red lines represent astrocyte scar. **b.** Glial scar depth was measured along its extent in the different experimental groups. **c.** Binary images of representative astrocytes from the glial scar were analysed. Scale bar 30 µm **d-f.** Morphological parameters were studied. Skeleton Analysis was used to assess the number of junctions and their branch length (**d**). Soma size (**e**) was manually measured. Fractal Analysis was used to measure convex hull area (**e**), and fractal dimension/complexity, span ratio, lacunarity, and circularity (**f**). Data are the mean ± SEM. Analyses were conducted on 15-20 cells (n=15-20) from at least three independent mice (N=3). ***vs Cort*$^{+/+}$ MCAO, *#vs* same experimental group at 6 months. $^{*/\#}p \leq 0.05$, $^{**/\#\#}p \leq 0.01$, $^{***/\#\#\#}p \leq 0.001$, $^{****/\#\#\#\#}p \leq 0.0001$.

Among TJs, ZO-1 disruption has been widely reported after ischemia [240–242], being of pivotal importance in BBB dysfunction and subsequent recovery. To study how this TJ was affected during stroke development and after cortistatin treatment, we analysed ZO-1 disruption. Interestingly, ZO-1 in the ischemic core increased its expression after MCAO procedure compared to the contralateral side (Figure 37c), in both young and middle-aged mice, (Figure 37d). However, ZO-1 presented a disorganized expression in both age groups after stroke, represented by an enhanced number of gaps. Although treatment with cortistatin revealed a similar presence of ZO-1 in the brain vessels, it significantly reduced the number of ZO-1 discontinuous expression in both age groups (Figure 37d).

Surprisingly, upon analysing the microscopy images, we found some nascent “vesicles” associated with vessels, positively stained for ZO-1 but not correlating with CD31 staining (Figure 37d). These structures exhibited characteristics that resembled vesicle budding. In the context of stroke, we concluded that they could potentially represent novel sprouting vessels [243]. Interestingly, these “vesicles” were significantly enhanced after cortistatin treatment in young and older mice after MCAO suggesting that cortistatin could be also implicated in the angiogenesis process. We also observed augmented ZO-1-positive “vesicles” in middle-aged mice post-MCAO that remained unchanged after treatment with cortistatin.

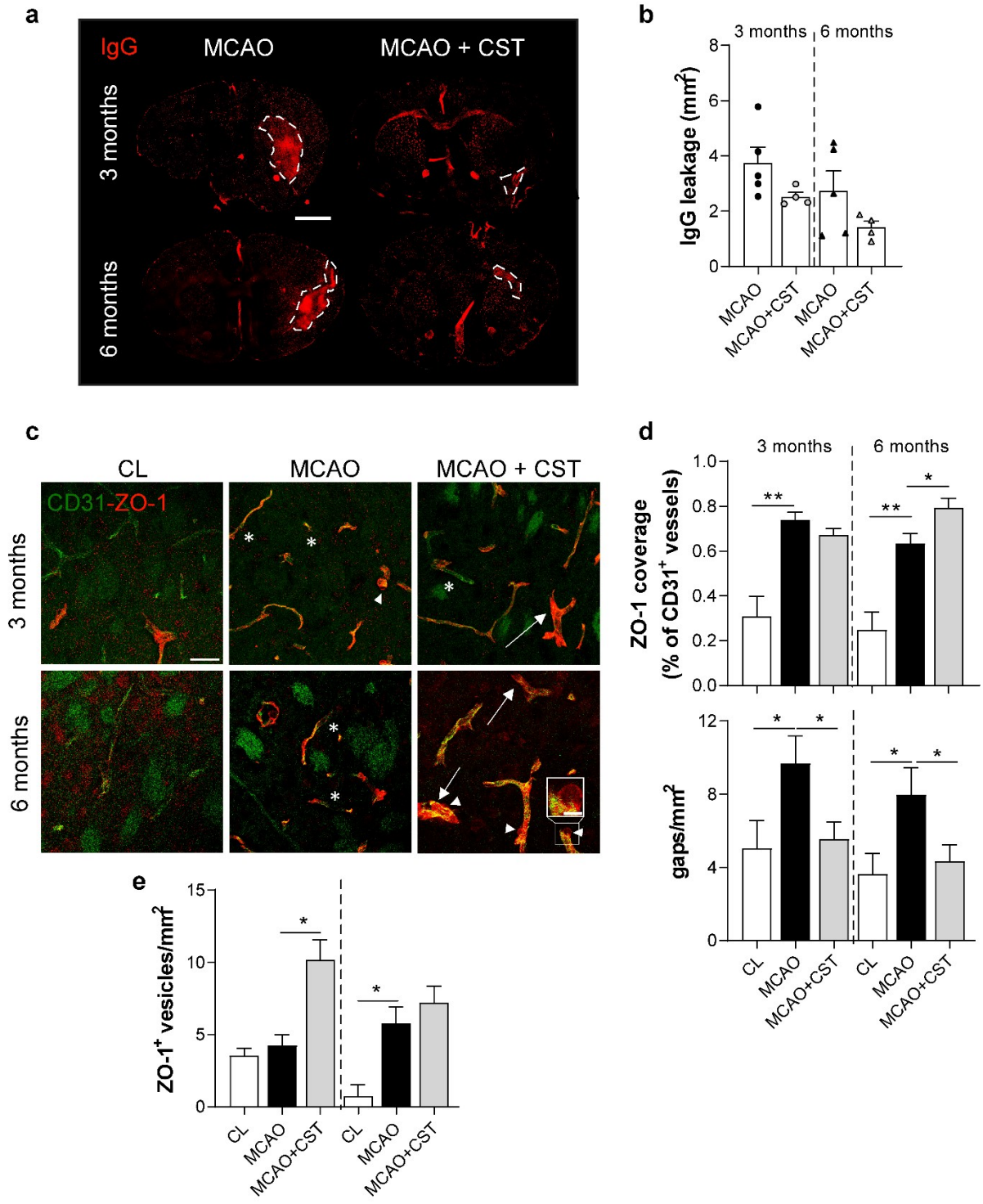

Figure 37. **Cortistatin modulates BBB leakage and brain endothelium disruption a.** Sections of *Cort*$^{+/+}$ young (3 months old) and middle-aged (6 months old) mice subjected to MCAO and treated with saline solution (MCAO) or with cortistatin (115 μg/kg) (MCAO+CST) at 24 h, stained with a secondary antibody for IgG. **b.** IgG^{+} area was calculated as a measurement of IgG leakage from blood. Sections from 4-8 independent mice were analysed. Scale bar 1,500 μm. **c.** Representative magnifications of the striatum of the different experimental groups following MCAO and their respective contralateral uninjured tissue (CL), stained with CD31 antibody for endothelial cells (green) and ZO-1 (red) for tight-junctions. Scale bar 30 μm. Magnifications of ZO-1^{+} vesicles are depicted in white squares. Scale bar 5 μm. **d.** ZO-1 coverage was measured as the % of

positive ZO-1 area that were covering the vessel ($CD31^+$ area), as well as the number of gaps in ZO-1 structure. **e.** The number of ZO-1-positive but CD31-negative vesicles/mm^2 was evaluated. 3 ROIs of 3-5 independent animals were analysed. Data are the mean ± SEM. *vs $Cort^{+/+}$ MCAO. $^{*/}p \leq 0.05$, $^{**}p \leq 0.01$.

Of note, the dynamics of BBB disruption are complex, encompassing various stages of acute damage and subsequent regenerative responses, including angiogenesis and the modification of the vascular tree [244].To investigate the enhanced number of ZO-1-positive emerging “vesicles” and the importance of this process in reoxygenation and stroke recovery, we examined the area occupied by vessels ($CD31^+$) and their diameter in the striatum core and the contralateral side of the mentioned mice (Figure 38a). As anticipated, vascular density was enhanced in young and middle-aged mice after MCAO, significantly increasing after cortistatin treatment in young animals (Figure 38b). However, vessel diameter was only augmented after MCAO in young animals, although cortistatin influenced it in both age groups (Figure 38c).

These results indicated that cortistatin protects against brain endothelium disruption and promotes angiogenesis and vascular remodelling events, potentially resulting in greater reperfusion to the damaged area and facilitating recovery mechanisms.

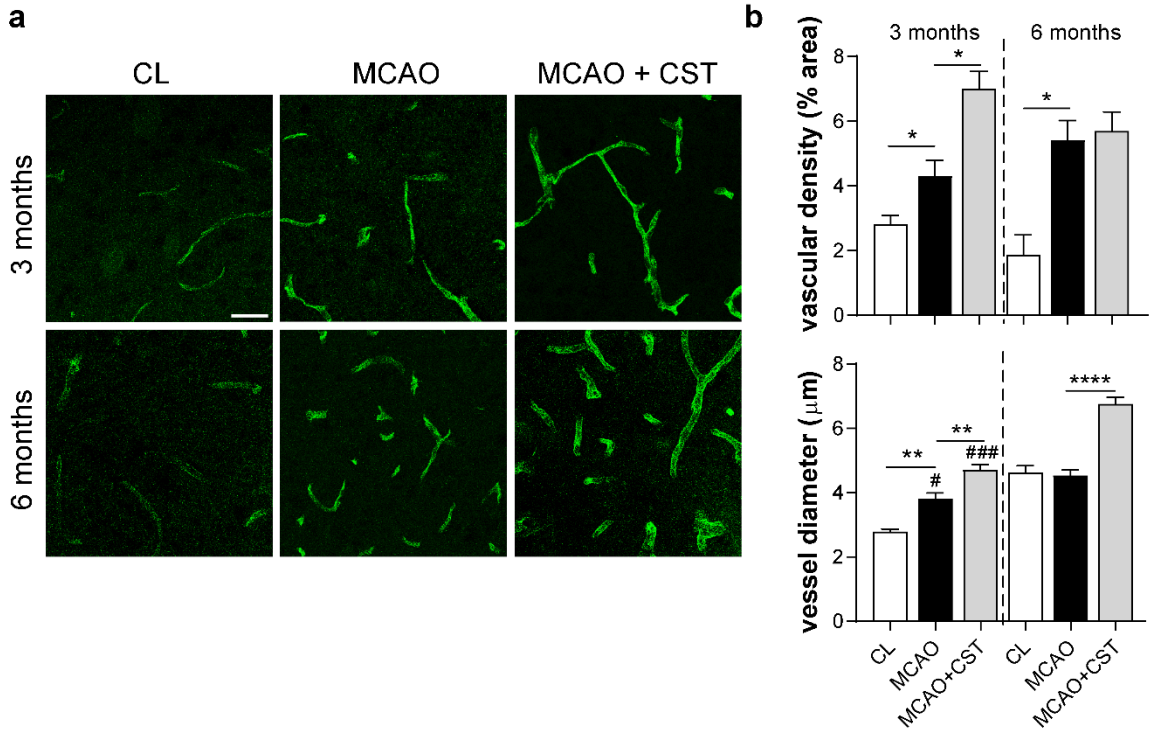

Figure 38. Cortistatin promotes angiogenesis and vascular remodelling after stroke. a. Representative images of endothelial cells (CD31, green) from the striatum of $Cort^{+/+}$ young (3 months old) and middle-aged (6 months old) mice subjected to MCAO and treated with saline solution (MCAO) or with cortistatin (115 μg/kg) (MCAO+CST) at 24 h. Their respective contralateral

uninjured tissue (CL) is also showed. Scale bar 30 μm. **b.** Vascular density, measured as the area of positive CD31. **c.** Vessel diameter was measured manually. Data are the mean ± SEM. 3 different ROIs from 3-5 mice were analysed. For vessel diameter, 10-20 measures of each vessel from 5-10 vessels from each image were analysed. ***vs Cort*$^{+/+}$ MCAO, *#vs* same experimental group at 6 months. $^{*/\#}p \leq 0.05$, $^{**/\#\#}p \leq 0.01$, $^{***/\#\#\#}p \leq 0.001$, $^{****/\#\#\#\#}p \leq 0.0001$.

4.2.4. Cortistatin reduces immune brain infiltration and attenuates ageing-exacerbated immune peripheral responses following a stroke

Following artery occlusion and prompted by ischemia and the ensuing reperfusion, a coordinated inflammatory process unfolds, involving not only the brain but also peripheral organs [10]. As a result, there is a rapid adhesion of leukocytes and platelets to the endothelium that, facilitated by the BBB breakdown, allows the infiltration of peripheral immune cells into the brain [116]. While this response is initially intended to resolve damage and protect the brain, it can become detrimental if it becomes chronic. Hence, improving BBB function and modulating immune cell infiltration in later stages might improve functional outcomes after stroke. To study the role of cortistatin in the regulation of the peripheral immune response dynamics, we examined immune infiltration in the ischemic core of young and middle-aged mice using a general leukocyte marker (*i.e.,* CD45). Notably, CD45+ cells were not detected on the contralateral side, whereas a significant number of cells infiltrated the ischemic region in MCAO mice regardless of age. Importantly, this immune infiltration significantly decreased after cortistatin treatment in both age groups (Figure 39a).

Following ischemia and BBB breakdown, cytokines and DAMPs generated by the brain injury enter the systemic circulation, reaching lymphoid organs and triggering the inflammatory response [10,116]. To characterize the impact of cortistatin on the systemic immune response 48 h after ischemia, we measured we measured pro-inflammatory cytokines/chemokines including IL-12, IL-6, and MCP-1, in serum. Remarkably, these factors seemed to be enhanced in old animals compared to young ones, although differences were not significant in any case. Treatment with cortistatin did not influence the levels of these mediators in young animals, but it appeared to reduce the levels in middle-aged mice, mainly for IL-12 (Figure 39b).

To sum up, these results indicate that cortistatin treatment administered at later stages (24 h), do not seem to impact behavioural outcomes but reduces neuronal damage, possibly mediated by the modulation of microglia activation and the formation of the astrocyte glial scar. Additionally, cortistatin regulates BBB dysfunction and facilitated

recovery processes such as angiogenesis. Finally, cortistatin appears to regulate immune cell infiltration in the brain and partially modulates the peripheral immune response.

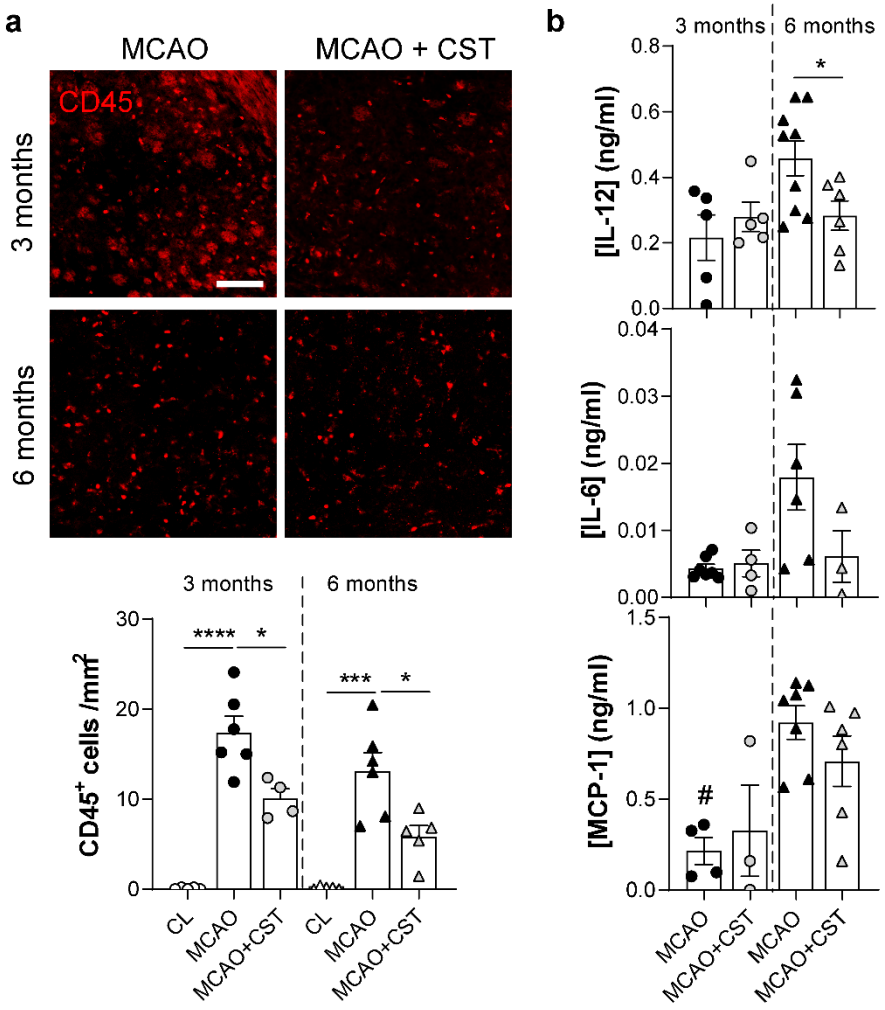

Figure 39. Cortistatin modulates immune infiltration and controls the peripheral immune response. a. Representative images from the striatum of *Cort*$^{+/+}$ young (3 months old) and middle-aged (6 months old) mice subjected to MCAO and treated with saline solution (MCAO) or with cortistatin (115 µg/kg) (MCAO+CST) at 24 h, stained with CD45 antibody (red) for leukocytes. 100 µm. Leukocyte density (number of cells/mm^2) was calculated in the striatum and in the contralateral side (CL) of the different experimental groups. **b.** IL-12, IL-6, and MCP-1 concentration (ng/ml) measured in serum by ELISA assay. Dots represent 3-9 independent mice. Data are the mean ± SEM. **vs Cort*$^{+/+}$ MCAO. *$^{/}$$p \leq 0.05$, ***$p \leq 0.001$, ****$p \leq 0.0001$.

4.3. The endogenous role of cortistatin in stroke pathophysiology and the impact of cortistatin deficiency

Given the potential therapeutic effect of cortistatin, we next aimed to elucidate the endogenous role of this neuropeptide in stroke pathogenesis. Previous results from our group and others have described exacerbated inflammatory responses in cortistatin-deficient mice [144], worsened outcomes in models of inflammatory or neuronal damage

[182,190,192], and the manifestation of a premature aging phenotype [245]. However, its role in stroke pathogenesis remains unknown. In light of this background, we conducted the MCAO procedure in young (3 months old) and middle-aged (6 months old) cortistatin-deficient mice. Besides, *Cort*$^{-/-}$ mice were treated with saline solution or cortistatin at 24 h, to assess whether the treatment could impact the potential phenotype. Wild-type mice of the same age injected with saline were used as controls (the data were incorporated in the graphs as a reference). As described above, neurological score, behavioural performances, ischemic volume, glial population dynamics, BBB breakdown, and immune dynamics were analysed at 48 h (Figure 40a).

4.3.1. Deficiency of cortistatin exacerbates neurodegeneration, a condition that is reversed after treatment

Young cortistatin-deficient mice displayed worsened neurological scores compared to wild-type mice (mean score 1-1.5, *i.e.,* moderate hypomobility, moderate motor incoordination, intermittent circling), which was significantly decreased by cortistatin treatment (Figure 40b). Similar trends were observed in middle-aged animals with 50% of *Cort*$^{-/-}$ mice exhibiting motor incoordination, intermittent circling, and tremor twitches (score 2-3). This was in contrast to the reduced number of cortistatin-treated and *Cort*$^{+/+}$ mice reaching this score (less than 24% in both cases), although the differences were not statistically significant (Figure 40b). To further investigate neurological deficits, we conducted wire-hanging and pole tests. As previously described for wild-type, young *Cort*$^{-/-}$ mice escaped fewer times and took longer after MCAO in the wire-hanging test (Figure 40c), with values slightly worse than in *Cort*$^{+/+}$ animals. Additionally, *Cort*$^{-/-}$ mice displayed a slightly non-significant higher number of turns after stroke in the pole test (Figure 40d), consistent with the overall poorer neurological score. Treatment with cortistatin did not significantly influence any of these parameters (Figure 40c). Notably, middle-aged *Cort*$^{-/-}$ mice seemed to display worse performances than young mice deficient in cortistatin as well as than their middle-age wild-type counterparts (Figure 40 c). Thus, 6-month-old *Cort*$^{-/-}$ mice took more time to escape with an increasing number of falls in the wire-hanging. Surprisingly, healthy and MCAO middle-age animals deficient in cortistatin showed similar performance in the pole test. The treatment with cortistatin in middle-aged animals did not impact these parameters (Figure 40d).

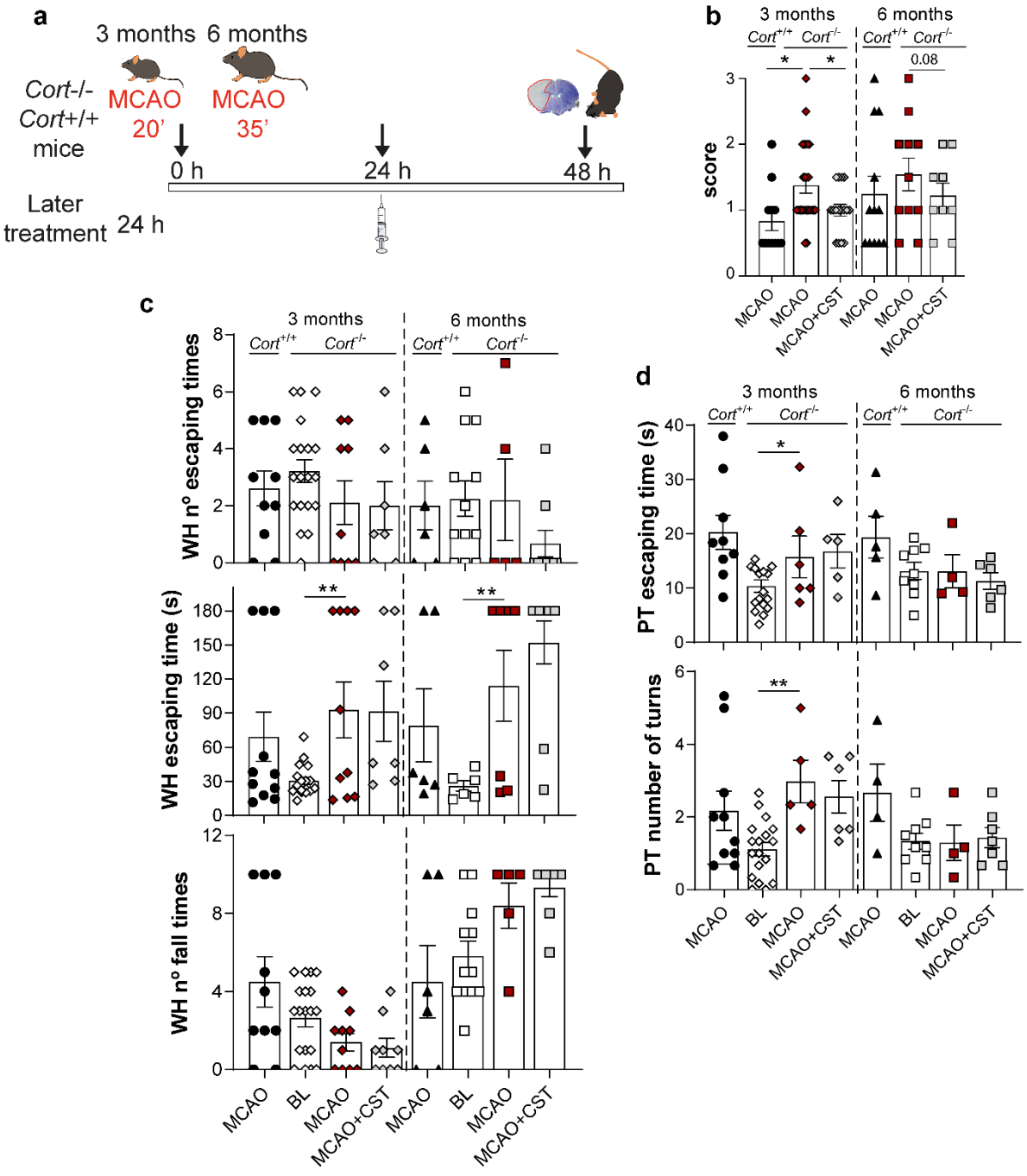

Figure 40. Cortistatin deficiency is associated with worse neurological deficits and poorer motor performance. a. Schematic representation of the timeline of the experiment. *Cort*$^{-/-}$ young (3 months old) and middle-aged (6 months old) mice subjected to MCAO treated with saline solution (MCAO) or with cortistatin (115 µg/kg) (MCAO+CST) at 24 h. Score at 48 h, behavioural outcomes, and ischemic lesion determination was assessed. *Cort*$^{+/+}$ mice from each age group subjected to MCAO were used as controls. **b.** Neurological score was graded from 0 to 3 evaluating motor, sensory, reflex, and balance in the mentioned mice. **c-d.** Behavioural assessment in wire-hanging and pole tests. **c.** In wire-hanging test, the number of escaping times towards one of the posts, the average time taken to reach one of the posts, and the number of falls onto the pad, were recorded. **d.** In the pole test, the time taken to escape and the number of turns while descending were recorded. In both cases, data of the performance 24 h before the procedure (baseline, BL) are

shown. Data are the mean ± SEM. N =6-12 mice/group from 3 independent experiments. *vs *Cort*$^{-/-}$ MCAO *$p \leq 0.05$.

We then sought to investigate the ischemic lesion volume through evaluation of CV and MAP-2 in these mice. Ischemic damage appeared more extensive in young *Cort*$^{-/-}$ mice compared to *Cort*$^{+/+}$ animals in CV staining (Figure 41a). Surprisingly, we did not observe larger lesions with CV methodology in older *Cort*$^{-/-}$ ice (Figure 41a). However, when we analysed damage in the striatum using MAP-2 staining we did observe larger lesions in *Cort*$^{-/-}$ mice at both ages (Figure 41b). The discrepancies between the trends of CV and MAP-2 staining may suggest that in older cortistatin-deficient mice, damage may primarily affect neuronal processes rather than neuronal bodies. Cortistatin treatment appeared to reduce the ischemic lesion in both age groups protecting both neuronal soma and dendrites, although the differences were not significant (Figure 41b).

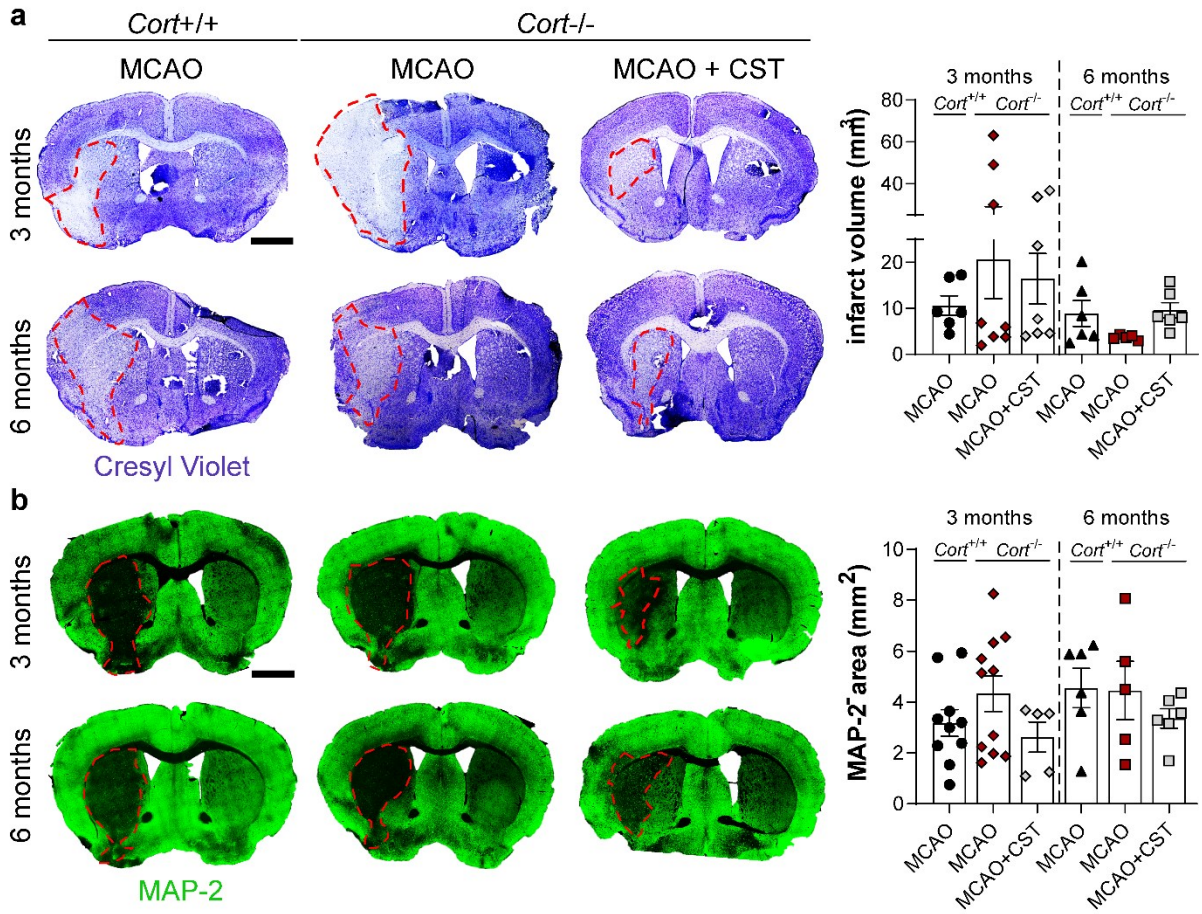

Figure 41. Cortistatin-deficient mice displays more severe neuronal lesions, which are reversed by cortistatin treatment. a-b. Representative brain coronal sections of *Cort*$^{-/-}$ young (3 months old) and middle-aged (6 months old) mice subjected to MCAO and treated with saline solution (MCAO) or with cortistatin (115 µg/kg) (MCAO+CST) at 24 h. *Cort*$^{+/+}$ mice from each age group subjected to MCAO were used as controls. Scale bar 1,500 µm. **a.** Sections were stained with CV (Nissl bodies) and the ischemic volume across the brain was calculated by measuring ten

CV-stained slices at 2 mm intervals. **b.** MAP-2 immunostaining identified dendrites and axonal processes. Ischemic area was assessed by measuring MAP-2^{-} area in a representative selected coronal section Data are the mean ± SEM. N =5-9 mice/group from 3 independent experiments.

4.3.2. In the absence of cortistatin, glial cells exhibited an impaired neuroinflammatory response which is modulated after cortistatin treatment

Given the exacerbated inflammatory responses in cortistatin-deficient mice [144], we proceed to investigate the neuroinflammatory response in these animals. Regarding microglia dynamics (Figure 42a), we observed an increase in microglia density in the infarct core of *Cort*$^{-/-}$ mice compared to their contralateral side in both age groups (Figure 42b). Besides, a higher number of cells were found in cortistatin-deficient mice compared to wild-type animals at 6 months. Although cortistatin treatment did not affect microglia density (Figure 42b), we noted a different activated morphotype of these cells in young and old mice compared to their contralateral counterparts and their corresponding wild-type mice (Figure 42c). In young mice deficient in cortistatin, we quantified a reduced number of junctions and branch length (Figure 42d), increased soma, reduced territory area (Figure 42e), increased fractal dimension and span ratio, and reduced lacunarity (Figure 42f). On the contrary, *Cort*$^{-/-}$ middle-aged mice showed a distinct activation pattern. In this case, hyper-ramification was significantly observed with a reduced number of junctions but larger branch lengths (Figure 42d), augmented soma but a greater occupied territory (Figure 42e), and reduced fractal dimension and circularity (Figure 42f). Importantly, cortistatin modulated this phenotype, leading to a mixed microglia population. While most features were partially recovered by cortistatin treatment, resembling microglia in MCAO wild-type mice, some properties such as soma size and complexity mirrored microglia found in healthy wild-type animals. This suggests that in cortistatin-deficient animals, cortistatin may modulate microglia activation in a different way compared to wild-type mice, effectively reversing its dysfunctional phenotype.

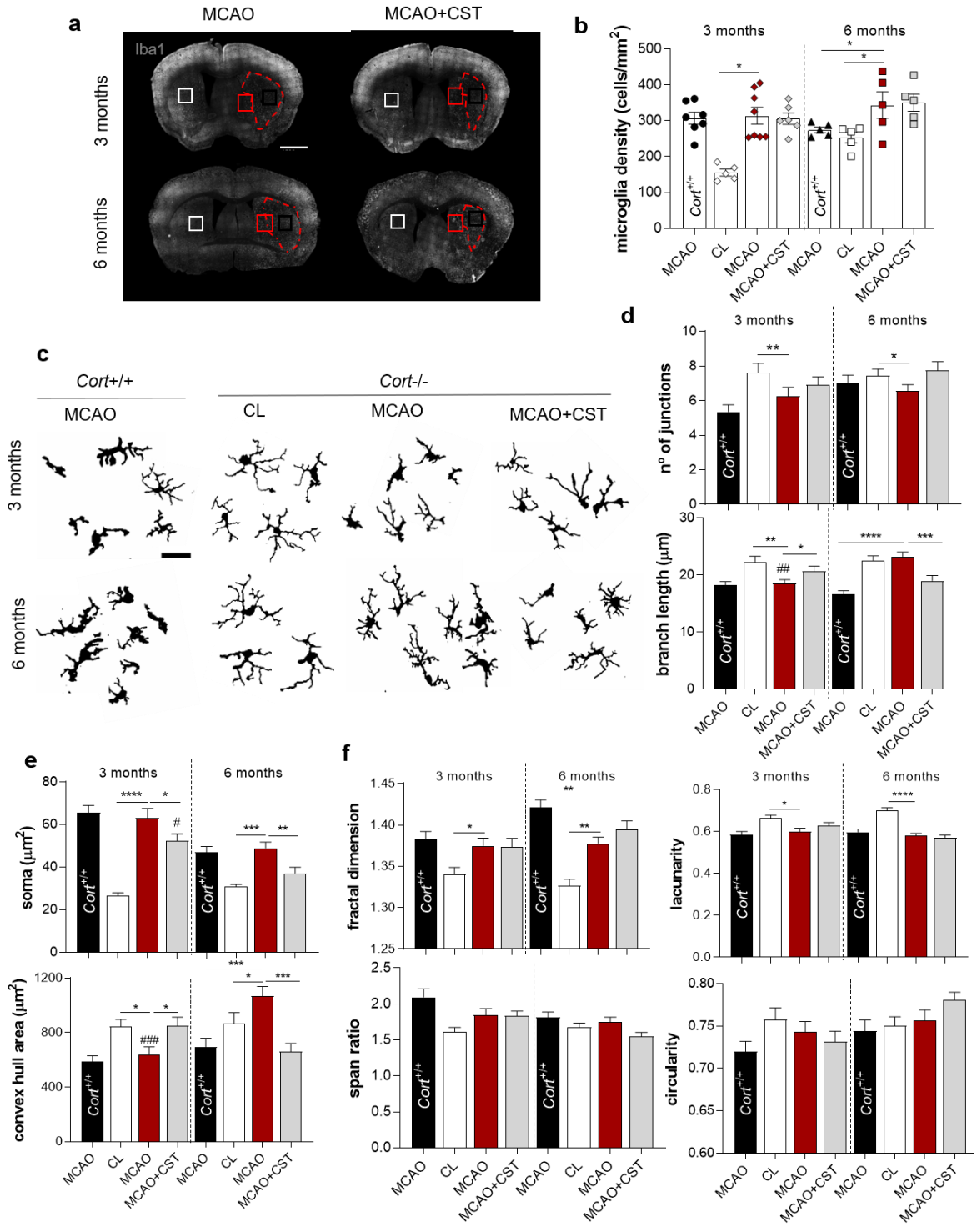

Figure 42. The deficiency of cortistatin leads to microglia dysfunctional response, reversed by cortistatin treatment. a. Representative brain coronal sections of *Cort*$^{-/-}$ young (3 months old) and middle-aged (6 months old) mice subjected to MCAO and treated with saline solution (MCAO) or with cortistatin (115 µg/kg) (MCAO+CST) at 24 h, stained with Iba1 antibody to identify microglia. *Cort*$^{+/+}$ mice from each age group subjected to MCAO were used as controls. Dashed red lines represent ischemic core. Scale bar 1,500 µm. **b.** Microglia density (number of cells/mm^2) was calculated in the ischemic core (striatum, black square) and in the contralateral side (CL) (striatum, white square) of the different experimental groups. **c.** Binary images of representative microglia were extracted from the ischemic penumbra (red square) and the CL (white square) from the

different experimental groups **d-f.** Morphological parameters evaluated in microglia. Skeleton Analysis was used to assess the number of junctions and their branch length (**d**). Soma size (**e**) was manually measured. Fractal Analysis was used to measure convex hull area (**e**), and fractal dimension/complexity, span ratio, lacunarity, and circularity (**f**). Data are the mean ± SEM. Analyses were conducted on 15-20 cells from at least three independent mice. ***vs* *Cort*$^{-/-}$ MCAO, *#vs* same experimental group at 6 months, $^{*/\#}p \leq 0.05$, $^{**/\#\#}p \leq 0.01$, $^{***/\#\#\#}p \leq 0.001$, $^{****/\#\#\#\#}p \leq 0.0001$.

Complementary, we studied astrocytic dynamics (Figure 43a). Surprisingly, an impaired glial scar was observed in cortistatin-deficient mice compared to wild-type controls, especially in the older ones, likely associated with age-related susceptibility (Figure 43b). The treatment with cortistatin reversed this feature up to baseline levels found in MCAO wild-type mice (Figure 43b). Considering this striking difference, we conducted a more detailed study of astrocyte morphology (Figure 43c). Notably, we observed that astrocytes from one or both age groups displayed an unusual phenotype characterized by smaller, non-ramified, elongated forms. In more detail, they displayed fewer junctions, shorter branch lengths (Figure 43d), smaller soma, reduced territory coverage (Figure 43e), decreased complexity, increased span ratios, and reduced circularity and lacunarity compared to wild-type astrocytes following MCAO. However, most of these aberrant parameters were reversed by the neuropeptide treatment (Figure 43d-f), as astrocytes were switched into a more activated and presumably functional phenotype (Figure 43c).

In summary, these findings reveal that cortistatin deficiency is associated with a dysfunctional glial phenotype, likely contributing to the more severe neuronal damage observed. However, cortistatin treatment reverses this dysfunctional phenotype and appears to shift microglia and astrocytes phenotype to a more reactive state. This change is likely essential in these animals to restrict neuronal damage.

4.3.3. Cortistatin deficiency is associated with enhanced BBB breakdown after stroke, but diminished following cortistatin administration

After investigating the role of cortistatin in glial dynamics in post-ischemic stroke and given the lack of knowledge on BBB dynamics in these animals after stroke, we conducted an analysis of IgG leakage (Figure 44a). In this case, we found an increased IgG leakage in *Cort*$^{-/-}$ mice, regardless of age, compared to wild-type controls, although the differences were not significant (Figure 44b). However, cortistatin treatment significantly reduced the augmented leakage in both age groups of these mice (Figure 44b). Regarding TJs disruption, we noted a reduction in the coverage of ZO-1 associated with an increased

number of gaps in ZO-1 structure in young *Cort*$^{-/-}$ animals following MCAO compared to wild-type mice. These features were reversed by cortistatin treatment.

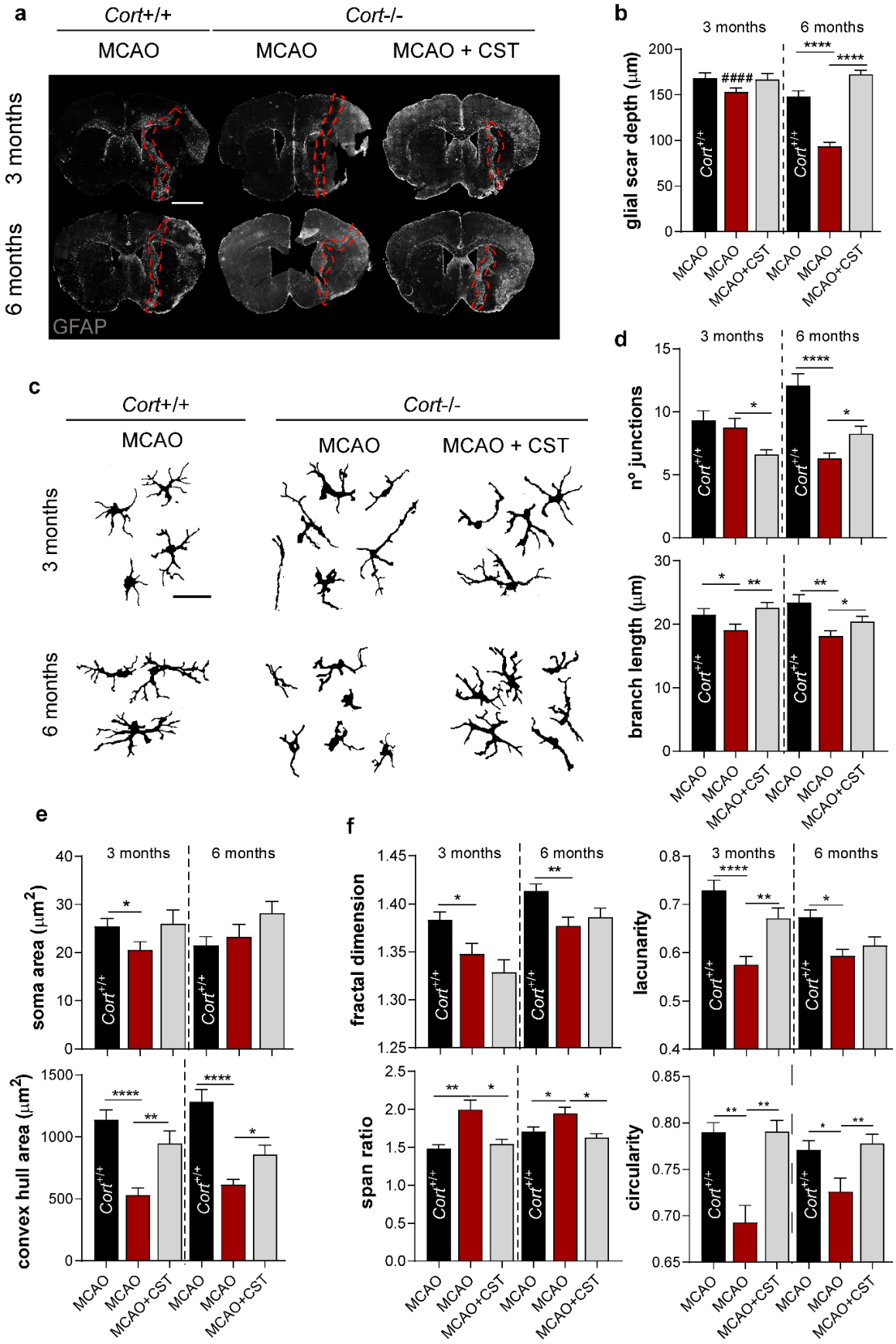

Figure 43. The deficiency of cortistatin induces impaired glial scar formation and dysfunctional astrocytes, which are modulated by exogenous cortistatin. a. Representative brain coronal sections of *Cort*$^{-/-}$ young (3 months old) and middle-aged (6 months old) mice subjected to MCAO and treated with saline solution (MCAO) or with cortistatin (115 µg/kg) (MCAO+CST) at 24 h. Sections were stained with GFAP antibody to identify astrocytes Scale bar 1,500 µm. Dashed red lines represent astrocyte scar. *Cort*$^{+/+}$ mice from each age group subjected to MCAO were used as controls. **b.** Glial scar depth was measured along its extent in the different experimental groups. 15-20 measures (n=15-20) of 4-7 mice were conducted **c.** Binary images of representative astrocytes in binary from the glial scar were analysed. Scale bar 30 µm. **d-f.** Morphological parameters were studied. Skeleton Analysis was used to assess the number of junctions and their branch length (**d**). Soma size (**e**) was manually measured. Fractal Analysis was used to measure convex hull area (**e**), and fractal dimension/complexity, span ratio, lacunarity, and circularity (**f**). Data are the mean ± SEM. Analyses were conducted on 15-20 cells from at least three independent mice. **vs Cort*$^{-/-}$MCAO, *#vs* same experimental group at 6 months. $^{*/\#}p \leq 0.05$, $^{**/\#\#}p \leq 0.01$, $^{***/\#\#\#}p \leq 0.001$, $^{****/\#\#\#\#}p \leq 0.0001$.

Interestingly, the reduced coverage found in these mice was associated with increased number of gaps in ZO-1 structure compared to wild-type mice, feature that was partially reversed after treatment in young mice (Figure 44c,d). Conversely, treatment in older *Cort*$^{-/-}$ mice did not influence the number of gaps, although it enhanced ZO-1 coverage (Figure 44c,d). Interestingly, we also studied in these animals the number of presumed sprouting vessels. Despite no differences were found between *Cort*$^{-/-}$ and *Cort*$^{+/+}$ mice after MCAO, the treatment with the neuropeptide significantly increased the number of ZO-1-positive vesicles, likely linked to the development of sprouting vessels (Figure 44c, d).

4.3.4. Angiogenesis is impaired in cortistatin-deficient middle-aged mice

Furthermore, we investigated brain endothelium dynamics given the impaired peripheral endothelium already described for these mice [146]. While we observed that the vascular density was similar compared to wild-type young mice, there was a significant reduction in vascular density in older mice (Figure 45a,b). As observed before in wild-type mice, cortistatin treatment significantly increased the amount of vessels/area. Despite not observing differences in vessel diameter *vs* wild-type mice, we observed greater vessel diameter after the treatment (Figure 45a,b).

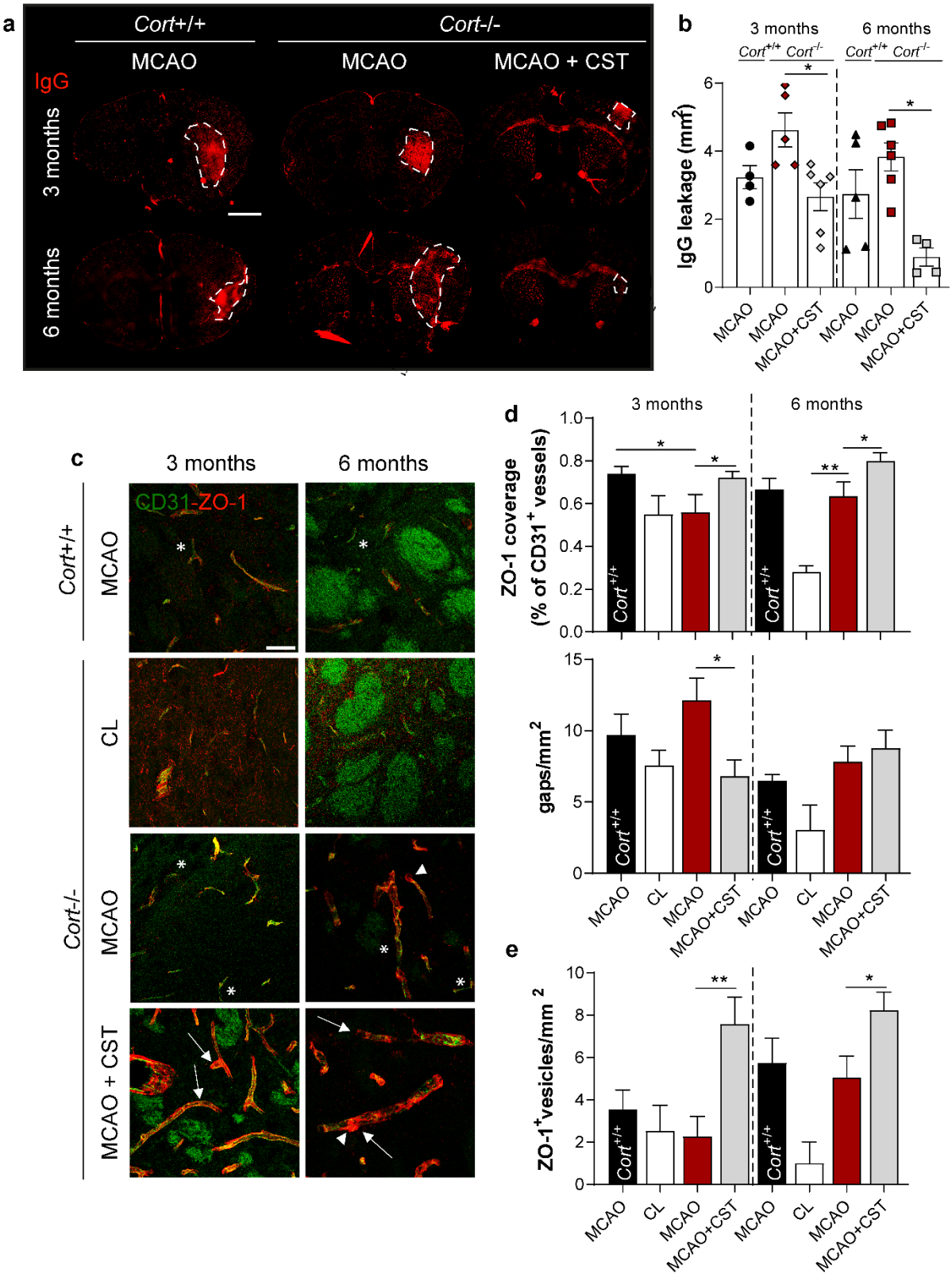

Figure 44. **Cortistatin-deficient mice exhibit more severe BBB breakdown and brain endothelium disruption in**. **a.** Representative brain coronal sections of *Cort*$^{-/-}$ young (3 months old) and middle-aged (6 months old) mice subjected to MCAO and treated with saline solution (MCAO) or with cortistatin (115 µg/kg) (MCAO+CST) at 24 h. *Cort*$^{+/+}$ mice from each age group subjected to MCAO were used as controls. Scale bar 1,500 µm. Sections are stained with a

secondary antibody for IgG. **b.** IgG$^+$ area was calculated as a measurement of IgG leakage from blood. Sections from 5-7 independent mice were analysed. **c**. Representative magnifications of the striatum of *Cort*$^{-/-}$ young (3 months old) and middle-aged (6 months old) subjected to MCAO treated with saline solution (MCAO) or with cortistatin (115 µg/kg) (MCAO+CST) at 24 h, stained with CD31 antibody for endothelial cells (green) and ZO-1 (red) for tight-junctions. Scale bar 30 µm. *Cort*$^{+/+}$ mice from each age group subjected to MCAO were used as controls. **d.** ZO-1 coverage was measured as the % of positive ZO-1 area that were covering the vessel (CD31$^+$ area) and the number of gaps in ZO-1 structure was also determined. **e.** The number of ZO-1-positive CD31-negative vesicles/mm^2 was evaluated. 3 ROIs of 3-5 independent animals were analysed. Data are the mean ± SEM. **vs Cort*$^{-/-}$ MCAO, **p* ≤ 0.05, ***p* ≤ 0.01.

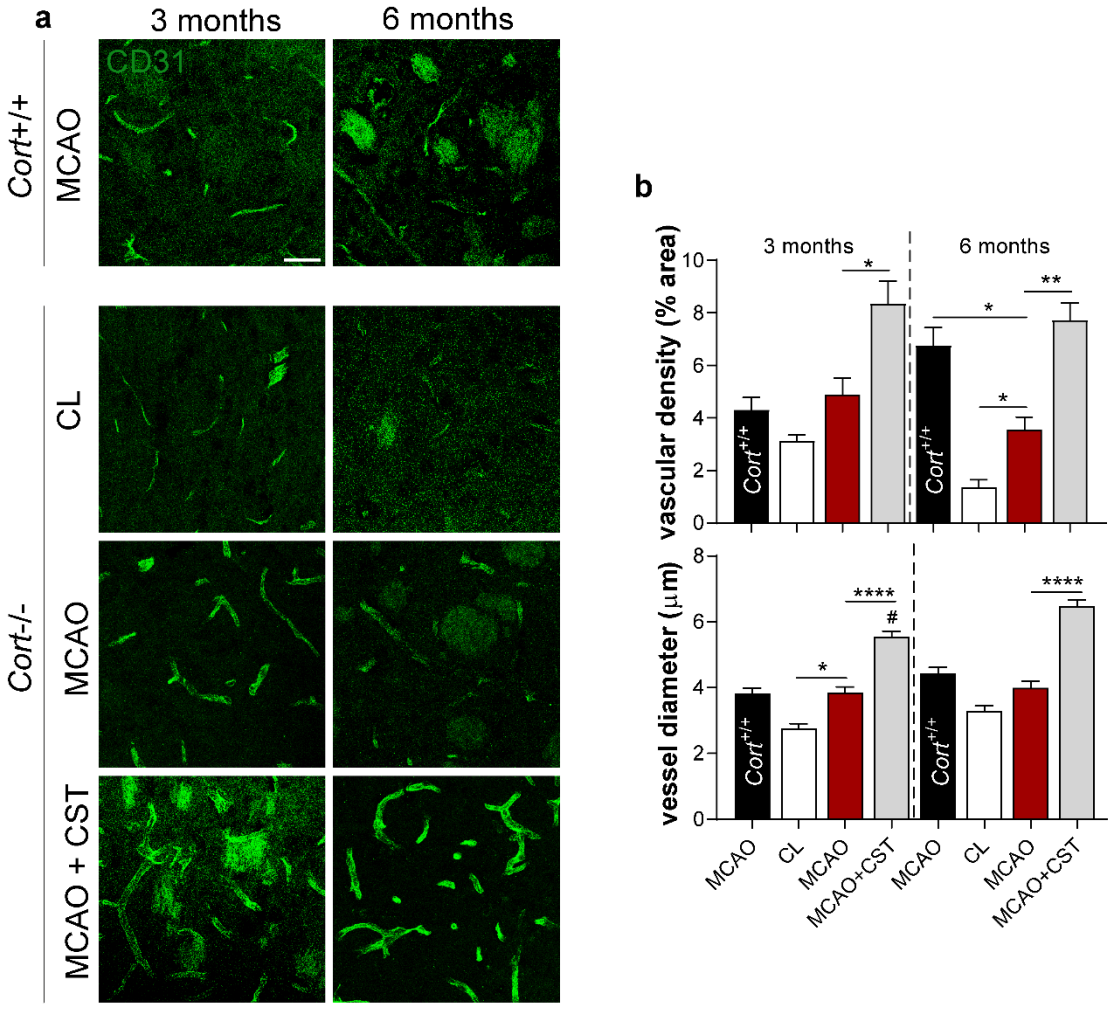

Figure 45. Impaired angiogenesis in cortistatin-deficient middle-aged mice. a. Representative images of endothelial cells (CD31, green) from the striatum of *Cort*$^{-/-}$ young (3 months old) and middle-aged (6 months old) mice subjected to MCAO and treated with saline solution (MCAO) or with cortistatin (115 µg/kg) (MCAO+CST) at 24 h. *Cort*$^{+/+}$ mice from each age group subjected to MCAO were used as controls**.** Scale bar 30 µm. **b.** Vascular density was measured in the ischemic striatum or its contralateral side (CL) in the in the different experimental groups as the area of positive CD31. Vessel diameter was manually measured. Data are the mean ± SEM. Three different ROIs from 3-5 mice were analysed. For vessel diameter, 10-20 measures of each vessel

from 5-10 vessels from each image were analysed. *vs *Cort*$^{-/-}$ MCAO, #vs same experimental group at 6 months. $^{*/\#}p \leq 0.05$, $^{**/\#\#}p \leq 0.01$, $^{***/\#\#\#}p \leq 0.001$, $^{****/\#\#\#\#}p \leq 0.0001$.

4.3.5. Cortistatin-deficient mice show enhanced immune infiltration and altered peripheral immune responses

Finally, given the proinflammatory basal state of these animals [144], and the enhanced proinflammatory responses in other models [182,190,192], we investigated immune infiltration and peripheral immune responses. Importantly, CD45 infiltration was enhanced in cortistatin-deficient mice compared to wild-type in young and middle-age animals but modulated after cortistatin treatment in both age groups (Figure 46a). Regarding serum cytokines levels after MCAO, IL-6, and MCP-1 were particularly elevated in *Cort*$^{-/-}$ mice compared to control mice especially in young animals (Figure 46b). As observed in wild-type animals, older mice seemed to display an exacerbated response, although differences did not reach statistical significance (Figure 46b). Notably, treatment with cortistatin seemed to modulate IL-12, IL-6, and MCP-1, with significant observed in the older mice (Figure 46b). These results suggest that the pro-inflammatory context in the periphery of cortistatin-deficient mice may contribute to a more adverse response towards the ischemic insult.

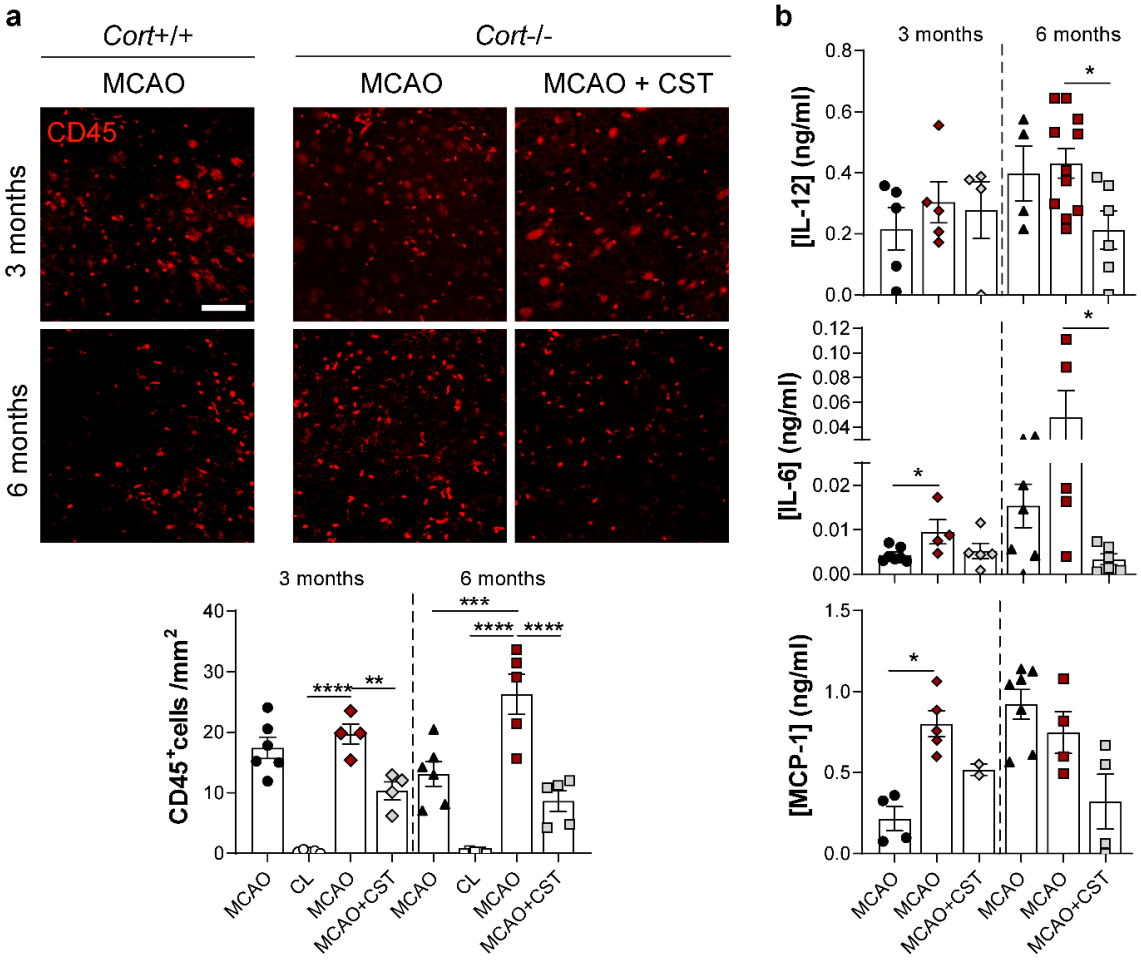

Figure 46. Deficiency of cortistatin provokes enhanced immune infiltration and altered immune peripheral response. a. Representative images of the striatum of *Cort*$^{-/-}$ young (3 months old) and middle-aged (6 months old) mice subjected to MCAO and treated with saline solution (MCAO) or with cortistatin (115 µg/kg) (MCAO+CST) at 24 h. *Cort*$^{+/+}$ mice from each age group subjected to MCAO were used as controls. Sections were stained with CD45 antibody for leukocytes (top)**.** Scale bar 100 µm. Leucocyte density (number of cells/mm^2) was calculated in the striatum and in the contralateral side (CL) of the different experimental groups (bottom). **b.** IL-12, IL-6, and MCP-1 concentration (ng/ml) measured in serum by ELISA assay. Data are the mean ± SEM. Dots represent 4-6 independent mice. **vs* *Cort*$^{-/-}$ MCAO *$p \leq 0.05$, **$p \leq 0.01$, ***$p \leq 0.001$, ****$p \leq 0.0001$.

In summary, *Cort*$^{-/-}$ mice displayed a more severe neurological deficit, dysfunctional microglia and astrocyte response, together with a disrupted BBB that leads to increased leakage and immune infiltration. Moreover, the immune peripheral response is enhanced compared to wild-type mice. The administration of exogenous cortistatin after stroke to mice lacking cortistatin, regulates the BBB breakdown and the local and peripheral immune activation. Despite the effect of cortistatin being exerted in a different way that when administered in MCAO wild-type animals it also leads to decreased neurodegeneration and neuroinflammation.

4.4. Study of the cellular and molecular mechanisms of cortistatin in brain endothelium dynamics

As previously mentioned, the breakdown of the BBB is a hallmark in many neurodegenerative and neuroinflammatory disorders, being particularly important in ischemic stroke. Notably, the integrity of the BBB can be compromised even with alterations restricted only to the BECs [112]. Following our previous results that demonstrated significant changes in brain endothelium and BBB dynamics after stroke (Figures 38-39, 44-45), we wanted to gain further insights into the mechanisms underlying cortistatin regulation in the endothelium after ischemic damage. To achieve this, we used BECs, from both mice and humans (including cell lines and primary cells), and exposed them to different stimuli simulating ischemic stroke.

4.4.1. Cortistatin modulates the permeability and integrity of mouse brain vascular endothelium after ischemic injury

We examined the effect of cortistatin in the dynamics of b.End5 cells exposed to brain ischemia-like insults, including inflammation (LPS), glucose deprivation (GD), or oxygen-glucose deprivation and reperfusion (OGD-R). When needed, cells were treated with cortistatin (100 nM). Control cells were subjected to normoxia/normoglycemia (NX/NG) conditions (Figure 47a).

First, we examined the expression of the cortistatin system (*i.e.,* cortistatin, somatostatin, and their receptors) in b.End5 cells in physiological conditions. Despite the fact that somatostatin, cortistatin, and ghrelin, along with their corresponding receptors have been identified in murine and human peripheral ECs [196,246], the expression of these neuropeptides and their receptors in BECs is either absent or poorly documented [194,196]. We observed that under physiological conditions *Sstr2* was preferentially expressed, while *Sstr1, Sstr4, and Ghsr* levels were lower. In turn, *Sstr3* and *Sstr5* expression was undetectable. Additionally, despite being expressed at low levels, we identified that *Cort* was preferentially expressed rather than *Sst* in these BECs (Figure 47b).

We then explored endothelial cell permeability to two different-size tracers (*i.e.,* EBA and NaF), after LPS, GD, and OGD-R insults. We observed an enhanced permeability after these three ischemic insults for both tracers. However, the treatment with cortistatin significantly reversed this increased permeability (Figure 47c). As we mentioned previously, BBB breakdown is normally related with TJs/AJs disruption, so we next studied their expression and distribution under the three insults. We reported that the disruption of the barrier after GD and OGD-R was accompanied by a delocalization and disruption of the TJ assembly (Figure 47d). Notably, the ischemic environment caused the alteration of the uniform pattern of ZO-1 in the membrane (Figure 47d), together with an increase in the intracellular expression of claudin-1, which is associated with BBB disruption, as reported by [247] (Figure 47e). However, cortistatin treatment not only restored ZO-1 integrity in the peripheral cell membrane (Figure 47d), as observed *in vivo* (Figure 38d), but also significantly decreased the accumulation of claudin-1 in the cytosol under both conditions (Figure 47e).

Moreover, in addition to maintaining and preserving BBB, ECs possess immunomodulatory potential and can display inflammatory responses following ischemic insults [248]. In this sense, we observed an altered inflammatory response in b.End5 cells subjected to GD or OGD-R, characterized by an increased production of IL-6 and MCP-1 proinflammatory factors, and reduced levels of nitrite, all of which are associated with BBB leakage [249] (Figure 47f,g). However, cortistatin treatment demonstrated an immunomodulatory effect on brain endothelium activation through the significant downregulation of TNF-α and MCP-1, although IL-6 and nitrite levels were not affected (Figure 47f,g). Finally, a significant reduction in the secreted levels of endogenous cortistatin was observed in OGD-R conditions (Figure 47h).

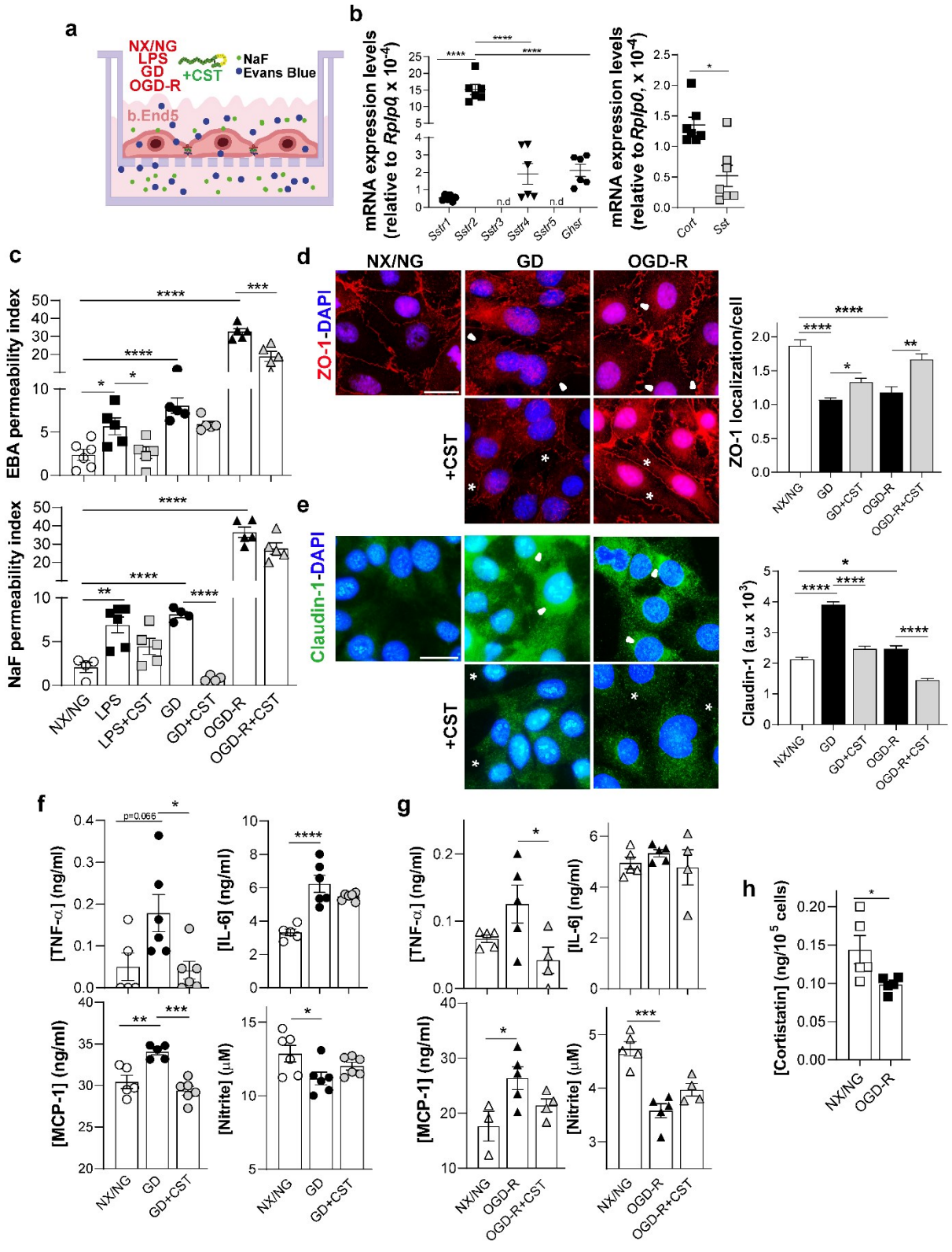

Figure 47. Cortistatin regulates b.End5 cell integrity after different ischemic insults. a. Schematic representation of the experimental design. Murine b.End5 cells were exposed to lipopolysaccharide (LPS), glucose deprivation (GD) for 24 h, or to 4 h of oxygen-glucose deprivation followed by 20 h of reoxygenation (OGD-R). Cortistatin (CST, 100 nM) was administered simultaneously to the insult (LPS+CST; GD+CST) or during recovery (OGD-R+CST). Cells

incubated in normoxia/normoglycemia (NX/NG) were used as controls. **b.** mRNA expression levels of cortistatin receptors (left, *Sstr1-5* and *Ghsr*) and ligands (right, somatostatin, *Sst* and cortistatin, *Cort*) in the brain endothelium under NX/NG. Data represent the mean mRNA expression levels quantified by real-time qPCR analyses and normalized to *Rplp0*. N = 5-7 cultures/group. **c**. Endothelial permeability was evaluated by EBA and NaF influx**.** Permeability was represented as the index (%) ofthe tracer permeability *vs* an empty-coated insert. N = 4-6 cultures/group. **d,e.** Representative immunofluorescence images showing the cellular distribution of ZO-1 (**d**, red) and claudin-1 (**e**, green) in b.End5 cells after GD or OGD-R in the absence or presence of cortistatin. **d.** ZO-1 delocalization (arrowheads highlighting gaps in ZO-1 structure in the membrane) was evaluated by calculating the ratio of ZO-1 staining intensity in the membrane *vs* the cytosol. After cortistatin treatment, ZO-1 rearrangement was observed in the membrane (asterisks). **e.** The cytosolic expression of claudin-1 in the cytosol was quantified by fluorescence intensity (expressed as arbitrary units, a.u). Claudin-1 displayed intracellular overexpression after GD/OGD-R (arrowheads). Cortistatin significantly reduced claudin-1 enhanced expression (asterisks). 25-50 selected ROIs from 4 independent fields were analysed. N = 6 cultures/group. Scale bar: 20 µm. **f**,**g.** Levels of inflammatory cytokines TNF-α, IL-6, chemokine MCP-1 (all in ng/ml), and nitrite (µM) were determined in culture supernatants after GD (**f**) or OGD-R (**g**) with or without cortistatin treatment. N = 4-6 cultures/group. h. Cortistatin protein levels were quantified in b.End5 supernatants after exposure to NX/NG and OGD-R. Results are normalized in ng protein/105 cells. N = 5 cultures/group. Data are the mean ± SEM. Dots represent individual values of independent cultures. *$p \leq 0.05$, **$p \leq 0.01$, ***$p \leq 0.001$, ****$p \leq 0.0001$.

Despite the fact that immortalized mouse brain endothelioma cell lines are commonly used, primary BECs appear to be a more biologically relevant alternative, since they better retain BBB properties *in vitro* [250]. Therefore, we set up an isolation protocol to isolate BECs from the adult CNS microvasculature (Figure 27). Similar to our observations in the cell line, cortistatin, somatostatin, and their receptors were also expressed by primary BECs under normal physiological conditions. As described in b.End5 cells, high levels of *Sstr2* and *Sstr4* were observed while *Sstr1*, *Sstr3*, *Sstr5,* and *Ghsr* displayed low levels. Notably, *Cort* endogenous expression was higher compared to *Sst* (Figure 48b).

To further support our previous findings with b.End5, we exposed BECs to OGD-R, as we considered it to be the most suitable insult to mimic the model of ischemic–reperfusion observed during MCAO procedure. BECs exhibited a significant increase in permeability (Figure 48c), impaired TJ architecture (*i.e.,* loss of ZO-1 and claudin-5 localization in the membrane and claudin-1 enhancement) (Figure 48d), and an exacerbated immune response after OGD-R (Figure 48e). Of note, cortistatin treatment effectively reversed BECs dysfunction to a homeostatic-like state, reducing permeability, preserving TJs, and downregulating the production of immune mediators, especially IL-6 and MCP-1 (Figure 48c-e). Importantly, as described in b.End5 cells, cortistatin secretion was reduced under OGD-R conditions (Figure 48f).

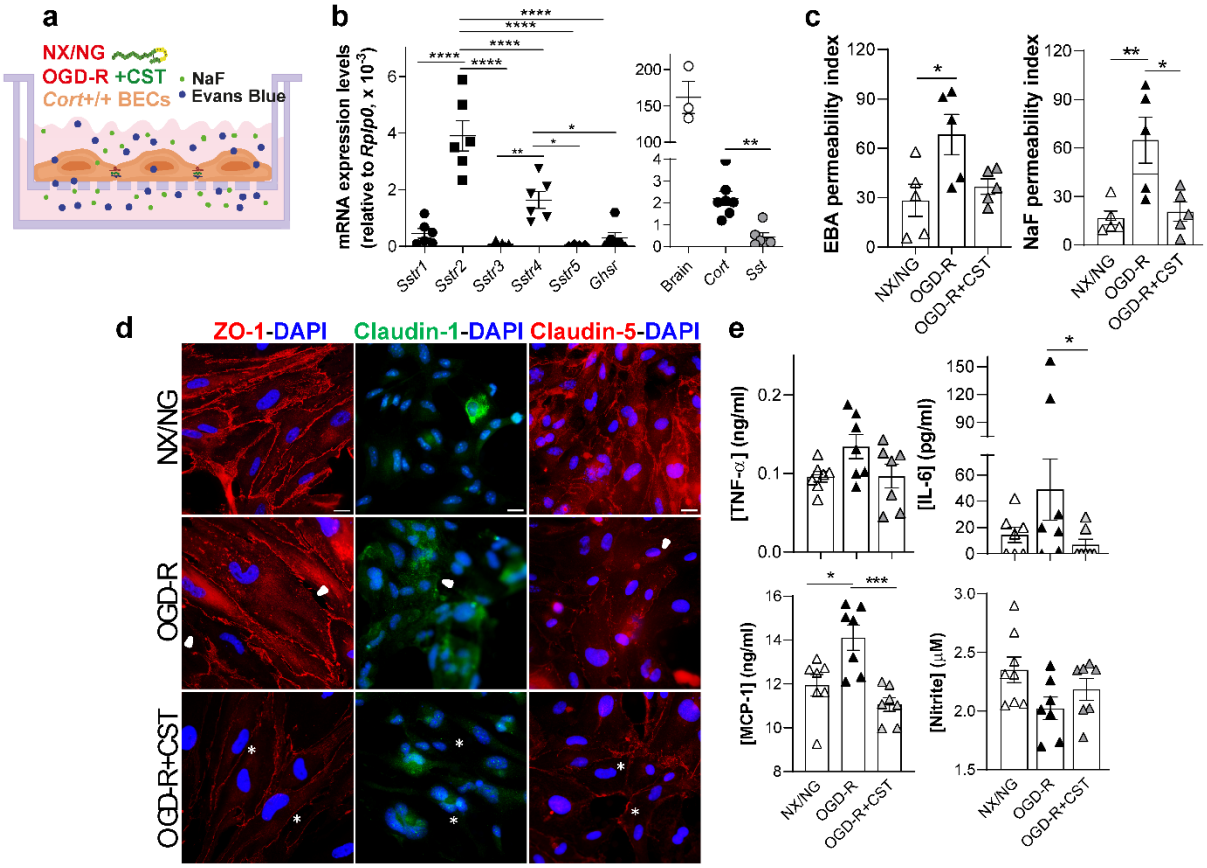

Figure 48. Cortistatin protects from murine brain endothelium breakdown after ischemic-like conditions. a. Schematic representation of the experimental design. Primary BECs (BECs) isolated from 8- week-old *Cort*$^{+/+}$ mice were exposed to OGD-R with or without cortistatin (CST, 100 nM). As controls, cells were incubated in normoxia/normoglycemia (NX/NG). **b.** mRNA expression levels of cortistatin receptors (left, *Sstr1-5* and *Ghsr*) and ligands (right, somatostatin, *Sst* and cortistatin, *Cort*) in the brain endothelium under NX/NG. Data represent the mean mRNA expression levels quantified by real-time qPCR analyses and normalized to *Rplp0*. N = 5-7 cultures/group. Mouse brain (n = 3) was used as an internal reference for endogenous *Cort* expression. **c.** Evaluation of endothelium functionality was examined by EBA and NaF permeability. Permeability was expressed as the index (%) of the tracer permeability *vs* an empty-coated insert. N = 5 cultures/group. **d.** Tight-junctions integrity evaluation. Representative immunofluorescence images of ZO-1 (red), claudin-1 (green), and claudin-5 (red) distribution in BECs after NX/NG, OGD-R, or OGD-R+CST. Arrowheads indicate disruptions in ZO-1 and claudin-5 along the cell membrane and the cytosolic overexpression of claudin-1. After cortistatin treatment, asterisks highlight the reestablishment of ZO-1 and claudin-5 continuous pattern in the membrane and the reduced claudin-1 intracellular location. Scale bar: 20 µm. **e.** Immune factor levels were evaluated in culture supernatants after NX/NG, OGD-R, or OGD-R+CST. N = 7 cultures/group. Each culture derived from 4 pooled brains. Data are the mean ± SEM. Dots represent the individual values from each independent culture. *$p \leq 0.05$, **$p \leq 0.01$, ***$p \leq 0.001$, ****$p \leq 0.0001$.

4.4.2. Cortistatin regulates the barrier properties of human brain endothelium after ischemic injury

Furthermore, we explored the potential role of cortistatin in human-derived brain ECs, aiming to better understand whether the dynamics of this neuropeptide in humans mirrored those in mice. Specifically, cells were incubated under hypoxia-reoxygenation (HPX-R) and OGD-R (Figure 49a), aiming to mimic ischemic–reperfusion injury. Unexpectedly, no changes in endothelial permeability between NX/NG and HPX-R conditions were detected (Figure 49b), likely due to the variability of serum-derived effects [251,252]. However, hBLECS showed a disorganization in ZO-1 structure (Figure 49c). Interestingly, treatment with cortistatin reduced permeability and restored ZO-1 presence in the cell membrane (Figure 49b,c). On the contrary, OGD-R increased endothelial permeability of hBLECs (Figure 49e). This increase was accompanied by increased ZO-1 disorganization (reduced ratio membrane/cytosol), as well as a depletion of claudin-5 expression in the membrane (Figure 49f). Paradoxically, although the addition of cortistatin significantly recovered the expression and architecture of ZO-1 and claudin-5 after OGD-R, it did not impact the permeability (Figure 49e,f). This conforms to other studies that reported dysfunctional and discontinuous junctional phenotypes without correlating with the permeability measures [253]. Notably, levels of cortistatin were decreased after the hypoxic-reoxygenation and OGD-R insults (Figure 49d,g).

Taken together, these data support our previous findings *in vivo* and demonstrate that cortistatin (and not somatostatin) plays a crucial role in the regulation of brain endothelium integrity and functionality at different levels after several ischemic injury-like conditions. In addition, our findings indicate that both murine and human brain ECs respond to ischemic conditions by modifying the expression of cortistatin (Figures 47-49).

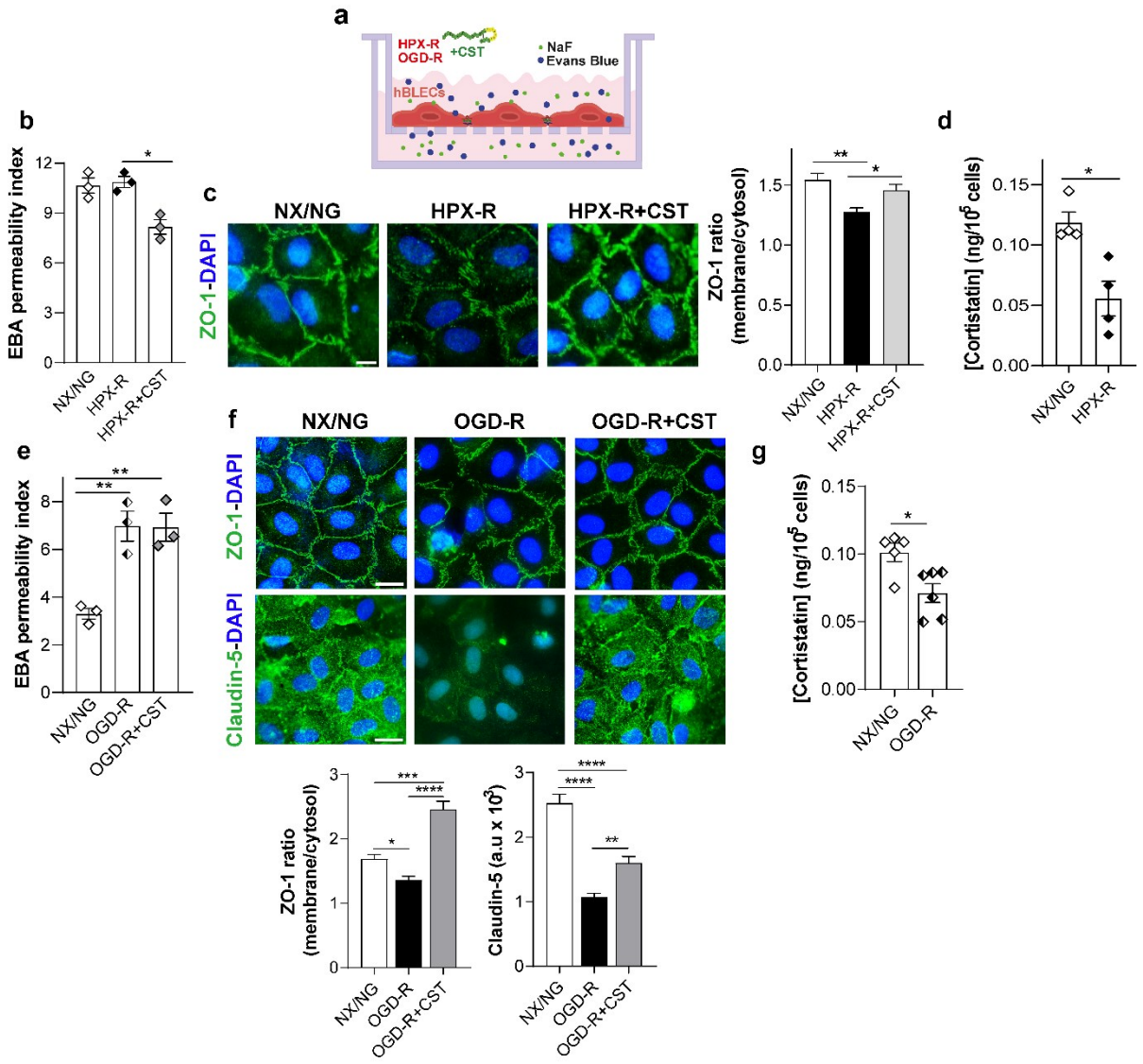

Figure 49. Role of cortistatin in the human brain endothelium. **a.** Schematic representation of the experimental design. Human brain-like endothelial cells (hBLECs) incubated for 4 h under hypoxia or oxygen-glucose deprivation, followed both by 20 h of reoxygenation (HPX-R/OGD-R) in the absence or presence of cortistatin (HPX-R + CST/OGD-R, 100 nM). **b,e.** Evaluation of endothelium integrity was represented as the index (%) of EBA permeability *vs* an empty-coated insert after HPX-R/HPX-R+CST (**b**) or OGD-R/OGD-R+CST (**e**). N = 3 cultures/group. Data are the mean ± SEM. Dots represent individual values from each independent culture. **c,f.** Representative immunofluorescence images of ZO-1 (green) after HPX-R/HPX-R+CST (**c**) and ZO-1 (green) and claudin-5 (green) after OGD-R/OGD-R+CST (**f**). Arrowheads indicate reduced and disrupted expression of ZO-1/claudin-5 (**c,f**) and asterisks highlight the restoration of junctional integrity exerted by cortistatin (**c,f**). Delocalization of ZO-1 was evaluated by the ratio of ZO-1 staining intensity in the membrane vs the cytosol (**c**). Claudin-5 expression was quantified by fluorescence intensity (expressed as arbitrary units, a.u) (**f**). Scale bar: 20 µm. Analysis was performed in 25–50 selected ROIs from 4 independent fields. N = 6 cultures/group. **d, g.** Cortistatin protein levels quantified in hBLECs supernatants after NX/NG, HPX-R (**d**), and OGD-R (**g**), as described. Results are normalized in ng protein/10^5 cells. N = 4 cultures/group. *$p \leq 0.05$, **$p \leq 0.01$, ***$p \leq 0.001$, ****$p \leq 0.0001$.

4.4.3. Deficiency of cortistatin exacerbates a dysfunctional brain endothelium response

Previous studies have demonstrated the regulatory role of cortistatin in the peripheral vascular system, showing exacerbated responses to vascular lesions in cortistatin-deficient mice [145–147]. Moreover, our *in vivo* study demonstrated that cortistatin-deficient mice presented a dysfunctional BBB after stroke (Figure 44). However, the precise mechanisms underlying the influence of cortistatin in brain endothelium functions are yet to be described. For this purpose, we isolated BECs from the brain microvasculature of wild-type (*Cort*$^{+/+}$) and cortistatin-deficient mice (*Cort*$^{+/-}$ and *Cort*$^{-/-}$) and subjected them to control (NX/NG) and ischemic (OGD-R) conditions (Figure 50a). Importantly, we observed an increase in endothelial permeability in cortistatin-deficient BECs compared to wild-type cells, both under control and ischemic conditions (Figure 50a). This enhanced permeability in cells with partial/complete absence of cortistatin was associated with a greater delocalization, disruption, and dysfunctional assembly of TJs and AJs in both control and ischemic conditions (Figure 50b,c). Specifically, ZO-1 suffered dramatic disintegration and redistribution in cortistatin-deficient cells under both conditions (NX/NG and OGD-R) (*i.e.,* reduced ratio between the location of ZO-1 in the membrane *vs* the cytosol) (Figure 50b). Additionally, cortistatin-deficient cells displayed a significant overexpression of claudin-1 (Figure 50b). Similar to ZO-1 findings, claudin-5 and VE-cadherin showed discontinuities in their junctional structures and a substantial reduction of expression in cortistatin-deficient BECs compared to wild-type cells (Figure 50c). Of note, the junctional disintegration of cortistatin-deficient cells under control conditions (NX/NG) closely resembled that observed in wild-type cells after OGD-R. Besides, we also conducted a rhodamine–phalloidin labelling (Figure 50c) to investigate the assembly of cytoskeleton-junctional proteins. Of note, F-actin is typically distributed in random fibres throughout the cytosol (as shown in NX/NG wild-type BECs) and undergoes a drastic reorganization into thick stress bundles after injury [254]. Surprisingly, thick stress bundles were observed in cortistatin-deficient cells even under control conditions, resembling those observed in wild-type cells after OGD-R (Figure 50c).

The lack of junctional integrity and increased permeability in cortistatin-deficient BECs that we reported were also correlated with an altered inflammatory phenotype (Figure 50d). Remarkably, we noted an increase in TNF-α, IL-6, and MCP-1 in BECS lacking the neuropeptide under control conditions, although some differences did not reach statistical significance. Importantly, decreased nitrite production was observed in both control and ischemic conditions (Figure 50d). Interestingly, endogenous levels of

cortistatin in *Cort*$^{+/-}$ endothelium in physiological conditions were similar to those secreted by wild-type cells under OGD-R (Figure 50e).

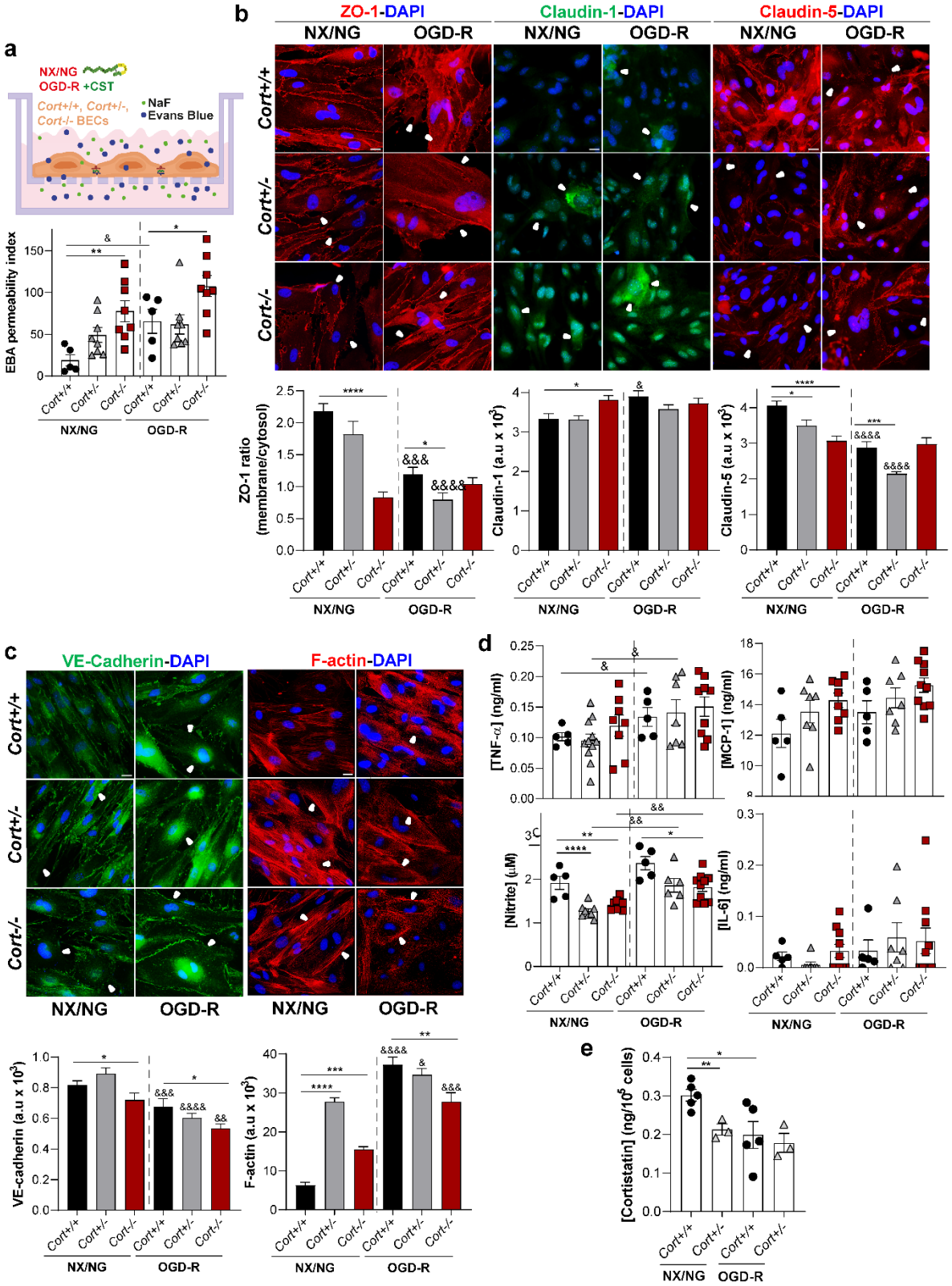

Figure 50. Cortistatin-deficient BECs show increased leakage, disrupted integrity, and exacerbated immune activation. a. BECs were isolated from wild-type (*Cort*$^{+/+}$) and cortistatin-deficient (partial: *Cort*$^{+/-}$; complete: *Cort*$^{-/-}$) mice and exposed to 4 h oxygen–glucose deprivation followed by 20 h of reoxygenation (OGD-R). Evaluation of endothelium integrity was represented as the index (%) of EBA permeability *vs* an empty-coated insert. N = 5–8 cultures/group. **b,c.** Representative immunofluorescence images of tight-junctions, adherens-junctions, and cytoskeleton proteins distribution in BECs incubated in basal conditions (NX/NG) and after OGD-R. **b.** Top, immunofluorescence of tight-junctions ZO-1 (red), claudin-1 (green), and claudin-5 (red). Arrowheads indicate membrane disruption in ZO-1 and claudin-5, or cytosolic overexpression of claudin-1. Bottom, delocalization of ZO-1 was evaluated through the ratio of ZO-1 staining intensity in the membrane vs the cytosol. Claudin-1 and claudin-5 cellular expression was quantified by fluorescence intensity (expressed as arbitrary units, a.u). **c.** Top, immunofluorescence of adherens-junction protein VE-cadherin (green) and F-actin labelling (red). Arrowheads show discontinuous expression of VE-cadherin and F-actin stress fibres. Bottom, expression was quantified by fluorescence intensity (a.u). 25–50 selected ROIs in 4 independent fields were analysed. N = 6 cultures/group. Scale bar: 20 µm. **d.** Levels of inflammatory factors were determined in culture supernatants after OGD-R. N = 5–10 cultures/group. **e.** Cortistatin protein levels quantified in *Cort*$^{+/+}$ and *Cort*$^{+/-}$ BECs supernatants after NX/NG and OGD-R. Results are normalized in ng protein/10^5 cells. Data are the mean ± SEM with dots representing individual values from independent cultures. Cells for each culture were derived from 4 pooled brains. **vs Cort*$^{+/+}$ either in NX/NG and OGD-R; $^{\&}$*vs* corresponding genotype (*Cort*$^{+/+}$, *Cort*$^{+/-}$, *Cort*$^{-/-}$) in NX/NG. $^{*/\&}p \leq 0.05$, $^{**/\&\&}p \leq 0.01$, $^{***/\&\&\&}p \leq 0.001$, $^{****/\&\&\&\&}p \leq 0.0001$.

Taken together, these findings indicate that brain ECs from cortistatin-deficient mice exhibit a leaky and inflammatory-like endothelium. This already occurs under physiological conditions, and is exacerbated under damage. Our findings indicate that cortistatin, potentially acting through Sstr4, Sstr2, or Sstr5, plays a crucial role in regulating the dynamics of the brain endothelium during physiology and ischemic injury, which could be determinant for BBB integrity.

4.4.4. Cortistatin-deficient brain endothelium displays dysregulated physiological pathways

To further investigate the molecular profile associated with the behaviour of the cerebral vascular endothelium in the absence of cortistatin, we compared the transcriptomes of *Cort*$^{+/+}$ and *Cort*$^{-/-}$ BECs under NX/NG or OGD-R using next-generation sequencing (RNA-seq). First, we verified that our samples showed strong enrichment of specific markers for BECs (*e.g.,* Cldn5, Pecam1/CD31, or Tjp1/ZO-1). In contrast, the barely detected expression of markers associated with pericytes (*Cspg4, Kcnj8, Vtn*), astrocytes (*Gfap, Aqp4, Gli1*), neurons (*Nefl, Gabra1, Reln*), oligodendrocytes (*Olig1, Mog, Mbp*), or microglia (*Ptprc, Itgam, Tnf*) (Appendix, Figure A1).

We identified 613 genes (139 upregulated and 474 downregulated) with significant differential expression (FDR < 0.05) in brain endothelium from cortistatin-deficient mice

compared to wild-type in an NX/NG environment (Figure 51a,b). On the other hand, we observed 407 genes (111 upregulated and 296 downregulated) differentially expressed in *Cort*$^{-/-}$ BECs compared to *Cort*$^{+/+}$ after OGD-R exposure (Figure 51d,e). Some of the top downregulated and upregulated genes were validated by qPCR showing a high degree of correlation with the RNA-seq quantification (Appendix, Figure A1). Notably, in these two comparisons, we observed that 226 DEGs in cortistatin-deficient BECs (more than half out of the total) were shared between NX/NG and OGD-R.

Subsequently, we conducted gene ontology terms overrepresentation analyses addressing biological processes (BP) (Figure 51c,d), molecular functions (MF), and cellular components (CC) (Appendix, Figure A2,3). Noteworthy, a great proportion of DEGs in *Cort*$^{-/-}$ BECs were associated with downregulated functional networks both in NX/NG and OGD-R (Figure 52c,f). These downregulated pathways included immune response, cell-matrix remodelling, cell signalling and transcription, brain endothelium dynamics, endothelial cell fate commitment, cell adhesion and migration, and cell metabolism. Taken together, these findings suggest that the absence of cortistatin may induce the downregulation of multiple molecular networks, potentially impacting not only physiological functions but also the responsiveness of BECs to ischemic injury conditions.

To further explore the characteristics that may be dysfunctional in cortistatin-deficient brain endothelium under physiological and injury conditions, we analysed the transcriptional profiles associated with the shift from a healthy (NX/NG) to an ischemic-reperfusion state (OGD-R), in both *Cort*$^{+/+}$ and *Cort*$^{-/-}$ BECs. We identified 83 differentially expressed genes (48 upregulated and 35 downregulated) in *Cort*$^{+/+}$ cells during the transition from NX/NG to OGD-R (Figure 52a,b). Surprisingly, we only detected 20 differentially expressed genes (3 upregulated and 17 downregulated) in *Cort*$^{-/-}$ BECs from the shift of NX/NG to OGD-R (Figure 52d,e). Regarding the ontology analyses, the majority of upregulated DEGs in *Cort*$^{+/+}$ BECs under OGD-R were involved in gene functions related to endothelial cell responses to injury (Figure 52c). Notably, these genes were associated not only with a detrimental response to damage but also with several processes aimed at a later balanced repair response (*i.e.,* regulation of leukocyte migration, cellular defence response, wounding response, remodelling of the ECM and cytoskeleton, regulation of apoptosis and cell proliferation, cellular response to oxygen, angiogenesis, and cell adhesion and migration) (Figure 52c). On the other hand, the majority of downregulated DEGs in *Cort*$^{-/-}$ BECs under OGD-R were predominantly associated with functions crucial for injury responses (*i.e.,* MAPK cascade, apoptosis, cell proliferation,

blood vessel remodelling, cell migration, and several metabolic pathways) (Figure 52f). Therefore, to effectively respond to damage would be challenging for these cells.

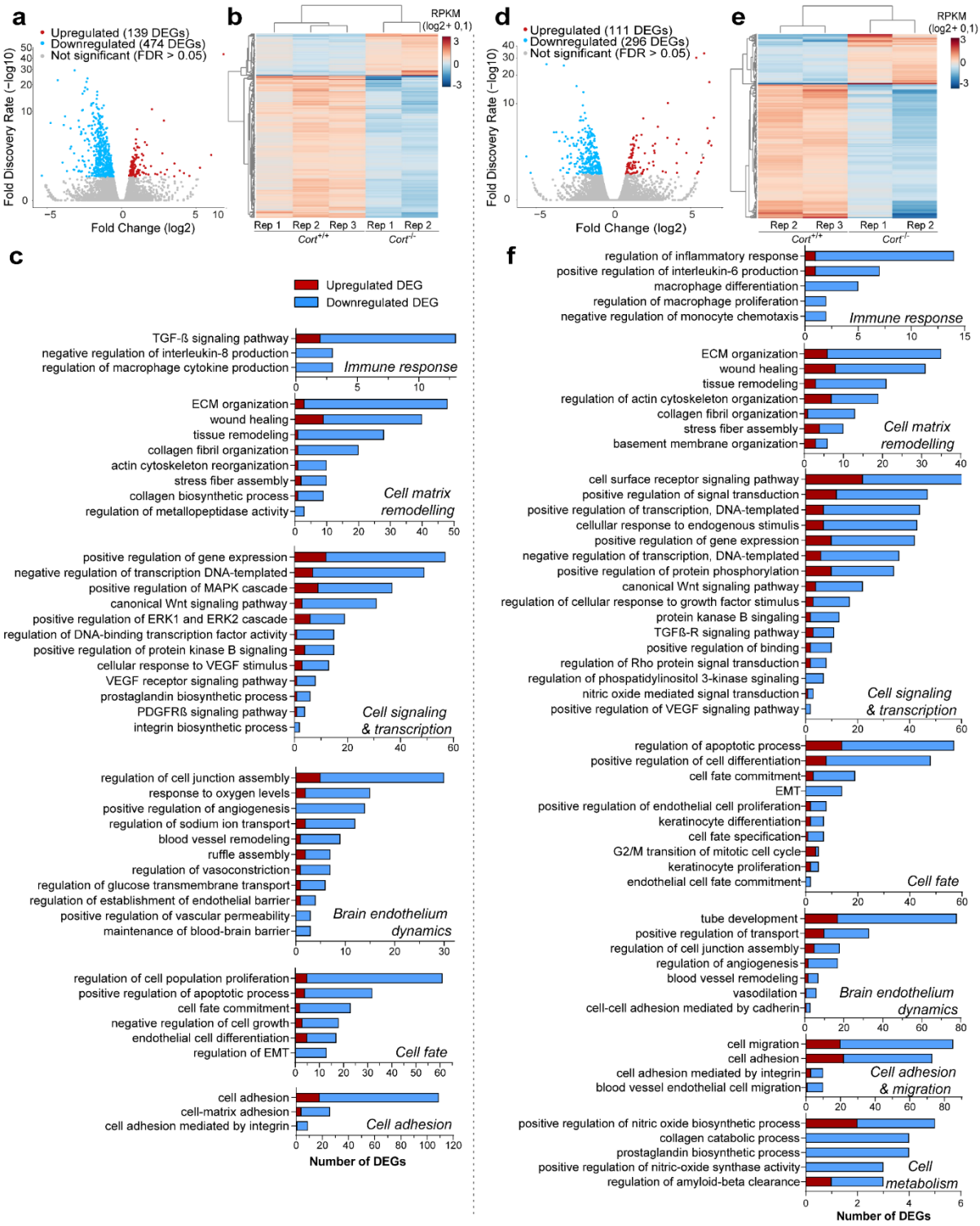

Figure 51. Deregulated gene pathways in cortistatin-deficient brain endothelium. Comparison of gene expression profiles from BECs isolated from *Cort*$^{+/+}$ vs *Cort*$^{-/-}$ mice in NX/NG or OGD-R conditions. Each biological replicate (Rep) was pooled from 3 mice per genotype. **a, d**. Volcano plots represent differentially expressed genes (DEGs) from *Cort*$^{-/-}$ *vs Cort*$^{+/+}$ BECs

incubated under NX/NG for 24 h (**a**) or under OGD-R (**d**). Each dot represents one gene. Significant DEGs (with false discovery rate, FDR, $p < 0.05$) from each comparison upregulated and downregulated are depicted in red and blue, respectively. Grey dots represent not significantly altered genes. The number of DEGs in each comparison is shown in the legend. **b,e**. Heatmaps and unsupervised hierarchical clustering of DEGs in *Cort*$^{-/-}$ *vs Cort*$^{+/+}$ BECs exposed to NX/NG (**b**) and in *Cort*$^{-/-}$ *vs Cort*$^{+/+}$ BECs exposed to OGD-R (**e**). **c, f.** Gene ontology (GO) terms for biological processes significantly overrepresented in *Cort*$^{-/-}$ *vs Cort*$^{+/+}$ BECs incubated under NX/NG (**c**) or OGD-R (**f**). GO terms were manually annotated into similar networks, including immune response, cell-matrix remodelling, cell signalling and transcription, brain endothelium dynamics, cell fate, cell adhesion and migration, and cell metabolism. Red and blue bar-segments correspond to the numbers of upregulated and downregulated DEGs, respectively. TGF-β, transforming growth factor beta; ECM, extracellular matrix; MAPK, mitogen-activated protein kinase; ERK, extracellular-signal-regulated kinase; VEGF, vascular endothelial growth factor; PDGFRβ, platelet-derived growth factor receptor beta; EMT, epithelial to mesenchymal transition.

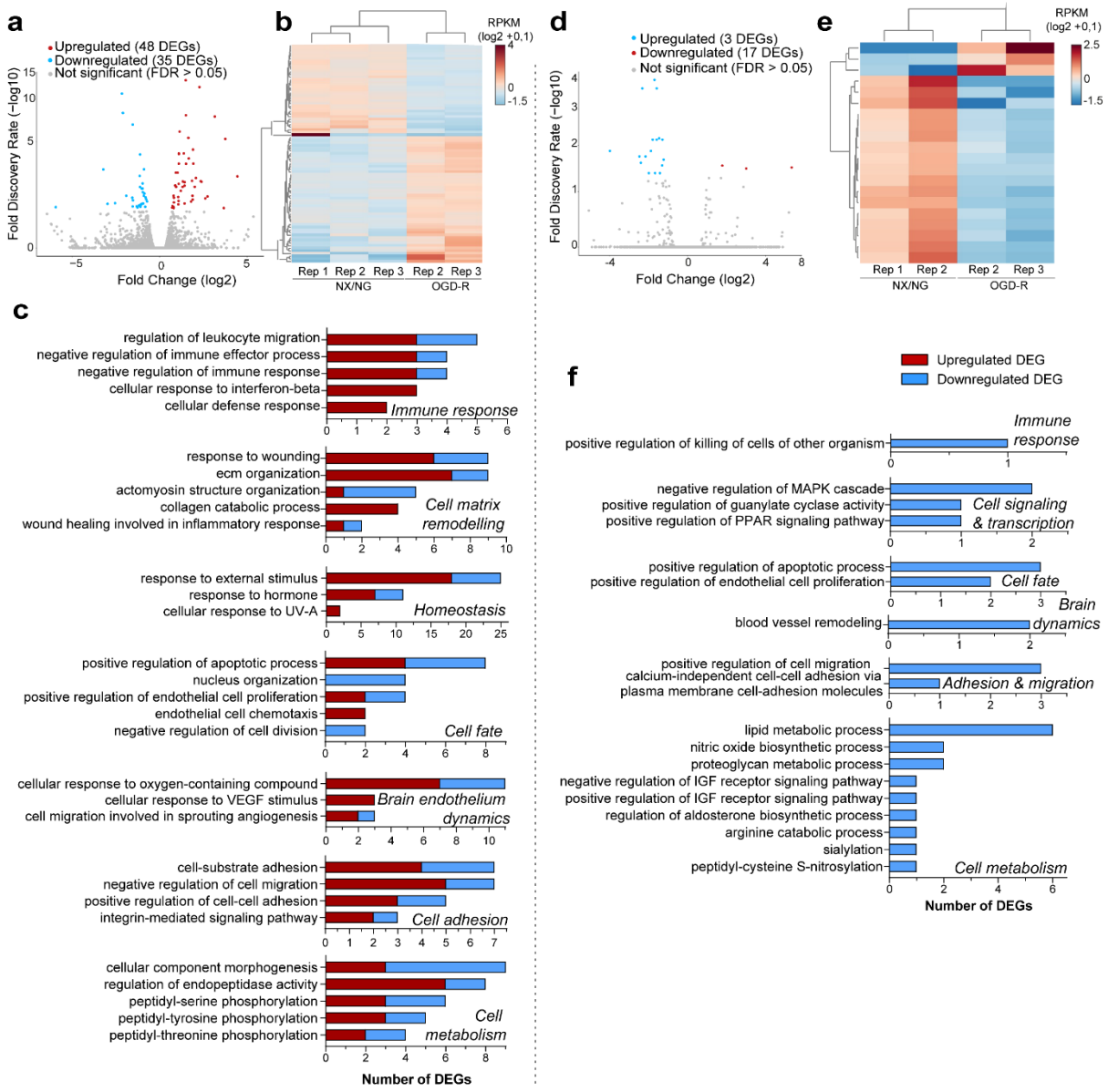

Figure 52. Lack of cortistatin affects the physiological dynamics of the brain endothelium and its ability to respond to damage. Comparison of gene expression profiles during the transition from basal (NX/NG) to ischemic (4 h) and reperfusion (OGD-R) (20 h) states in *Cort*$^{+/+}$ and *Cort*$^{-/-}$ BECs. Each biological replicate (Rep) was pooled from 3 mice per genotype. **a**, **d.** Volcano plots represent DEGs from *Cort*$^{+/+}$ BECs under OGD-R *vs* NX/NG (**a**), or *Cort*$^{-/-}$ BECs incubated under OGD-R *vs* NX/NG (**d**). Each dot represents one gene. Significant DEGs (with false discovery rate, FDR, $p < 0.05$) from each comparison upregulated and downregulated are depicted in red and blue, respectively. Grey dots represent not significantly altered genes. The number of DEGs in each comparison is shown in the legend. **b,e.** Heatmaps and unsupervised hierarchical clustering of DEGs in *Cort*$^{+/+}$ BECs under OGD-R *vs* NX/NG (**b**) and DEGs in *Cort*$^{-/-}$ BECs under OGD-R *vs* NX/NG (**e**).**c,f.** GO terms for biological processes significantly overrepresented in *Cort*$^{+/+}$ BECs under OGD-R *vs* NX/NG (**c**) and DEGs in *Cort*$^{-/-}$ BECs under OGD-R *vs* NX/NG (**f**). GO terms were manually annotated into similar networks, including immune response, cell-matrix remodelling, cell signalling and transcription, homeostasis, cell fate, brain endothelium dynamics, cell adhesion and migration, and cell metabolism. Red and blue bar-segments correspond to the numbers of upregulated and downregulated DEGs, respectively. ECM, extracellular matrix, VEGF, vascular endothelial growth factor, MAPK, mitogen-activated protein kinase, PPAR, peroxisome proliferator-activated receptor.

Next, we performed a more thorough examination of the DEGs involved in these pathways in the four different comparisons. We classified them based on the extent of their expression changes (*i.e.,* $\log_2$ fold change) and the biological relevance of their functions to the general brain endothelial dynamics (Figure 53a-i). These included ECM, cell-cell contact, BBB dynamics, cell fate, transporters, immune response, response to oxygen, signalling, among others. The analysis of the ECM cluster (Figure 53a) revealed that most of the genes were downregulated in both control (NX/NG) and ischemic (OGD-R) conditions in *Cort*$^{-/-}$ brain endothelium (Figure 53a). These included genes encoding collagens and other ECM components (*e.g., Col1a2, Col5a3, Col6a3, Pcolce,* or *Vcan)*, metallopeptidases (including, *Adamts1, Adamts2, Adamtsl3*), metalloproteinases (*i.e., Mmp2, Mmp19*), MMPs inhibitors (*i.e., Timp1, Timp2, Timp3*), as well as genes related to actin cytoskeleton dynamics (*e.g., Eps8, Cracd,* or *Wasf3*), among others. Importantly, we found that *Cobl* and *Arhgap28*, linked to cytoskeleton disassembly, were upregulated in cortistatin-deficient BECs under NX/NG (Figure 53a), supporting the results *in vitro* (Figure 50d). Conversely, the ECM components *Col5a3, Col15a1,* the metalloproteinases *Mmp3, Mmp10,* or *Mmp28,* the metalloproteinase inhibitor *Timp1*, or the enzyme *Has2* were upregulated in *Cort*$^{+/+}$ cells under OGD-R conditions, following the canonical response to damage and recovery (Figure 53a). Nevertheless, in *Cort*$^{-/-}$ cells from the shift of NX/NG to OGD-R, we did not report differential expression for any of these or related genes (Figure 53a).

Moreover, several genes involved in cell adhesion/migration (*e.g, Tln2, Sned1, H19, Pkp1*), as well as some integrins (*i.e., Itga10, Itgb5, or Itgbl1*), were downregulated

in cortistatin-deficient cells compared to wild-type cells during both NX/NG and OGD-R (Figure 53b). Of note, *Itga3* and *Itga4*, involved in immune cell activation and chemoattraction (Figure 53b), and *Epcam*, involved in adhesion and migration (Figure 53h) were upregulated in the *Cort*$^{-/-}$ cells.

Furthermore, we observed that genes linked to BBB integrity were affected. For instance, we found that cadherins such as *Pcdh18, Pcdh19,* and *Cdh11* were downregulated in control conditions in *Cort*$^{-/-}$ BECs (Figure 53c). Interestingly, genes linked to BBB breakdown and TJ disintegration [247,255,256] were upregulated in cortistatin-deficient brain endothelium during OGD-R (*i.e., Cldn4, Cldn6*, *Cldn9*, *Cdh1*, *Mylk*, and *Myh14*) or even in NX/NG conditions (*i.e., Cldn1* and *F11r*) (Figure 53b,h). This supports our previous findings where we observed lack of integrity of *Cort*$^{-/-}$ BECs (Figure 50c-e). We also found that many master regulators of vascular remodelling (including *Agt,* or *Plpp3*), vasoregulation (*e.g., Angpt1, Ptgs1,* or *S1pr3*), and angiogenesis (*e.g., Vegfa, Vegfd, Bdnf, Pdpn,* or *Sema3c*) were already downregulated in *Cort*$^{-/-}$ BECs under a physiological stage and some also reduced after OGD-R (Figure 53b,c). Conversely, only a few pro-angiogenic genes such as *Srpx2, Stab1,* or Notch-dependent *Pcdh12* were upregulated (Figure 53c).

Additionally, we observed that cortistatin deficiency was markedly associated with an upregulation of genes related to DNA damage (*i.e., Dffa* and *Gadd45a*) (Figure 53d). Concurrently, there was a downregulation of master regulators of apoptosis such as *Nr4a1, Egr1, Fas,* or *Ret*, among others, suggesting a potential challenge for these cells in managing such processes (Figure 53d). This dysregulation was accompanied by an upregulation of genes related to cell cycle such as *Chmp4c*, *Ticrr,* and *Clspn* (Figure 53d). Finally, there was a marked downregulation of genes related to endothelial proliferation and differentiation (*e.g., Igf2, Pdpn,* or *Lingo1*) (Figure 53d). Importantly, some of these genes, essential for the damage response (*e.g., Casp12, Egr1, Fos* and *Nr4a1*) [257], were upregulated in *Cort*$^{+/+}$ BECs in the shift from NX/NG to OGD-R, while none of these genes, or others functionally related, showed significant changes in cortistatin-deficient endothelium (Figure 53d).

Moreover, we found that several BBB transporters, crucial for metabolic and ionic endothelial homeostasis (*e.g., Slc4a4, Slc7a2, Slc22a18, Slco2a1, Atp1b1, Lrp1,* or *Aqp1*) were downregulated in the absence of cortistatin in both NX/NG and OGD-R (Figure 53e). Conversely, *Slco4a1* and *Atp8a1*, known to be detrimental to brain connectivity when

elevated [258,259], exhibited an upregulation in *Cort*$^{-/-}$ BECs in basal and injured stages (Figure 53e).

Regarding genes involved in immune response pathways, we found that factors linked to an anti-inflammatory, immunoregulatory, and protective response (*e.g., Il34* or *Tnfrsf1b*) [260–262], were downregulated in *Cort*$^{-/-}$ cells in NX/NG, OGD-R, or both (Figure 53f). On the contrary, related genes normally associated with the activation and chemoattraction of immune cells (*e.g., Lcp1, Ccl9*, *Il16*, *Cd93*, *Ulbp1, Itga3,* and *Itga4*) were upregulated in both physiological and injured *Cort*$^{-/-}$ BECs (Figure 53f). Importantly, genes required for the inflammatory-driven repair response, such as *Gbp2, Gbp3, Il11, Il33*, and *Egr1*, were only upregulated in *Cort*$^{+/+}$ cells after OGD-R conditions (Figure 53f). None of these DEGs, or others, related to immune pathways showed significant expression changes in *Cort*$^{-/-}$ BECs during the shift from physiological to ischemic states (Figure 53f).

Notably, some genes related to the hypoxia response with neuroprotective roles (including *Fos, Gbp2, Nr4a1, Mmp3, Spp1,* and *Nr1d1*) [257] were only upregulated in wild-type endothelium after ischemic conditions (Figure 53g). In turn, some of them (*i.e., Nr4a1* or *Spp1*) were downregulated under physiological or OGD-R conditions in cortistatin-deficient endothelium (Figure 53g). Alternatively, genes related to ROS modulation (*e.g., Cryab, Sod3,* or *Vnn1*) were downregulated in *Cort*$^{-/-}$ BECs even under both conditions (Figure 53g), suggesting an inactive response to ROS after injury. Except for *Nos2* downregulation, none of these genes showed differential expression in *Cort*$^{-/-}$ BECs in the shift from normoxic to ischemic states (Figure 53g).

Surprisingly, we observed some epithelial cells markers (*i.e., Epcam*), or genes related to the keratinization process (*i.e., Krt7, Krt8, Krt18,* and *Myh14)* (Figure 53g) among the top 25 upregulated DEGs in *Cort*$^{-/-}$ BECs after ischemic damage.

Finally, we found that many genes belonging to important signalling networks regulating endothelial cell biology were downregulated in the *Cort*$^{-/-}$ BECs under physiological and ischemic conditions. These genes were involved in pathways such as Wnt (*e.g., Fzd1, Fzd2, Apc2, Rspo2,* or *Ptk7*), TGF-β (*e.g., Ltbp1, Ltbp3,* or *Ltbp4*), MAPK (including *Angpt1, Ntrk3*) and Notch (*i.e., Notch2,* and *Notch3*) (Figure 53i). Besides, various growth factors crucial for endothelium homeostasis (*e.g., Igf2, Pdgfc, Vegfa,* or *Igfbp4*) were also downregulated in *Cort*$^{-/-}$ BECs in control conditions (Figure 53i). Interestingly, some kinases (*i.e., Mapk6, Ntrk3, Ddr2*), phosphatases (*i.e., Ptprk*), and growth factors (*i.e., Igf1, Sox17, Pdgfb,* and *Pdgfra*) were upregulated in *Cort*$^{-/-}$ cells in NX/NG, probably as a compensatory effect. Except for *Igf1*, none of the mentioned genes

showed differences in the transition from normoxic to ischemic state in either *Cort*$^{+/+}$ or *Cort*$^{-/-}$ BECs (Figure 53i).

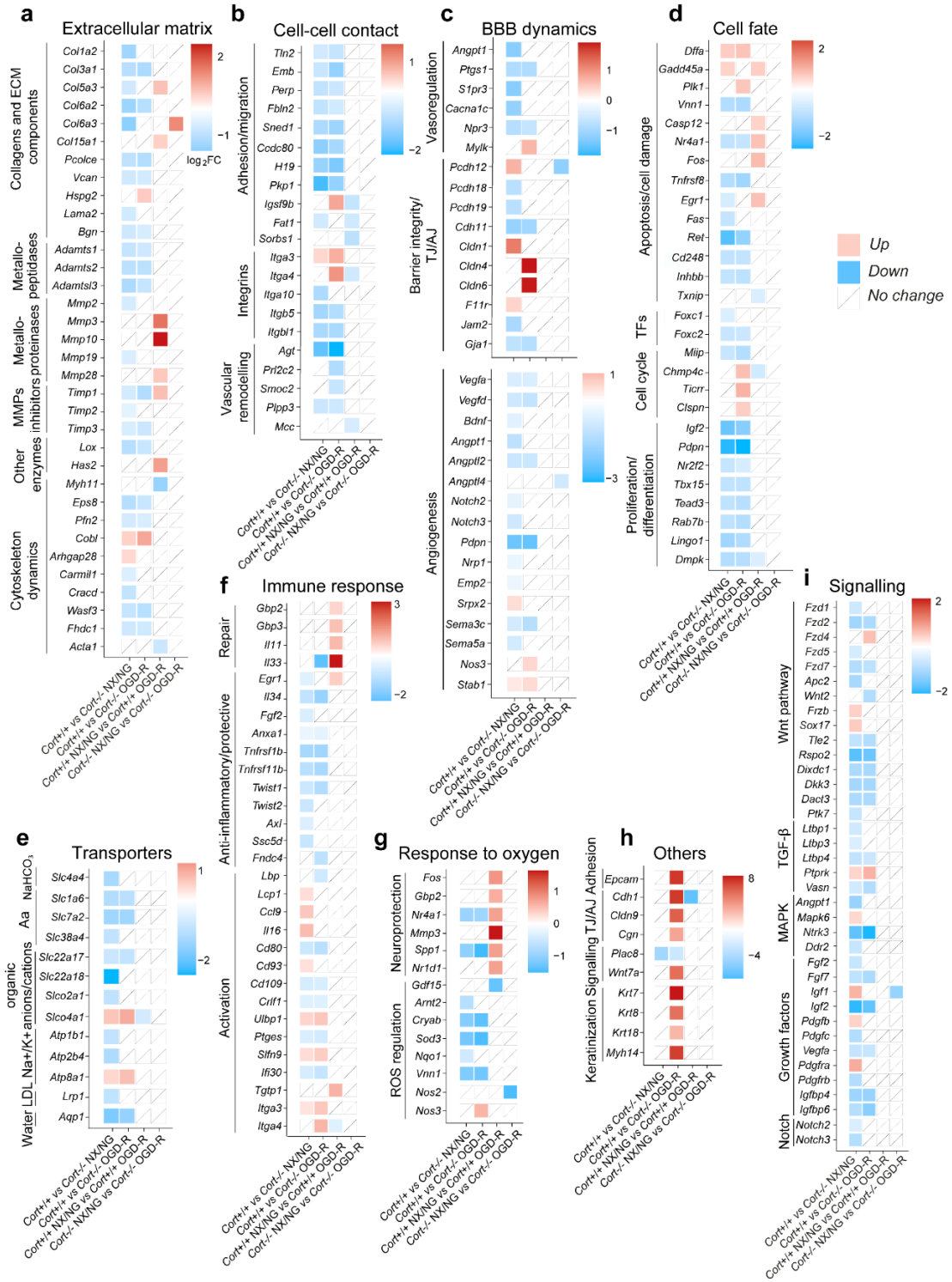

Figure 53. Transcriptional alterations in cortistatin-deficient brain endothelium. a-i. Gene sets for *Cort*$^{+/+}$ and *Cort*$^{-/-}$ BECs displayed in figures 51-52 were manually classified into gene networks crucial for brain endothelium dynamics: extracellular matrix components (**a**), cell–cell contact mediators (**b**), BBB dynamics (**c**), cell fate agents (**d**) endothelial transporters (**e**), immune response (**f**), response to oxygen (**g**), others (**h**), (genes with the highest fold change from each

one of the other different categories), and signalling pathways (**i**). The relative fold change expression (log_2FC) for each DEG in each experimental group is shown by shades of red (upregulated) and blue (downregulated). Genes that do not have significant expression changes are displayed by a white box. MMPs, matrix metalloproteinases, TJ/AJs, tight-junctions/adherens-junctions, TFs, transcription factors, AA, amino acids, LDL, low-density lipoprotein, MAPKs, mitogen-activated protein kinases.

Collectively, these results demonstrate that the absence of cortistatin induces the downregulation of transcriptional programs not only in conditions of damage but also in physiological states. While *Cort*$^{+/+}$ BECs appears to exhibit a canonical balanced response to damage, these pathways are impaired in *Cort*$^{-/-}$ BECs under both conditions.

4.4.5. Cortistatin protects the integrity, regulates the junction assembly, and reverses immune activation of cortistatin-deficient brain endothelium

To validate the regulatory role of cortistatin in brain endothelium dynamics, we finally investigated whether the treatment could rescue the observed phenotype in cortistatin-deficient BECs following ischemic conditions. Our findings showed that the addition of exogenous cortistatin after OGD-R significantly reduced the enhanced endothelial permeability in both wild-type cells and cells with partial or complete cortistatin deficiency (Figure 54a). This restoration of barrier permeability was accompanied by the reestablishment of the functional intercellular architecture of the endothelium (Figure 54b,c). Notably, cortistatin treatment recovered the uniform and settled location of ZO-1 and claudin-5 along the membrane, the increased and robust expression of VE-cadherin, the reduced presence of cytosolic claudin-1, and the physiological randomised distribution of stress fibres (Figure 54b,c). Moreover, cortistatin treatment could reverse back to the homeostatic state the dysregulated immune response exerted by the ischemic-injured endothelium (Figure 54d). Specifically, levels of TNF-α and MCP-1 were significantly reduced in *Cort*$^{+/+}$, *Cort*$^{+/-}$, and *Cort*$^{-/-}$ BECs compared to non-treated cells (Figure 54d). Interestingly, cortistatin treatment significantly enhanced the reduced levels of nitrite in cortistatin-deficient endothelium, probably as a compensatory effect (Figure 54d).

Regarding the direct connection between disrupted permeability, inflammatory response in the endothelium, and cell migration, we next investigated whether cortistatin could regulate immune trafficking within wild-type and cortistatin-deficient brain endothelium (Figure 54e). In particular, we analysed the dynamics of infiltrating macrophages and T cells in control and treated endothelium that had been previously activated by TNF-α. Transendothelial migration of T cells and macrophages was enhanced

in cortistatin-deficient endothelium (*Cort*$^{+/-}$ and *Cort*$^{-/-}$ BECs). However, cortistatin treatment significantly modulated the migration of both cell types (Figure 54e).

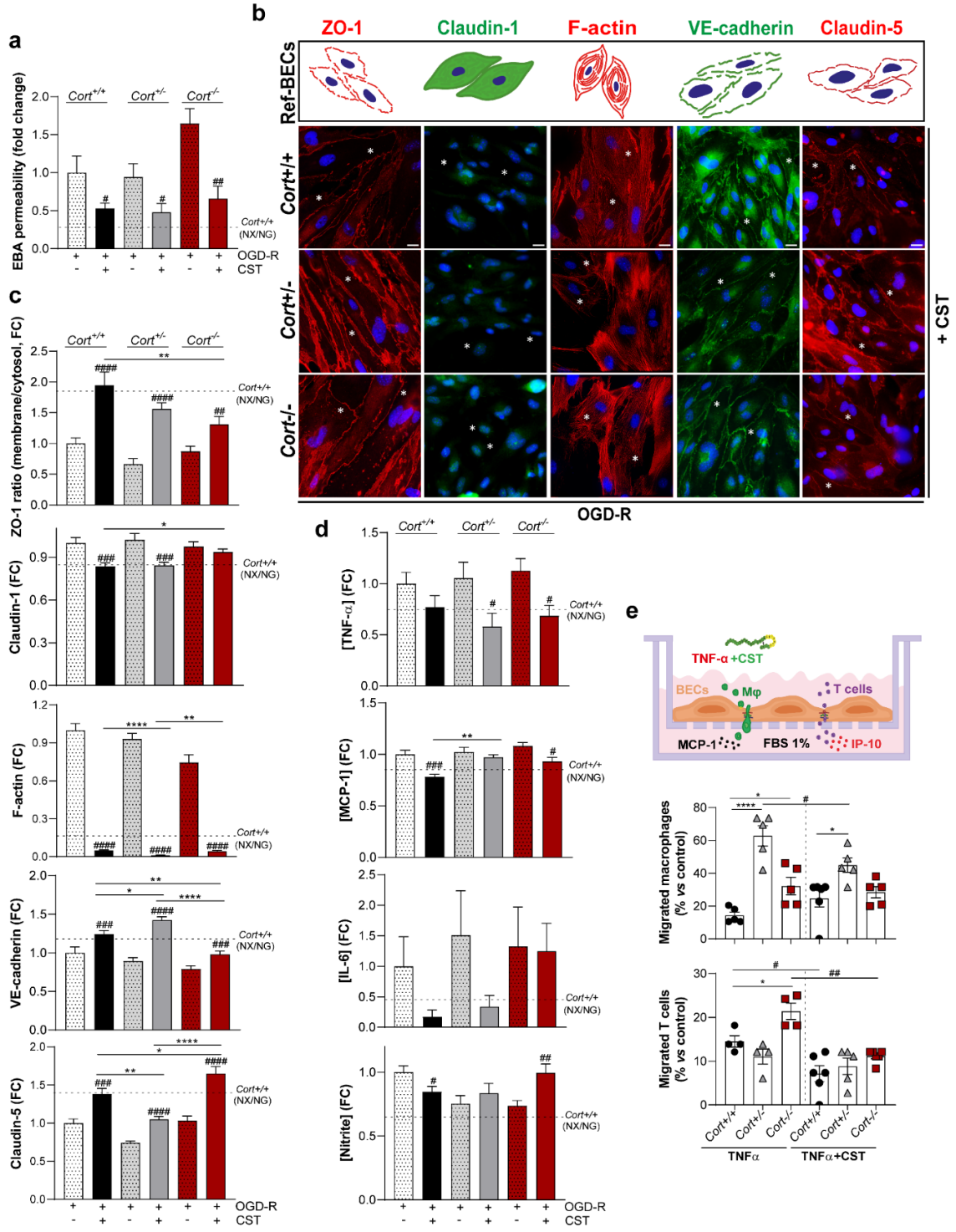

Figure 54. Cortistatin restores the integrity and function of brain endothelial cells following ischemic-like conditions. **a.** Endothelial permeability to EBA was measured in wild-type and cortistatin-deficient BECs after OGD-R in the presence or absence of cortistatin (100 nM, OGD-R + CST) as previously described. N = 5–8 cultures/group. **b.** Immunofluorescence representative images of tight-junctions (ZO-1, claudin-1, claudin-5), adherens-junctions (VE-cadherin), and F-

actin distribution in wild-type and cortistatin-deficient BECs after OGD-R treated with cortistatin. Asterisks indicate continuous membrane expression of ZO-1 (red), claudin-5 (red), and VE-cadherin (green), reduced cytosolic expression claudin-1 (green), and random distribution of F-actin fibres (red), compared to BECs exposed to OGD-R without cortistatin addition (as shown in Fig. 21b–c, represented by schematic illustrations in the top of the figure: Ref-BECs). Scale bar: 20 µm. **c.** ZO-1 location was quantified as the ratio of ZO-1 intensity in the membrane *vs* the cytosol. Claudin-1, claudin-5, VE-cadherin, and F-actin expression was quantified by fluorescence intensity (a.u). 25–50 ROIs from 4 independent fields were evaluated. N = 6 cultures/group. **d.** Levels of inflammatory mediators determined in culture supernatants. N = 8 cultures/group. Data in **a**, **c**, and **d**, are represented as the fold-change (FC) *vs* the reference values of OGD-R wild-type BECs in each quantification (set at 1). In each case, *Cort*$^{+/+}$ BECs in NX/NG are represented as a basal condition reference (dashed line). **e**. Top, schematic representation of transendothelial migration assay. Wild-type mice macrophages and T cells were incubated for 24 h at the top of *Cort*$^{+/+}$, *Cort*$^{+/-}$, and *Cort*$^{-/-}$ BECs-covered transwells, previously activated with TNF-α (10 ng/ml, 24 h). The migration assay was performed using MCP-1 (50 µg/ml) or IP-10 (50 µg/ml), as macrophages and T-cell chemoattractants, respectively. CST (100 nM) was applied when indicated. Bottom, data represented the percentage of migrated immune cells *vs* the control (empty-coated insert). N = 4–6 cultures/group. Data are the mean ± SEM with dots representing individual values of independent cultures. Cells in each culture were derived from 4 pooled brains. **vs* *Cort*$^{+/+}$ BECs exposed to OGD-R + CST; $^{\#}$*vs* BECs of corresponding genotype (*Cort*$^{+/+}$, *Cort*$^{+/-}$, *Cort*$^{-/-}$) exposed to OGD-R.$^{*/\#}p \leq 0.05$, $^{**/\#\#}p \leq 0.01$, $^{***/\#\#\#}p \leq 0.001$, $^{****/\#\#\#\#}p \leq 0.0001$.

Finally, we examined the leakage of the barrier in wild-type and cortistatin-deficient mice using a different model of BBB disruption than that of MCAO. In this study, 1-year-old mice were administered with LPS (*i.e.,* model of mild neuroinflammation [263]) and cortistatin for 6 h. One hour before sacrifice, mice were intravenously injected with Evans Blue, which binds to albumin in the blood, allowing the assessment of the leakage of this molecule into the brain. Importantly, cortistatin treatment effectively reversed the increased leakage observed in both genotypes following LPS injection (Figure 55). Notably, cortistatin-deficient mice exhibited a great barrier disruption even in physiological conditions, resembling the wild-type barrier phenotype after LPS injection. Collectively, these results support the hypothesis that cortistatin-deficient mice present a dysfunctional blood-brain barrier under physiological conditions, which is further exacerbated upon injury.

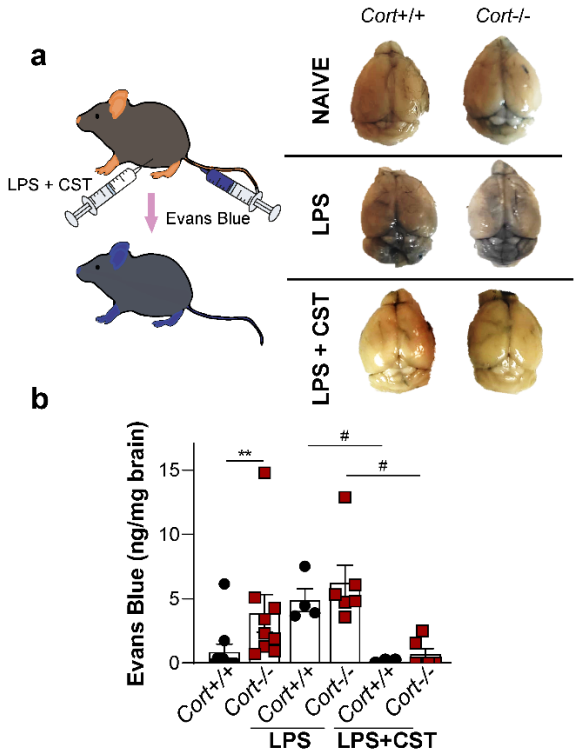

Figure 55. Cortistatin reduces BBB leakage in a mild model of neuroinflammation by LPS. **a. Left**, 1-year-old wild-type and cortistatin-deficient mice were subjected to a mild-neuroinflammation model by intraperitoneally administering LPS (6 mg/kg) and cortistatin (1 nmol in PBS, immediately after LPS) for 6 hours.1 h before sacrifice Evans-Blue (2% in PBS) was injected via the tail vein. PBS was administered in control mice. Brains were then collected and minced in N,N-dimethylformamide at 55 ºC for 24 hours to determine EB content **Right**, representative images of wild-type and cortistatin-deficient brains showing EB leakage after LPS or LPS+CST. **b.** Quantification of Evans blue (ng/mg brain). The data represent the mean ± SEM, with dots indicating individual mice (N = 4–8/group). *vs *Cort*$^{+/+}$, $^{\#}$vs LPS in either *Cort*$^{+/+}$ or *Cort*$^{-/-}$ mice, $^{*/\#}p \leq 0.05$, $^{**/\#}p \leq 0.01$.

5. Discussion

5. Discussion

5.1. Stroke from bench to bedside. Pitfalls and new possibilities

Despite several efforts, stroke remains the second leading cause of death worldwide. So far, intravenous rtPA and mechanical removal of arterial blood clots are the only available treatments for acute ischemic stroke. However, the narrow therapeutic window and the limited availability of Care Units specialized for stroke limit the availability of both treatments [264]. Moreover, the intricate and still not fully understood pathophysiology of stroke complicates stroke management, as a plethora of simultaneous cellular and molecular mechanisms involving the brain, vascular system, and peripheral organs are underlying. In this sense, the use of cytoprotective approaches that modulate multiple facets of the ischaemic cascade is far more attractive than the traditional approach of targeting individual aspects of the ischemic cascade, often focused on neuro-centric mechanisms. Notably, current knowledge underscores the importance of regulating and balancing neurotoxic processes instead of completely halting specific pathways, as doing so may inadvertently impede neuroprotective mechanisms. Moreover, a better understanding of the complex relationship between the nervous, the vascular, and the immune systems seems to be of crucial importance in stroke prognosis. In this context, we propose that the neuropeptide cortistatin, a crucial link between the CNS and the immune system, with anti-inflammatory, neuroprotective, and immunomodulatory properties, could function as an endogenous pleiotropic key mechanism in the pathophysiology of ischemic stroke, as well as a potential therapeutic agent. To test this hypothesis, we initially explored the potential therapeutic properties of this neuropeptide in a preclinical model of stroke (MCAO) at different time points to determine the most efficient time window. Once the optimal time window of the neuropeptide was determined, we conducted the model in wild-type and cortistatin-deficient mice following cortistatin administration. Finally, to account for the aging risk factor, we performed the experiments in young (3 months old) and middle-aged mice (6 months old).

At this point, an important topic to discuss related to the failure of bench-to-bedside translation is the reproducibility of ischemic stroke mouse models. Models of stroke have gained popularity in bench research, with the MCAO model standing out as the most studied and utilized in stroke research for various reasons. These include its minimal invasion (*i.e.,* it does not require craniotomy), its ability to precisely regulate the duration of ischemia, and the control of reperfusion by withdrawing the suture [265]. Additionally, it better mimics clinical stroke in humans because it efficiently reproduces the recanalization

of an embolized or thrombosed vessel, resembling the clinical interventions of rtPA administration or EVT [266]. However, as we and others showed [265–267], the variability of this model is high and not entirely clear, likely due to various factors, including differences in the composition of the circle of Willis, the collateral circulation, the distribution of grey and white matter, and other neuro-morphological features strain-specific [266]. These may ultimately impact the results from the experiment. Additionally, factors such as surgical expertise, the specific MCAO method employed, the occlusion time, the diameter and coating of the filament, and anaesthesia can also affect the reproducibility of this model and its translation to the clinic [265]. Therefore, meticulous fine-tuning of MCAO parameters is indispensable to ensure a highly reproducible and minimally invasive model. As previously reported, opting for milder models by reducing occlusion time and using thinner filaments yields more consistent and smaller infarct sizes, along with decreased mortality rates, which allows to use a reduced number of rodents [268]. Importantly, this approach closely mirrors the clinical scenario of stroke in humans, as more than half of the patients who suffer from MCA stroke have rather small lesions (4-14% of the affected hemisphere) [269].

In preliminary experiments of this thesis project (data not shown), we employed larger occlusion times and the filament thickness typically commercialized for animals of the same age and weight. However, this approach resulted in low surgery success. The low reperfusion rates led to the exclusion of many animals from the study, together with high mortality rates among the animals that experimented reperfusion. This was likely associated with the adverse effects that thick filaments may have on the endothelium, a phenomenon reported by others [270]. These effects include damaging the carotid intima, which can cause thrombosis and further compromise blood flow, affecting histopathological results [265,270]. Consequently, we decided to adopt thinner filaments and adjust the occlusion duration to 20 min of occlusion for young animals and 35 min for middle-aged. This adjustment was based on our observations that a 20-minute occlusion in middle-aged did not consistently induce lesions (data not shown). As a result of these modifications and refined skills, we noted an improvement in the success of the surgical procedures, with almost all animals experiencing reperfusion, and enhanced survival rates in all genotypes and ages.

Finally, it is important to bear in mind that stroke predominantly affects the elderly, with aging not merely being a risk factor but also linked to increased vulnerability and diminished capacity to recover from brain injury [271]. Despite this, the majority of studies are currently conducted in young animals, leaving the impact of aging relatively

unexplored. To account for the age-related factor, we performed the aforementioned experiments using both young (3 months old) and middle-aged mice (6 months old). Typically, older animals (15-24 months old) are employed for studying the aging component in strokes [272,273]. However, cortistatin-deficient mice already manifest an elevated susceptibility to various injury models [141,144,182,190,192], as well as a premature aging-like phenotype that is evident as early as 6 months (unpublished data from Ignacio Serrano's thesis [245]). Consequently, the use of older animals might have compromised the success of the model due to the probable high mortality of these animals. Moreover, it is important to note that the incidence rates in people under the age of 70 have worryingly raised in the last 20 years, accounting for 63% of strokes. Therefore, studies conducted in middle-aged are also of great relevance [1]. Finally, although other risk factors such as atherosclerosis, diabetes, hypertension, and other health conditions were not included in this preliminary study, they are the subject of current and future studies in our research group.

5.2. Therapeutic role of cortistatin. Neurological and motor deficits

Currently, the primary focus of available stroke therapy is directed towards reperfusing the penumbra and salvaging as much tissue as fast as possible, to ensure a more favourable clinical outcome. This underscores the critical importance of the "time is brain" mantra [274]. However, the existing endovascular treatments have a narrow time window. Unfortunately, a significant percentage of patients cannot benefit from these treatments due to exclusion criteria, categorized according to Behrndtz et al. as "too risky" (*e.g.,* anticoagulant use, comorbidities), "too large" (large lesion size), "too late" (late presentation of stroke or the so-called "wake-up" strokes), or "too mild" (clinically mild/remitting symptoms) [275]. Regrettably, among the eligible patients (3-8.5%), success is achieved in less than half of these cases, leaving most patients without treatment options [276]. It is crucial to recognize that stroke pathophysiology is a complex process that unfolds in a spatio-temporally variable manner. Neglecting these characteristics, most cytoprotective therapies have focused on irrelevant therapeutic windows in terms of the pathophysiology of stroke, often focusing on the hyper-acute phase to fall into the range of rtPA, or slightly later without distinguishing between phases. These both have led to poor prognosis in many cases [264]. Moreover, each patient may tolerate ischemia differently due to differences in collateral circulation, cerebral reserve, or size of the lesion [277]. Therefore, we advocate that the focus should be on cytoprotective factors in the later stages of stroke when the core hypoxic-reperfusion neuronal damage has already occurred but other important processes have just unfolded (*i.e.,* neuroinflammation,

immune infiltration, cytotoxicity). This would provide a broader treatment window, allowing for the enrolment of a substantial number of patients.

For this reason, our initial goal was to explore the potential therapeutic effect of cortistatin at later stages (24 h post-stroke), to investigate whether this neuropeptide could exert beneficial effects beyond the currently limited timeframe. Moreover, to establish an effective and protective time window, we examined the immediate effect of the neuropeptide after reperfusion (0 h+ 24 h) when damage has just begun influencing the starting inflammatory/cytotoxic processes, or at early times (4 h+ 24 h) when these responses have already unfolded, but damage due to reperfusion is still occurring.

Importantly, treatment with the neuropeptide at later stages demonstrated beneficial effects, reducing infarct volume and enhancing glial protective-like responses, as well as inducing a sightly improvement of motor deficits. Surprisingly, our findings showed that immediate treatment with cortistatin worsened neuronal damage, neurological scores, and motor performance. Interestingly, a reduced microglial density in the ischemic core and an impaired astrocyte scar were also observed. These detrimental effects associated with the immediate treatment might appear contradictory to the protective effects observed at 24 h and with the observed beneficial effects of cortistatin treatment in other neurological disorders [144,181,182]. However, they align with the known potent anti-inflammatory properties of cortistatin. In this sense, in our study and the mentioned by others, cortistatin was injected at later stages of the disease once the damage was well-established, exerting a modulation of the probable detrimental glial response. Therefore, our findings do not imply that cortistatin is neurotoxic, but rather suggest that the initial local neuroinflammatory response, essential for constraining damage (*i.e.,* forming a glial scar) and engulfing debris and dead cells (microglia), is halted by the immunoregulatory action of the neuropeptide, leading to detrimental neurological outcomes. Indeed, blocking this crucial early response has shown detrimental outcomes in other early therapies. For example, Szalay and colleagues showed that microglia depletion led to a striking increase in infarct size, which was reversed by microglial repopulation [278]. Moreover, the anti-inflammatory role of cortistatin at acute stages might be blocking immune trafficking to the brain. Notably, neutrophils, macrophages, and T cells, among their multiple roles, are recognized for signalling to diverse cells, including microglia, astrocytes, or endothelial cells, influencing their function in a polarizing manner during stroke [279]. In particular, it is well described that the presence of immune cells in the brain during early stages contributes to the neuroinflammatory response of microglia, a critical event in the responsiveness to ischemia. For example, Benakis and collaborators described that the

cytokine/chemokine secretion pattern of different populations of T helper cells is crucial for modulating the activation of microglia in stroke [280]. This data may also correlate with the lack of clinical success observed in some immunomodulatory/anti-inflammatory drugs injected at early stages [264]. Altogether, these findings highlight the pivotal role played by the inflammatory response in the regenerative process following a stroke, and that this process cannot be completely halted. Indeed, the inflammatory response may only become harmful when it becomes chronic or magnified, possibly associated with the severity of the injury or due to concurrent disease conditions or risk factors [264]. As a result, we advocate that modulating and controlling this response, rather than attempting to completely halt it, appears to be a more desirable approach.

On the other hand, the treatment with cortistatin at early stages (4 h + 24 h) did not result in a reduced infarct volume, nor in beneficial effects in terms of neurological scores or neuronal lesion. However, cortistatin treatment modulated and enhanced glial scar, although it did not affect microglia response in this case. This may be due to the fact that treatment at 4 h might block microglia, which is known to respond early, and not astrocytes activation, which is known to happen at later stages. Considering that the beneficial effects of cortistatin are more pronounced at later stages rather than earlier, further studies will explore whether the therapeutic window of cortistatin can be shortened or more precisely adjusted. Moreover, it is important to consider that, in the immediate and early treatments, two doses of cortistatin were administered at hyper-acute and acute stages. This is in contrast to the single injection at the acute stage of the later treatment, which might be influencing the observed outcomes. However, the striking differences between them suggest that the first time point administration of cortistatin appears to be crucial for the later development of the stroke response.

In light of these preliminary results, we then focused on the later treatment due to its potentially broader therapeutic window, allowing for more flexibility in the application of the treatment or concurrent administration with other treatments (*i.e.,* rtPA). To collectively examine the potential effect of the neuropeptide, we evaluated neurodegeneration, glial population dynamics, BBB breakdown, brain vasculature alterations/regenerative process, and immune response 48 h following MCAO.

According to our previous results with C57BL/6J animals performed in DNF to identify the best time window for cortistatin administration, our findings in the animal experimental facility showed that cortistatin treatment in later stages also reduced lesion sizes, although it did not show a significant improvement in the neurological score of wild-

type mice. These consistent observations conducted in different animal facilities indicate that the model and the experimental procedure were successfully and accurately performed. In general, we observed the non-significant differences in score despite an evident reduction in the neuronal lesion may be attributed to the use of a mild model of stroke rather than a severe one. Indeed, in the mild model clinical manifestations are very similar between low scores, making challenging to observe the correlation with infarct volume and scores [281]. However, cortistatin-deficient mice exhibited worsened neurological scores in both age groups compared to wild-type mice. Accordingly, a higher susceptibility of cortistatin-deficient mice has been observed in other injury models [144,182,190,192]. Importantly, cortistatin treatment reduced neurological scores in cortistatin-deficient young and middle-aged mice. The capacity of cortistatin to regulate neurological deficits in old mice and animals more susceptible to stroke with severe clinical manifestations (*i.e.,* cortistatin-deficient mice), is very promising, suggesting that this neuropeptide could also target challenging stroke manifestations effectively.

Interestingly, although after stroke mice exhibit multiple sensorimotor deficits and neurological impairments similar to human patients [211,282], behavioural stroke phenotypes are highly heterogeneous in mice. Therefore, a comprehensive functional assessment requires supplementing neurological scores with an extensive battery of tests to more accurately represent the specific aspects of stroke pathology [269]. Unfortunately, there is no universally standardized battery of behavioural tests in the field, and specific tests are often applied and modified to meet the requirements of each particular study [269]. To closely mimic human outcomes, in our study we conducted several tests (*i.e.,* rotarod, wire-hanging, and pole test). However, the locomotor ability of animals, individual variations, different protocols, or animal facility environment, can severely impact the performance of any test [269,282]. Moreover, while training can reduce individual variation, occasional failure to perform the task may be attributed to a lack of experience rather than functional deficits [282].

Notably, despite observing more severe neurological deficits in cortistatin-deficient mice compared to wild-type mice, this did not always correlate with worse motor performance in the behavioural tests. These paradoxical effects may be influenced by the exacerbated anxiety-like behaviour exhibited by these animals, driven by elevated glucocorticoids as a compensatory mechanism for cortistatin deficiency [144]. This intriguing behaviour has been previously described by Souza-Moreira and colleagues, who reported that cortistatin-deficient mice entered fewer times and spent decreased time in the open arms of the elevated plus-maze. The mice also explored peripheral areas of the

open field for longer durations when compared to wild-type mice [144]. In this sense, an anxiety-like behaviour could have provoked animals to move faster, potentially covering up any underlying poorer performance in motor tasks.

Surprisingly, cortistatin treatment did not seem to affect the performance of motor and coordination tests in either young wild-type or cortistatin-deficient mice, although it reduced neuronal lesions and clinical manifestations. Additionally, cortistatin treatment even showed a trend towards a negative impact on motor and coordination tests in 6-months mice of both genotypes. However, this decline in motor performance did not correlate either with severe lesions, as it was observed in the immediate treatment. In fact, these animals exhibited improved neurological scores after cortistatin treatment. Upon careful observation, mice seemed to be apathetic, passive, and uninterested during the test, and they did not appear to fall or escape less due to motor deficits as seen in the immediate treatment. These impressive results would probably be related to the capacity of cortistatin to reduce locomotor activity [168]. Further experiments are necessary to determine whether repetitive treatments with cortistatin would reverse these outcomes and to elucidate why older animals, but not younger ones, suffered from this condition.

Altogether, we consider that the acute time point and the sole administration of cortistatin may be masking its possible protective effects. A more extended and repetitive treatment of the neuropeptide to evaluate outcomes at later stages (*e.g.,* 7 or 14 days) could potentially be beneficial, as reported in other models [182,190,192]. Moreover, we acknowledge as a limitation that the battery of tests performed might not be well-adjusted to the deficits present in these animals. In this sense, the chosen acute end-point of the experiment (*i.e.,* 48 h) prevents us from studying memory or sensory deficits, which would be crucial for a comprehensive assessment of neurological dysfunction after stroke. Additionally, the intrinsic anxiety-like behaviour of cortistatin-deficient mice and the capacity of cortistatin to reduce locomotor activity should be considered for further experiments conducted at later times, which should aim to address these concerns collectively.

On a different note, the major immediate consequence of acute stroke is irreversible neuronal cell death and brain damage [270]. Particularly, ischemic stroke in humans and MCAO model in rodents is characterized by an ischemic core and a distinguishable penumbra [283]. Interestingly, despite the apparent absence of impact on neurological deficits, cortistatin treatment did reduce the lesion size, especially targeting the core and the penumbra, in wild-type animals from both age groups. Importantly, cortistatin treatment

seemed to target the viability of dendritic processes and neuron bodies, as reported by both CV and MAP-2 staining. Importantly, beyond the traditional CV staining, MAP-2 offers a more accurate insight into the initial stages of neuron death even if the process is not complete yet, which in turn offers potential opportunities for intervention [238]. The original definition of penumbra was a transient state of “neuronal lethargy” with electrical failure and potassium release but not terminal depolarization. Today, the concept has evolved and penumbra is generally considered as “time-sensitive hypo-perfused brain tissue with decreased oxygen and glucose availability”, a salvageable tissue treatable through intervention, or a potential target for neuroprotection [284]. In this sense, the reduced lesion size observed in the striatum following cortistatin treatment in MAP-2 indicates that cortistatin efficiently targets these initial critical stages of neuronal death, while also protecting neuronal bodies (Figure 56).

Conversely, despite exhibiting poorer neurological deficits, we did not observe more severe lesions in cortistatin-deficient animals compared to wild-type. In this line, our results conform to other studies reporting that infarct size does not always correlate with neurological function and functional outcomes [269,270,285]. This suggests that the evaluation of stroke outcomes does not only have to rely on ischemic volumes. Notably, no differences were observed in older animals in any of the genotypes. Despite this being surprising, several studies in rodents and humans have reported that aging is not necessarily correlated to developing a larger infarct size, even if aged individuals recover less effectively than younger ones [272,273,286]. For instance, Gullota and collaborators reported worsened neurological outcomes and higher mortality rates, but without increased neuronal lesions [286,287]. This may be attributed to the fact that, although the timing of neuronal loss in aged rats is accelerated, the process of neuronal degeneration ultimately converges on a similar endpoint in young and old individuals [286]. This would explain the lack of differences between young and middle-aged mice, both in wild-type or cortistatin-deficient mice. Hence, we advocate that the reductions in ischemic lesions by cortistatin in both age groups and genotypes is of particular interest and value.

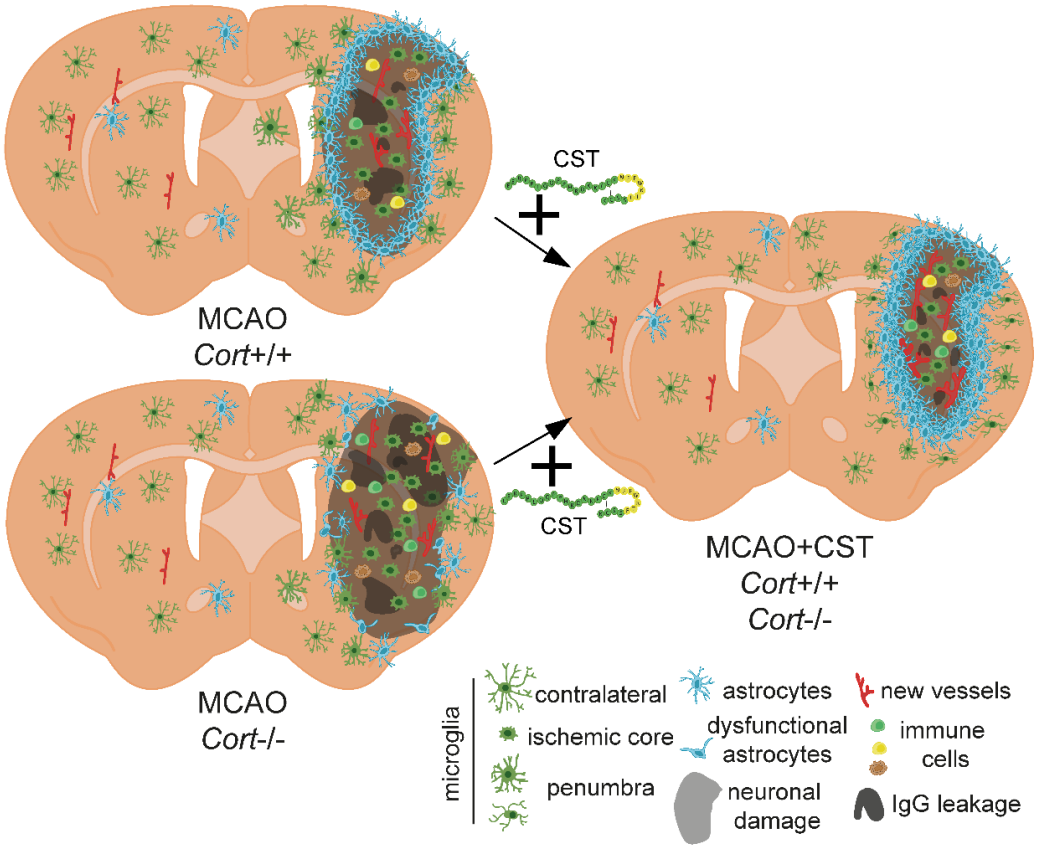

Figure 56. Schematic illustration of the proposed role of cortistatin in stroke pathophysiology 48 h after the onset. Top left, wild-type mice response after stroke (*i.e.,* neuronal mild damage, microglia proliferation in the ischemic core, microglia activation in the penumbra, astrocyte scar formation, mild BBB leakage, immune infiltration, and angiogenesis promotion). **Bottom left**, deregulated response after stroke of cortistatin-deficient mice (*i.e.,* severe neurological damage, microglia proliferation in the core, hyper-ramified microglia in the penumbra, enhanced BBB disruption, impaired glial scar, elevated immune infiltration, and deregulated angiogenesis. **Right**, cortistatin treatment reversed all the mentioned deficits in both conditions (*i.e.,* reduces neurological damage, enhances microglia proliferation in the core, regulates protective microglia in the penumbra, increases glial scar formation, reduces BBB leakage and immune infiltration, and promotes angiogenesis.

The neuroprotective effects of cortistatin reported above agree with previous investigations conducted by our group and others, which have recently demonstrated that cortistatin treatment exerts a protective effect over the neurons from the substantia nigra pars compacta (SNPc) and the striatum of a mouse model of Parkinson [181], and neurons from the SNpc of LPS-treated mice [245]. Besides, cortistatin has been reported to protect dopaminergic neurons in mesencephalic cultures exposed to the MMP toxin [181], and primary cortical neurons following β-amyloid intoxication [288]. However, the precise mechanisms underlying the influence of cortistatin in neurological lesions are not fully understood (*i.e.,* whether it directly inhibits apoptosis, neuronal degeneration, oxidative damage, or a combination of these factors). Accordingly, the questions of whether

cortistatin exerts a direct neuroprotective effect on neurons or if, conversely, it is exerting other responses (*i.e.,* anti-inflammatory, immunomodulatory effects) on different cells, indirectly benefiting neurons, stand and remain a possibility that cannot be discarded.

5.3. Role of cortistatin in neuroinflammatory responses

For many decades the primary focus of therapies for ischemic stroke has been the rescue of neurons in the penumbra region, to prevent the expansion of the infarct core. However, it is now evident that excitotoxicity, oxidative stress, neuroinflammation, or peripheral immune response can all lead to secondary neuronal cell death [289], becoming increasingly clear that simply focusing on neuronal death would be oversimplistic [274]. Therefore, in this thesis we also aimed to explore additional potential roles of cortistatin in stroke pathophysiology, particularly elucidating its impact on the neuroinflammatory response.

It has been reported that during the first hours following ischemic stroke, microglia are rapidly activated and accumulate in large numbers at the site of the infarction and the peri-infarct zone [290]. The source of these cells is still subject of debate, with three different origins suggested: local self-renewal of reactive microglia, pericytes/endogenous progenitors, or infiltration of blood-derived cells [291]. In this sense, our observations revealed an enhanced number of microglia in the ischemic core following cortistatin treatment in wild-type mice in both age groups, suggesting that these cells could be involved in the phagocytosis of dead neurons, as a clearly reduced area of neurological lesion was found in treated-mice. Interestingly, an elevated number of microglial cells were found also in MCAO cortistatin-deficient middle-aged mice compared to wild-type that was unaltered following cortistatin treatment (Figure 56).

Whether the phagocytic function of microglia in stroke is advantageous or detrimental remains uncertain, emphasizing the importance of maintaining a delicate balance for an improved stroke prognosis. Specifically, some studies reported that enhancing the phagocytic capability of microglia in a MCAO model can foster efficient clearance of tissue debris, reorganizing neuronal network [292]. Conversely, others report that excessively activated microglia in models of focal cerebral ischemia induced by endothelin-1, engulfed live or stressed neuronal cells and resulted in neurological deficits and brain atrophy post-stroke [293]. Besides, perivascular microglia have been observed to phagocytose endothelial cells, leading to blood vessel damage and BBB breakdown [290,294]. Hence, it is important to consider that microglial phagocytosis after stroke is an intricate and intriguing biological progress that may depend on factors such as the severity

of initial ischemia, the location within the lesion, and the specific time points after stroke. Notably, previous studies from our group have demonstrated that while wild-type microglia undergo activation, produce neurotrophic and regenerative mediators, and efficiently eliminate debris, cortistatin-deficient microglia exert deficient phagocytosis in physiological and demyelinating environments [183]. This supports the idea that the increased number of microglia in the ischemic core of cortistatin-treated wild-type mice would be efficiently phagocyting dead cells. On the contrary, although elevated density was also found in cortistatin-deficient animals, this would be likely a compensatory effect, since microglia would not be as efficiently involved in phagocytosis.

While most cells are engulfing dead neurons in the ischemic core, in the peri-infarct area they exhibit a different phenotypic polarization into either protective or detrimental forms, depending on surrounding factors [294,295]. Recent studies have unveiled that the initially predominant microglia, which are protective and characterized by phagocytosis, reduced production of inflammatory factors, and enhanced neuroprotective factors, is temporary. In turn, more proinflammatory and less phagocyting microglia are eventually dominant in the chronic phases, ultimately impairing axon regrowth [295]. Traditionally, this process has been characterized based on basic metrics such as long processes, indicating ramified microglia, or short processes indicating activated microglia. In any case, microglia undergo changes across multiple scales following injury (*e.g.,* branch configuration, degree and length of branching, soma size and shape, diameter, cell territory, cytoskeletal organization, relative cytoplasmic volume, membrane configuration, and receptor distribution), that goes far beyond the oversimplified paradigm of M1/M2 dichotomy [296]. Indeed, recent studies have defined at least 6 transcriptionally different microglial subsets following stroke [297]. This highlights the large heterogeneity among microglia after stroke and the need for further investigations into microglial subtypes or specific functions. However, determining when a cell transitions from ramified to activated or vice versa in a still photo poses some challenges. Is it when the ramifications shorten or when the soma swells? On another level, how should we interpret a brain area with half of the microglia falling into one category and the other half into another? [27]. To address these challenges, researchers have recently fashioned different tools to quantitatively address morpho-function and to precisely assess morphological features of microglia (*e.g.,* Fractal Analysis or Skeleton Analysis). These methods are increasingly widespread and have been proven to be successful when analysing microglia, in an accessible and cost-effective manner [27]. However, it is key to recognize that while a form-function model serves as a starting point, further studies integrating at the same time function,

morphology, transcriptome, metabolome, and proteome, through high-dimensional techniques should be conducted [289]. Finally, it is important to consider that besides microglia morpho-functional changes, these cells undergo an activation pattern that differs in space and time. Hence, different morphological phenotypes across areas (*i.e.,* marginal zone, penumbra, and core) may reflect the transition in microglia function and the different pathological states of ischemic damage [291]. Emphasizing the study of microglia in the penumbra, which is the region subjected to the most intense cellular and molecular changes, seems essential for better a understanding of stroke dynamics [284].

Therefore, we conducted an exhaustive morphological quantitative analysis of microglia activation in the peri-infarct area. In our study, several parameters of branching, soma volume, complexity, or lacunarity collectively showed marked activated microglia after MCAO in wild-type mice, regardless of age. Interestingly, microglia from both age groups behaved differentially after cortistatin treatment, with microglia shifting to a more physiological state in middle-aged mice. Similar to the effect on lesion size, the more pronounced modulation of microglia by cortistatin in older animals holds promise for targeting a broader age range, potentially benefiting the elderly (Figure 56).

This modulation of microglia morpho-function also conformed with previous results from our group and others in other neuroinflammatory models (*i.e.,* multiple sclerosis, Parkinson, and sepsis) [144,180,181,183,245]. These studies reported that microglia seemed to return to a physiological ramified-like state after cortistatin treatment, which was markedly correlated with better prognosis of the disease. Notably, young wild-type and cortistatin-deficient microglia displayed a similar phenotype after stroke, but we observed hyper-ramified microglia in middle-aged *Cort*$^{-/-}$ mice compared to wild-type mice and their respective young mice. Interestingly, other studies have reported hyper-ramification of microglia in response to acute and chronic stress and excitotoxicity, a response that might be implicated in synaptic modifications [25,298]. For instance, Hinwood and colleagues reported that chronic stress resulted in hyper-ramified microglia in the prefrontal cortex of rats, correlating with enhanced activation of neurons in that region and impaired spatial working memory [299]. This is in line with the stress-like behaviour exhibited by these animals and may imply an over-activation of these cells prior to ischemia which may negatively impact the posterior neurological damage. Accordingly, other studies from the group reported exacerbated inflammatory responses in cortistatin-deficient microglia [144]. Importantly, cortistatin treatment modulated this phenotype, resembling microglia found in MCAO wild-type mice in some properties while mirroring the microglia observed in healthy wild-type animals in most of the parameters. This suggests that in cortistatin-deficient

animals, cortistatin may modulate microglia activation differently compared to wild-type mice, effectively reversing its dysfunctional phenotype.

At this point, it is important to emphasize that the observed ramified state (*i.e.,* similar to the contralateral healthy microglia) following cortistatin treatment in both genotypes does not imply a state of inactivity. On the contrary, considering the immunomodulatory properties of cortistatin, we propose that these microglia actually remain highly active, potentially secreting factors that contribute to the recovery of brain homeostasis, while exhibiting less detrimental functions. This also agrees with previous reports in neuron-glia cultures treated with the neuropeptide [144].

Numerous questions surrounding the transitions between the different microglial subsets remain unanswered, and the specific molecular cues prompting this transition are yet to be identified [30]. In this sense, our study suggests that cortistatin could be one of these important factors. In particular, cortistatin is capable of regulating microglia proliferation towards a more phagocyting and protective-like phenotype, and of modulating the transition of activated pro-inflammatory-like microglia to a more protective-like state in the penumbra. Altogether, our study supports the notion that modulating microglia, rather than suppressing its activity, seems to be crucial for maintaining brain homeostasis. Indeed, as we showed with the immediate treatment of cortistatin, activation of microglia in the hyper-acute stages appears to be indispensable for improved recovery. However, sustained activation of microglia over time is not beneficial either. As our study and others have reported [144,183,300,301], treatments in the later stages have demonstrated that shifting microglia towards a more anti-inflammatory phenotype contributes to the recovery processes. Accordingly, our study demonstrates that the detrimental outcomes of microglia activation are clearly counterbalanced by beneficial effects, including phagocytosis and release of trophic factors. Further studies will address the exact mechanisms through which microglia can exert this immunomodulatory role.

Beyond microglia, astrocytes greatly contribute to the neuroinflammatory response. As mentioned in the Introduction section, after ischemic damage astrocytes proliferate and migrate creating a barrier around the edges of severely damaged tissue from the surrounding viable neural tissue [39]. Notably, the molecular and cellular mechanisms that underlie the formation of the glial scar and astrocyte activation are not completely understood. These likely involve a complex and balanced interplay of molecular signals that can simultaneously boost phagocytosis and debris clearance, which would be essential for the protection and conservation of the still-healthy tissue [39,46,47]. Similar

to microglia, an A1/A2 paradigm for astrocyte morphology and function has been proposed [302]. However, the spatiotemporal heterogeneity of activated astrocytes has demonstrated that this classification is too simple and highly questionable, so additional parameters far from traditional approaches should be considered.

In this research, we observed that cortistatin treatment enhanced the thickness of the glial scar in young and middle-aged animals. After conducting quantitative analyses of the morpho-function of these astrocytes conforming the glial scar, we observed an activated-like phenotype. The thicker glial scar produced by these astrocytes may be closely related to the observed protection of the neuronal tissue. Surprisingly, we described an impaired glial scar formation in cortistatin-deficient mice in both age groups (Figure 36). Interestingly, although very scarce, these astrocytes display a completely different phenotype from wild-type mice after stroke, exhibiting small, non-ramified, elongated forms, not previously described in the bibliography. Interestingly, these results did not align with previous results from astrocytes in cortistatin-deficient mice in other neuroinflammatory models, such as sepsis [245], EAE [144,183], or Parkinson [181]. In detail, these studies showed no impaired response of astrocytes in cortistatin-deficient mice, rather, an upregulated astrogliosis was observed, which was reversed by cortistatin treatment. However, it is interesting to note that in these models, damage was evaluated at chronic stages, where the astrocyte response might be chronic and detrimental. As demonstrated in our study, and similar to microglia, inhibiting glial scar formation in acute stages with immediate cortistatin treatment was proved to be detrimental to neuronal damage. Therefore, the most beneficial response in stroke at this stage would be to enhance the astrocytic response, as the underlying astrocytes would likely adopt a protective phenotype towards neurons. Accordingly, defective astrocyte scar formation in various transgenic loss-of-function models of ischemia has been shown to result in increased lesion size, demyelination, and death of local neurons, leading to decreased recovery of function [46–49]. Additionally, GFAP or vimentin KO-mice (*i.e.,* model of inhibited astrogliosis) exhibit more severe lesions, impaired recovery of sensorimotor function, and aberrant restoration of global neuronal connectivity. Besides, maladaptive plasticity responses have been also noted in these mice, implying that astrocyte activation is crucial for neuroprotection against stroke [303]. Nevertheless, it is important to mention that uncontrolled astrogliosis and excessive scar formation over time may ultimately be harmful (*e.g.,* exacerbating inflammation or interfering with synapse sprouting or axon growth during the recovery phase). Future studies would address the role of cortistatin in modulating such response at later stages. Provided that astrocytes display very

heterogenous responses of astrocytes in the progression of strokes, adopting a simplistic therapeutic strategy of inhibiting or promoting the proliferation of reactive astrocytes may not be a suitable approach [39]. Instead, a more conscious and nuanced strategy would involve the modulation of the role of astrocyte towards the most protective function for the brain tailored to each stage of the disease.

Interestingly, although to a lesser extent, fibroblasts also migrate with astrocytes to the injured area and contribute to the formation of the glial scar [39,304,305]. Importantly, these cells give rise to fibrous scars that mature and coagulate over time, persisting for a period, much more extended than astrocytes. While such a response may be beneficial in other tissues, it impedes axon growth in the brain [39]. In this context, cortistatin may also target these cells, since recently published results have described anti-fibrotic properties of the neuropeptide not only in effector cells but also in the surrounding microenvironment [192].

Finally, different studies indicate that experimental stroke in rodents favours SVZ neurogenesis, prompting the migration of SVZ-derived neuronal precursor cells towards the ischemic penumbra. There, these cells do not only survive but also differentiate and integrate new synapses [306,307]. Through as yet unknown mechanisms, these cells seem to contribute to the reduction of the infarct size and the improvement of neurological function [308]. Interestingly, it has been recently reported that reactive astrocytes play a crucial role in SVZ neurogenesis following stroke [307]. Specifically, it appears that reactive astrocytes, through their elongated processes, disrupt the migratory scaffold for neuroblasts, leading to SVZ reorganization after a stroke [309]. In this sense, the activation of these astrocytes after cortistatin treatment could be also prompting neurogenesis in the SVZ or the hippocampus. Despite further studies should investigate this aspect, other neuropeptides (*i.e.,* neuropeptide Y, VIP, or galanin) have been reported to regulate proliferation and neurogenesis [310,311].

5.4. Role of cortistatin in BBB breakdown and brain endothelial disruption

BBB breakdown stands out as a primary hallmark of stroke, manifesting shortly after artery occlusion and persisting for several days to weeks. However, the conventional classification of BBB alterations after stroke is again too simple and restricted to “opening” or “closing” (*i.e.,* "bad" or " good”) being this dichotomy completely outdated. Instead, BBB permeability exhibits a multiphasic pattern across various stroke stages (*i.e.,* hyperacute, acute, subacute, and chronic stages), each associated with distinct biological events [112]. In this study, we have focused on its acute phase, where the permeability is at its highest

and neuroinflammatory response can aggravate the injury [112]. Notably, our findings revealed an increased IgG leakage after stroke in wild-type animals, being slightly more pronounced in cortistatin-deficient animals (Figure 56). This observation is consistent with the increased BBB leakage observed in a different model of mild-neuroinflammation induced by bacterial LPS, that also courses with BBB disruption. Notably, cortistatin-deficient mice exhibited BBB disruption even under physiological conditions, confirming the great susceptibility of the barrier of these animals. This susceptibility might greatly predispose them to vascular-associated disorders and likely disturb transport, detoxification, and protection mechanisms of the brain. Importantly, apart from the hypoxic damage to NVU components, the leakage of proteins from plasma (*i.e.,* albumin and immunoglobulins) can lead to the formation of vasogenic edema, which reduces vascular diameter, and results in hypoperfusion within the NVU [312]. Notably, the treatment with cortistatin mitigated this increased leakage, especially in cortistatin-deficient mice, and could therefore be an important therapeutic advantage for this severe complication.

The disruption of the BBB is generally linked to endothelial damage and disrupted TJs and AJs. In this sense, we focused our study on the endogenous and therapeutic role of cortistatin in endothelial dynamics after ischemic injury and reperfusion. We found that cortistatin-deficient BECs exhibited both *in vivo* and *in vitro* a disrupted BBB endothelium in physiological conditions, exacerbated after ischemic damage (*i.e.,* enhanced permeability, TJ-AJs disruption, increased pro-inflammatory state). Importantly, the exogenous addition of cortistatin reversed all these features (Figure 57).

Numerous studies have established that disturbances in the content, cellular distribution, and/or post-translational modifications of TJs and AJs in ECs, participate in BBB disruption post-stroke. Notably, these alterations can even initiate neurodegenerative/neuroinflammatory diseases [55,75]. Importantly, together with playing a role in BBB structure, recent research has unveiled additional non-canonical functions for TJs and AJs. These include cell proliferation, differentiation, angiogenesis, inflammatory processes, and gene regulation [59,74]. In this study, cortistatin deficiency resulted in reduced protein levels and altered cell distribution *in vitro* of claudin-5, VE-cadherin, and ZO-1 (also demonstrated *in vivo*), although without significantly affecting their transcript levels. However, we found a downregulated expression of other TJ/AJ genes such as *Pcdh18, Pcdh19, Cdh11, Jam2, or Gja1*, crucial for connecting adjacent ECs [313,314]. Similarly, others have reported that delocalization, decreased expression, or increased phosphorylation of ZO-1 following hypoxic damage impact BBB function [53,315]. Changes in the phosphorylation status of ZO-1, ZO-2, and claudin-5 have also

been linked to alterations in BBB permeability [76,316]. Additionally, ZO-1 and VE-cadherin were downregulated in stroke mice [317]. Furthermore, the reduced expression of claudin-5 has been related to BBB dysfunction in ischemic stroke [240]. Claudin-5 knock-out mice also exhibited a size-selective BBB disruption for molecules < 800 Da, dying within 10 days after birth. This highlights the important role of this molecule in BBB homeostasis [61,64,318]. Moreover, supporting our results, various studies have also demonstrated that different insults may not impact TJ expression, but they can influence their cellular redistribution and functional organization. For example, ZO-1 translocation from the membrane to the cytosol, without changes in its expression, adversely affected barrier integrity and led to TJ disorganization [319].

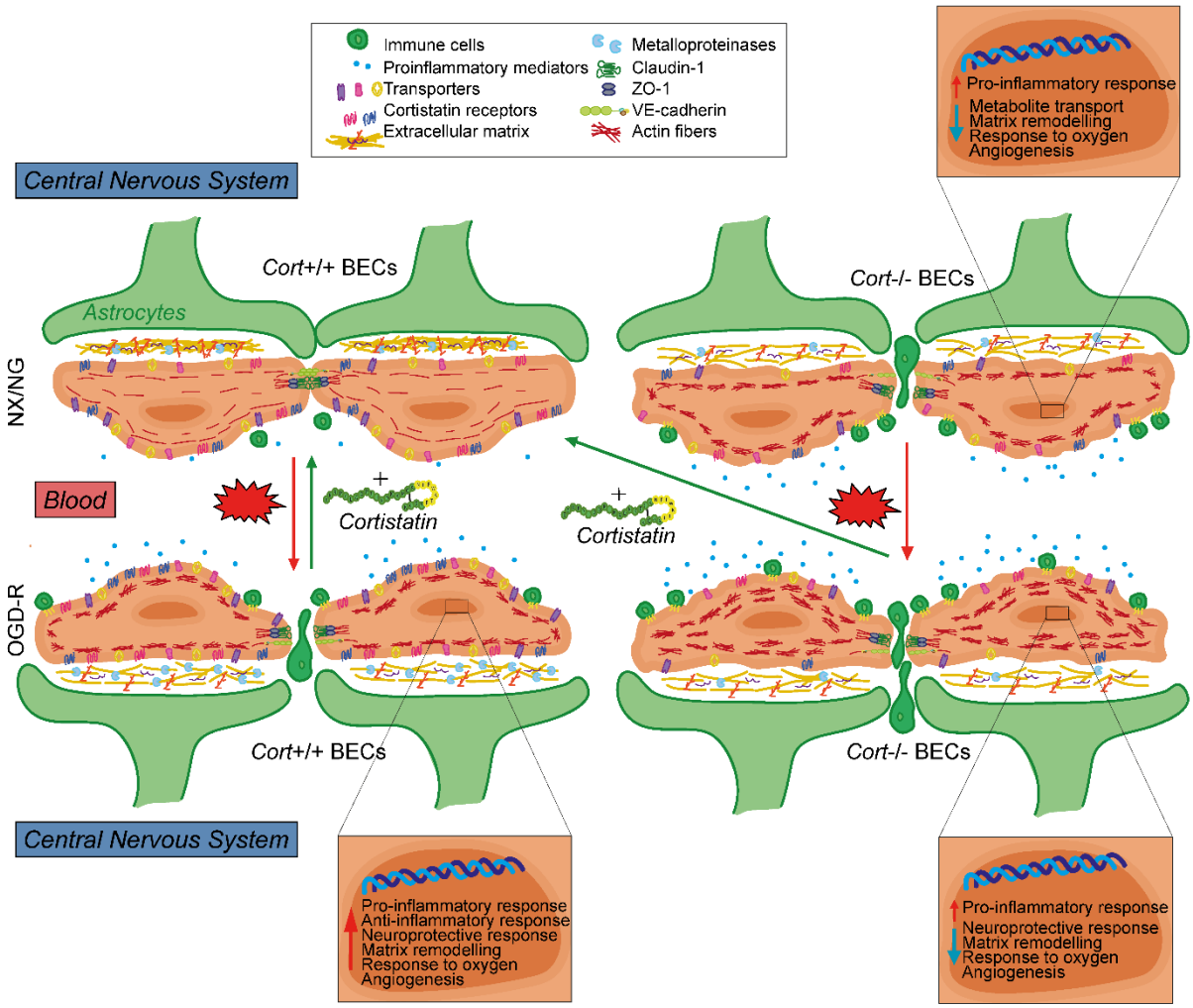

Figure 57. Schematic illustration of the proposed role of cortistatin in the modulation of brain endothelium under physiological and ischemic conditions. **Top left**, *Cort*$^{+/+}$ BECs under normoxia/normoglycemia (NX/NG) conditions exhibit homeostatic endothelial barrier integrity. **Bottom left,** following ischemic damage (OGD-r) (red arrow), *Cort*$^{+/+}$ BECs experimented a canonical response (*i.e.,* tight-junctions disruption, reorganization of actin in stress fibres, ECM remodelling, immune cell infiltration, and proinflammatory mediators release). Simultaneously,

there was an upregulation of protective and reparative transcriptional pathways (*e.g.,* anti-inflammatory response or angiogenesis) (zoom for details). Importantly, these changes were reversed with cortistatin treatment (green arrow). **Top right,** *Cort*$^{-/-}$BECs in physiological conditions displayed similar features to *Cort*$^{+/+}$ BECs after OGD-R (except for a decrease in the number of transporters and cortistatin receptors), but a distinctive genetic programming (*i.e.,* dysregulated ECM remodelling, exacerbated immune response, and downregulation of protective pathways related to damage response) (zoom for details). **Bottom right**, *Cort*$^{-/-}$BECs in OGD-R conditions (red arrow), did not show significant transcriptional changes compared to *Cort*$^{-/-}$ BECs in NX/NG. However, they presented exacerbated stress fibre formation, enhanced immune response and downregulation of metabolites transporters. Importantly, cortistatin reversed these changes back to physiological conditions (top left, green arrow).

Complementary to downregulation, we found increased protein levels of claudin-1 and a dysregulated distribution in cortistatin-deficient BECs (Figure 57). Accordingly, we found an overexpression of *Cldn1, Cldn4, Cldn6, Cldn9, Cgn, Cdh1,* and *F11r* associated with exacerbated inflammation, perturbation of the TJ assembly [247,320] and even with mesenchymal transformation or tumour progression [321,322]. Despite controversial reports about the role of claudin-1 [320,323,324], several studies indicate that claudin-1 increases in the disrupted endothelium, it affects claudin-5 assembly, and its cytosolic accumulation has been correlated with TJ arrangement deficits and limited full recovery of the BBB [64,247]. Emerging evidence also suggests that claudin proteins can localize to sites outside of the tight-junction complex. Indeed, claudin-1 seems to be representative of a type of claudin that shuttle between the cytoplasm and nucleus, acquiring non-canonical functions. These include cell proliferation, differentiation, angiogenesis, and inflammatory processes, or regulation of gene expression [74,325]. In fact, reducing claudin-1 was beneficial for modulating BBB permeability and endothelial inflammatory phenotype [247]. Altogether, our results point to the relevance of cortistatin in maintaining a properly sealed and healthy barrier. This is supported by the disrupted expression of ZO-1, VE-cadherin, and claudin-5, together with the cytosolic overexpression of ZO-1 and claudin-1 in cortistatin-deficient ECs, in both ischemic and physiological conditions.

Furthermore, TJs and AJs are connected to actin cytoskeleton through intracellular proteins, providing structural stability to the BBB. Several studies have reported that the rapid polymerization of actin filaments and their spatial redistribution into stress fibres are often associated with TJ instability, endothelial barrier dysfunction, and hyperpermeability [254]. In this context, we observed that, in addition to TJ disruption, endothelium from cortistatin-deficient mice also exhibited an elevated formation of F-actin stress fibres. This increase was correlated with marked cytoskeletal disassembly in both uninjured and injured conditions. Both TJ disruption and cytoskeleton disorganization in cortistatin-deficient endothelium were also linked to the dysregulation of some functional pathways

involving actin cytoskeleton reorganization and stress fibre assembly. These pathways include genes such as *Wasf3, Cracd*, or *Cobl*, suggesting that these cells are not able to properly regulate this process, being exacerbated. Moreover, we found a downregulation of some kinases/phosphatases (including *Mapk6, Ntrk3, Dmpk,* and *Ptprk*), which have been described as crucial regulators of TJ/AJs organization/dissociation [326].

The cytoskeleton also acts as a physical and biochemical link between the brain endothelium and the ECM [327]. The alterations and reduction of ECM components such as collagens, fibronectin, laminin, agrin, or perlecan have been also linked to BBB leakage and stroke [92]. For instance, it has been reported that alterations in collagens-associated genes predispose to haemorrhages in humans [328], and decreased expression of these components was found 24–72 h post-stroke [96]. Our investigations showed a notable dysregulation in genes encoding for ECM components (including *Col1a2, Col3a1, Pcolce, Vcan, Lama2,* or *Bgn)* in cortistatin-deficient endothelium after physiological and ischemic conditions. This suggests a disruption in the structure of the endothelium and a higher predisposition to vascular pathologies including stroke. Notably, during BBB disruption after stroke, the downregulation of ECM is accompanied by an upregulation of factors related to ECM remodelling, such as MMPs or metallopeptidases [92]. Given the increased leakiness of cortistatin-deficient vessels and the downregulation of ECM components, an upregulation of these proteins would have been expected. Conversely, we found a downregulation of these genes and derived factors (*e.g., Adamts1, Mmp2, Timp1,* or *Lox)* in *Cort*$^{-/-}$ BECs in both physiological and ischemic conditions. Notably, most of these genes were upregulated in *Cort*$^{+/+}$ cells after damage. It is important to note that, although the upregulation of MMPs is a hallmark of stroke, ECM components also undergo alterations and modifications driven by these enzymes in physiological conditions, enabling the correct functioning of the cell. Additionally, these alterations are necessary to induce angiogenesis and vascular remodelling after injury [93,329]. Besides, it is also essential not to overlook other critical roles of ECM beyond its physical and mechanical properties. For example, ECM is pivotal in cell-cell signalling and matrix-cell signalling, with integrins complexes acting as the main receptors. In summary, an unbalanced ratio of ECM components and/or dysfunction of integrins can lead to BBB abnormalities, as multiple endothelial functions are affected (*i.e.,* survival, migration, differentiation, and cell adhesion) [92]. Taken together, these results suggest that cortistatin-deficient mice would not have the capacity to remodel their endothelium upon physiological conditions or ischemic damage, likely provoking BBB disruption (Figure 57).

Furthermore, one strength of the BBB is that it provides all the necessary components for brain homeostasis, while simultaneously protecting the brain from toxins in the bloodstream [330]. We observed that a great range of transporters involved in AA, organic cations/anions, ions, and water transporters were downregulated (Figure 57). In this sense, the downregulation of *Aqp1* has been related to leaky vessels and brain edema, which would suggest that the disrupted permeability observed in these animals is not only related to TJs disruption but also to a downregulation of the water transport [331]. The downregulation of other genes that encode for transporters related to ion dynamics would likely contribute to this higher susceptibility.

On another aspect, BECs have not been traditionally considered to function as classical immune cells. However, an increasing number of studies demonstrate that these cells are intricately in inflammatory responses across various tissues (reviewed in [248]). In particular, BECs are known to rapidly and actively participate in CNS inflammation, recruiting immune cells to the sites of tissue injury [332]. In fact, extensive literature described the participation of cytokines and chemokines in the loss of BBB integrity, TJ remodelling, stress fibre formation, and immune cell infiltration (reviewed in Sonar and Lal, 2018). Our data revealed a dysregulated immune response in cortistatin-deficient brain endothelium, characterized by the production of inflammatory factors (*i.e.,* IL-6, TNF-α, and MCP-1), enhanced immune cell migration, upregulated integrin signalling, and downregulated immunoregulatory and reparative pathways (*e.g.,* regulation of immune response, regulation of macrophage differentiation, regulation of cytokine production). These findings underscore the crucial role of cortistatin as a modulator in the immune response of these cells, thanks to its immunomodulatory and anti-inflammatory role.

Additionally, we observed reduced nitrite levels in BECs after OGD-R, with a particularly large decrease in *Cort*$^{-/-}$ BECs, feature that was reversed by cortistatin treatment. Nitric oxide is a crucial mediator of immunity and inflammation [335], and stands as one of the most important signalling molecules in the regulation of cerebrovascular homeostasis and CBF [336]. In both cerebral and peripheral endothelium, diminished availability of endothelial NO has been associated with vasoconstriction, increased arterial blood pressure, platelet aggregation, immune cell adhesion, and inflammation. In fact, reduced availability of endothelial NO has been identified in aged endothelium [312] and has been shown to play an essential role in the initiation and progression of vascular diseases such as atherosclerosis [336]. Interestingly, we observed that the reduced levels of nitrite were enhanced after cortistatin treatment, suggesting that the preservation of endothelial NO production by cortistatin may be crucial for preventing cerebrovascular

diseases. The reduction of NO production has been involved with several mechanisms, including impaired activity of eNOS, which has been reported in aging and other disorders [312]. However, we found a noticeable upregulation of *Nos3* (encoding for endothelial NO synthase, eNOS) in *Cort*$^{-/-}$ BECs after OGD-R. Indeed, another possible mechanism that has been previously described by others, involves impaired mitochondria function and anti-oxidant defence. In short, increased O_2-anions can react with NO to form the potent free radical peroxynitrite [337], reducing NO availability [312]. Accordingly, we found that genes encoding for antioxidant enzymes such as *Sod3, Nqo1*, or *Vnn1* among others, were downregulated. Consistent with these findings, Zhao et al. reported accelerated mitochondrial damage, elevated ROS levels, and impaired respiratory chain function in cells from the nucleus pulposus of *Cort*$^{-/-}$ mice. These are features that were reversed by cortistatin treatment [338]. Altogether, these observations suggest that the enhanced inflammatory phenotype of cortistatin-deficient endothelium, coupled with their compromised response to oxidative stress and vascular homeostasis, could contribute to brain endothelium dysfunction. In contrast, treatment with cortistatin seems to contribute to vascular homeostasis.

On the other hand, we observed the notable downregulation of pathways related to apoptosis and cell survival in cortistatin-BECs. Despite being less vulnerable than neurons, BECs also experience dysfunction or death after ischemia-reperfusion. Surprisingly, some genes associated with the negative response to apoptosis and the promotion of cell survival *(i.e., Ret, Foxc1,* or *Foxc2)* were downregulated. However, it is important to take into account that, just like phagocytosis, physiological apoptosis is crucial for removing damaged cells and facilitating tissue homeostasis [339]. In this sense, dysregulated cell death could be detrimental to the tissue as cells would be releasing cytotoxic factors. Indeed, we found the upregulation of some genes related to DNA damage such as *Gadd45a, Dffa, Plk1,* or *Clspn* in cortistatin-deficient endothelium compared to wild-type. Besides, we observed that several markers of neurodegeneration and aging (*Cmpk2, Capn11, Galnt3, Ubiad1,* and *Eno1b* among others) were upregulated in *Cort*$^{-/-}$ endothelium. On the contrary, upon damage, *Cort*$^{+/+}$ BECs upregulated some genes that may be needed for the response to damage (*i.e., Egr1* or *Nr4a1*), whereas none of these genes were upregulated or downregulated in *Cort*$^{-/-}$ BECs.

Moreover, we observed a downregulation of genes related to endothelial-mesenchymal transition (EMT), which refers to ECs transdifferentiating into mesenchymal-like cells during embryonic development and certain diseases, including atherosclerosis, fibrosis, or hypertension, but not extensively studied in stroke [340]. The induction of EMT

in BECs can lead to vascular remodelling in the infarct lesion, potentially contributing to angiogenesis and the remodelling of damaged vessels. In this line, the downregulation of genes related to differentiation and proliferation in cortistatin-deficient mice suggests a potential negative impact on angiogenesis and vascular remodelling.

Unexpectedly, elevated expression of epithelial markers such as *Krt7, Krt8, Krt18, Cdh1*, and *Epcam* was observed in cortistatin-deficient BECs. These genes are typically associated with choroid plexus epithelial cells [341], which can unintentionally contaminate primary isolates of brain microvascular ECs. However, the differentially increased expression of these factors was specifically identified in *Cort*$^{-/-}$ BECs. This finding supports the hypothesis that endogenous cortistatin plays a role in endothelial cell determination, specifically promoting endothelial commitment over an epithelial-like fate. Notably, regulatory factors governing specification of ECs fate were found to be downregulated in cortistatin-deficient endothelium. Accordingly, other studies from our group have demonstrated the endogenous role of cortistatin as a controller of cell fate in fibrosis [192].

Lastly, from a molecular point of view, our study unveiled the downregulation of relevant gene networks in cortistatin-deficient endothelium (Figure 57). Several of these networks are crucial for physiological and injury responses including matrix remodelling, cytoskeleton architecture, junction assembly, angiogenesis, apoptosis, endothelial commitment, and immune activity. Among the affected pathways, we identified VEGF-VEGFR2-Nrp1, TGF-β-Nrp1 and Notch signalling (all pivotal for angiogenesis), Wnt pathway (critical for BBB maturation and barriergenesis), Ang1/Tie2 interaction (critical for TJs stabilization), and semaphorins signalling (key in vascular remodelling and growth and barrier properties). While further research is needed to explore the specific contribution of cortistatin in each functional network, our results and pioneering transcriptomics datasets highlight the key role of endogenous cortistatin in finely modulating these interconnected pathways.

Taken together, our findings suggest that while wild-type BECs exhibited a canonical balanced response to ischemic damage by upregulating the pathways linked to recovery (including ECM reorganization, angiogenesis, cell fate determination, and response to hypoxia), these responses were impaired in cortistatin-deficient endothelium (Figure 57). Understanding the mechanisms underlying brain endothelium dysregulation could potentially guide care decisions and the development of new therapeutic targets against stroke. Importantly, the investigation of multifactorial factors looks promising for the treatment and prevention of neuroinflammatory/neurodegenerative disorders.

Cortistatin is a case example of this type of factors, targeting and modulating whole components of the TJ complex, crucial molecular pathways, endothelial permeability, and immune dysregulation. Furthermore, the modulation of BBB breakdown would also directly tackle the ongoing challenge of achieving drug delivery to the injured brain, since the alterations in the endothelium and the accumulation of blood-derived toxics often restrict the transport of drugs to the brain [59].

Regarding experimental designs, while mouse models are of paramount importance to BBB research, they are not 100 % reliable and cannot precisely replicate the human barrier. Alternatively, human BBB primary cells are exceptionally challenging to obtain, mainly because of availability would depend on biopsies from unhealthy individuals or commercial vendors with limited information on cell sources [342]. Nonetheless, advancements in stem cell technology have facilitated the development of improved human BBB models [342], particularly based on human pluripotent stem cells and human cord blood-derived stem cells. In our study, we employed the latter [343], reporting protective properties of cortistatin in TJ integrity and permeability similar to those observed in mice. Intriguingly, we found that hypoxia-reoxygenation (HPX-R) did not enhance permeability compared to control conditions. Previous studies have demonstrated that in normal culture conditions, serum-derived factors can compromise barrier properties while keeping TJs intact [344–346]. Moreover, it has been observed that the administration of serum during the reoxygenation phase can limit differences in permeability [251,252]. Nevertheless, although permeability levels were similar, the ZO-1 membrane expression was significantly decreased in HPX-R *vs* NX/NG conditions, indicating that HPX had already an effect on the continuity of the TJs. Importantly, under the same conditions, cortistatin not only reduced permeability but also prevented the loss of expression of ZO-1. Both results suggest that cortistatin was able to induce tighter barrier properties. Given these results, we extended our investigation to OGD-R studies in these cells, with the aim of further elucidating the role of cortistatin under ischemic conditions. However, human models incorporate a wide range of variables, including different durations of oxygen-glucose deprivation and reoxygenation, the composition of the culture medium during OGD and reperfusion (including the presence or absence of serum, glucose, endothelial growth factors), among other factors. While these variables have been all been well-established and standardized for mouse BECs, this is not the case yet for human cells. In this assay, cells subjected to OGD-R showed increased permeability, accompanied by significant disruption of ZO-1 and reduced claudin-5 expression in the cell membrane, compared with the continuous distribution of ZO-1 and

claudin-5 in cells incubated under NX/NG conditions. Surprisingly, the addition of cortistatin had no effect on permeability but significantly affected the recovery of ZO-1 and the distribution and integrity of claudin-5. While discontinuous junctions are typically indicative of decreased barrier function and increased permeability, recent works have demonstrated that global permeability measures may not necessarily correlate with the junction phenotype (*i.e.,* permeability measure remains the same with continuous and discontinuous arrangement of TJs) [253].

Finally, it is crucial to note the participation of the rest of the components of the NVU in brain endothelium physiology and further disruption. For instance, beyond their role in scar formation, astrocytes serve as a critical cellular link between the neuronal circuitry and blood vessels, enabling them to regulate blood flow in response to neuronal activity signalling. However, after ischemic damage, astrocytes can release MMPs that affect brain endothelium integrity [309]. Similarly, activation of pericytes may further aggravate BBB breakdown, through detaching and migrating from the vessel, which normally implies secreting MMPs [106]. In this sense, previous studies from the group have shown an exacerbated activated phenotype of these cells in cortistatin-deficient cells in physiological and LPS conditions (unpublished results from Irene García's master thesis), reporting also a therapeutic role of cortistatin deactivating this exacerbated response. Future studies will address the exact role of cortistatin in these cells under ischemic injury conditions, as well as their role in reparative further responses in the context of the BBB.

On the other hand, the late stages of BBB also involve regenerative processes, such as angiogenesis and the modification of the vascular tree. Angiogenesis is a complex, multi-step process that entails the formation of new blood vessels from pre-existing ones. ECs surrounding the infarct region start to proliferate as early as 12–24 h following ischemia, leading to an increase in vascular density between the second and third days. This process can persist for up to 90 days after stroke [347,348]. Angiogenesis is a natural defense mechanism that helps to restore cerebral blood flow, oxygen and glucose supply. These, in turn, facilitates neuronal regeneration, promoting the reconstruction of synaptic connections between neurons. All of the above determine the degree of functional recovery of the patient [347]. In this context, our research has demonstrated that cortistatin treatment increases vascular density, vessel diameter and seems to enhance the number of sprouting vessels (Figure 56). However, newly formed vessels after stroke typically exhibit immaturity and higher permeability than normal vessels, due to a lack of TJs [348]. Hence, caution is advisable when aiming to promote angiogenesis with a treatment, as it may worsen outcomes in stroke patients. Therefore, strategies that not only stimulate

angiogenesis but also promote TJ formation and maintain BBB integrity in these new vessels offer a more promising and safer approach for enhancing stroke recovery. In this context, our research has demonstrated that cortistatin treatment particularly enhances the formation of new vessels whereas conveniently promoting TJs, AJs, and cytoskeleton reorganization, and increase integrity. Accordingly, these were correlated with a reduction of post-injury permeability *in vitro*, and a reduced BBB leakage *in vivo*. Overall, these findings suggest that cortistatin could be used as a novel therapeutic agent focusing on angiogenesis-derived responses. However, a comprehensive understanding of the exact role of cortistatin in other components of the NVU (*i.e.,* pericytes, astrocytes) should be addressed in order to gain further insights into the precise mechanisms underlying cortistatin regulation.

Beyond an efficient treatment, we reported that cortistatin also seems to play an endogenous crucial role in brain angiogenesis, since middle-aged cortistatin-deficient mice showed impaired angiogenesis after stroke. Accordingly, our transcriptomic analyses in cortistatin-deficient cells revealed reduced expression of *Vegfa*, *Vegfd*, *Bdnf*, *Angpt1*, *Angptl2*, *Angptl4*, and other angiogenic-related factors, in both control and ischemic-like conditions. This suggests that the impaired angiogenesis observed in cortistatin-deficient mice might be partly related to the reduction of these factors. Interestingly, Notch signalling was also impaired in cortistatin-deficient endothelium. In addition to its various roles in cell fate determination, Notch directly and indirectly regulates a cohort of genes involved in angiogenesis, including VEGF receptors and EphrinB2 [349]. Specifically, Notch has been reported to be critical for both sprouting angiogenesis and vessel maturation. In particular, it has been shown that during the formation of a new capillary, Notch drives the differentiation of the leading endothelial cell, also referred to as tip cell, and the subsequent growing cell, the stalk cell. Notch is also involved in regulating vessel stability [349]. Furthermore, we observed the evident downregulation of *Pdpn*, which is also involved in angiogenesis and vessel stability. Studies investigating *Pdpn* deficiency or modification have reported that it leads to defective recruitment of ECM and pericytes, and eventually to BBB breakdown and large haemorrhages [350–352]. Finally, the formation of new vessels also creates an appropriate microenvironment for cell migration, enabling neuroblasts migrate from the SVZ to the peri-infarct region. Similarly, growth factors released by ECs (*e.g.,* VEGF, BDNF, or EGF) are indispensable for the proliferation of neuroblasts [347]. We did not observe a significantly reduced vessel density in young cortistatin-deficient mice following stroke, but we propose that the alteration of these

pathways in cortistatin-deficient endothelium both in ischemic and physiological conditions may have ultimately caused the reduced density that we did observe in middle-aged mice.

5.5. Involvement of cortistatin in immune peripheral-brain connection

Finally, it is crucial to acknowledge that a stroke is a complex process that do not only concerns the brain, but also peripheral organs organism-wide. Shortly after the interruption of blood flow and the subsequent hypoxia, ECs express selectins in response to oxidative damage. These molecules quickly engage circulating innate immune cells, triggering the rapid pro-inflammatory response in the periphery. Moreover, the degradation of BBB components facilitates the extravasation of these cells, at different time intervals and with variable cadences. Our investigation shows that cortistatin modulates immune infiltration in the brain of both wild-type and cortistatin-deficient mice in both age groups (Figure 56). Similar effects of cortistatin treatment were found by others in an EAE model [144]. Accordingly, our research indicates that cortistatin can modulate the transmigration of macrophages and T cells across the endothelium. Similarly, other studies from the group have also reported the regulatory role of cortistatin modulating and decreasing the binding of immune cells to the peripheral endothelium [145], which was related to beneficial responses. To what extent cortistatin is involved in regulating adhesion molecules, whether is directly affecting immune cells instead, or both, are points that we cannot fully elucidate at this point. In fact, cortistatin exerts immunomodulatory activities in activated macrophages *in vitro,* suggesting that we cannot dismiss the latter [138]. Importantly, several treatments targeting leukocyte trafficking have also shown beneficial outcomes including E- or P-selectin [353,354], ICAM-1, CD18, or CD11b blocking [355]. However, clinical trials of anti-ICAM-1 [356] or anti-CD18 [357] compounds have not proven their efficacy, or have resulted in higher mortality [358]. As highlighted when addressing the neuroinflammatory response, we again advocate that understanding each specific mechanism at each specific stage seems to be paramount to achieve a better modulation of the overall response.

Furthermore, we found that cortistatin-deficient endothelium from middle-aged mice presented a greater number of infiltrated immune cells in the brain parenchyma after injury (Figure 56). Indeed, we reported an enhanced migration of macrophages and T cells through the brain endothelium (Figure 57). Despite the precise underlying mechanisms are not completely understood [359,360], endogenous cortistatin may be regulating the adhesion molecules present in these cells, since in cortistatin-deficient BECs the integrins *Itga3* and *Itga4* were upregulated. Besides, we cannot dismiss the involvement of the

disrupted endothelium of these animals in enhanced leukocyte migration, nor the contribution of inflammatory factors or chemokines from the rest of the cells of the parenchyma.

Beyond periphery-only effects, the elevation of inflammatory mediators following ischemia occurs both centrally and peripherally [131]. First, microglia, astrocytes, BECs, and neurons in the brain produce cytokines in response to ischemic injury, reaching the systemic circulation through disrupted BBB or CSF drainage lymphatic pathways [361]. Subsequently, circulating cytokines, among other factors, trigger the immune response in lymphoid organs, and increase the production of inflammatory mediators in circulating and splenic immune cells [116]. In general, an increased production of pro-inflammatory cytokines and a decreased production of anti-inflammatory cytokines is correlated with poorer clinical outcomes and larger infarct size in animal models [361]. In this sense, we observed an enhanced proinflammatory response (*i.e.,* IL-6, IL-12, MCP-1) in middle-aged mice compared to young animals, likely associated with an aging-related factor. Moreover, we found an enhanced production of these mediators in cortistatin-deficient mice conforming to previously reported studies [144], and being the increased production significantly reduced after cortistatin treatment in both age groups.

Among the several cytokines involved in stroke pathophysiology, IL-6 is a pleiotropic pro-inflammatory cytokine known for its role in increasing leukocyte migration, modulating the production of chemokines, and enhancing the expression of adhesion molecules [362]. Elevated levels of IL-6 in serum within the first 24 h following a stroke have been associated with a decline in the functional state of patients [362–364]. Notably, the concentration of IL-6 in serum on the 1st and 6th day after an ischemic stroke is linked to long-term post-stroke outcomes, including disability degree and mortality at 3 months and/or 1 year after the event [362,364]. Interestingly, Shenhar-Tsarfaty and colleagues demonstrated that an increase in IL-6 within the first 24 h after hospital admission is a highly sensitive stroke biomarker and an important prognostic factor for the survival of stroke patients within the first year [362,365]. Another important cytokine involved in stroke dynamics is IL-12, which plays a proinflammatory role in immune response. Specifically, IL-12 increases the production and action of several pro-inflammatory cytokines and chemokines, promoting the release of adhesion molecules by BECs, which subsequently enhances immune cell adhesion. Moreover, IL-12 functions as a cofactor in the polarization of T cell response. Specifically, antigen-presenting cells produced IL-12, IL-23, and IL-27 during antigen presentation to naive T cells [366]. Similar to IL-6, IL-12 is

increased in serum of stroke patients or patients with myocardial infarction and severe brain injury [367].

Regarding chemokines, MCP-1 (also known as CCL2) and its corresponding receptor, CCR2, among other cytokines, are involved in regulating the inflammatory response in ischemia. In particular, it has been reported that MCP-1 modulates immune cell recruitment and adhesion to brain endothelium [359,368]. Notably, MCP-1 expression becomes enhanced in the ischemic penumbra, cerebrospinal fluid, and serum after stroke, and positively correlates with lesion enlargement [369,370]. All these findings add evidence to the detrimental role that CCL2/CCR2 signalling pathways play in ischemic stroke [370]. Knocking out the CCR2 receptor of chemokine MCP-1 (CCL2) in animal models results in the depletion of cell migration and the reduction of the size of the ischemic area [362]. In other studies aiming to define stroke subtypes, MCP-1 levels were also specifically associated with the risk of ischemic stroke [371].

Collectively, the enhanced levels of these inflammatory mediators in cortistatin-deficient mice might contribute to the elevated presence of immune infiltrating cells in the brain parenchyma. Moreover, these factors would contribute to the disrupted BBB and the polarized inflammatory phenotype of microglia and immune cells observed in these mice. Moreover, their elevated presence in plasma would contribute to the enhanced susceptibility to stroke exhibited by these animals, since these factors would also target other peripheral organs. Importantly, these results underline the endogenous role of cortistatin as a mediator/brake in excessive inflammation, together with its potent anti-inflammatory properties when used as therapy.

Nevertheless, the Janus-faced nature of peripheral inflammation cannot be dismissed. In summary, the same factors may either contribute to tissue damage or protection, depending on the temporal-spatial context of their expression [372]. For example, IL-6 serves as a neurotrophic factor in the late phase. In fact, some studies reported that intravenous administration of IL-6 improves functional outcomes and reduces stroke volume in mice [373], or promotes angiogenesis after a stroke [372]. Hence, considering the dual role of cytokines in both the acute and the recovery phases, blocking them can have undesired effects [374]. In this context, it is important that cortistatin modulated but not reduced completely the levels of these cytokines/chemokines. Besides, it is crucial to consider that these experiments were conducted in the acute phase, where cytokines typically exert a pro-inflammatory/detrimental function. Future studies should address the dynamics of cortistatin regulation over cytokines and chemokines production

in later stages. Finally, it is essential to consider that, aside from studying peripheral cytokines in serum, a deeper understanding of the role of cortistatin in the local cytokine response in the brain, would be of crucial importance [361]. In this sense, the capacity of cortistatin to efficiently modulate the immune response in BECs in our study, as well as in other NVU cells such as astrocytes or microglia [144], suggests that this neuropeptide would regulate both locally and peripherally the immune response.

5.6. Possible mechanisms underlying cortistatin role after stroke

The interactions among the endocrine, nervous, and immune systems are mediated by intricate networks of cells and molecules, which are in constant communication to generate a variety of coordinated responses to potential threats. This biological dialogue is based on the immune system notifying the neuroendocrine system when a systemic immune/inflammatory response to infection or tissue injury is underway. In response, the nervous system orchestrates the febrile response and influences behaviour, encompassing sleep, feeding, and locomotion [375]. Reciprocally, the immune system is under the regulation of the nervous system. Both stress and immune stimuli activate various neuronal mechanisms in the hypothalamus, initiating anti-inflammatory and immunosuppressive molecular pathways that are generally, aiming to limit the immune response [375].

One of the main axes in the neuroendocrine interplay is the hypothalamus–pituitary–adrenal (HPA) axis. In particular, upon stress stimuli, the corticotropin-releasing hormone (CRH) is released by the hypothalamus, binding to its receptor in the pituitary gland and releasing adrenocorticotropic hormone (ACTH). Subsequently, circulating ACTH activates glucocorticoid synthesis and secretion from the adrenal gland [376]. Interestingly, the activation of the HPA axis correlates with higher rates of post-stroke morbidity and mortality in humans [377]. Moreover, enhanced plasma glucocorticoid levels are related to increased infarct volume and poor functional recovery in mice [378]. Interestingly, cortistatin-deficient mice present high levels of glucocorticoids that might be affecting their increased susceptibility to strokes. Conversely, cortistatin treatment in humans reduced the exacerbated response of the HPA axis. Besides, it is known that common post-stroke complications such as immune depression, cognitive impairment, and infections are directly or indirectly impacted by the dysregulated neuroendocrine axis [376]. In this sense, other studies have reported that the high levels of peripheral glucocorticoids in cortistatin-deficient mice may provoke an immune suppressive phenotype in these animals after some injury models [144,202]. However, this paradoxical

effect was only reported in systemic models and not in acute models or in the individual response of neuroimmune cell populations [182,190,192]. Accordingly, the inflammatory phenotype of cortistatin-deficient cells (*i.e.,* microglia, astrocytes, and BECs) suggests that none of the immunosuppressor effects associated with glucocorticoids are either observed in the context of stroke. In fact, *Anxa1*, a glucocorticoid-induced endothelial factor correlated with BBB disruption [379], was downregulated in BECs lacking cortistatin.

This complex interplay is possible thanks to the presence of a biochemical common language of neurotransmitters, neuropeptides, and hormones. In addition to our current study, previous studies have long demonstrated the protective effect of neuropeptides in stroke. For example, a study conducted over 20 years ago documented a reduction in lesion size in rats following treatment with somatostatin, octreotide (a somatostatin analogue), and cortistatin in a permanent MCAO model at seven days [201]. However, the exact mechanisms underlying this effect were not elucidated, and no subsequent studies have further investigated cortistatin. Interestingly, in this study cortistatin was administered immediately after MCAO and, contrary to our findings, neuroprotective effects were reported. Nevertheless, differences in the ischemic model (*i.e.,* permanent rather than transient), the choice of the organism, the observation of effects at later stages rather than acutely, and especially the administration via for the neuropeptide (*i.e.,* intra-cerebrovascular rather than intraperitoneally) may contribute to the observed differences. Additionally, various studies have demonstrated that ghrelin administration reduces the infarct volume and improves neurological deficits, in a MCAO model in rats [380,381], as well as positively impacting BBB [382]. In these models, elevated levels of ghrelin in serum were found, probably as a compensatory neuroprotective effect against ischemia [383,384]. Accordingly, although not in stroke, cortistatin expression was also found elevated in other vascular disorders, such as mouse arteries subjected to blood-flow alterations, in plasma of patients with coronary artery lesions, and in hearts of mice with autoimmune myocarditis [145,146]. These all suggest that in response to certain acute injuries, neuropeptide secretion would be enhanced as a compensatory mechanism. Interestingly, local levels of cortistatin and somatostatin were decreased in the ischemic core but enhanced in the penumbra in a mouse model of stroke [206]. Accordingly, we found in our study that BECs from mice and humans showed decreased cortistatin levels upon oxygen-glucose deprivation injury. Furthermore, levels of cortistatin were impaired in the temporal lobule of AD patients [203] or in the retina of patients with diabetic retinopathy [205]. Additionally, a depletion in the short arm of chromosome 1 (*i.e.,* syndrome of monosomy 1.36p), where the cortistatin gene is located, is associated with low levels of

cortistatin in humans and severe brain and development disorders (*e.g.,* intellectual disability, vision and hearing problems, renal anomalies, or cardiomyopathy) [385]. Altogether, these findings indicate that while neuropeptide levels may increase in the acute phase of damage, they subsequently decrease in chronic stages, correlating with a worse prognosis of the disease. This implies that restoring neuropeptide levels, especially in the chronic stages of neurodegenerative/neuroinflammatory disorders, could represent a novel neuroprotective mechanism. Future studies will investigate whether the dynamic changes in these neuropeptides could also serve as biomarkers of the prognosis of stroke or other neuroimmune conditions.

Further comprehending the relationship between the structure and function of these neuropeptides and their receptors (*i.e.,* receptor signalling, internalization, and homo- and heterodimerization) in a physiological and pathologic context will pave the way for the development of innovative pharmacological agents [375]. In this context, cortistatin is known to bind to Sstr, Ghsr, and Mgrx2 receptors, as well as to others yet unknown. However, from a molecular point of view, the exact mechanism through which cortistatin acts through their receptors exerting protective properties in stroke is still unknown. Probably, the potential capability of cortistatin to synergistically signal through somatostatin/ghrelin receptors (in addition to a yet unknown specific receptor) could confer an advantage over the individual regulation of stroke physiopathology exerted by somatostatin/ghrelin. Moreover, the intriguing possibility that cortistatin exerts its mechanisms through different cell types (*i.e.,* neurons, microglia, astrocytes, pericytes, BECs, or immune cells) could also confer an advantage against other potential therapeutics.

Regarding stroke, the role of the different receptors is not well-known, and only a handful of studies have addressed them. For instance, Stumm and colleagues reported that an upregulation of *Sstr2* was found in pyramidal neurons after focal ischemia, related to more severe ischemic lesions. Additionally, they found that *Sstr2*-deficient mice exhibited more protective outcomes than wild-type mice [206]. Intriguingly, Sstr2 agonists only promoted neuronal death in ischemic conditions [206]. Notably, levels of S*str2* and S*str4* decreased from the first 6 h in the ischemic core. However, these levels seem to increase in the periinfarct area [206]. Interestingly, Yua and colleagues described that Sstr1 contributes to neuronal apoptosis after an intracerebral haemorrhage model in rats [386]. In addition, *Sstr1* knockdown specifically resulted in reduced neuronal apoptosis. Similarly, other reports in the same model indicated an elevated expression of S*str3*, which correlated with increased neuronal apoptosis [387]. The reported detrimental effects of

Sstr in stroke did not correlate with the neuroprotective properties of Ghsr that have been demonstrated after ischemia-reperfusion. In particular, *Ghsr*$^{-/-}$ mice have greater loss of dopamine neurons in the SNpc than wild-type mice in a model of Parkinson's (reviewed in Spencer et al., 2013). However, the exact interplay cortistatin-Ghsr during strokes has not been described yet.

It is important to take into account that the activation of somatostatin/ghrelin receptors by cortistatin can trigger diverse signalling pathways, exerting different effects than those of somatostatin or ghrelin [389–391]. For example, somatostatin inhibits cAMP accumulation, while cortistatin has been reported to stimulate it [392]. Therefore, though somatostatin receptors have been reported to be augmented upon ischemic stroke, being associated with poor outcomes, we advocate that the binding of cortistatin might induce different actions compared to somatostatin or agonists. The signalling through these receptors may contribute to the observed beneficial neuroprotective effects in stroke. Further studies should address the specific mechanisms underlying the effects of cortistatin, and the binding to these receptors particularly in ischemia.

This hypothesis is supported by the finding that Sstr4 and Sstr2 were the two major receptors expressed in BECs, and that cortistatin may have exerted beneficial effects though their interaction. While future experiments would be necessary to characterize cortistatin-induced intracellular pathways, we advocate that the binding of cortistatin to these receptors might be also regulating brain endothelium integrity. Similarly, somatostatin, ghrelin, and receptors-agonists have been reported to have protective effects over the endothelium [194,198,393]. In particular, cortistatin promotes peripheral protective vascular responses after injury via somatostatin/ghrelin receptors, by inducing cAMP and inhibiting calcium rise [146]. Interestingly, increased levels of cAMP are associated with greater endothelial TJ integrity [394], cytoskeleton and actin filaments stabilization, reinforcement of cell-matrix interactions [395], and anti-inflammatory actions [178,396]. Further studies will address the differential expression of these ligands and receptors upon ischemic damage in the different cell populations involved in stroke.

5.7. Clinical potential role of cortistatin and concluding remarks

Finally, it is important to highlight that the successful use of cortistatin at clinical levels has already been demonstrated, providing assurances of its potential use in clinics. In contrast to other existing anti-inflammatory or neuroprotective drugs for strokes, neuropeptides are physiological compounds, so they are intrinsically nontoxic. Moreover, neuropeptides are small and hydrophilic molecules, being rapidly cleared from the body through natural

detoxification/excretion mechanisms and renal excretion [375]. Furthermore, any of the potential side effects derived from their general actions (*i.e.,* hypotension, decreased gut motility, or diarrhoea) have been reported [375]. Besides, most of these neuropeptides, including cortistatin, have already been administered systemically and locally to humans, demonstrating its clinical efficiency in patients with acromegalia, prolactinoma [161], or Cushing Disease [160]. In each of these disorders, cortistatin has been shown to reduce the secretion of the growth hormone, prolactin levels, and the activity of the HPA, respectively [160,161].

Nevertheless, due to their peptide nature, and although they can rapidly access the site of inflammation, these molecules have a short life in body fluids and tissues (*e.g.,* cortistatin lasts only 2 min in plasma) because of their rapid degradation by endopeptidases [162]. In this regard, various approaches have been proposed to enhance their stability, namely amino acid sequence modifications, co-administration with peptidase inhibitors, the use of lentiviral vectors, encapsulation into nanoparticles, micelles, liposomes, among other engineering structures that increase their protection, stability and bioavailability. These would allow the release of the bioactive neuropeptide in a controlled manner [162]. For instance, our research group has developed a stable analogue of cortistatin by selectively substituting AA in the naive peptide. Noteworthy, this analogue showed more than ten-fold higher half-life in plasma and similar therapeutic effects, when compared to cortistatin in experimental chronic IBD [397].

Beyond the peptide-specific characteristics, another challenge that has to be addressed is the promiscuity of neuropeptides, as they can bind several receptors and act through a plethora of different cell types. This fact, together with their production in multiple body locations, increase the risk of generating pleiotropic and undesired side effects. Therefore, in recent years there has been a growing interest in designing modified neuropeptides combined with compounds that protect them from peptidase-induced degradation but that also facilitate their specific release at the target site. In this sense, a latent form of the cytokine interferon-β [398] has been modified and adapted for VIP and MSH [399], demonstrating increased efficiency in treating experimental inflammatory disorders. Building upon this approach, it has been recently designed a latent form of cortistatin [162]. This innovative design involves a molecular shield provided by the latency-associated peptide (LAP) of TGF-β1 linked to the cortistatin sequence via a cleavage site recognized by MMP. Within this construct, LAP serves to protect cortistatin from degradation by tissue endopeptidases, preventing its binding to receptors until it reaches a MMP-cleavage site [162]. This allows the release of bioactive cortistatin

exclusively in regions of the body with an abundance of these enzymes, such as foci of inflammation or severe damage. Further studies would be needed to address whether these newly engineered forms of cortistatin elicit the same beneficial effects in stroke, or may even offer enhanced protection.

In summary, this study, conform to others and highlights the importance of a better understanding of the spatio-temporal changes in stroke. In particular, it is evident that the evolutionary process has favoured an acute response to address body damage, with an attempt to ensure the repair of the injury, though at a certain cost [39]. Therefore, rather than aiming to completely halt specific processes, the focus on stroke therapies should be shifted towards regulating and balancing them to prevent chronic detrimental responses. Indeed, interrupting certain neurotoxic processes (*e.g.,* glial activation, or immune response) might unintentionally hamper neuroprotective mechanisms (*e.g.,* angiogenesis) [400]. Moreover, our study highlights the importance of addressing the most effective therapeutic window for potential therapeutic compounds, as well as identifying possible detrimental effects in its time-dependent administration. Additionally, our study underscores the importance of the use of several motor and cognitive tests to better understand clinical deficits and, beyond acute stages, our design also emphasises the necessity of investigating potential therapeutic compounds at later chronic stages.

In conclusion, cortistatin emerges as a pleiotropic endogenous key factor and a potential therapeutic agent in stroke management. In particular, its capacity to concurrently modulate several pathological features, such as clinical manifestations, neurological damage, glial over-reaction, or astrocyte scar, holds significant promise compared to interventions targeting only a single aspect. Furthermore, our findings indicate that cortistatin is particularly involved in protecting BBB from post-stroke breakdown, exerting anti-inflammatory and brain endothelium reparative properties, through organizing endothelial junction proteins and reducing immune exacerbated responses. Additionally, cortistatin emerges as a critical factor modulating the intricate interplay between the CNS and the immune system, regulating exacerbated cellular and molecular responses from both systems that could impact brain homeostasis. Finally, its efficient application at later times and across different ages and phenotypes could open the door for extending a therapeutical time window, which is unfortunately very narrow or non-existent for many patients who do not meet the clinical criteria. The useful insights derived from this study have the potential to contribute to the development of novel therapeutic strategies not only for stroke, but also for other CNS pathologies associated with BBB dysfunction, glial over-reactivity, or impaired CNS-immune system interplay.

6. Conclusions/ Conclusiones

6. Conclusions

1. Cortistatin emerges as a potential therapeutic agent for stroke by modulating the deregulated response of microglia, impaired glial scar formation, and blood-brain barrier breakdown, which collectively reduces ischemic lesions and protects against the progression of neurodegeneration. This beneficial effect of cortistatin is observed in both young and middle-aged animals.

2. Cortistatin plays a crucial role as a modulator of the neuroimmune response during stroke since it can regulate exacerbated inflammatory mediators in the periphery but also locally in the brain endothelium, while also modulating immune traffic to the brain.

3. The therapeutic window of cortistatin extends to later stages (24 h post-stroke) and demonstrates efficacy regardless of age and genotype. This potential broadening of the current narrow therapeutic window addresses the challenge of exclusion criteria in clinical practice.

4. Acute responses and biological interactions at initial stages, such as microglia response or glial scar formation, are vital for ultimate stroke recovery and should not be halted. This implies that cortistatin and other agents with anti-inflammatory actions might not be suitable for administration at very early stages.

5. The deficiency of endogenous cortistatin leads to altered glial response, compromised glial scar formation, disrupted blood-brain barrier, and exacerbated immune response, resulting in worse clinical manifestations.

6. Cortistatin plays a particularly important role in mouse and human brain endothelium, regulating the integrity of tight-junctions and adherens-junctions, and modulating barrier permeability and immune dysregulation in both physiological and injured conditions.

7. The endogenous lack of cortistatin in brain endothelium is correlated with disrupted and/or deactivated molecular pathways involved in physiological and repair processes after injury, such as extracellular matrix remodelling, angiogenesis, transport, cell fate, signalling, or immune response. These pathways become dysfunctional rendering cortistatin-deficient brain endothelium unresponsive to further injury.

8. The use of cortistatin as a treatment emerges as an innovative therapeutic approach for addressing stroke and other neurogenerative/neuroinflammatory conditions associated with dysfunction in the blood-brain barrier, glial over-reactivity, or deregulated interplay between the central nervous system and the immune system.

Conclusiones

1. Cortistatina emerge como un potencial agente terapéutico para el accidente cerebrovascular al modular la respuesta desregulada de la microglía, la formación alterada de la cicatriz glial y la ruptura de la barrera hematoencefálica. Esta acción colectiva reduce las lesiones isquémicas y protege contra la progresión de la neurodegeneración. El efecto beneficioso de cortistatina se observa tanto en animales jóvenes como de mediana edad.

2. Cortistatina desempeña un papel crucial como modulador de la respuesta neuroinmunológica durante el accidente cerebrovascular. En concreto, puede regular los mediadores inflamatorios elevados en periferia, así como localmente en el endotelio cerebral, y modular el tráfico de células inmunitarias hacia el cerebro.

3. La ventana terapéutica de cortistatina se extiende hasta etapas tardías (24 horas después del accidente cerebrovascular) y demuestra eficacia independientemente de la edad y el genotipo de los animales. Esta potencial ampliación de la estrecha ventana terapéutica actual aborda el desafío de los criterios de exclusión en la práctica clínica.

4. La respuesta aguda y las interacciones biológicas durante las etapas iniciales del ictus, como la respuesta de la microglía o la formación de la cicatriz glial, son vitales para la recuperación del accidente cerebrovascular y no deben detenerse. Esto implica que cortistatina y otros agentes con acciones antiinflamatorias probablemente no deban administrarse en etapas muy tempranas.

5. La deficiencia endógena de cortistatina conduce a una respuesta glial alterada, una formación comprometida de la cicatriz glial, una disrupción de la barrera hematoencefálica y una respuesta inmunológica exacerbada, lo que conjuntamente resulta en peores manifestaciones clínicas.

6. Cortistatina desempeña un papel particularmente importante en el endotelio cerebral de ratones y humanos, regulando la integridad de las uniones estrechas

y las uniones adherentes, la permeabilidad de la barrera y la desregulación inmunológica tanto en condiciones fisiológicas como de daño.

7. La falta endógena de cortistatina en el endotelio cerebral se correlaciona con vías moleculares desreguladas y/o desactivadas que están involucradas en procesos fisiológicos y de reparación después de un daño, como la remodelación de la matriz extracelular, la angiogénesis, el transporte, el destino celular, la señalización o la respuesta inmunológica. Estas vías se vuelven disfuncionales, haciendo que el endotelio cerebral deficiente en cortistatina no sea capaz de responder funcionalmente a daños posteriores.

8. El uso de cortistatina como tratamiento representa un enfoque terapéutico innovador para abordar el accidente cerebrovascular, así como otras condiciones neurodegenerativas/neuroinflamatorias asociadas con disfunciones en la barrera hematoencefálica, con una exacerbada reactividad glial o con la interacción desregulada entre el sistema nervioso central y el sistema inmunológico.

7. References

7. References

1. Feigin VL, Stark BA, Johnson CO, Roth GA, Bisignano C, Abady GG, et al. Global, regional, and national burden of stroke and its risk factors, 1990–2019: a systematic analysis for the Global Burden of Disease Study 2019. The Lancet Neurology. 2021;20:795–820.

2. Lapchak PA, Yang G-Y, editors. Translational Research in Stroke [Internet]. Singapore: Springer Singapore; 2017 [cited 2023 Feb 16]. Available from: http://link.springer.com/10.1007/978-981-10-5804-2

3. Buscemi L, Price M, Bezzi P, Hirt L. Spatio-temporal overview of neuroinflammation in an experimental mouse stroke model. Sci Rep. 2019;9:507.

4. Ohashi SN, DeLong JH, Kozberg MG, Mazur-Hart DJ, van Veluw SJ, Alkayed NJ, et al. Role of Inflammatory Processes in Hemorrhagic Stroke. Stroke. 2023;54:605–19.

5. Correa-Paz C, da Silva-Candal A, Polo E, Parcq J, Vivien D, Maysinger D, et al. New Approaches in Nanomedicine for Ischemic Stroke. Pharmaceutics. 2021;13:757.

6. Owolabi MO, Thrift AG, Mahal A, Ishida M, Martins S, Johnson WD, et al. Primary stroke prevention worldwide: translating evidence into action. Lancet Public Health. 2022;7:e74–85.

7. Campbell BCV, De Silva DA, Macleod MR, Coutts SB, Schwamm LH, Davis SM, et al. Ischaemic stroke. Nat Rev Dis Primers. 2019;5:1–22.

8. Herpich F, Rincon F. Management of Acute Ischemic Stroke. Critical Care Medicine. 2020;48:1654.

9. Hui C, Tadi P, Patti L. Ischemic Stroke. StatPearls [Internet]. Treasure Island (FL): StatPearls Publishing; 2023 [cited 2023 Aug 28]. Available from: http://www.ncbi.nlm.nih.gov/books/NBK499997/

10. Iadecola C, Anrather J. The immunology of stroke: from mechanisms to translation. Nat Med. 2011;17:796–808.

11. Cai W, Liu H, Zhao J, Chen LY, Chen J, Lu Z, et al. Pericytes in Brain Injury and Repair After Ischemic Stroke. Transl Stroke Res. 2017;8:107–21.

12. Peng L, Hu G, Yao Q, Wu J, He Z, Law BY-K, et al. Microglia autophagy in ischemic stroke: A double-edged sword. Frontiers in Immunology [Internet]. 2022 [cited 2023 Jul 24];13. Available from: https://www.frontiersin.org/articles/10.3389/fimmu.2022.1013311

13. Ludwig PE, Reddy V, Varacallo M. Neuroanatomy, Central Nervous System (CNS). StatPearls [Internet]. Treasure Island (FL): StatPearls Publishing; 2023 [cited 2023 Aug 25]. Available from: http://www.ncbi.nlm.nih.gov/books/NBK442010/

14. Ashley K, Lui F. Physiology, Nerve. StatPearls [Internet]. Treasure Island (FL): StatPearls Publishing; 2023 [cited 2023 Aug 28]. Available from: http://www.ncbi.nlm.nih.gov/books/NBK551652/

15. Girijala RL, Sohrabji F, Bush RL. Sex differences in stroke: Review of current knowledge and evidence. Vasc Med. 2017;22:135–45.

16. Tuazon JP, Castelli V, Lee J-Y, Desideri GB, Stuppia L, Cimini AM, et al. Neural Stem Cells. In: Ratajczak MZ, editor. Stem Cells: Therapeutic Applications [Internet]. Cham: Springer International Publishing; 2019 [cited 2023 Aug 28]. p. 79–91. Available from: https://doi.org/10.1007/978-3-030-31206-0_4

17. Rahman AA, Amruta N, Pinteaux E, Bix GJ. Neurogenesis After Stroke: A Therapeutic Perspective. Transl Stroke Res. 2021;12:1–14.

18. Huang S, Ren C, Luo Y, Ding Y, Ji X, Li S. New insights into the roles of oligodendrocytes regulation in ischemic stroke recovery. Neurobiology of Disease. 2023;184:106200.

19. Kuhn S, Gritti L, Crooks D, Dombrowski Y. Oligodendrocytes in Development, Myelin Generation and Beyond. Cells. 2019;8:1424.

20. Ma Y, Wang J, Wang Y, Yang G-Y. The biphasic function of microglia in ischemic stroke. Progress in Neurobiology. 2017;157:247–72.

21. Matute C, Domercq M, Pérez-Samartín A, Ransom BR. Protecting White Matter From Stroke Injury. Stroke. 2013;44:1204–11.

22. Seo JH, Miyamoto N, Hayakawa K, Pham L-DD, Maki T, Ayata C, et al. Oligodendrocyte precursors induce early blood-brain barrier opening after white matter injury. J Clin Invest [Internet]. 2013 [cited 2023 Aug 25];123. Available from: https://www.jci.org/articles/30852

23. Li Q, Barres BA. Microglia and macrophages in brain homeostasis and disease. Nat Rev Immunol. 2018;18:225–42.

24. Colonna M, Butovsky O. Microglia Function in the Central Nervous System During Health and Neurodegeneration. Annual Review of Immunology. 2017;35:441–68.

25. Vidal-Itriago A, Radford RAW, Aramideh JA, Maurel C, Scherer NM, Don EK, et al. Microglia morphophysiological diversity and its implications for the CNS. Frontiers in Immunology [Internet]. 2022 [cited 2023 Jul 24];13. Available from: https://www.frontiersin.org/articles/10.3389/fimmu.2022.997786

26. Nimmerjahn A, Kirchhoff F, Helmchen F. Resting Microglial Cells Are Highly Dynamic Surveillants of Brain Parenchyma in Vivo. Science. 2005;308:1314–8.

27. Karperien A, Ahammer H, Jelinek H. Quantitating the subtleties of microglial morphology with fractal analysis. Frontiers in Cellular Neuroscience [Internet]. 2013 [cited 2023 Oct 19];7. Available from: https://www.frontiersin.org/articles/10.3389/fncel.2013.00003

28. Jiang X, Andjelkovic AV, Zhu L, Yang T, Bennett MVL, Chen J, et al. Blood-brain barrier dysfunction and recovery after ischemic stroke. Progress in Neurobiology. 2018;163–164:144–71.

29. Benakis C, Garcia-Bonilla L, Iadecola C, Anrather J. The role of microglia and myeloid immune cells in acute cerebral ischemia. Frontiers in Cellular Neuroscience [Internet]. 2015 [cited 2023 Jul 24];8. Available from: https://www.frontiersin.org/articles/10.3389/fncel.2014.00461

30. Qin C, Zhou L-Q, Ma X-T, Hu Z-W, Yang S, Chen M, et al. Dual Functions of Microglia in Ischemic Stroke. Neurosci Bull. 2019;35:921–33.

31. Stuckey SM, Ong LK, Collins-Praino LE, Turner RJ. Neuroinflammation as a Key Driver of Secondary Neurodegeneration Following Stroke? International Journal of Molecular Sciences. 2021;22:13101.

32. Wang H, Li J, Zhang H, Wang M, Xiao L, Wang Y, et al. Regulation of microglia polarization after cerebral ischemia. Frontiers in Cellular Neuroscience [Internet]. 2023 [cited 2023 Oct 17];17. Available from: https://www.frontiersin.org/articles/10.3389/fncel.2023.1182621

33. Mota M, Porrini V, Parrella E, Benarese M, Bellucci A, Rhein S, et al. Neuroprotective epi-drugs quench the inflammatory response and microglial/macrophage activation in a mouse model of permanent brain ischemia. Journal of Neuroinflammation. 2020;17:361.

34. Zhang X, Zhu X-L, Ji B-Y, Cao X, Yu L-J, Zhang Y, et al. LncRNA-1810034E14Rik reduces microglia activation in experimental ischemic stroke. J Neuroinflammation. 2019;16:75.

35. Choi JY, Kim JY, Kim JY, Park J, Lee WT, Lee JE. M2 Phenotype Microglia-derived Cytokine Stimulates Proliferation and Neuronal Differentiation of Endogenous Stem Cells in Ischemic Brain. Exp Neurobiol. 2017;26:33–41.

36. Jiang G-L, Yang X-L, Zhou H-J, Long J, Liu B, Zhang L-M, et al. cGAS knockdown promotes microglial M2 polarization to alleviate neuroinflammation by inhibiting cGAS-STING signaling pathway in cerebral ischemic stroke. Brain Res Bull. 2021;171:183–95.

37. Sofroniew MV, Vinters HV. Astrocytes: biology and pathology. Acta Neuropathol. 2010;119:7–35.

38. Zhou B, Zuo Y-X, Jiang R-T. Astrocyte morphology: Diversity, plasticity, and role in neurological diseases. CNS Neuroscience & Therapeutics. 2019;25:665–73.

39. Shen X-Y, Gao Z-K, Han Y, Yuan M, Guo Y-S, Bi X. Activation and Role of Astrocytes in Ischemic Stroke. Frontiers in Cellular Neuroscience [Internet]. 2021 [cited 2023 Jul 21];15. Available from: https://www.frontiersin.org/articles/10.3389/fncel.2021.755955

40. Guillamón-Vivancos T, Gómez-Pinedo U, Matías-Guiu J. Astrocytes in neurodegenerative diseases (I): function and molecular description. Neurologia. 2015;30:119–29.

41. Linnerbauer M, Rothhammer V. Protective Functions of Reactive Astrocytes Following Central Nervous System Insult. Frontiers in Immunology [Internet]. 2020 [cited 2023 Jul 28];11. Available from: https://www.frontiersin.org/articles/10.3389/fimmu.2020.573256

42. Sahlender DA, Savtchouk I, Volterra A. What do we know about gliotransmitter release from astrocytes? Philosophical Transactions of the Royal Society B: Biological Sciences. 2014;369:20130592.

43. Chen Z, Yuan Z, Yang S, Zhu Y, Xue M, Zhang J, et al. Brain Energy Metabolism: Astrocytes in Neurodegenerative Diseases. CNS Neuroscience & Therapeutics. 2023;29:24–36.

44. Sofroniew MV. Astrocyte barriers to neurotoxic inflammation. Nat Rev Neurosci. 2015;16:249–63.

45. Anderson MA, Ao Y, Sofroniew MV. Heterogeneity of reactive astrocytes. Neuroscience Letters. 2014;565:23–9.

46. Burda JE, Sofroniew MV. Reactive Gliosis and the Multicellular Response to CNS Damage and Disease. Neuron. 2014;81:229–48.

47. Wanner IB, Anderson MA, Song B, Levine J, Fernandez A, Gray-Thompson Z, et al. Glial Scar Borders Are Formed by Newly Proliferated, Elongated Astrocytes That Interact to Corral Inflammatory and Fibrotic Cells via STAT3-Dependent Mechanisms after Spinal Cord Injury. J Neurosci. 2013;33:12870–86.

48. Faulkner JR, Herrmann JE, Woo MJ, Tansey KE, Doan NB, Sofroniew MV. Reactive astrocytes protect tissue and preserve function after spinal cord injury. J Neurosci. 2004;24:2143–55.

49. Herrmann JE, Imura T, Song B, Qi J, Ao Y, Nguyen TK, et al. STAT3 is a critical regulator of astrogliosis and scar formation after spinal cord injury. J Neurosci. 2008;28:7231–43.

50. Sandoval KE, Witt KA. Blood-brain barrier tight junction permeability and ischemic stroke. Neurobiology of Disease. 2008;32:200–19.

51. Candelario-Jalil E, Dijkhuizen RM, Magnus T. Neuroinflammation, Stroke, Blood-Brain Barrier Dysfunction, and Imaging Modalities. Stroke. 2022;53:1473–86.

52. Castillo-González J, Ruiz JL, Serrano-Martínez I, Forte-Lago I, Ubago-Rodriguez A, Caro M, et al. Cortistatin deficiency reveals a dysfunctional brain endothelium with impaired gene pathways, exacerbated immune activation, and disrupted barrier integrity. Journal of Neuroinflammation. 2023;20:226.

53. Ballabh P, Braun A, Nedergaard M. The blood–brain barrier: an overview: Structure, regulation, and clinical implications. Neurobiology of Disease. 2004;16:1–13.

54. Muoio V, Persson PB, Sendeski MM. The neurovascular unit - concept review. Acta Physiol. 2014;210:790–8.

55. Keaney J, Campbell M. The dynamic blood-brain barrier. FEBS J. 2015;282:4067–79.

56. Pearce JMS. The blood brain barrier and Lina Solomonovna Stern (Shtern). Advances in Clinical Neuroscience and Rehabilitation [Internet]. 2022 [cited 2023 Aug 23]; Available from: https://acnr.co.uk/articles/the-blood-brain-barrier-and-lina-solomonovna-stern-shtern/

57. Saunders NR, Dreifuss J-J, Dziegielewska KM, Johansson PA, Habgood MD, Møllgård K, et al. The rights and wrongs of blood-brain barrier permeability studies: a walk through 100 years of history. Front Neurosci. 2014;8:404.

58. Daneman R, Prat A. The Blood–Brain Barrier. Cold Spring Harb Perspect Biol. 2015;7:a020412.

59. Sweeney MD, Zhao Z, Montagne A, Nelson AR, Zlokovic BV. Blood-Brain Barrier: From Physiology to Disease and Back. Physiological Reviews. 2019;99:21–78.

60. Pong S, Karmacharya R, Sofman M, Bishop JR, Lizano P. The Role of Brain Microvascular Endothelial Cell and Blood-Brain Barrier Dysfunction in Schizophrenia. Complex Psychiatry. 2020;6:30–46.

61. Hashimoto Y, Greene C, Munnich A, Campbell M. The CLDN5 gene at the blood-brain barrier in health and disease. Fluids and Barriers of the CNS. 2023;20:22.

62. Lv J, Hu W, Yang Z, Li T, Jiang S, Ma Z, et al. Focusing on claudin-5: A promising candidate in the regulation of BBB to treat ischemic stroke. Progress in Neurobiology. 2018;161:79–96.

63. Farquhar MG, Palade GE. Junctional complexes in various epithelia. J Cell Biol. 1963;17:375–412.

64. Gonçalves A, Ambrósio AF, Fernandes R. Regulation of claudins in blood-tissue barriers under physiological and pathological states. Tissue Barriers. 2013;1:e24782.

65. Van Itallie CM, Anderson JM. Claudin interactions in and out of the tight junction. Tissue Barriers. 2013;1:e25247.

66. Abbott NJ, Rönnbäck L, Hansson E. Astrocyte–endothelial interactions at the blood–brain barrier. Nat Rev Neurosci. 2006;7:41–53.

67. Hartsock A, Nelson WJ. Adherens and Tight Junctions: Structure, Function and Connections to the Actin Cytoskeleton. Biochim Biophys Acta. 2008;1778:660–9.

68. Popoff MR, Geny B. Multifaceted role of Rho, Rac, Cdc42 and Ras in intercellular junctions, lessons from toxins. Biochimica et Biophysica Acta (BBA) - Biomembranes. 2009;1788:797–812.

69. Stamatovic SM, Johnson AM, Keep RF, Andjelkovic AV. Junctional proteins of the blood-brain barrier: New insights into function and dysfunction. Tissue Barriers. 2016;4:e1154641.

70. Zihni C, Mills C, Matter K, Balda MS. Tight junctions: from simple barriers to multifunctional molecular gates. Nat Rev Mol Cell Biol. 2016;17:564–80.

71. Zhao F, Deng J, Yu X, Li D, Shi H, Zhao Y. Protective effects of vascular endothelial growth factor in cultured brain endothelial cells against hypoglycemia. Metab Brain Dis. 2015;30:999–1007.

72. Kotini M, Barriga EH, Leslie J, Gentzel M, Rauschenberger V, Schambony A, et al. Gap junction protein Connexin-43 is a direct transcriptional regulator of N-cadherin in vivo. Nat Commun. 2018;9:3846.

73. Vargas-Rodríguez P, Cuenca-Martagón A, Castillo-González J, Serrano-Martínez I, Luque RM, Delgado M, et al. Novel Therapeutic Opportunities for Neurodegenerative Diseases with Mesenchymal Stem Cells: The Focus on Modulating the Blood-Brain Barrier. International Journal of Molecular Sciences. 2023;24:14117.

74. Hagen SJ. Non-canonical functions of claudin proteins: Beyond the regulation of cell-cell adhesions. Tissue Barriers. 2017;5:e1327839.

75. Zlokovic BV. The Blood-Brain Barrier in Health and Chronic Neurodegenerative Disorders. Neuron. 2008;57:178–201.

76. Knox EG, Aburto MR, Clarke G, Cryan JF, O'Driscoll CM. The blood-brain barrier in aging and neurodegeneration. Mol Psychiatry. 2022;27:2659–73.

77. Nian K, Harding IC, Herman IM, Ebong EE. Blood-Brain Barrier Damage in Ischemic Stroke and Its Regulation by Endothelial Mechanotransduction. Frontiers in Physiology [Internet]. 2020 [cited 2023 Oct 11];11. Available from: https://www.ncbi.nlm.nih.gov/pmc/articles/PMC7793645/

78. Foroutan S, Brillault J, Forbush B, O'Donnell ME. Moderate-to-severe ischemic conditions increase activity and phosphorylation of the cerebral microvascular endothelial cell Na+-K+-Cl− cotransporter. American Journal of Physiology-Cell Physiology. 2005;289:C1492–501.

79. Vemula S, Roder KE, Yang T, Bhat GJ, Thekkumkara TJ, Abbruscato TJ. A Functional Role for Sodium-Dependent Glucose Transport across the Blood-Brain Barrier during Oxygen Glucose Deprivation. J Pharmacol Exp Ther. 2009;328:487–95.

80. Vadlapudi AD, Vadlapatla RK, Mitra AK. Sodium dependent multivitamin transporter (SMVT): a potential target for drug delivery. Curr Drug Targets. 2012;13:994–1003.

81. Wang J. The Plasma Membrane Monoamine Transporter (PMAT): Structure, Function, and Role in Organic Cation Disposition. Clin Pharmacol Ther. 2016;100:489–99.

82. Iwao B, Yara M, Hara N, Kawai Y, Yamanaka T, Nishihara H, et al. Functional expression of choline transporter like-protein 1 (CTL1) and CTL2 in human brain microvascular endothelial cells. Neurochemistry International. 2016;93:40–50.

83. Ponka P, Lok CN. The transferrin receptor: role in health and disease. Int J Biochem Cell Biol. 1999;31:1111–37.

84. Sorets AG, Rosch JC, Duvall CL, Lippmann ES. Caveolae-mediated transport at the injured blood–brain barrier as an underexplored pathway for central nervous system drug delivery. Current Opinion in Chemical Engineering. 2020;30:86–95.

85. Knowland D, Arac A, Sekiguchi KJ, Hsu M, Lutz SE, Perrino J, et al. Stepwise Recruitment of Transcellular and Paracellular Pathways Underlies Blood-Brain Barrier Breakdown in Stroke. Neuron. 2014;82:603–17.

86. Shi Y, Zhang L, Pu H, Mao L, Hu X, Jiang X, et al. Rapid endothelial cytoskeletal reorganization enables early blood–brain barrier disruption and long-term ischaemic reperfusion brain injury. Nat Commun. 2016;7:10523.

87. Choi K-H, Kim H-S, Park M-S, Kim J-T, Kim J-H, Cho K-A, et al. Regulation of Caveolin-1 Expression Determines Early Brain Edema After Experimental Focal Cerebral Ischemia. Stroke. 2016;47:1336–43.

88. Huang Q, Zhong W, Hu Z, Tang X. A review of the role of cav-1 in neuropathology and neural recovery after ischemic stroke. Journal of Neuroinflammation. 2018;15:348.

89. Profaci CP, Munji RN, Pulido RS, Daneman R. The blood–brain barrier in health and disease: Important unanswered questions. Journal of Experimental Medicine. 2020;217:e20190062.

90. Ransohoff RM, Engelhardt B. The anatomical and cellular basis of immune surveillance in the central nervous system. Nat Rev Immunol. 2012;12:623–35.

91. Xu L, Nirwane A, Yao Y. Basement membrane and blood–brain barrier. Stroke Vasc Neurol. 2018;4:78–82.

92. Baeten KM, Akassoglou K. Extracellular matrix and matrix receptors in blood–brain barrier formation and stroke. Developmental Neurobiology. 2011;71:1018–39.

93. Ma Z, Mao C, Jia Y, Fu Y, Kong W. Extracellular matrix dynamics in vascular remodeling. American Journal of Physiology-Cell Physiology. 2020;319:C481–99.

94. Schöller K, Trinkl A, Klopotowski M, Thal SC, Plesnila N, Trabold R, et al. Characterization of microvascular basal lamina damage and blood-brain barrier dysfunction following subarachnoid hemorrhage in rats. Brain Res. 2007;1142:237–46.

95. Baumann E, Preston E, Slinn J, Stanimirovic D. Post-ischemic hypothermia attenuates loss of the vascular basement membrane proteins, agrin and SPARC, and the blood-brain barrier disruption after global cerebral ischemia. Brain Res. 2009;1269:185–97.

96. Fukuda S, Fini CA, Mabuchi T, Koziol JA, Eggleston LL, del Zoppo GJ. Focal cerebral ischemia induces active proteases that degrade microvascular matrix. Stroke. 2004;35:998–1004.

97. Cao L, Zhou Y, Chen M, Li L, Zhang W. Pericytes for Therapeutic Approaches to Ischemic Stroke. Frontiers in Neuroscience [Internet]. 2021 [cited 2023 Jul 29];15. Available from: https://www.frontiersin.org/articles/10.3389/fnins.2021.629297

98. Sweeney MD, Ayyadurai S, Zlokovic BV. Pericytes of the neurovascular unit: key functions and signaling pathways. Nat Neurosci. 2016;19:771–83.

99. Hu S, Yang B, Shu S, He X, Sang H, Fan X, et al. Targeting Pericytes for Functional Recovery in Ischemic Stroke. Neuromol Med [Internet]. 2023 [cited 2023 Jul 29]; Available from: https://doi.org/10.1007/s12017-023-08748-z

100. Zhou S-Y, Guo Z-N, Zhang D-H, Qu Y, Jin H. The Role of Pericytes in Ischemic Stroke: Fom Cellular Functions to Therapeutic Targets. Frontiers in Molecular Neuroscience [Internet]. 2022 [cited 2023 Jul 29];15. Available from: https://www.frontiersin.org/articles/10.3389/fnmol.2022.866700

101. Armulik A, Abramsson A, Betsholtz C. Endothelial/Pericyte Interactions. Circulation Research. 2005;97:512–23.

102. Uemura MT, Maki T, Ihara M, Lee VMY, Trojanowski JQ. Brain Microvascular Pericytes in Vascular Cognitive Impairment and Dementia. Frontiers in Aging Neuroscience [Internet]. 2020 [cited 2023 Aug 24];12. Available from: https://www.frontiersin.org/articles/10.3389/fnagi.2020.00080

103. Attwell D, Mishra A, Hall CN, O'Farrell FM, Dalkara T. What is a pericyte? J Cereb Blood Flow Metab. 2016;36:451–5.

104. Hartmann DA, Underly RG, Grant RI, Watson AN, Lindner V, Shih AY. Pericyte structure and distribution in the cerebral cortex revealed by high-resolution imaging of transgenic mice. NPh. 2015;2:041402.

105. Tu Z, Li Y, Smith DS, Sheibani N, Huang S, Kern T, et al. Retinal Pericytes Inhibit Activated T Cell Proliferation. Invest Ophthalmol Vis Sci. 2011;52:9005–10.

106. Dalkara T, Alarcon-Martinez L, Yemisci M. Pericytes in Ischemic Stroke. In: Birbrair A, editor. Pericyte Biology in Disease [Internet]. Cham: Springer International Publishing; 2019 [cited 2023 Jul 29]. p. 189–213. Available from: https://doi.org/10.1007/978-3-030-16908-4_9

107. Duz B, Oztas E, Erginay T, Erdogan E, Gonul E. The effect of moderate hypothermia in acute ischemic stroke on pericyte migration: An ultrastructural study. Cryobiology. 2007;55:279–84.

108. MacVicar BA, Newman EA. Astrocyte Regulation of Blood Flow in the Brain. Cold Spring Harb Perspect Biol. 2015;7:a020388.

109. Liebner S, Dijkhuizen RM, Reiss Y, Plate KH, Agalliu D, Constantin G. Functional morphology of the blood–brain barrier in health and disease. Acta Neuropathol. 2018;135:311–36.

110. Daneman R, Zhou L, Kebede AA, Barres BA. Pericytes are required for blood-brain barrier integrity during embryogenesis. Nature. 2010;468:562–6.

111. Obermeier B, Daneman R, Ransohoff RM. Development, maintenance and disruption of the blood-brain barrier. Nat Med. 2013;19:1584–96.

112. Bernardo-Castro S, Sousa JA, Brás A, Cecília C, Rodrigues B, Almendra L, et al. Pathophysiology of Blood–Brain Barrier Permeability Throughout the Different Stages of Ischemic Stroke and Its Implication on Hemorrhagic Transformation and Recovery. Frontiers in Neurology [Internet]. 2020 [cited 2023 Aug 18];11. Available from: https://www.frontiersin.org/articles/10.3389/fneur.2020.594672

113. Zheng X, Ren B, Gao Y. Tight junction proteins related to blood-brain barrier and their regulatory signaling pathways in ischemic stroke. Biomedicine & Pharmacotherapy. 2023;165:115272.

114. Carmeliet P, Jain RK. Molecular mechanisms and clinical applications of angiogenesis. Nature. 2011;473:298–307.

115. Hayashi T, Noshita N, Sugawara T, Chan PH. Temporal Profile of Angiogenesis and Expression of Related Genes in the Brain after Ischemia. J Cereb Blood Flow Metab. 2003;23:166–80.

116. Iadecola C, Buckwalter MS, Anrather J. Immune responses to stroke: mechanisms, modulation, and therapeutic potential. J Clin Invest. 2020;130:2777–88.

117. Pleşeru A-M, Mihailă RG. The role of thrombin in central nervous system activity and stroke. Clujul Med. 2018;91:368–71.

118. Choi YH, Laaker C, Hsu M, Cismaru P, Sandor M, Fabry Z. Molecular Mechanisms of Neuroimmune Crosstalk in the Pathogenesis of Stroke. International Journal of Molecular Sciences. 2021;22:9486.

119. Qiu Y, Zhang C, Chen A, Wang H, Zhou Y, Li Y, et al. Immune Cells in the BBB Disruption After Acute Ischemic Stroke: Targets for Immune Therapy? Frontiers in Immunology [Internet]. 2021 [cited 2023 Jul 21];12. Available from: https://www.frontiersin.org/articles/10.3389/fimmu.2021.678744

120. Youngchaiyud U, Coates AS, Whittingham S, Mackay IR. Cellular-Immune Response to Myelin Protein: Absence in Multiple Sclerosis and Presence in Cerebrovascular Accidents. Australian and New Zealand Journal of Medicine. 1974;4:535–8.

121. Ortega SB, Torres VO, Latchney SE, Whoolery CW, Noorbhai IZ, Poinsatte K, et al. B cells migrate into remote brain areas and support neurogenesis and functional recovery after focal stroke in mice. Proceedings of the National Academy of Sciences. 2020;117:4983–93.

122. Zhang D, Ren J, Luo Y, He Q, Zhao R, Chang J, et al. T Cell Response in Ischemic Stroke: From Mechanisms to Translational Insights. Frontiers in Immunology [Internet]. 2021 [cited 2023 Aug 21];12. Available from: https://www.frontiersin.org/articles/10.3389/fimmu.2021.707972

123. Jenkins MK, Khoruts A, Ingulli E, Mueller DL, McSorley SJ, Reinhardt RL, et al. In vivo activation of antigen-specific CD4 T cells. Annu Rev Immunol. 2001;19:23–45.

124. Liesz A, Karcher S, Veltkamp R. Spectratype analysis of clonal T cell expansion in murine experimental stroke. J Neuroimmunol. 2013;257:46–52.

125. Zhang Z, Lv M, Zhou X, Cui Y. Roles of peripheral immune cells in the recovery of neurological function after ischemic stroke. Frontiers in Cellular Neuroscience [Internet]. 2022 [cited 2023 Aug 21];16. Available from: https://www.frontiersin.org/articles/10.3389/fncel.2022.1013905

126. Jayaraj RL, Azimullah S, Beiram R, Jalal FY, Rosenberg GA. Neuroinflammation: friend and foe for ischemic stroke. Journal of Neuroinflammation. 2019;16:142.

127. Xie L, Yang S-H. Interaction of astrocytes and T cells in physiological and pathological conditions. Brain Research. 2015;1623:63–73.

128. Ao L, Yan Y-Y, Zhou L, Li C, Li W-T, Fang W, et al. Immune Cells After Ischemic Stroke Onset: Roles, Migration, and Target Intervention. J Mol Neurosci. 2018;66:342–55.

129. Jian Z, Liu R, Zhu X, Smerin D, Zhong Y, Gu L, et al. The Involvement and Therapy Target of Immune Cells After Ischemic Stroke. Frontiers in Immunology [Internet]. 2019 [cited 2023 Aug 21];10. Available from: https://www.frontiersin.org/articles/10.3389/fimmu.2019.02167

130. Wang Y, Liu J, Wang X, Liu Z, Li F, Chen F, et al. Frequencies of circulating B- and T-lymphocytes as indicators for stroke outcomes. Neuropsychiatr Dis Treat. 2017;13:2509–18.

131. Famakin BM. The Immune Response to Acute Focal Cerebral Ischemia and Associated Post-stroke Immunodepression: A Focused Review. Aging Dis. 2014;5:307–26.

132. Peh A, O'Donnell JA, Broughton BRS, Marques FZ. Gut Microbiota and Their Metabolites in Stroke: A Double-Edged Sword. Stroke. 2022;53:1788–801.

133. Clemente JC, Ursell LK, Parfrey LW, Knight R. The Impact of the Gut Microbiota on Human Health: An Integrative View. Cell. 2012;148:1258–70.

134. Braniste V, Al-Asmakh M, Kowal C, Anuar F, Abbaspour A, Tóth M, et al. The gut microbiota influences blood-brain barrier permeability in mice. Sci Transl Med [Internet]. 2014 [cited 2023 Feb 16];6. Available from: https://www.science.org/doi/10.1126/scitranslmed.3009759

135. Benakis C, Brea D, Caballero S, Faraco G, Moore J, Murphy M, et al. Commensal microbiota affects ischemic stroke outcome by regulating intestinal γδ T cells. Nat Med. 2016;22:516–23.

136. Delgado M, Gonzalez-Rey E. Role of Cortistatin in the Stressed Immune System. In: Savino W, Guaraldi F, editors. Frontiers of Hormone Research [Internet]. S. Karger AG; 2017 [cited 2023 Feb 16]. p. 110–20. Available from: https://www.karger.com/Article/FullText/452910

137. Gonzalez-Rey E, Chorny A, Delgado M. Regulation of immune tolerance by anti-inflammatory neuropeptides. Nat Rev Immunol. 2007;7:52–63.

138. Gonzalez-Rey E, Chorny A, Robledo G, Delgado M. Cortistatin, a new antiinflammatory peptide with therapeutic effect on lethal endotoxemia. Journal of Experimental Medicine. 2006;203:563–71.

139. Wu R, Dong W, Zhou M, Cui X, Hank Simms H, Wang P. Ghrelin improves tissue perfusion in severe sepsis via downregulation of endothelin-1. Cardiovasc Res. 2005;68:318–26.

140. Gonzalez-Rey E, Chorny A, Varela N, O'Valle F, Delgado M. Therapeutic effect of urocortin on collagen-induced arthritis by down-regulation of inflammatory and Th1 responses and induction of regulatory T cells. Arthritis Rheum. 2007;56:531–43.

141. Morell M, Souza-Moreira L, Caro M, O'Valle F, Forte-Lago I, de Lecea L, et al. Analgesic effect of the neuropeptide cortistatin in murine models of arthritic inflammatory pain. Arthritis Rheum. 2013;65:1390–401.

142. Fernandez-Martin A, Gonzalez-Rey E, Chorny A, Martin J, Pozo D, Ganea D, et al. VIP prevents experimental multiple sclerosis by downregulating both inflammatory and autoimmune components of the disease. Ann N Y Acad Sci. 2006;1070:276–81.

143. Pedreño M, Morell M, Robledo G, Souza-Moreira L, Forte-Lago I, Caro M, et al. Adrenomedullin protects from experimental autoimmune encephalomyelitis at multiple levels. Brain Behav Immun. 2014;37:152–63.

144. Souza-Moreira L, Morell M, Delgado-Maroto V, Pedreño M, Martinez-Escudero L, Caro M, et al. Paradoxical Effect of Cortistatin Treatment and Its Deficiency on Experimental Autoimmune Encephalomyelitis. The Journal of Immunology. 2013;191:2144–54.

145. Delgado-Maroto V, Benitez R, Forte-Lago I, Morell M, Maganto-Garcia E, Souza-Moreira L, et al. Cortistatin reduces atherosclerosis in hyperlipidemic ApoE-deficient mice and the formation of foam cells. Sci Rep. 2017;7:46444.

146. Duran-Prado M, Morell M, Delgado-Maroto V, Castaño JP, Aneiros-Fernandez J, de Lecea L, et al. Cortistatin Inhibits Migration and Proliferation of Human Vascular Smooth Muscle Cells and Decreases Neointimal Formation on Carotid Artery Ligation. Circ Res. 2013;112:1444–55.

147. Delgado-Maroto V, Falo CP, Forte-Lago I, Adan N, Morell M, Maganto-Garcia E, et al. The neuropeptide cortistatin attenuates experimental autoimmune myocarditis via inhibition of cardiomyogenic T cell-driven inflammatory responses. British Journal of Pharmacology. 2017;174:267–80.

148. Gonzalez-Rey E, Fernandez-Martin A, Chorny A, Delgado M. Therapeutic effect of urocortin and adrenomedullin in a murine model of Crohn's disease. Gut. 2006;55:824–32.

149. Gonzalez-Rey E, Varela N, Sheibanie AF, Chorny A, Ganea D, Delgado M. Cortistatin, an antiinflammatory peptide with therapeutic action in inflammatory bowel disease. Proc Natl Acad Sci U S A. 2006;103:4228–33.

150. Campos-Salinas J, Cavazzuti A, O'Valle F, Forte-Lago I, Caro M, Beverley SM, et al. Therapeutic Efficacy of Stable Analogues of Vasoactive Intestinal Peptide against Pathogens. Journal of Biological Chemistry. 2014;289:14583–99.

151. Campos-Salinas J, Caro M, Cavazzuti A, Forte-Lago I, Beverley SM, O'Valle F, et al. Protective role of the neuropeptide urocortin II against experimental sepsis and leishmaniasis by direct killing of pathogens. J Immunol. 2013;191:6040–51.

152. Gonzalez-Rey E, Chorny A, Delgado M. VIP: an agent with license to kill infective parasites. Ann N Y Acad Sci. 2006;1070:303–8.

153. Gonzalez-Rey E, Delgado M. Anti-inflammatory neuropeptide receptors: new therapeutic targets for immune disorders? Trends in Pharmacological Sciences. 2007;28:482–91.

154. Souza-Moreira L, Delgado-Maroto V, Morell M, O'Valle F, Del Moral RG, Gonzalez-Rey E. Therapeutic effect of ghrelin in experimental autoimmune encephalomyelitis by inhibiting antigen-specific Th1/Th17 responses and inducing regulatory T cells. Brain Behav Immun. 2013;30:54–60.

155. Delgado M, Pozo D, Ganea D. The Significance of Vasoactive Intestinal Peptide in Immunomodulation. Pharmacol Rev. 2004;56:249–90.

156. Lee JY, Oh TH, Yune TY. Ghrelin inhibits hydrogen peroxide-induced apoptotic cell death of oligodendrocytes via ERK and p38MAPK signaling. Endocrinology. 2011;152:2377–86.

157. Maki T, Takahashi Y, Miyamoto N, Liang AC, Ihara M, Lo EH, et al. Adrenomedullin promotes differentiation of oligodendrocyte precursor cells into myelin-basic-protein expressing oligodendrocytes under pathological conditions in vitro. Stem Cell Research. 2015;15:68–74.

158. Prasse A, Zissel G, Lützen N, Schupp J, Schmiedlin R, Gonzalez-Rey E, et al. Inhaled vasoactive intestinal peptide exerts immunoregulatory effects in sarcoidosis. Am J Respir Crit Care Med. 2010;182:540–8.

159. Youssef G, Javitt J, Al-Saadi M, Zahiruddin F, Beshay S, Bittar M. Rapid Recovery from Critical COVID-19 Respiratory Failure after treatment with VI [Internet]. 2020 [cited 2023 Oct 9]. Available from: https://europepmc.org/article/PPR/PPR216291

160. Giordano R, Picu A, Bonelli L, Broglio F, Prodam F, Grottoli S, et al. The activation of somatostatinergic receptors by either somatostatin-14 or cortistatin-17 often inhibits ACTH hypersecretion in patients with Cushing's disease. European Journal of Endocrinology. 2007;157:393–8.

161. Grottoli S, Gasco V, Broglio F, Baldelli R, Ragazzoni F, Gallenca F, et al. Cortistatin-17 and Somatostatin-14 Display the Same Effects on Growth Hormone, Prolactin, and Insulin Secretion in Patients with Acromegaly or Prolactinoma. The Journal of Clinical Endocrinology & Metabolism. 2006;91:1595–9.

162. Campos-Salinas J, Barriga M, Delgado M. Therapeutic Effect of a Latent Form of Cortistatin in Experimental Inflammatory and Fibrotic Disorders. Pharmaceutics. 2022;14:2785.

163. Saver JL. Time Is Brain—Quantified. Stroke. 2006;37:263–6.

164. Xiong Y, Wakhloo AK, Fisher M. Advances in Acute Ischemic Stroke Therapy. Circulation Research. 2022;130:1230–51.

165. Fisher M, Savitz SI. Pharmacological brain cytoprotection in acute ischaemic stroke — renewed hope in the reperfusion era. Nat Rev Neurol. 2022;18:193–202.

166. Smith CJ, Denes A, Tyrrell PJ, Di Napoli M. Phase II anti-inflammatory and immune-modulating drugs for acute ischaemic stroke. Expert Opin Investig Drugs. 2015;24:623–43.

167. Veltkamp R, Gill D. Clinical Trials of Immunomodulation in Ischemic Stroke. Neurotherapeutics. 2016;13:791–800.

168. de Lecea L, Criado JR, Prospero-Garcia O, Gautvik KM, Schweitzer P, Danielson PE, et al. A cortical neuropeptide with neuronal depressant and sleep-modulating properties. Nature. 1996;381:242–5.

169. de Lecea L. Cortistatin—Functions in the central nervous system. Molecular and Cellular Endocrinology. 2008;286:88–95.

170. Spier AD, de Lecea L. Cortistatin: a member of the somatostatin neuropeptide family with distinct physiological functions. Brain Research Reviews. 2000;33:228–41.

171. Sunkin SM, Ng L, Lau C, Dolbeare T, Gilbert TL, Thompson CL, et al. Allen Brain Atlas: an integrated spatio-temporal portal for exploring the central nervous system. Nucleic Acids Research. 2013;41:D996–1008.

172. Karlsson M, Zhang C, Méar L, Zhong W, Digre A, Katona B, et al. A single–cell type transcriptomics map of human tissues. Science Advances. 2021;7:eabh2169.

173. Gonzalez-Rey E, Pedreño M, Delgado-Maroto V, Souza-Moreira L, Delgado M. Lulling immunity, pain, and stress to sleep with cortistatin: Cortistatin is a neuroimmune mediator. Ann NY Acad Sci. 2015;1351:89–98.

174. Gonzalez-Rey E, Delgado M. Emergence of cortistatin as a new immunomodulatory factor with therapeutic potential in immune disorders. Molecular and Cellular Endocrinology. 2008;286:135–40.

175. Robas N, Mead E, Fidock M. MrgX2 Is a High Potency Cortistatin Receptor Expressed in Dorsal Root Ganglion*. Journal of Biological Chemistry. 2003;278:44400–4.

176. Ibáñez-Costa A, Luque RM, Castaño JP. Cortistatin: A new link between the growth hormone/prolactin axis, stress, and metabolism. Growth Hormone & IGF Research. 2017;33:23–7.

177. Siehler S, Nunn C, Hannon J, Feuerbach D, Hoyer D. Pharmacological profile of somatostatin and cortistatin receptors. Mol Cell Endocrinol. 2008;286:26–34.

178. Deghenghi R, Papotti M, Ghigo E, Muccioli G. Cortistatin, but not somatostatin, binds to growth hormone secretagogue (GHS) receptors of human pituitary gland. J Endocrinol Invest. 2001;24:RC1-3.

179. Chiu C-T, Wen L-L, Pao H-P, Wang J-Y. Cortistatin Is Induced in Brain Tissue and Exerts Neuroprotection in a Rat Model of Bacterial Meningoencephalitis. The Journal of Infectious Diseases. 2011;204:1563–72.

180. Wen Q, Ding Q, Wang J, Yin Y, Xu S, Ju Y, et al. Cortistatin-14 Exerts Neuroprotective Effect Against Microglial Activation, Blood-brain Barrier Disruption, and Cognitive Impairment in Sepsis-associated Encephalopathy. J Immunol Res. 2022;2022:3334145.

181. Serrano-Martínez I, Pedreño M, Castillo-González J, Ferraz-de-Paula V, Vargas-Rodríguez P, Forte-Lago I, et al. Cortistatin as a novel multimodal therapy for the treatment of Parkinson´s Disease. International Journal of Molecular Science. 2023;

182. Falo CP, Benitez R, Caro M, Morell M, Forte-Lago I, Hernandez-Cortes P, et al. The Neuropeptide Cortistatin Alleviates Neuropathic Pain in Experimental Models of Peripheral Nerve Injury. Pharmaceutics. 2021;13:947.

183. Pérez Falo C. Papel del neuropéptido cortistatina en la fisiopatología de los procesos de des- y remielinización en el sistema nervioso [Internet] [http://purl.org/dc/dcmitype/Text]. Universidad de Granada; 2021 [cited 2023 Nov 27]. p. 1. Available from: https://dialnet.unirioja.es/servlet/tesis?codigo=295627

184. Morell M, Camprubí-Robles M, Culler MD, de Lecea L, Delgado M. Cortistatin attenuates inflammatory pain via spinal and peripheral actions. Neurobiology of Disease. 2014;63:141–54.

185. Markovics A, Szőke É, Sándor K, Börzsei R, Bagoly T, Kemény Á, et al. Comparison of the Anti-inflammatory and Anti-nociceptive Effects of Cortistatin-14 and Somatostatin-14 in Distinct In Vitro and In Vivo Model Systems. J Mol Neurosci. 2012;46:40–50.

186. Méndez-Díaz M, Guevara-Martínez M, Alquicira CR, Guzmán Vásquez K, Prospéro-García O. Cortistatin, a modulatory peptide of sleep and memory, induces analgesia in rats. Neurosci Lett. 2004;354:242–4.

187. Dalm V, van Hagen PM, van Koetsveld PM, Achilefu S, Houtsmuller AB, Pols DHJ, et al. Expression of somatostatin, cortistatin, and somatostatin receptors in human monocytes, macrophages, and dendritic cells. Am J Physiol Endocrinol Metab. 2003;285:E344-353.

188. Qiu C, Li J, Luo D, Chen X, Qu R, Liu T, et al. Cortistatin protects against inflammatory airway diseases through curbing CCL2 and antagonizing NF-κB signaling pathway. Biochem Biophys Res Commun. 2020;531:595–601.

189. Gonzalez-Rey E, Chorny A, Moral RGD, Varela N, Delgado M. Therapeutic effect of cortistatin on experimental arthritis by downregulating inflammatory and Th1 responses. Annals of the Rheumatic Diseases. 2007;66:582–8.

190. Barriga M, Benitez R, Ferraz-de-Paula V, Garcia-Frutos M, Caro M, Robledo G, et al. Protective role of cortistatin in pulmonary inflammation and fibrosis. British Journal of Pharmacology. 2021;178:4368–88.

191. Barriga M, Benitez R, Robledo G, Caro M, O'Valle F, Campos-Salinas J, et al. Neuropeptide Cortistatin Regulates Dermal and Pulmonary Fibrosis in an Experimental Model of Systemic Sclerosis. Neuroendocrinology. 2021;112:784–95.

192. Benitez R, Caro M, Andres-Leon E, O'Valle F, Delgado M. Cortistatin regulates fibrosis and myofibroblast activation in experimental hepatotoxic- and cholestatic-induced liver injury. British Journal of Pharmacology. 2022;179:2275–96.

193. Zhang B, Liu Y, Sui Y-B, Cai H-Q, Liu W-X, Zhu M, et al. Cortistatin Inhibits NLRP3 Inflammasome Activation of Cardiac Fibroblasts During Sepsis. Journal of Cardiac Failure. 2015;21:426–33.

194. Basivireddy J, Somvanshi RK, Romero IA, Weksler BB, Couraud P-O, Oger J, et al. Somatostatin preserved blood brain barrier against cytokine induced alterations: Possible role in multiple sclerosis. Biochemical Pharmacology. 2013;86:497–507.

195. Cardelli P, Fiori A, Corleto VD, Savi MR, Granata F, Ceci F, et al. Inhibitory effect of somatostatin on neutral amino acid transport in isolated brain microvessels: Somatostatin and amino acid transport in brain microvessels. Journal of Neurochemistry. 2001;78:349–57.

196. Li R, Yao G, Zhou L, Zhang M, Yan J. The ghrelin-GHSR-1a pathway inhibits high glucose-induced retinal angiogenesis in vitro by alleviating endoplasmic reticulum stress. Eye and Vision. 2022;9:20.

197. Li M, Wang S, Wang S, Zhang L, Wu D, Yang R, et al. Occludin downregulation in high glucose is regulated by SSTR2 via the VEGF/NRP1/Akt signaling pathway in RF/6A cells. Experimental and Therapeutic Medicine. 2017;14:1732–8.

198. Monte MD, Cammalleri M, Martini D, Casini G, Bagnoli P. Antiangiogenic Role of Somatostatin Receptor 2 in a Model of Hypoxia-Induced Neovascularization in the Retina: Results from Transgenic Mice. Investigative Ophthalmology & Visual Science. 2007;48:3480–9.

199. Zaniolo K, Sapieha P, Shao Z, Stahl A, Zhu T, Tremblay S, et al. Ghrelin Modulates Physiologic and Pathologic Retinal Angiogenesis through GHSR-1a. Investigative Ophthalmology & Visual Science. 2011;52:5376–86.

200. Aslam M, Idrees H, Ferdinandy P, Helyes Z, Hamm C, Schulz R. Somatostatin Primes Endothelial Cells for Agonist-Induced Hyperpermeability and Angiogenesis In Vitro. Int J Mol Sci. 2022;23:3098.

201. Rauca C, Schäfer K, Höllt V. Effects of somatostatin, octreotide and cortistatin on ischaemic neuronal damage following permanent middle cerebral artery occlusion in the rat. Naunyn-Schmiedeberg's Arch Pharmacol. 1999;360:633–8.

202. Córdoba-Chacón J, Gahete MD, Pozo-Salas AI, Martínez-Fuentes AJ, de Lecea L, Gracia-Navarro F, et al. Cortistatin is not a somatostatin analogue but stimulates prolactin release and inhibits GH and ACTH in a gender-dependent fashion: potential role of ghrelin. Endocrinology. 2011;152:4800–12.

203. Gahete MD, Rubio A, Durán-Prado M, Avila J, Luque RM, Castaño JP. Expression of Somatostatin, cortistatin, and their receptors, as well as dopamine receptors, but not of neprilysin, are reduced in the temporal lobe of Alzheimer's disease patients. J Alzheimers Dis. 2010;20:465–75.

204. Winsky-Sommerer R, Spier AD, Fabre V, Lecea L de, Criado JR. Overexpression of the human β-amyloid precursor protein downregulates cortistatin mRNA in PDAPP mice. Brain Research. 2004;1023:157–62.

205. Carrasco E, Hernández C, de Torres I, Farrés J, Simó R. Lowered cortistatin expression is an early event in the human diabetic retina and is associated with apoptosis and glial activation. Mol Vis. 2008;14:1496–502.

206. Stumm RK. Somatostatin Receptor 2 Is Activated in Cortical Neurons and Contributes to Neurodegeneration after Focal Ischemia. Journal of Neuroscience. 2004;24:11404–15.

207. Buscemi L, Price M, Castillo-González J, Chatton J-Y, Hirt L. Lactate Neuroprotection against Transient Ischemic Brain Injury in Mice Appears Independent of HCAR1 Activation. Metabolites. 2022;12:465.

208. Rousselet E, Kriz J, Seidah NG. Mouse Model of Intraluminal MCAO: Cerebral Infarct Evaluation by Cresyl Violet Staining. JoVE (Journal of Visualized Experiments). 2012;e4038.

209. Shvedova M, Islam MR, Armoundas AA, Anfinogenova ND, Wrann CD, Atochin DN. Modified Middle Cerebral Artery Occlusion Model Provides Detailed Intraoperative Cerebral Blood Flow Registration and Improves Neurobehavioral Evaluation. J Neurosci Methods. 2021;358:109179.

210. Lee S, Hong Y, Park S, Lee S-R, Chang K-T, Hong Y. Comparison of surgical methods of transient middle cerebral artery occlusion between rats and mice. J Vet Med Sci. 2014;76:1555–61.

211. Balkaya M, Kröber JM, Rex A, Endres M. Assessing post-stroke behavior in mouse models of focal ischemia. J Cereb Blood Flow Metab. 2013;33:330–8.

212. Hoffman E, Winder SJ. A Modified Wire Hanging Apparatus for Small Animal Muscle Function Testing. PLoS Curr. 2016;8:ecurrents.md.1e2bec4e78697b7b0ff80ea25a1d38be.

213. Zhang Q, Heng Y, Mou Z, Huang J, Yuan Y, Chen N. Reassessment of subacute MPTP-treated mice as animal model of Parkinson's disease. Acta Pharmacol Sin. 2017;38:1317–28.

214. Schindelin J, Arganda-Carreras I, Frise E, Kaynig V, Longair M, Pietzsch T, et al. Fiji: an open-source platform for biological-image analysis. Nat Methods. 2012;9:676–82.

215. Fernández-Arjona M del M, Grondona JM, Granados-Durán P, Fernández-Llebrez P, López-Ávalos MD. Microglia Morphological Categorization in a Rat Model of Neuroinflammation by Hierarchical Cluster and Principal Components Analysis. Front Cell Neurosci. 2017;11:235.

216. Young K, Morrison H. Quantifying Microglia Morphology from Photomicrographs of Immunohistochemistry Prepared Tissue Using ImageJ. JoVE. 2018;57648.

217. Doube M, Kłosowski MM, Arganda-Carreras I, Cordelières FP, Dougherty RP, Jackson JS, et al. BoneJ: Free and extensible bone image analysis in ImageJ. Bone. 2010;47:1076–9.

218. Karperien A. FracLac for ImageJ. 1999; Available from: http://rsb.info.nih.gov/ij/plugins/fraclac/FLHelp/Introduction.htm

219. Welser-Alves JV, Boroujerdi A, Milner R. Isolation and Culture of Primary Mouse Brain Endothelial Cells. In: Milner R, editor. Cerebral Angiogenesis: Methods and Protocols [Internet]. New York, NY: Springer; 2014 [cited 2023 Feb 17]. p. 345–56. Available from: https://doi.org/10.1007/978-1-4939-0320-7_28

220. Takata F, Dohgu S, Yamauchi A, Matsumoto J, Machida T, Fujishita K, et al. In Vitro Blood-Brain Barrier Models Using Brain Capillary Endothelial Cells Isolated from Neonatal and Adult Rats Retain Age-Related Barrier Properties. Liebner S, editor. PLoS ONE. 2013;8:e55166.

221. De Jesus A, Pusec CM, Nguyen T, Keyhani-Nejad F, Gao P, Weinberg SE, et al. Optimized protocol to isolate primary mouse peritoneal macrophage metabolites. STAR Protocols. 2022;3:101668.

222. Ray A, Dittel BN. Isolation of Mouse Peritoneal Cavity Cells. J Vis Exp. 2010;1488.

223. Kim Y, Lee S, Zhang H, Lee S, Kim H, Kim Y, et al. CLEC14A deficiency exacerbates neuronal loss by increasing blood-brain barrier permeability and inflammation. J Neuroinflammation. 2020;17:48.

224. Ruiz JL, Terrón-Camero LC, Castillo-González J, Fernández-Rengel I, Delgado M, Gonzalez-Rey E, et al. reanalyzerGSE: tackling the everlasting lack of reproducibility and reanalyses in transcriptomics [Internet]. bioRxiv; 2023 [cited 2023 Jul 14]. p. 2023.07.12.548663. Available from: https://www.biorxiv.org/content/10.1101/2023.07.12.548663v1

225. Andrés-León E, Rojas AM. miARma-Seq, a comprehensive pipeline for the simultaneous study and integration of miRNA and mRNA expression data. Methods. 2019;152:31–40.

226. Nikolayeva O, Robinson MD. edgeR for Differential RNA-seq and ChIP-seq Analysis: An Application to Stem Cell Biology. In: Kidder BL, editor. Stem Cell Transcriptional Networks:

Methods and Protocols [Internet]. New York, NY: Springer; 2014 [cited 2023 Feb 17]. p. 45–79. Available from: https://doi.org/10.1007/978-1-4939-0512-6_3

227. Brionne A, Juanchich A, Hennequet-Antier C. ViSEAGO: a Bioconductor package for clustering biological functions using Gene Ontology and semantic similarity. BioData Mining. 2019;12:16.

228. Alexa A, Rahnenfuhrer J. topGO: Enrichment Analysis for Gene Ontology [Internet]. Bioconductor version: Release (3.16); 2023 [cited 2023 Mar 2]. Available from: https://bioconductor.org/packages/topGO/

229. Maglott D, Ostell J, Pruitt KD, Tatusova T. Entrez Gene: gene-centered information at NCBI. Nucleic Acids Research. 2011;39:D52–7.

230. Sayers EW, Bolton EE, Brister JR, Canese K, Chan J, Comeau DC, et al. Database resources of the national center for biotechnology information. Nucleic Acids Research. 2022;50:D20–6.

231. R Core Team. R: A language and environment for statistical computing [Internet]. 2022. Available from: https://www.R-project.org/

232. Huber W, Carey VJ, Gentleman R, Anders S, Carlson M, Carvalho BS, et al. Orchestrating high-throughput genomic analysis with Bioconductor. Nat Methods. 2015;12:115–21.

233. Wickham H. ggplot2: Elegant Graphics for Data Analysis [Internet]. Springer-Verlag New York; 2016. Available from: https://ggplot2.tidyverse.org

234. Wickham H. ggplot2. WIREs Computational Statistics. 2011;3:180–5.

235. Schep AN, Kummerfeld SK. iheatmapr: Interactive complex heatmaps in R. Journal of Open Source Software. 2017;2:359.

236. Wen Q, Ding Q, Wang J, Yin Y, Xu S, Ju Y, et al. Cortistatin-14 Exerts Neuroprotective Effect Against Microglial Activation, Blood-brain Barrier Disruption, and Cognitive Impairment in Sepsis-associated Encephalopathy. Journal of Immunology Research. 2022;2022:e3334145.

237. Türeyen K, Vemuganti R, Sailor KA, Dempsey RJ. Infarct volume quantification in mouse focal cerebral ischemia: a comparison of triphenyltetrazolium chloride and cresyl violet staining techniques. Journal of Neuroscience Methods. 2004;139:203–7.

238. Kharlamov A, LaVerde GC, Nemoto EM, Jungreis CA, Yushmanov VE, Jones SC, et al. MAP2 immunostaining in thick sections for early ischemic stroke infarct volume in non-human primate brain. Journal of Neuroscience Methods. 2009;182:205–10.

239. Thal S, Luh C, Schaible E-V, Timaru-Kast R, Hedrich J, Luhmann H, et al. Volatile Anesthetics Influence Blood-Brain Barrier Integrity by Modulation of Tight Junction Protein Expression in Traumatic Brain Injury. PloS one. 2012;7:e50752.

240. Abdullahi W, Tripathi D, Ronaldson PT. Blood-brain barrier dysfunction in ischemic stroke: targeting tight junctions and transporters for vascular protection. Am J Physiol Cell Physiol. 2018;315:C343–56.

241. Jiao H, Wang Z, Liu Y, Wang P, Xue Y. Specific Role of Tight Junction Proteins Claudin-5, Occludin, and ZO-1 of the Blood–Brain Barrier in a Focal Cerebral Ischemic Insult. J Mol Neurosci. 2011;44:130–9.

242. Zhang S, An Q, Wang T, Gao S, Zhou G. Autophagy- and MMP-2/9-mediated Reduction and Redistribution of ZO-1 Contribute to Hyperglycemia-increased Blood–Brain Barrier Permeability During Early Reperfusion in Stroke. Neuroscience. 2018;377:126–37.

243. Zhu H, Zhang Y, Zhong Y, Ye Y, Hu X, Gu L, et al. Inflammation-Mediated Angiogenesis in Ischemic Stroke. Front Cell Neurosci. 2021;15:652647.

244. Rust R. Insights into the dual role of angiogenesis following stroke. J Cereb Blood Flow Metab. 2020;40:1167–71.

245. Serrano-Martínez I, Castillo-González J, Vargas-Rodríguez P, Forte-Lago I, Gonzalez-Rey E. Cortistatin as an endogenous regulator of neuroinflammation and neurodegeneration in aging. (Granada, Spain); 2023.

246. Yan S, Li M, Chai H, Yang H, Lin PH, Yao Q, et al. TNF-α decreases expression of somatostatin, somatostatin receptors, and cortistatin in human coronary endothelial cells. Journal of Surgical Research. 2005;123:294–301.

247. Sladojevic N, Stamatovic SM, Johnson AM, Choi J, Hu A, Dithmer S, et al. Claudin-1-Dependent Destabilization of the Blood–Brain Barrier in Chronic Stroke. J Neurosci. 2019;39:743–57.

248. O'Carroll SJ, Kho DT, Wiltshire R, Nelson V, Rotimi O, Johnson R, et al. Pro-inflammatory TNFα and IL-1β differentially regulate the inflammatory phenotype of brain microvascular endothelial cells. J Neuroinflammation. 2015;12:131.

249. Yang T, Roder KE, Abbruscato TJ. Evaluation of bEnd5 cell line as an in vitro model for the blood–brain barrier under normal and hypoxic/aglycemic conditions. Journal of Pharmaceutical Sciences. 2007;96:3196–213.

250. Coisne C, Dehouck L, Faveeuw C, Delplace Y, Miller F, Landry C, et al. Mouse syngenic in vitro blood-brain barrier model: a new tool to examine inflammatory events in cerebral endothelium. Lab Invest. 2005;85:734–46.

251. Gerhartl A, Pracser N, Vladetic A, Hendrikx S, Friedl H-P, Neuhaus W. The pivotal role of micro-environmental cells in a human blood–brain barrier in vitro model of cerebral ischemia: functional and transcriptomic analysis. Fluids and Barriers of the CNS. 2020;17:19.

252. Kuntz M, Mysiorek C, Pétrault O, Boucau M-C, Aijjou R, Uzbekov R, et al. Transient oxygen–glucose deprivation sensitizes brain capillary endothelial cells to rtPA at 4h of reoxygenation. Microvascular Research. 2014;91:44–57.

253. Gray KM, Jung JW, Inglut CT, Huang H-C, Stroka KM. Quantitatively relating brain endothelial cell–cell junction phenotype to global and local barrier properties under varied culture conditions via the Junction Analyzer Program. Fluids Barriers CNS. 2020;17:16.

254. Lai C-H, Kuo K-H, Leo JM. Critical role of actin in modulating BBB permeability. Brain Research Reviews. 2005;50:7–13.

255. Babinska A, Kedees MH, Athar H, Ahmed T, Batuman O, Ehrlich YH, et al. F11-receptor (F11R/JAM) mediates platelet adhesion to endothelial cells: role in inflammatory thrombosis. Thromb Haemost. 2002;88:843–50.

256. Beard RS, Haines RJ, Wu KY, Reynolds JJ, Davis SM, Elliott JE, et al. Non-muscle Mlck is required for β-catenin- and FoxO1-dependent downregulation of Cldn5 in IL-1β-mediated barrier dysfunction in brain endothelial cells. J Cell Sci. 2014;127:1840–53.

257. Sperandio S, Fortin J, Sasik R, Robitaille L, Corbeil J, de Belle I. The transcription factor Egr1 regulates the HIF-1α gene during hypoxia. Molecular Carcinogenesis. 2009;48:38–44.

258. Kerr DJ, Marsillo A, Guariglia SR, Budylin T, Sadek R, Menkes S, et al. Aberrant hippocampal Atp8a1 levels are associated with altered synaptic strength, electrical activity, and autistic-like behavior. Biochimica et Biophysica Acta (BBA) - Molecular Basis of Disease. 2016;1862:1755–65.

259. Zhao Z, Nelson AR, Betsholtz C, Zlokovic BV. Establishment and Dysfunction of the Blood-Brain Barrier. Cell. 2015;163:1064–78.

260. Chadwick W, Magnus T, Martin B, Keselman A, Mattson MP, Maudsley S. Targeting TNF-α receptors for neurotherapeutics. Trends Neurosci. 2008;31:504–11.

261. Jin S, Sonobe Y, Kawanokuchi J, Horiuchi H, Cheng Y, Wang Y, et al. Interleukin-34 Restores Blood–Brain Barrier Integrity by Upregulating Tight Junction Proteins in Endothelial Cells. PLOS ONE. 2014;9:e115981.

262. Mizuno T, Doi Y, Mizoguchi H, Jin S, Noda M, Sonobe Y, et al. Interleukin-34 Selectively Enhances the Neuroprotective Effects of Microglia to Attenuate Oligomeric Amyloid-β Neurotoxicity. The American Journal of Pathology. 2011;179:2016–27.

263. Jangula A, Murphy EJ. Lipopolysaccharide-induced blood brain barrier permeability is enhanced by alpha-synuclein expression. Neuroscience Letters. 2013;551:23–7.

264. Drieu A, Levard D, Vivien D, Rubio M. Anti-inflammatory treatments for stroke: from bench to bedside. Ther Adv Neurol Disord. 2018;11:1756286418789854.

265. Wang J, Zhang P, Tang Z. Animal models of transient ischemic attack: a review. Acta Neurol Belg. 2020;120:267–75.

266. Liu F, McCullough LD. Middle Cerebral Artery Occlusion Model in Rodents: Methods and Potential Pitfalls. BioMed Research International. 2011;2011:e464701.

267. Trotman-Lucas M, Wong R, Allan SM, Gibson CL. Improved reperfusion following alternative surgical approach for experimental stroke in mice [Internet]. F1000Research; 2020 [cited 2023 Nov 23]. Available from: https://f1000research.com/articles/9-188

268. Li Y, Tan L, Yang C, He L, Liu L, Deng B, et al. Distinctions between the Koizumi and Zea Longa methods for middle cerebral artery occlusion (MCAO) model: a systematic review and meta-analysis of rodent data. Sci Rep. 2023;13:10247.

269. Pinto R, Magalhães A, Sousa M, Melo L, Lobo A, Barros P, et al. Bridging the Transient Intraluminal Stroke Preclinical Model to Clinical Practice: From Improved Surgical Procedures to a Workflow of Functional Tests. Frontiers in Neurology [Internet]. 2022 [cited 2023 Nov 20];13. Available from: https://www.frontiersin.org/articles/10.3389/fneur.2022.846735

270. Fan C, Zhang L, He Z, Shao P, Ding L, Wang G, et al. Reduced Severity of Outcome of Recurrent Ipsilateral Transient Cerebral Ischemia Compared with Contralateral Transient Cerebral Ischemia in Rats. Journal of Stroke and Cerebrovascular Diseases. 2017;26:2915–25.

271. Yousufuddin M, Young N. Aging and ischemic stroke. Aging (Albany NY). 2019;11:2542–4.

272. Ritzel RM, Lai Y-J, Crapser JD, Patel AR, Schrecengost A, Grenier JM, et al. Aging alters the immunological response to ischemic stroke. Acta Neuropathol. 2018;136:89–110.

273. Sieber MW, Claus RA, Witte OW, Frahm C. Attenuated Inflammatory Response in Aged Mice Brains following Stroke. PLoS One. 2011;6:e26288.

274. Ermine CM, Bivard A, Parsons MW, Baron J-C. The ischemic penumbra: From concept to reality. International Journal of Stroke. 2021;16:497–509.

275. Behrndtz AB, Damsbo AG, Blauenfeldt RA, Andersen G, Speiser LO, Simonsen CZ. Too risky, too large, too late, or too mild—Reasons for not treating ischemic stroke patients and the related outcomes. Frontiers in Neurology [Internet]. 2022 [cited 2023 Nov 22];13. Available from: https://www.frontiersin.org/articles/10.3389/fneur.2022.1098779

276. Bambauer KZ, Johnston SC, Bambauer DE, Zivin JA. Reasons Why Few Patients With Acute Stroke Receive Tissue Plasminogen Activator. Archives of Neurology. 2006;63:661–4.

277. Wang D, Wang Y. Tissue window, not the time window, will guide acute stroke treatment. Stroke Vasc Neurol [Internet]. 2019 [cited 2023 Nov 23];4. Available from: https://svn.bmj.com/content/4/1/1

278. Szalay G, Martinecz B, Lénárt N, Környei Z, Orsolits B, Judák L, et al. Microglia protect against brain injury and their selective elimination dysregulates neuronal network activity after stroke. Nat Commun. 2016;7:11499.

279. Liu P, Li H, Dong M, Gu X, Xu S, Xia S, et al. Infiltrating myeloid cell-derived properdin markedly promotes microglia-mediated neuroinflammation after ischemic stroke. Journal of Neuroinflammation. 2023;20:260.

280. Benakis C, Simats A, Tritschler S, Heindl S, Besson-Girard S, Llovera G, et al. T cells modulate the microglial response to brain ischemia. Rothlin CV, Foster J, editors. eLife. 2022;11:e82031.

281. Bieber M, Gronewold J, Scharf A-C, Schuhmann MK, Langhauser F, Hopp S, et al. Validity and Reliability of Neurological Scores in Mice Exposed to Middle Cerebral Artery Occlusion. Stroke. 2019;50:2875–82.

282. Ruan J, Yao Y. Behavioral tests in rodent models of stroke. Brain Hemorrhages. 2020;1:171–84.

283. Fluri F, Schuhmann MK, Kleinschnitz C. Animal models of ischemic stroke and their application in clinical research. Drug Des Devel Ther. 2015;9:3445–54.

284. Walther J, Kirsch E, Hellwig L, Schmerbeck S, Holloway P, Buchan A, et al. Reinventing the Penumbra — the Emerging Clockwork of a Multi-modal Mechanistic Paradigm. Translational Stroke Research. 2022;14:1–24.

285. Ardelt AA, Anjum N, Rajneesh KF, Kulesza P, Koehler RC. Estradiol augments peri-infarct cerebral vascular density in experimental stroke. Experimental Neurology. 2007;206:95–100.

286. Popa-Wagner A, Carmichael ST, Kokaia Z, Kessler C, Walker L. The Response of the Aged Brain to Stroke: Too Much, Too Soon? Current neurovascular research. 2007;4:216–27.

287. Gullotta GS, De Feo D, Friebel E, Semerano A, Scotti GM, Bergamaschi A, et al. Age-induced alterations of granulopoiesis generate atypical neutrophils that aggravate stroke pathology. Nat Immunol. 2023;24:925–40.

288. Rubio A, Sánchez-Mut JV, García E, Velasquez ZD, Oliver J, Esteller M, et al. Epigenetic control of somatostatin and cortistatin expression by β amyloid peptide. Journal of Neuroscience Research. 2012;90:13–20.

289. Fan P, Wang S, Chu S, Chen N. Time-dependent dual effect of microglia in ischemic stroke. Neurochemistry International. 2023;169:105584.

290. Jia J, Yang L, Chen Y, Zheng L, Chen Y, Xu Y, et al. The Role of Microglial Phagocytosis in Ischemic Stroke. Frontiers in Immunology [Internet]. 2022 [cited 2023 Nov 15];12. Available from: https://www.frontiersin.org/articles/10.3389/fimmu.2021.790201

291. Zhang S. Microglial activation after ischaemic stroke. Stroke Vasc Neurol. 2019;4:71–4.

292. Kawabori M, Kacimi R, Kauppinen T, Calosing C, Kim JY, Hsieh CL, et al. Triggering Receptor Expressed on Myeloid Cells 2 (TREM2) Deficiency Attenuates Phagocytic Activities of Microglia and Exacerbates Ischemic Damage in Experimental Stroke. J Neurosci. 2015;35:3384–96.

293. Neher JJ, Emmrich JV, Fricker M, Mander PK, Théry C, Brown GC. Phagocytosis executes delayed neuronal death after focal brain ischemia. Proceedings of the National Academy of Sciences. 2013;110:E4098–107.

294. Jolivel V, Bicker F, Binamé F, Ploen R, Keller S, Gollan R, et al. Perivascular microglia promote blood vessel disintegration in the ischemic penumbra. Acta Neuropathol. 2015;129:279–95.

295. Xu X, Gao W, Li L, Hao J, Yang B, Wang T, et al. Annexin A1 protects against cerebral ischemia–reperfusion injury by modulating microglia/macrophage polarization via FPR2/ALX-dependent AMPK-mTOR pathway. Journal of Neuroinflammation. 2021;18:119.

296. Paolicelli RC, Sierra A, Stevens B, Tremblay M-E, Aguzzi A, Ajami B, et al. Microglia states and nomenclature: A field at its crossroads. Neuron. 2022;110:3458–83.

297. Li X, Lyu J, Li R, Jain V, Shen Y, del Águila Á, et al. Single-cell transcriptomic analysis of the immune cell landscape in the aged mouse brain after ischemic stroke. Journal of Neuroinflammation. 2022;19:83.

298. Fujikawa R, Jinno S. Identification of hyper-ramified microglia in the CA1 region of the mouse hippocampus potentially associated with stress resilience. European Journal of Neuroscience. 2022;56:5137–53.

299. Hinwood M, Morandini J, Day TA, Walker FR. Evidence that Microglia Mediate the Neurobiological Effects of Chronic Psychological Stress on the Medial Prefrontal Cortex. Cerebral Cortex. 2012;22:1442–54.

300. Li F, Zhao H, Han Z, Wang R, Tao Z, Fan Z, et al. Xuesaitong May Protect Against Ischemic Stroke by Modulating Microglial Phenotypes and Inhibiting Neuronal Cell Apoptosis via the STAT3 Signaling Pathway. CNS Neurol Disord Drug Targets. 2019;18:115–23.

301. Wang D, Liu F, Zhu L, Lin P, Han F, Wang X, et al. FGF21 alleviates neuroinflammation following ischemic stroke by modulating the temporal and spatial dynamics of microglia/macrophages. Journal of Neuroinflammation. 2020;17:257.

302. Li L, Zhou J, Han L, Wu X, Shi Y, Cui W, et al. The Specific Role of Reactive Astrocytes in Stroke. Frontiers in Cellular Neuroscience [Internet]. 2022 [cited 2023 Nov 23];16. Available from: https://www.ncbi.nlm.nih.gov/pmc/articles/PMC8934938/

303. Aswendt M, Wilhelmsson U, Wieters F, Stokowska A, Schmitt FJ, Pallast N, et al. Reactive astrocytes prevent maladaptive plasticity after ischemic stroke. Progress in Neurobiology. 2022;209:102199.

304. Xu L, Nirwane A, Xu T, Kang M, Devasani K, Yao Y. Fibroblasts repair blood-brain barrier damage and hemorrhagic brain injury via TIMP2. Cell Reports. 2022;41:111709.

305. Xu L, Yao Y. Central Nervous System Fibroblast-Like Cells in Stroke and Other Neurological Disorders. Stroke. 2021;52:2456–64.

306. Arvidsson A, Collin T, Kirik D, Kokaia Z, Lindvall O. Neuronal replacement from endogenous precursors in the adult brain after stroke. Nat Med. 2002;8:963–70.

307. Young CC, van der Harg JM, Lewis NJ, Brooks KJ, Buchan AM, Szele FG. Ependymal Ciliary Dysfunction and Reactive Astrocytosis in a Reorganized Subventricular Zone after Stroke. Cerebral Cortex. 2013;23:647–59.

308. Zhang RL, Chopp M, Gregg SR, Toh Y, Roberts C, LeTourneau Y, et al. Patterns and Dynamics of Subventricular Zone Neuroblast Migration in the Ischemic Striatum of the Adult Mouse. J Cereb Blood Flow Metab. 2009;29:1240–50.

309. Choudhury GR, Ding S. Reactive astrocytes and therapeutic potential in focal ischemic stroke. Neurobiology of Disease. 2016;85:234–44.

310. Weir K, Kim DW, Blackshaw S. A potential role for somatostatin signaling in regulating retinal neurogenesis. Sci Rep. 2021;11:10962.

311. Zaben MJ, Gray WP. Neuropeptides and hippocampal neurogenesis. Neuropeptides. 2013;47:431–8.

312. Cai W, Zhang K, Li P, Zhu L, Xu J, Yang B, et al. Dysfunction of the neurovascular unit in ischemic stroke and neurodegenerative diseases: An aging effect. Ageing Research Reviews. 2017;34:77–87.

313. Cong X, Kong W. Endothelial tight junctions and their regulatory signaling pathways in vascular homeostasis and disease. Cellular Signalling. 2020;66:109485.

314. Tietz S, Engelhardt B. Brain barriers: Crosstalk between complex tight junctions and adherens junctions. Journal of Cell Biology. 2015;209:493–506.

315. Fischer S, Wobben M, Marti HH, Renz D, Schaper W. Hypoxia-induced hyperpermeability in brain microvessel endothelial cells involves VEGF-mediated changes in the expression of zonula occludens-1. Microvasc Res. 2002;63:70–80.

316. Spindler KR, Hsu T-H. Viral disruption of the blood–brain barrier. Trends in Microbiology. 2012;20:282–90.

317. Zeng X, He G, Yang X, Xu G, Tang Y, Li H, et al. Zebularine protects against blood-brain-barrier (BBB) disruption through increasing the expression of zona occludens-1 (ZO-1) and vascular endothelial (VE)-cadherin. Bioengineered. 2022;13:4441–54.

318. Nitta T, Hata M, Gotoh S, Seo Y, Sasaki H, Hashimoto N, et al. Size-selective loosening of the blood-brain barrier in claudin-5–deficient mice. Journal of Cell Biology. 2003;161:653–60.

319. Sajja RK, Prasad S, Cucullo L. Impact of altered glycaemia on blood-brain barrier endothelium: an in vitro study using the hCMEC/D3 cell line. Fluids Barriers CNS. 2014;11:8.

320. Schlingmann B, Overgaard CE, Molina SA, Lynn KS, Mitchell LA, Dorsainvil White S, et al. Regulation of claudin/zonula occludens-1 complexes by hetero-claudin interactions. Nat Commun. 2016;7:12276.

321. Yan T, Tan Y, Deng G, Sun Z, Liu B, Wang Y, et al. TGF-β induces GBM mesenchymal transition through upregulation of CLDN4 and nuclear translocation to activate TNF-α/NF-κB signal pathway. Cell Death Dis. 2022;13:1–11.

322. Zavala-Zendejas VE, Torres-Martinez AC, Salas-Morales B, Fortoul TI, Montaño LF, Rendon-Huerta EP. Claudin-6, 7, or 9 Overexpression in the Human Gastric Adenocarcinoma Cell Line AGS Increases Its Invasiveness, Migration, and Proliferation Rate. Cancer Investigation. 2011;29:1–11.

323. Liebner S, Fischmann A, Rascher G, Duffner F, Grote E-H, Kalbacher H, et al. Claudin-1 and claudin-5 expression and tight junction morphology are altered in blood vessels of human glioblastoma multiforme. Acta Neuropathol. 2000;100:323–31.

324. Pfeiffer F, Schäfer J, Lyck R, Makrides V, Brunner S, Schaeren-Wiemers N, et al. Claudin-1 induced sealing of blood–brain barrier tight junctions ameliorates chronic experimental autoimmune encephalomyelitis. Acta Neuropathol. 2011;122:601–14.

325. Alshbool FatimaZ, Mohan S. Emerging Multifunctional Roles of Claudin Tight Junction Proteins in Bone. Endocrinology. 2014;155:2363–76.

326. Rao RK, Basuroy S, Rao VU, Karnaky KJ Jr, Gupta A. Tyrosine phosphorylation and dissociation of occludin–ZO-1 and E-cadherin–β-catenin complexes from the cytoskeleton by oxidative stress. Biochemical Journal. 2002;368:471–81.

327. Kassianidou E, Kumar S. A biomechanical perspective on stress fiber structure and function. Biochim Biophys Acta. 2015;1853:3065–74.

328. Gould DB, Phalan FC, van Mil SE, Sundberg JP, Vahedi K, Massin P, et al. Role of COL4A1 in small-vessel disease and hemorrhagic stroke. N Engl J Med. 2006;354:1489–96.

329. Bauer AT, Bürgers HF, Rabie T, Marti HH. Matrix Metalloproteinase-9 Mediates Hypoxia-Induced Vascular Leakage in the Brain via Tight Junction Rearrangement. J Cereb Blood Flow Metab. 2010;30:837–48.

330. Qosa H, Miller DS, Pasinelli P, Trotti D. Regulation of ABC Efflux Transporters at Blood-Brain Barrier in Health and Neurological Disorders. Brain Res. 2015;1628:298–316.

331. Jiang Y, Liu H, Liu W, Tong H, Chen C, Lin F, et al. Endothelial Aquaporin-1 (AQP1) Expression Is Regulated by Transcription Factor Mef2c. Mol Cells. 2016;39:292–8.

332. Ludewig P, Winneberger J, Magnus T. The cerebral endothelial cell as a key regulator of inflammatory processes in sterile inflammation. Journal of Neuroimmunology. 2019;326:38–44.

333. Sonar SA, Lal G. Blood-brain barrier and its function during inflammation and autoimmunity. J Leukoc Biol. 2018;103:839–53.

334. de Vries HE, Blom-Roosemalen MCM, Oosten M van, de Boer AG, van Berkel TJC, Breimer DD, et al. The influence of cytokines on the integrity of the blood-brain barrier in vitro. Journal of Neuroimmunology. 1996;64:37–43.

335. Garg N, Syngle A, Krishan P. Nitric Oxide: Link between Inflammation and Endothelial Dysfunction in Rheumatoid Arthritis. Int J Angiol. 2017;26:165–9.

336. Zhu J, Song W, Li L, Fan X. Endothelial nitric oxide synthase: a potential therapeutic target for cerebrovascular diseases. Molecular Brain. 2016;9:30.

337. van der Loo B, Labugger R, Skepper JN, Bachschmid M, Kilo J, Powell JM, et al. Enhanced Peroxynitrite Formation Is Associated with Vascular Aging. Journal of Experimental Medicine. 2000;192:1731–44.

338. Zhao Y, Qiu C, Wang W, Peng J, Cheng X, Shangguan Y, et al. Cortistatin protects against intervertebral disc degeneration through targeting mitochondrial ROS-dependent NLRP3 inflammasome activation. Theranostics. 2020;10:7015–33.

339. Zille M, Farr TD, Przesdzing I, Müller J, Sommer C, Dirnagl U, et al. Visualizing cell death in experimental focal cerebral ischemia: promises, problems, and perspectives. J Cereb Blood Flow Metab. 2012;32:213–31.

340. Chen D, Li L, Wang Y, Xu R, Peng S, Zhou L, et al. Ischemia-reperfusion injury of brain induces endothelial-mesenchymal transition and vascular fibrosis via activating let-7i/TGF-βR1 double-negative feedback loop. FASEB J. 2020;34:7178–91.

341. Ghersi-Egea J-F, Strazielle N, Catala M, Silva-Vargas V, Doetsch F, Engelhardt B. Molecular anatomy and functions of the choroidal blood-cerebrospinal fluid barrier in health and disease. Acta Neuropathol. 2018;135:337–61.

342. Thomsen MS, Humle N, Hede E, Moos T, Burkhart A, Thomsen LB. The blood-brain barrier studied in vitro across species. PLOS ONE. 2021;16:e0236770.

343. Cecchelli R, Aday S, Sevin E, Almeida C, Culot M, Dehouck L, et al. A Stable and Reproducible Human Blood-Brain Barrier Model Derived from Hematopoietic Stem Cells. PLOS ONE. 2014;9:e99733.

344. Hinkel S, Mattern K, Dietzel A, Reichl S, Müller-Goymann CC. Parametric investigation of static and dynamic cell culture conditions and their impact on hCMEC/D3 barrier properties. Int J Pharm. 2019;566:434–44.

345. Nitz T, Eisenblätter T, Psathaki K, Galla H-J. Serum-derived factors weaken the barrier properties of cultured porcine brain capillary endothelial cells in vitro. Brain Research. 2003;981:30–40.

346. Qi D, Lin H, Hu B, Wei Y. A review on in vitro model of the blood-brain barrier (BBB) based on hCMEC/D3 cells. Journal of Controlled Release. 2023;358:78–97.

347. Ma Y, Yang S, He Q, Zhang D, Chang J. The Role of Immune Cells in Post-Stroke Angiogenesis and Neuronal Remodeling: The Known and the Unknown. Frontiers in Immunology [Internet]. 2021 [cited 2023 Nov 15];12. Available from: https://www.frontiersin.org/articles/10.3389/fimmu.2021.784098

348. Yang Y, Torbey MT. Angiogenesis and Blood-Brain Barrier Permeability in Vascular Remodeling after Stroke. Curr Neuropharmacol. 2020;18:1250–65.

349. Kofler NM, Shawber CJ, Kangsamaksin T, Reed HO, Galatioto J, Kitajewski J. Notch Signaling in Developmental and Tumor Angiogenesis. Genes Cancer. 2011;2:1106–16.

350. Lowe KL, Finney BA, Deppermann C, Hägerling R, Gazit SL, Frampton J, et al. Podoplanin and CLEC-2 drive cerebrovascular patterning and integrity during development. Blood. 2015;125:3769–77.

351. Wang Y, Peng D, Huang Y, Cao Y, Li H, Zhang X. Podoplanin: Its roles and functions in neurological diseases and brain cancers. Frontiers in Pharmacology [Internet]. 2022 [cited 2023 Nov 17];13. Available from: https://www.frontiersin.org/articles/10.3389/fphar.2022.964973

352. Xia L, Ju T, Westmuckett A, An G, Ivanciu L, McDaniel JM, et al. Defective angiogenesis and fatal embryonic hemorrhage in mice lacking core 1–derived O-glycans. J Cell Biol. 2004;164:451–9.

353. Huang J, Choudhri TF, Winfree CJ, McTaggart RA, Kiss S, Mocco J, et al. Postischemic cerebrovascular E-selectin expression mediates tissue injury in murine stroke. Stroke. 2000;31:3047–53.

354. Mocco J, Choudhri T, Huang J, Harfeldt E, Efros L, Klingbeil C, et al. HuEP5C7 as a humanized monoclonal anti-E/P-selectin neurovascular protective strategy in a blinded placebo-controlled trial of nonhuman primate stroke. Circ Res. 2002;91:907–14.

355. Kanemoto Y, Nakase H, Akita N, Sakaki T. Effects of anti-intercellular adhesion molecule-1 antibody on reperfusion injury induced by late reperfusion in the rat middle cerebral artery occlusion model. Neurosurgery. 2002;51:1034–41; discussion 1041-1042.

356. Investigators EAST. Use of anti-ICAM-1 therapy in ischemic stroke: Results of the Enlimomab Acute Stroke Trial. Neurology. 2001;57:1428–34.

357. Becker KJ. Anti-leukocyte Antibodies: LeukArrest (Hu23F2G) and Enlimomab (R6.5) in Acute Stroke. Current Medical Research and Opinion. 2002;18:s18–22.

358. Malone K, Amu S, Moore AC, Waeber C. Immunomodulatory Therapeutic Strategies in Stroke. Front Pharmacol. 2019;10:630.

359. Fang T, Yin X, Wang Y, Wang H, Wang X, Xue Y. Lymph Node Metastasis-Related Gene ITGA4 Promotes the Proliferation, Migration, and Invasion of Gastric Cancer Cells by Regulating Tumor Immune Microenvironment. J Oncol. 2022;2022:1315677.

360. Li Y, Li F, Bai X, Li Y, Ni C, Zhao X, et al. ITGA3 Is Associated With Immune Cell Infiltration and Serves as a Favorable Prognostic Biomarker for Breast Cancer. Frontiers in Oncology. 2021;11.

361. Doll DN, Barr TL, Simpkins JW. Cytokines: Their Role in Stroke and Potential Use as Biomarkers and Therapeutic Targets. Aging Dis. 2014;5:294–306.

362. Pawluk H, Woźniak A, Grześk G, Kołodziejska R, Kozakiewicz M, Kopkowska E, et al. The Role of Selected Pro-Inflammatory Cytokines in Pathogenesis of Ischemic Stroke. Clinical Interventions in Aging. 2020;15:469–84.

363. Bustamante A, Sobrino T, Giralt D, García-Berrocoso T, Llombart V, Ugarriza I, et al. Prognostic value of blood interleukin-6 in the prediction of functional outcome after stroke: A systematic review and meta-analysis. Journal of Neuroimmunology. 2014;274:215–24.

364. Shaafi S, Sharifipour E, Rahmanifar R, Hejazi S, Andalib S, Nikanfar M, et al. Interleukin-6, a reliable prognostic factor for ischemic stroke. Iran J Neurol. 2014;13:70–6.

365. Shenhar-Tsarfaty S, Assayag EB, Bova I, Shopin L, Fried M, Berliner S, et al. Interleukin-6 as an Early Predictor for One-Year Survival following an Ischaemic Stroke/Transient Ischaemic Attack. International Journal of Stroke. 2010;5:16–20.

366. Zhu H, Hu S, Li Y, Sun Y, Xiong X, Hu X, et al. Interleukins and Ischemic Stroke. Front Immunol. 2022;13:828447.

367. Han D, Liu H, Gao Y. The role of peripheral monocytes and macrophages in ischemic stroke. Neurol Sci. 2020;41:3589–607.

368. Hughes PM, Allegrini PR, Rudin M, Perry VH, Mir AK, Wiessner C. Monocyte Chemoattractant Protein-1 Deficiency is Protective in a Murine Stroke Model. J Cereb Blood Flow Metab. 2002;22:308–17.

369. Fang W, Zhai X, Han D, Xiong X, Wang T, Zeng X, et al. CCR2-dependent monocytes/macrophages exacerbate acute brain injury but promote functional recovery after ischemic stroke in mice. Theranostics. 2018;8:3530–43.

370. Qin C, Yang S, Chu Y-H, Zhang H, Pang X-W, Chen L, et al. Signaling pathways involved in ischemic stroke: molecular mechanisms and therapeutic interventions. Sig Transduct Target Ther. 2022;7:1–29.

371. Georgakis MK, Malik R, Björkbacka H, Pana TA, Demissie S, Ayers C, et al. Circulating Monocyte Chemoattractant Protein-1 and Risk of Stroke. Circulation Research. 2019;125:773–82.

372. Gertz K, Kronenberg G, Kälin RE, Baldinger T, Werner C, Balkaya M, et al. Essential role of interleukin-6 in post-stroke angiogenesis. Brain. 2012;135:1964–80.

373. Grønhøj MH, Clausen BH, Fenger CD, Lambertsen KL, Finsen B. Beneficial potential of intravenously administered IL-6 in improving outcome after murine experimental stroke. Brain, Behavior, and Immunity. 2017;65:296–311.

374. Cao Y, Yue X, Jia M, Wang J. Neuroinflammation and anti-inflammatory therapy for ischemic stroke. Heliyon. 2023;9:e17986.

375. Souza-Moreira L, Campos-Salinas J, Caro M, Gonzalez-Rey E. Neuropeptides as Pleiotropic Modulators of the Immune Response. Neuroendocrinology. 2011;94:89–100.

376. Kim S, Park ES, Chen PR, Kim E. Dysregulated Hypothalamic–Pituitary–Adrenal Axis Is Associated With Increased Inflammation and Worse Outcomes After Ischemic Stroke in Diabetic Mice. Frontiers in Immunology [Internet]. 2022 [cited 2023 Nov 22];13. Available from: https://www.frontiersin.org/articles/10.3389/fimmu.2022.864858

377. Barugh AJ, Gray P, Shenkin SD, MacLullich AMJ, Mead GE. Cortisol levels and the severity and outcomes of acute stroke: a systematic review. J Neurol. 2014;261:533–45.

378. Zucchi FC, Matthies N-F, Badr N, Metz GA. Stress-induced glucocorticoid receptor activation determines functional recovery following ischemic stroke. Experimental & Translational Stroke Medicine. 2010;2:18.

379. Cristante E, McArthur S, Mauro C, Maggioli E, Romero IA, Wylezinska-Arridge M, et al. Identification of an essential endogenous regulator of blood–brain barrier integrity, and its pathological and therapeutic implications. Proc Natl Acad Sci U S A. 2013;110:832–41.

380. Cheyuo C, Wu R, Zhou M, Jacob A, Coppa G, Wang P. Ghrelin Suppresses Inflammation and Neuronal Nitric Oxide Synthase in Focal Cerebral Ischemia Via the Vagus Nerve. Shock. 2011;35:258.

381. Miao Y, Xia Q, Hou Z, Zheng Y, Pan H, Zhu S. Ghrelin protects cortical neuron against focal ischemia/reperfusion in rats. Biochemical and Biophysical Research Communications. 2007;359:795–800.

382. Ku JM, Andrews ZB, Barsby T, Reichenbach A, Lemus MB, Drummond GR, et al. Ghrelin-Related Peptides Exert Protective Effects in the Cerebral Circulation of Male Mice Through a Nonclassical Ghrelin Receptor(s). Endocrinology. 2015;156:280–90.

383. Seyhanli ES, Lok U, Gulacti U, Buyukaslan H, Atescelik M, Yildiz M, et al. Assessment of serum and urine ghrelin levels in patients with acute stroke. Int J Clin Exp Med. 2015;8:722–9.

384. Xu X, Zhu Y, Chuai J. Changes in Serum Ghrelin and Small Intestinal Motility in Rats with Ischemic Stroke. The Anatomical Record. 2012;295:307–12.

385. Jordan VK, Zaveri HP, Scott DA. 1p36 deletion syndrome: an update. TACG. 2015;8:189–200.

386. Yuan D, Shen J, Yan Y, Wu X, Li A, Guo A, et al. Upregulated Expression of SSTR1 is Involved in Neuronal Apoptosis and is Coupled to the Reduction of bcl-2 Following Intracerebral Hemorrhage in Adult Rats. Cell Mol Neurobiol. 2014;34:951–61.

387. Yao Q, Liu Q, Xu H, Wu Z, Zhou L, Gu Z, et al. Upregulated Expression of SSTR3 is Involved in Neuronal Apoptosis After Intracerebral Hemorrhage in Adult Rats. Cellular and Molecular Neurobiology. 2017;37.

388. Spencer SJ, Miller AA, Andrews ZB. The Role of Ghrelin in Neuroprotection after Ischemic Brain Injury. Brain Sci. 2013;3:344–59.

389. Córdoba-Chacón J, Gahete MD, Duran-Prado M, Pozo-Salas AI, Malagón MM, Gracia-Navarro F, et al. Identification and characterization of new functional truncated variants of somatostatin receptor subtype 5 in rodents. Cell Mol Life Sci. 2010;67:1147–63.

390. Durán-Prado M, Malagón MM, Gracia-Navarro F, Castaño JP. Dimerization of G protein-coupled receptors: New avenues for somatostatin receptor signalling, control and functioning. Molecular and Cellular Endocrinology. 2008;286:63–8.

391. Jiang H, Smith R. Modification of ghrelin and somatostatin signaling by formation of GHSR-1a／SSTR5 heterodimers. The Endocrine Society's 89th Annual Meeting. 2007;P9: 299.

392. Sánchez-Alavez M, Gómez-Chavarín M, Navarro L, Jiménez-Anguiano A, Murillo-Rodríguez E, Prado-Alcalá RA, et al. Cortistatin modulates memory processes in rats. Brain Research. 2000;858:78–83.

393. Li R, Yao G, Zhou L, Zhang M, Yan J. The ghrelin-GHSR-1a pathway inhibits high glucose-induced retinal angiogenesis in vitro by alleviating endoplasmic reticulum stress. Eye and Vision. 2022;9:20.

394. Hurst RD, Clark JB. Alterations in Transendothelial Electrical Resistance by Vasoactive Agonists and Cyclic AMP in a Blood-Brain Barrier Model System. Neurochem Res. 1998;23:149–54.

395. Lampugnani MG, Giorgi M, Gaboli M, Dejana E, Marchisio PC. Endothelial cell motility, integrin receptor clustering, and microfilament organization are inhibited by agents that increase intracellular cAMP. Lab Invest. 1990;63:521–31.

396. Dixit VD, Schaffer EM, Pyle RS, Collins GD, Sakthivel SK, Palaniappan R, et al. Ghrelin inhibits leptin- and activation-induced proinflammatory cytokine expression by human monocytes and T cells. J Clin Invest. 2004;114:57–66.

397. Rol Á, Todorovski T, Martin-Malpartida P, Escolà A, Gonzalez-Rey E, Aragón E, et al. Structure-based design of a Cortistatin analogue with immunomodulatory activity in models of inflammatory bowel disease. Nat Commun. 2021;12:1869.

398. Adams G, Vessillier S, Dreja H, Chernajovsky Y. Targeting cytokines to inflammation sites. Nat Biotechnol. 2003;21:1314–20.

399. Vessillier S, Adams G, Montero-Melendez T, Jones R, Seed M, Perretti M, et al. Molecular engineering of short half-life small peptides (VIP, αMSH and γ3MSH) fused to latency-associated peptide results in improved anti-inflammatory therapeutics. Annals of the Rheumatic Diseases. 2012;71:143–9.

400. Datta A, Saha C, Godse P, Sharma M, Sarmah D, Bhattacharya P. Neuroendocrine regulation in stroke. Trends in Endocrinology & Metabolism. 2023;34:260–77.

8. Appendix

8. Appendix

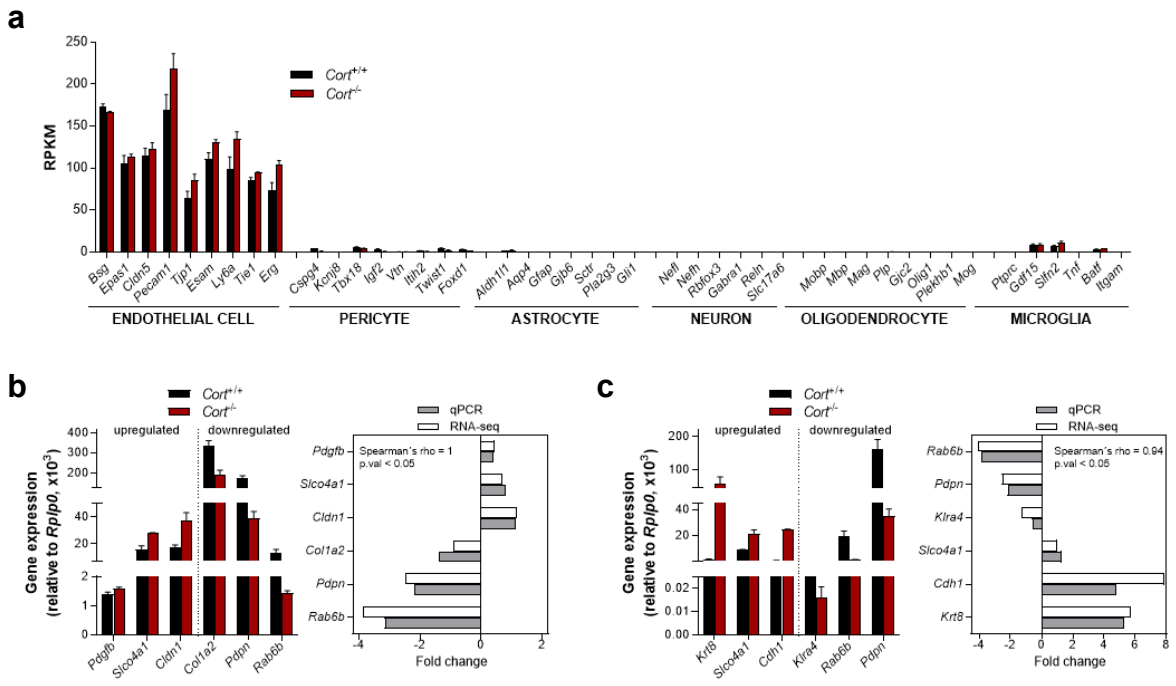

Figure A1. Analysis of specific markers in BECs and validation of gene expression. a. The expression of signature markers for components of the NVU (*i.e.,* BECs, pericytes, astrocytes, neurons, oligodendrocytes, and microglia) was analysed in wild-type and cortistatin-deficient BECs in normal conditions (NX/NG). Data are expressed as reads per kilobase of transcript per million reads mapped (RPKM). **b.c.** Validation of RNA-seq data. The expression of selected upregulated or downregulated differentially expressed genes (DEGs) in *Cort*-/- BECs *vs* wild-type BECs under NX/NG (**b**) and OGD-R (**c**) was quantified by real-time qPCR (left panel in b and c). Fold-change expression of these DEGs was compared using both RNA-seq and real-time qPCR analyses (right panel in b and c) showing large significant correlation with Spearman´s rho test. N = 2-3 samples/group. Data are the mean ± SEM.

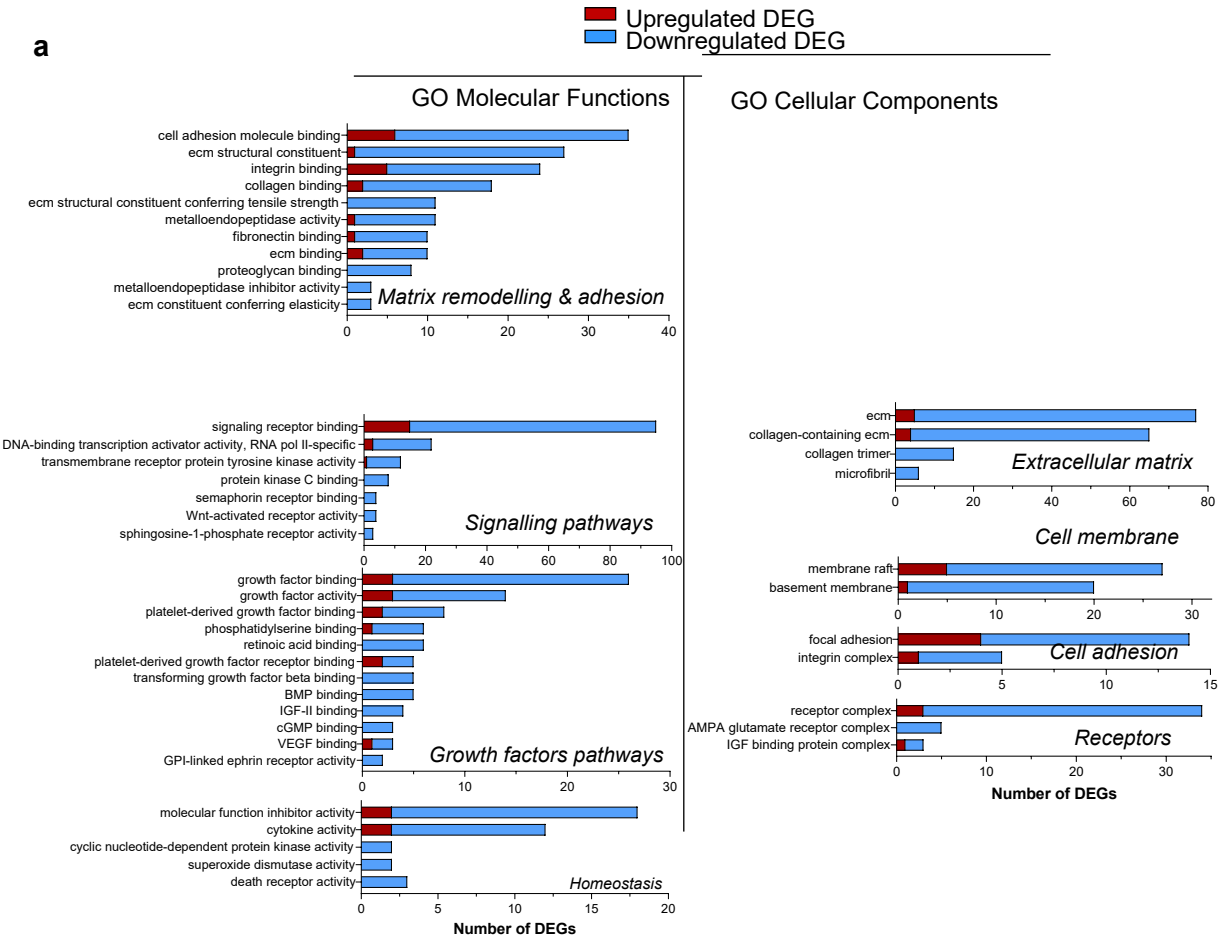
a
Upregulated DEG
Downregulated DEG
GO Molecular Functions
GO Cellular Components
cell adhesion molecule binding
ecm structural constituent
integrin binding
collagen binding
ecm structural constituent conferring tensile strength
metalloendopeptidase activity
fibronectin binding
ecm binding
proteoglycan binding
metalloendopeptidase inhibitor activity
ecm constituent conferring elasticity
Matrix remodelling & adhesion
signaling receptor binding
DNA-binding transcription activator activity, RNA pol II-specific
transmembrane receptor protein tyrosine kinase activity
protein kinase C binding
semaphorin receptor binding
Wnt-activated receptor activity
sphingosine-1-phosphate receptor activity
Signalling pathways
growth factor binding
growth factor activity
platelet-derived growth factor binding
phosphatidylserine binding
retinoic acid binding
platelet-derived growth factor receptor binding
transforming growth factor beta binding
BMP binding
IGF-II binding
cGMP binding
VEGF binding
GPI-linked ephrin receptor activity
Growth factors pathways
molecular function inhibitor activity
cytokine activity
cyclic nucleotide-dependent protein kinase activity
superoxide dismutase activity
death receptor activity
Homeostasis
Number of DEGs
ecm
collagen-containing ecm
collagen trimer
microfibril
Extracellular matrix
Cell membrane
membrane raft
basement membrane
focal adhesion
integrin complex
Cell adhesion
receptor complex
AMPA glutamate receptor complex
IGF binding protein complex
Receptors
Number of DEGs

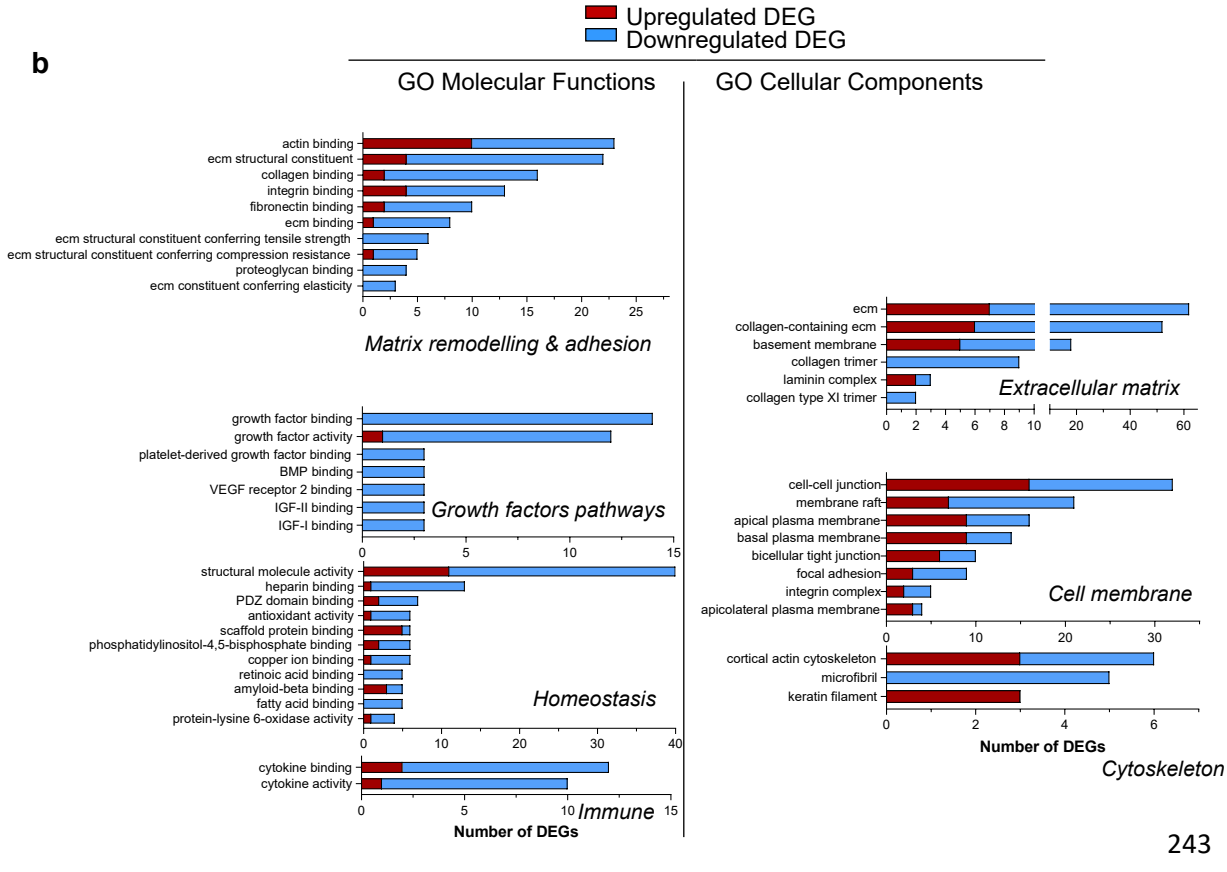
b
Upregulated DEG
Downregulated DEG
GO Molecular Functions
GO Cellular Components
actin binding
ecm structural constituent
collagen binding
integrin binding
fibronectin binding
ecm binding
ecm structural constituent conferring tensile strength
ecm structural constituent conferring compression resistance
proteoglycan binding
ecm constituent conferring elasticity
Matrix remodelling & adhesion
growth factor binding
growth factor activity
platelet-derived growth factor binding
BMP binding
VEGF receptor 2 binding
IGF-II binding
IGF-I binding
Growth factors pathways
structural molecule activity
heparin binding
PDZ domain binding
antioxidant activity
scaffold protein binding
phosphatidylinositol-4,5-bisphosphate binding
copper ion binding
retinoic acid binding
amyloid-beta binding
fatty acid binding
protein-lysine 6-oxidase activity
Homeostasis
cytokine binding
cytokine activity
Immune
Number of DEGs
ecm
collagen-containing ecm
basement membrane
collagen trimer
laminin complex
collagen type XI trimer
Extracellular matrix
cell-cell junction
membrane raft
apical plasma membrane
basal plasma membrane
bicellular tight junction
focal adhesion
integrin complex
apicolateral plasma membrane
Cell membrane
cortical actin cytoskeleton
microfibril
keratin filament
Number of DEGs
Cytoskeleton

Figure A2. Characterization of gene pathways in wild-type *vs* cortistatin-deficient brain endothelium. Gene ontology (GO) terms of molecular functions (MF, left panel in **a** and **b**) and cellular components (CC, right panel in **a** and **b**) significantly overrepresented in *Cort*$^{-/-}$ *vs Cort*$^{+/+}$ BECs incubated under NX/NG **(a)** or OGD-R **(b)**. Data were grouped into similar gene sets and manually annotated into several MF and CC terms networks. For MF, these include matrix remodelling and adhesion, cell signalling, growth factors pathways, homeostasis or immune response; and for CC, terms such as extracellular matrix, cell membrane, cell adhesion, receptors or cytoskeleton. Red and blue bar-segments correspond to numbers of upregulated and downregulated DEGs, respectively.

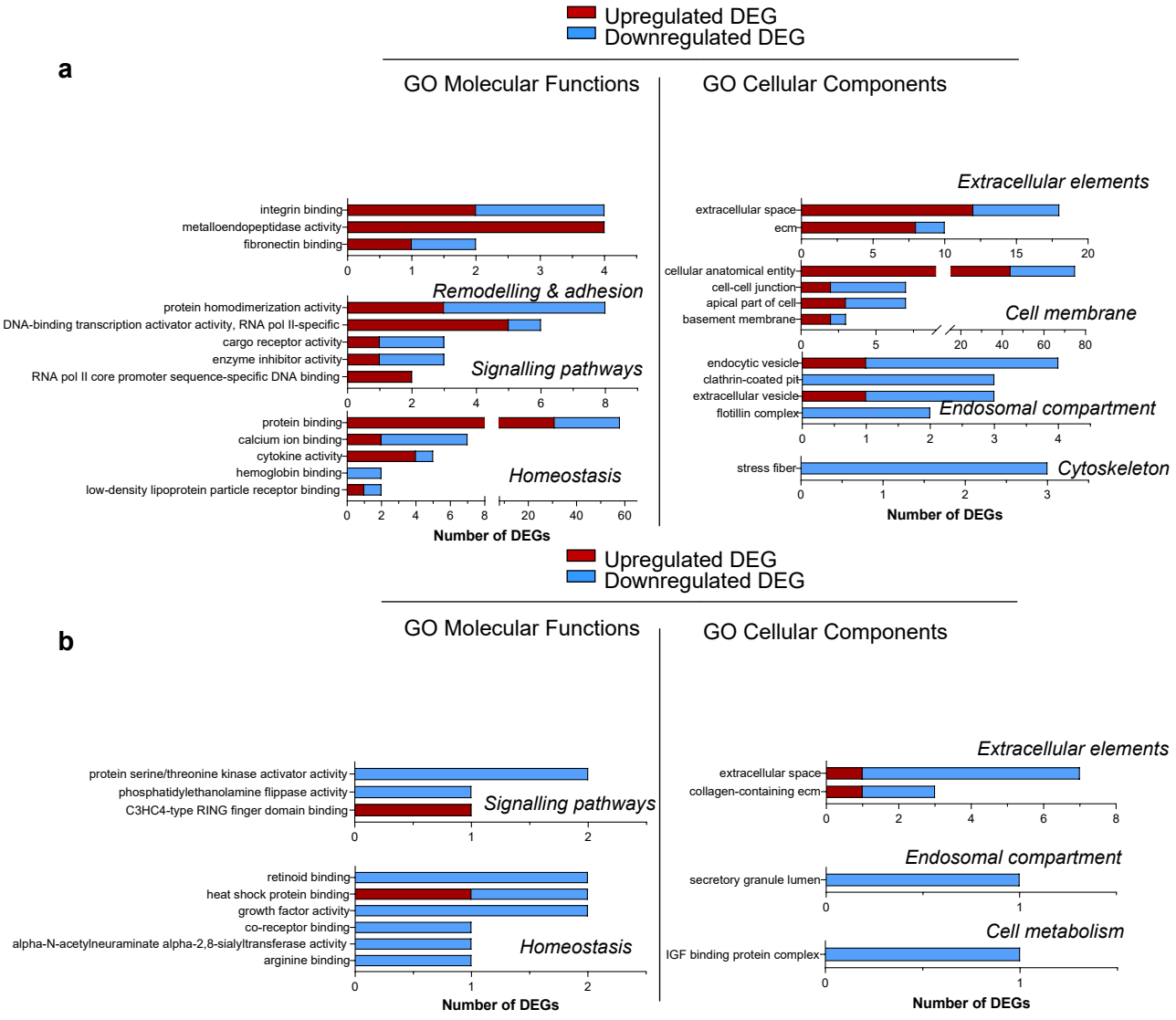

Figure A3. Characterization of gene pathways in the dynamics of *Cort*$^{+/+}$ and *Cort*$^{-/-}$ brain endothelium. Gene ontology (GO) terms of molecular functions (MF, left panel in **a** and **b**) and cellular components (CC, right panel in **a** and **b**) significantly overrepresented in BECs following progression from the basal (NX/NG) to ischemic and repairing (OGD-R) states in *Cort*$^{+/+}$ (**a**) and *Cort*$^{-/-}$ BECs (**b**). Data were grouped into similar gene sets and manually annotated into several networks for MF and CC terms including matrix remodelling and adhesion, cell signalling, or homeostasis for MF; and extracellular elements, cell membrane, endosomal compartment, cytoskeleton, or cell metabolism for CC. Red and blue bar-segments correspond to numbers of upregulated and downregulated DEGs, respectively.

9. Publications

Castillo-González *et al.*
Journal of Neuroinflammation (2023) 20:226
https://doi.org/10.1186/s12974-023-02908-5

Journal of Neuroinflammation

RESEARCH

Open Access

Cortistatin deficiency reveals a dysfunctional brain endothelium with impaired gene pathways, exacerbated immune activation, and disrupted barrier integrity

Julia Castillo-González[1], José Luis Ruiz[1], Ignacio Serrano-Martínez[1], Irene Forte-Lago[1], Ana Ubago-Rodriguez[1], Marta Caro[1], Jesús Miguel Pérez-Gómez[2,3,4,5], Alejandro Benítez-Troncoso[1], Eduardo Andrés-León[1], Macarena Sánchez-Navarro[1], Raúl M. Luque[2,3,4,5] and Elena González-Rey[1*]

Abstract

Background Brain activity governing cognition and behaviour depends on the fine-tuned microenvironment provided by a tightly controlled blood–brain barrier (BBB). Brain endothelium dysfunction is a hallmark of BBB breakdown in most neurodegenerative/neuroinflammatory disorders. Therefore, the identification of new endogenous molecules involved in endothelial cell disruption is essential to better understand BBB dynamics. Cortistatin is a neuroimmune mediator with anti-inflammatory and neuroprotective properties that exerts beneficial effects on the peripheral endothelium. However, its role in the healthy and injured brain endothelium remains to be evaluated. Herein, this study aimed to investigate the potential function of endogenous and therapeutic cortistatin in regulating brain endothelium dysfunction in a neuroinflammatory/neurodegenerative environment.

Methods Wild-type and cortistatin-deficient murine brain endothelium and human cells were used for an in vitro barrier model, where a simulated ischemia-like environment was mimicked. Endothelial permeability, junction integrity, and immune response in the presence and absence of cortistatin were evaluated using different size tracers, immunofluorescence labelling, qPCR, and ELISA. Cortistatin molecular mechanisms underlying brain endothelium dynamics were assessed by RNA-sequencing analysis. Cortistatin role in BBB leakage was evaluated in adult mice injected with LPS.

Results The endogenous lack of cortistatin predisposes endothelium weakening with increased permeability, tight-junctions breakdown, and dysregulated immune activity. We demonstrated that both damaged and uninjured brain endothelial cells isolated from cortistatin-deficient mice, present a dysregulated and/or deactivated genetic programming. These pathways, related to basic physiology but also crucial for the repair after damage (e.g., extracellular matrix remodelling, angiogenesis, response to oxygen, signalling, and metabolites transport), are dysfunctional and make brain endothelial barrier lacking cortistatin non-responsive to any further injury. Treatment with cortistatin reversed in vitro hyperpermeability, tight-junctions disruption, inflammatory response, and reduced in vivo BBB leakage.

*Correspondence:
Elena González-Rey
elena.g@csic.es
Full list of author information is available at the end of the article

Conclusions The neuropeptide cortistatin has a key role in the physiology of the cerebral microvasculature and its presence is crucial to develop a canonical balanced response to damage. The reparative effects of cortistatin in the brain endothelium were accompanied by the modulation of the immune function and the rescue of barrier integrity. Cortistatin-based therapies could emerge as a novel pleiotropic strategy to ameliorate neuroinflammatory/neurodegenerative disorders with disrupted BBB.

Keywords Blood–brain barrier, Cortistatin, Tight-junctions, Brain endothelium transcriptome, Oxygen–glucose deprivation, Ischemia, Endothelial immune activation

Introduction

The blood–brain barrier (BBB) is a highly dynamic interface between the central nervous system (CNS) and the peripheral circulation [1]. BBB is comprised of brain endothelial cells (BECs) surrounded by astrocyte end-feet and pericytes, all of them embedded in an extracellular matrix network [2]. The function of the BBB is intricately controlled as it provides a tight regulation of ions and nutrient influx, restricts the transport of harmful agents, and selectively limits the traffic of immune cells and inflammatory mediators [1]. Brain endothelial cells show unique features compared to other endothelial peripheral cells that allow this fine regulation. Among them, it is the presence of tight-junction (TJ) and adherens-junction (AJ) proteins, which attach adjacent endothelial cells and connect to cytoskeletal proteins, such as actin, thereby maintaining the structural integrity of the endothelium [3]. In addition, endothelial cells exhibit a low rate of pinocytosis, present several transporters that facilitate nutrient uptake and waste elimination, and express low levels of leukocyte adhesion molecules [1]. BBB disruption is a key feature of most neuroinflammatory/neurodegenerative disorders, such as Parkinson's and Alzheimer's disease, or brain ischemia. This provokes an imbalance in the transport of and/or permeability to proteins, inflammatory cells, or pathogens, leading to brain homeostasis failure, glial activation, and neuronal dysfunction [4]. Importantly, BECs dysfunction is sufficient to promote BBB breakdown, and this is mainly attributed to the loss of junction integrity [3]. Therefore, the identification of new endogenous molecules that target endothelial cell dysfunction seems essential to better understand and promote BBB stability and maintenance.

Cortistatin is a cyclic neuropeptide first discovered in the brain cortex and hippocampus but widely distributed in the immune system [5, 6]. Highly homologous to somatostatin (SST), cortistatin can bind to somatostatin receptors (SSTR1–5) sharing functional properties with SST. However, cortistatin displays unique functions in the nervous system and peripheral tissues [7, 8] by interacting with other receptors different from those of SST, including the ghrelin receptor (GHSR1α), the Mas gene-related receptor X-2 (MRGPRX2), and a still unidentified cortistatin-selective receptor. In fact, cortistatin has been described as a potent anti-inflammatory molecule that protects against the development and progression of several inflammatory and autoimmune disorders (reviewed in [5]). Specifically, multiple studies have reported that cortistatin treatment exerts immunomodulatory and neuroprotective effects in models of neuroinflammatory/neuroimmune injury, such as excitotoxicity [9], meningoencephalitis [10], multiple sclerosis [11], or neuropathic pain [12]. In all of them, cortistatin reduced inflammatory mediators and modulated glial cell function while maintaining their tissue-surveillance activities. Interestingly, the lack of cortistatin has been reported to cause an exacerbated pro-inflammatory basal state in the CNS and periphery, accompanied by decreased expression of neurotrophic factors [5, 11]. Moreover, cortistatin plays a key role in peripheral vascular function, as it has been shown that the arterial endothelium expresses cortistatin and its receptors, especially in response to injury, and that cortistatin impairs the binding of immune cells to the peripheral endothelium [13–15].

Hence, the anti-inflammatory, immunomodulatory, and neuroprotective properties of cortistatin, together with its critical function in the dynamics and activation of immune cell populations in the periphery and in the glial niche, highlight the key role of cortistatin in brain-injury disorders. Taking into account the relevance of the brain barrier for CNS homeostasis and the protective properties of cortistatin in the peripheral endothelium, an effect of cortistatin in regulating BBB physiology and its breakdown would be expected. However, nothing is known about the role of this neuropeptide in either the brain endothelium or the integrity of the BBB. Therefore, in this study we aimed to investigate the potential function of cortistatin in regulating brain endothelium dysfunction in a neuroinflammatory/neurodegenerative environment and to elucidate the relevance of the absence of cortistatin in BBB dynamics.

Materials and methods

Animals

All procedures described in this study were approved by the Animal Care and Use Board and the Ethical

Committee of the Spanish National Research Council (Animal Care Unit Committee IPBLN-CSIC # protocol CEEA OCT/2017.EGR), in accordance with the guidelines from Directive 2010/63/EU of the European Parliament on the protection of animals used for scientific purposes. Transgenic mice lacking the cortistatin gene (*Cort*$^{-/-}$) were a kind gift from Dr. Luis de Lecea (Stanford University, La Jolla, CA, USA). They were generated and also maintained as hemizygotes (*Cort*$^{+/-}$) in a C57BL/6J background as previously described [7, 12] and in Additional file 1.

Cell culture

Preparation of b.End5 cells

The mouse brain endothelioma cell line b.End5 (Sigma-Aldrich, #96091930) was used as a BBB in vitro model [16]. b.End5 cells were incubated as reported in Additional file 1. Before procedures, adherent cells were rinsed in 1 × phosphate buffer solution (PBS) and detached by adding 0.1% trypsin–EDTA, followed by the addition of an equal volume of fresh medium. The cell suspensions were centrifuged for 5 min at 150 rcf. The supernatant was then removed and cells were resuspended in fresh medium, counted, and allowed to grow at 37 °C and 5% CO_2 in a humidified incubator.

Isolation of mouse brain endothelial cells (BECs)

To isolate endothelial cells (ECs) from mouse brain microvasculature, we followed a dissociation protocol [17] with some modifications. Additional details can be found in Additional file 1. Prior to cell seeding for experiments, adherent BECs were trypsinized (0.05% trypsin–EDTA), centrifuged for 5 min at 290 rcf, and brought to suspension as described above for b.End5 cells.

Human BBB model

A human BBB model was generated by differentiating cord blood-derived hematopoietic cells into ECs, followed by the induction of BBB properties by co-culturing them with pericytes (see Additional file 1), as previously described [18]. After 6–8 days of co-culture, ECs acquired BBB properties (therefore, named human brain-like endothelial cells, hBLECs), and were used in permeability assays.

Brain endothelium barrier model

To establish the brain endothelium barrier model, mouse ECs (b.End5, BECs) (5×10^4 cells/well) were seeded on the top of a PET transwell insert (0.33 cm^2, 8 µm pore size, Corning) previously coated with rat collagen-I (50 µg/ml) and fibronectin (20 µg/ml, Invitrogen). For hBLECs, inserts with cells from co-cultures were placed into new wells without pericytes. Cells were grown to confluence in their respective culture media. We considered that endothelial cell barrier integrity in murine monocultures was established when the transendothelial electrical resistance (EVOM^2 Epithelial Voltohmmeter, World Precision Instruments) was above 200 Ω × cm^2. TEER measurements under NX/NG conditions were evaluated in random transwells from each assay prior to any experimental procedure for b.End5 (550 ± 25.17 Ω × cm^2), BECs isolated from *Cort*$^{+/+}$ (585.7 ± 22.15 Ω × cm^2), *Cort*$^{+/-}$ (505.5 ± 27.78 Ω × cm^2), and *Cort*$^{-/-}$ (525 ± 25.28 Ω × cm^2) mice. Human barrier integrity was also evaluated by measuring the permeability of Lucifer yellow ($Pc < 15 \cdot 10^{-6}$ cm/s) as described below and detailed in Additional file 1.

Establishment of brain injury-like conditions

Mouse ECs were exposed to bacterial lipopolysaccharide (LPS) inflammation, glucose deprivation (GD), or oxygen–glucose deprivation and reoxygenation (OGD-R), while hBLECs were incubated in a hypoxic environment as well as in OGD-R conditions. For inflammatory damage, LPS from *E. coli* 055:B5 (10 µg/ml, Sigma) was added to the cells for 24 h. For GD conditions, b.End5 were washed twice and placed in glucose and serum-free b.End5 culture medium for 24 h. For OGD-R, mouse cells were placed in their respective glucose and serum-free culture media and incubated in a sealed hypoxic workstation (1% O_2, 94% N_2, 5% CO_2, 37 °C; In vivo$_2$, Ruskin Technologies) for 4 h. Immediately after OGD, cultures were returned to normoxic (NX) and normoglycemic (NG) conditions (21% O_2, 5.5 mM glucose), and incubated in 10% FBS medium for 20 h to mimic reperfusion. hBLECs were incubated under hypoxic conditions (HPX, 1% O_2) for 4 h in normal sECM/5% FBS medium and then returned to control conditions for 20 h (HPX-R). For OGD, hBLECs were incubated in a hypoxic chamber for 6 h. Subsequently, cells were returned to NX conditions for 18 h. Unlike from hypoxia, OGD and OGD-R conditions were performed in endothelial cell medium in the absence of serum, glucose or other commercial growth factors. When needed, mouse cortistatin-29 or human cortistatin-17 (CST; Bachem) (100 nM) were added for 24 h immediately after LPS and GD, or for 20 h during reoxygenation in OGD-R or HPX-R conditions. For each cell type, controls were incubated simultaneously in normal medium in a NX/NG environment (21% O_2, 5.5 mM glucose at 37 °C).

Endothelial permeability in vitro models

After LPS, GD, OGD-R or HPX-R incubations, Evans Blue-Albumin (Sigma, EBA, 67 kDa) and sodium fluorescein (Sigma, NaF, 376 Da) influx was determined as described [19] (details in Additional file 1). The

permeability coefficient (Pc) of the tracer was expressed as cm/min of the tracer diffusing from the luminal to the abluminal side as $Pc = (C_A/t)^*(1/A)^*(V/C_L)$. C_A is the tracer concentration in the abluminal side, t is the time (60 min), A is the total surface of the insert membrane, V is the final volume, and C_L is the initial known tracer concentration in the luminal side. To avoid inter-variability between assays, permeability was finally represented as the index (%) between the Pc of each well and the Pc of the control transwell (maximal influx of each tracer in an ECs-free coated insert).

Immunocytochemistry

After exposure to insults, cultured mouse/human ECs were fixed with 4% paraformaldehyde (Sigma) for 10 min at RT. For claudin-5 staining, hBLECs were fixed with cold methanol and rinsed twice with cold PBS. Specific immunodetection was performed as described in Additional file 1. Cells from four different fields for each cell culture were imaged at 63 × magnification in a LEICA DMi8 S Platform Life cell microscope, selecting different region-of-interest (ROI) with the same exposure parameters. At least six independent experiments (cell cultures) were performed and a total of 25–50 selected ROIs were examined for each group. Image fluorescence analyses (mean grey value) were performed with ImageJ Fiji free software (https://fiji.sc).

Determination of inflammatory factors and cortistatin

The concentration of inflammatory mediators and cortistatin in b.End5/BECs/hBLECs culture media was determined by ELISA assay. The amount of nitric oxide was estimated from the accumulation of nitrite by the Griess assay. Details can be found in Additional file 1.

Transendothelial migration assay

Before migration experiments, immune cells were isolated from 8-week-old *Cort*$^{+/+}$ mice. Macrophages and T cells were isolated as described in Additional file 1. Immune migration was evaluated in a BECs monolayer grown onto coated inserts of 24-well plates, as described above. 24 h before the assay, cells were activated with TNF-α (10 ng/ml, BD Pharmigen). On the day of the experiment, transwells inserts were transferred to a new 24-well culture plate containing 1% FBS medium in the bottom side supplemented with MCP-1 (50 µg/ml, Bionova) or IP-10 (50 µg/ml, Bionova) for macrophages and T cells, respectively. Immediately, immune cells (2×10^5/transwell) were added to the upper side of the transwell in contact with BECs. When indicated, mouse cortistatin-29 (100 nM) was added to both sides of the transwell. After 24 h, migrated T cells were counted on the bottom side using a Neubauer chamber (VWR). Macrophages were identified at the bottom of the well after plate fixation and DAPI staining. As a positive control of migration, macrophages/T cells were incubated in a BECs-free coated transwell. The number of migrated cells was represented as the percentage of immune migrated cells vs the positive control.

In vivo blood–brain barrier permeability assay

BBB integrity was analysed by evaluating Evans blue extravasation. For this, 1-year-old *Cort*$^{+/+}$ and *Cort*$^{-/-}$ mice were injected intraperitoneally with LPS from *E.coli* 055:B5 (6 mg/kg, Sigma) inducing mild neuroinflammation [20]. Immediately after LPS injection, 1 nmol of CST-29 (resuspended in PBS, Bachem) was intraperitoneally injected. 5 h after LPS and LPS + CST injection, Evans Blue (EB, 2% in saline, 4 ml/kg) was injected through the tail vein. Control animals were injected with vehicle (PBS). After 1 h, mice were sacrificed by intraperitoneal injection of pentobarbital and intracardially perfused with PBS. EB quantification was performed as indicated in Additional file 1. Data were represented as µg of dye per mg of brain tissue.

RNA extraction and determination of gene expression

Following incubation under different conditions, mouse b.End5 and BECs were collected and lysed in TriPure reagent (Roche) for RNA isolation. After RNA isolation, cDNA synthesis from 1 µg RNA was performed using the RevertAid First Strand cDNA Synthesis Kit (ThermoFisher) and random hexamers in a CFX Connect QPCR System (Biorad), under the following conditions: incubation at 25 °C/5 min, reverse transcription at 42 °C/60 min, inactivation at 70 °C/5 min. Gene expression of cortistatin–somatostatin system and inflammation-related genes was determined by a microfluidic-based qPCR dynamic array, as previously described [21]. Conventional qPCR was used to validate differentially expressed genes selected from our transcriptomic studies. Specific primers for mouse transcripts are listed in Additional file 1: Tables S1, S2. Details for each approach are described in Additional file 1.

Next-generation transcriptome sequencing (RNA-seq)

RNA (200 ng) from primary *Cort*$^{+/+}$ and *Cort*$^{-/-}$ BECs cultures exposed to NX/NG or OGD-R conditions for 24 h was used to prepare mRNA libraries with Illumina stranded mRNA Prep Ligation kit (Illumina). Three independent biological replicates were performed, with RNA Integrity Number coefficients > 9.9 (Bioanalyzer RNA 6000 Nano-chip, Agilent). Quality and size distribution of mRNA libraries were validated by Bioanalyzer High Sensitivity DNA assay and concentration was measured on the Qubit fluorometer (ThermoFisher).

Final libraries were pooled in equimolecular ratios and diluted/denatured as recommended by Illumina NextSeq 500 library preparation guide. The 75 × 2nt paired-end sequencing was conducted on a NextSeq 500 sequencer. The average number of sequencing reads above a quality threshold of Q > 30 was 91.5%. We obtained a mean GC content of 51.3%, and 40,407,022 paired-end reads and > 28,000 transcripts on average. Considering the low levels of cortistatin expression, we have implemented the reanalyzerGSE software [22, 23] for transcriptomic studies. This pipeline was implemented in the RNA-seq analysis to identify differentially expressed genes (DEGs) and to prevent the exclusion of low expressed genes with potential biological relevance (see details in Additional file 1). Both multidimensional scaling (Principal Coordinates Analysis, PCoA) and unsupervised hierarchical clustering of normalized samples were used to assess the divergence and the replicability of the samples included in each one of the independent comparisons (Additional file 1: Fig. S1). DEGs with a False Discovery Rate (FDR) ≤ 0.05 were calculated by comparing: (i) $Cort^{-/-}$ vs $Cort^{+/+}$ samples for each condition (NX/NG and OGD-R); (ii) NX/NG vs OGD-R for each genotype ($Cort^{-/-}$ and $Cort^{+/+}$). The Fold Change (log_2FC) was used to evaluate the degree of expression change of each gene. To investigate the potential effects and relevance of DEGs, functional enrichment analyses based on the Gene Ontology (GO) database were performed as indicated in Additional file 1.

Statistical analysis

Data are expressed as the mean ± SEM. All experiments were randomized and blinded for researchers. The number of independent animals or cell cultures is shown, and statistical analysis was performed using these independent values. Statistical differences comparing two groups were conducted using the unpaired Student's *t* test (for parametric data, and normal distribution) or the non-parametric Mann–Whitney *U* test. For three or more groups with normal distribution and parametric data, one-way ANOVA with appropriate post-hoc tests for multiple comparisons were utilized (with small number of data Bonferroni post-hoc test was preferentially used vs Tukey post-hoc test). Non-parametric data from three or more groups was analysed by Kruskal–Wallis test and Dunn's post-hoc test. When standard deviations were assumed as different, Brown–Forsythe and Welch ANOVA test were applied with Dunnett T3 post-hoc test. Spearman's rho non-parametric test was used for correlation studies. All analyses were performed using GraphPad Prism v8.3.0 software. We considered *P* values < 0.05 (two-tailed) as significant.

Data availability

RNA-seq data are available in the GEO repository under accession number GSE207405, https://www.ncbi.nlm.nih.gov/geo/query/acc.cgi?acc=GSE207405.

Results

Brain endothelium expresses the components of the cortistatin pathway

ECs from peripheral murine and human vessels express the neuropeptides somatostatin, cortistatin, and ghrelin, and their corresponding receptors [24, 25]. However, the expression of these neuropeptides and their receptors in brain ECs is either absent or poorly documented [24, 26]. Thus, using methodologies with different sensitivity, we first investigated the relative expression of the components related to the cortistatin–somatostatin system in b.End5 murine brain ECs. A variable expression level for each SSTR was found under physiological conditions (Additional file 1: Fig. S2a, b). We observed that *Sstr4, Sstr1* and *Sstr2* seem to be preferentially expressed, while *Sstr3*, *Sstr5 and Ghsr* levels were low or undetectable. Low levels of cortistatin and somatostatin, were also detected by both Fluidigm and conventional qPCR techniques. Interestingly, we found a preferential expression for endogenous *Cort* vs *Sst* in the brain endothelial cells (Additional file 1: Fig. S2a, b).

Cortistatin regulates the permeability and integrity of the brain vascular endothelium after injury

BBB breakdown is a hallmark in most neurodegenerative/neuroinflammatory disorders and injured brain ECs are enough to disrupt the BBB. In this sense, previous results showed the critical role of cortistatin in the regulation of the peripheral vascular endothelium [13–15]. Therefore, we evaluated the possible influence of this neuropeptide on the integrity of the brain endothelium. First, we characterized the effect of cortistatin in b.End5 cells exposed to different insults mimicking brain injury-like conditions (Fig. 1a).

Specifically, we observed increased endothelial cell permeability after incubation with bacterial LPS, glucose deprivation (GD), or oxygen–glucose deprivation and reoxygenation (OGD-R) (Fig. 1b). However, the addition of exogenous cortistatin to b.End5 cultures significantly reversed this increased permeability (Fig. 1b). The lack of endothelial integrity was accompanied by a delocalization and disruption of the TJ assembly (Fig. 1c, d). GD and OGD-R caused the disruption of ZO-1 (Zonula occludens-1) uniform pattern in the membrane (Fig. 1c), as well as the increase of claudin-1 intracellular

expression (correlated with BBB disruption, as shown by [27]) (Fig. 1d).

Cortistatin restored ZO-1 integrity in the peripheral cell membrane (Fig. 1c) and significantly reduced claudin-1 cytosolic accumulation under both conditions (Fig. 1d). Moreover, injured ECs developed an altered inflammatory response, characterized by an augmented production of the proinflammatory factors IL-6 and MCP-1, and reduced levels of nitrite, quantified as a major metabolite of nitric oxide, all linked to BBB leakage [16] (Fig. 1e, f). Cortistatin treatment exerted an immunomodulatory effect on brain endothelium activation by significantly downregulating TNF-α and MCP-1, without affecting nitrite levels (Fig. 1e, f). Moreover, cortistatin addition seems to modulate to basal levels the OGD-R-derived dysregulated expression of other immune mediators, inflammasome components and endothelial-derived agents being only significant for *Il6ra* (Additional file 1: Fig. S3a–c). Although some biological trends can be observed, exposure to OGD-R and/or treatment with cortistatin did not significantly affect the expression levels of *Cort*, *Sst* or their receptors (Additional file 1: Fig. S2c). Notably, during injury conditions, the secreted levels of endogenous cortistatin were reduced significantly (Additional file 1: Fig. S2d).

Despite the fact that immortalized mouse brain endothelioma cell lines have been widely used, primary murine brain endothelial cells (BECs) have been shown to better retain several phenotypic properties of the BBB in vitro, due to their specialization with complex TJs [28]. Thus, we examined the role of cortistatin in murine BECs isolated from the adult CNS microvasculature (Fig. 2a). As described above for the cell line, cortistatin–somatostatin system was also expressed by primary BECs under homeostatic conditions. Although we found some variability for the expression levels of the receptors and neuropeptides according to the different methodologies, low levels of *Sstr3* and *Ghsr1a* were observed, while *Sstr2* and *Sstr4* significantly displayed the highest expression (Fig. 2b; Additional file 1: Fig. S4). Of note, endogenous *Cort* expression was higher compared to *Sst*. Next, to further support our previous results with b.End5, BECs were incubated under OGD-R as the preferred insult to mimic the model of ischemic–reperfusion injury to study BBB disruption. ECs significantly increased permeability, showing a compromised TJ architecture and an exacerbated immune response (Fig. 2c, d). Treatment with exogenous cortistatin reversed brain endothelial cell dysfunction back to the homeostatic state, decreasing permeability, preserving functional proteins for the barrier formation (Fig. 2d) and downregulating the production of immune mediators, such as MCP-1 and IL-6 (Fig. 2e). Importantly, secretion of cortistatin was reduced under OGD-R conditions (Additional file 1: Fig. S6c).

In addition, we also evaluated the potential role of cortistatin in human-derived brain ECs under ischemic–reperfusion injury mimicked by hypoxia– and oxygen–glucose deprivation assays combined with reoxygenation (Fig. 3; Additional file 1: Fig. S5).

Although no changes were detected in the endothelial barrier permeability between NX/NG and HPX-R conditions (Fig. 3b), probably due to the variability of serum-derived effects [29, 30], only the injured endothelial cells showed a disruptive presence of ZO-1 (Fig. 3c). Incubation with cortistatin reduced permeability in hypoxic cells and recovered intact ZO-1 presence in the cell membrane (Fig. 3b, c). As expected, OGD-R did induce an increase in barrier permeability of hBLECs. This increase was associated with a reduced expression of ZO-1 and an increase in ZO-1 disorganization, as well as claudin-5 membrane depletion (Additional file 1: Fig. S5a, b). Paradoxically, the addition of cortistatin significantly recovered the junctional expression and architecture of ZO-1 and claudin-5, although no changes

(See figure on next page.)

Fig. 1 Cortistatin regulates the integrity of b.End5 cells exposed to different insults. **a** Schematic representation of the experimental design. Murine b.End5 cells were exposed to lipopolysaccharide (LPS), glucose deprivation (GD) for 24 h, or to 4 h of oxygen–glucose deprivation followed by 20 h of reoxygenation (OGD-R). Cortistatin (CST, 100 nM) was applied simultaneously to the insult (LPS + CST; GD + CST) or during recovery (OGD-R + CST). Cells incubated in normoxia/normoglycemia (NX/NG) were used as a reference. **b–d** Endothelial integrity was assessed by evaluating permeability to Evans Blue-Albumin (EBA) and Sodium Fluorescein (NaF) (**b**), and tight-junctions assembly (**c, d**). **b** Permeability is represented as the index (%) of the tracer permeability vs an empty-coated insert. $N = 4–6$ cultures/group. **c, d** Representative immunofluorescence images of the cellular distribution of ZO-1 (**c**, red) and claudin-1 (**d**, green) in b.End5 cells after GD or OGD-R in the absence or presence of cortistatin. Delocalization of ZO-1 was evaluated through the ratio of ZO-1 staining intensity in the membrane vs the cytosol (**c**, arrowheads indicate gaps in ZO-1 membrane location). After cortistatin addition, ZO-1 junctional rearrangement was observed in the membrane (asterisks). Claudin-1 intracellular overexpression was quantified by fluorescence intensity (**d**). Cytosolic expression of claudin-1 was augmented in GD/OGD-R (arrowheads). Cortistatin drastically decreased claudin-1 intracellular expression (asterisks). 25–50 selected ROIs in 4 independent fields were analysed (expressed as arbitrary units, a.u). $N = 6$ cultures/group. Scale bar: 20 µm. **e, f** Levels of inflammatory cytokines TNF-α, IL-6, chemokine MCP-1 (all in ng/ml) and nitrite (µM) were determined in culture supernatants after GD (**e**) or OGD-R (**f**) with or without cortistatin addition. $N = 4–6$ cultures/group. Data are the mean ± SEM with dots representing individual values of the independent cultures. $^{*}p \le 0.05$, $^{**}p \le 0.01$, $^{***}p \le 0.001$, $^{****}p \le 0.0001$

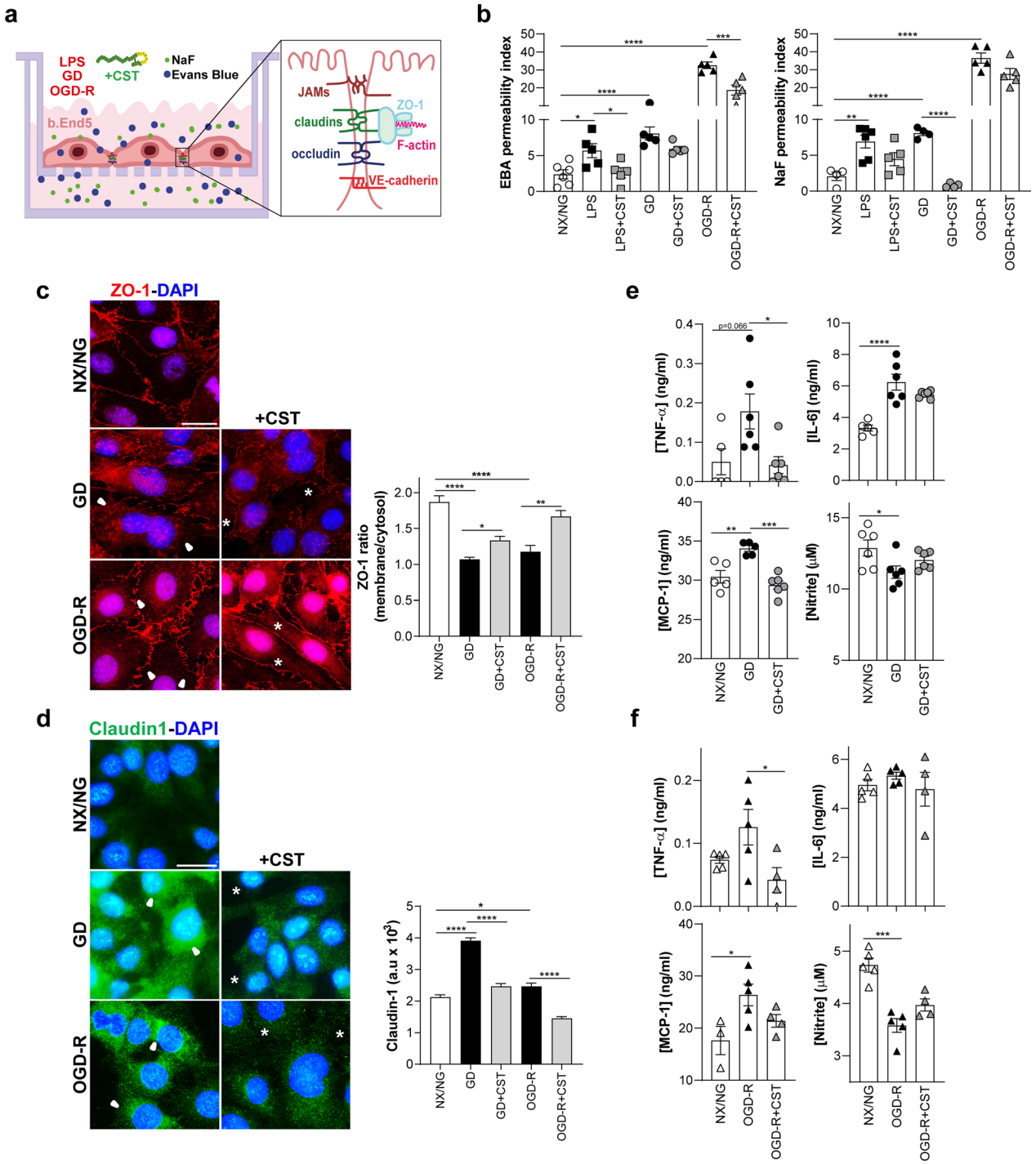

Fig. 1 (See legend on previous page.)

were observed in the permeability of OGD-R-injured cells (Additional file 1: Fig. S5a, b). While discontinuous junctions are typically indicative of decreased barrier function and increased permeability, recent works have demonstrated that global permeability measures (as the ones used for transwell experiments) may not correlate with the junction phenotype (i.e., permeability measure remains the same with continuous and discontinuous arrangement of TJs) [31]. Interestingly, as we observed in the murine endothelial cells, healthy hBLECs predominantly expressed cortistatin, while somatostatin levels were almost undetectable (Additional file 1: Fig. S5c).

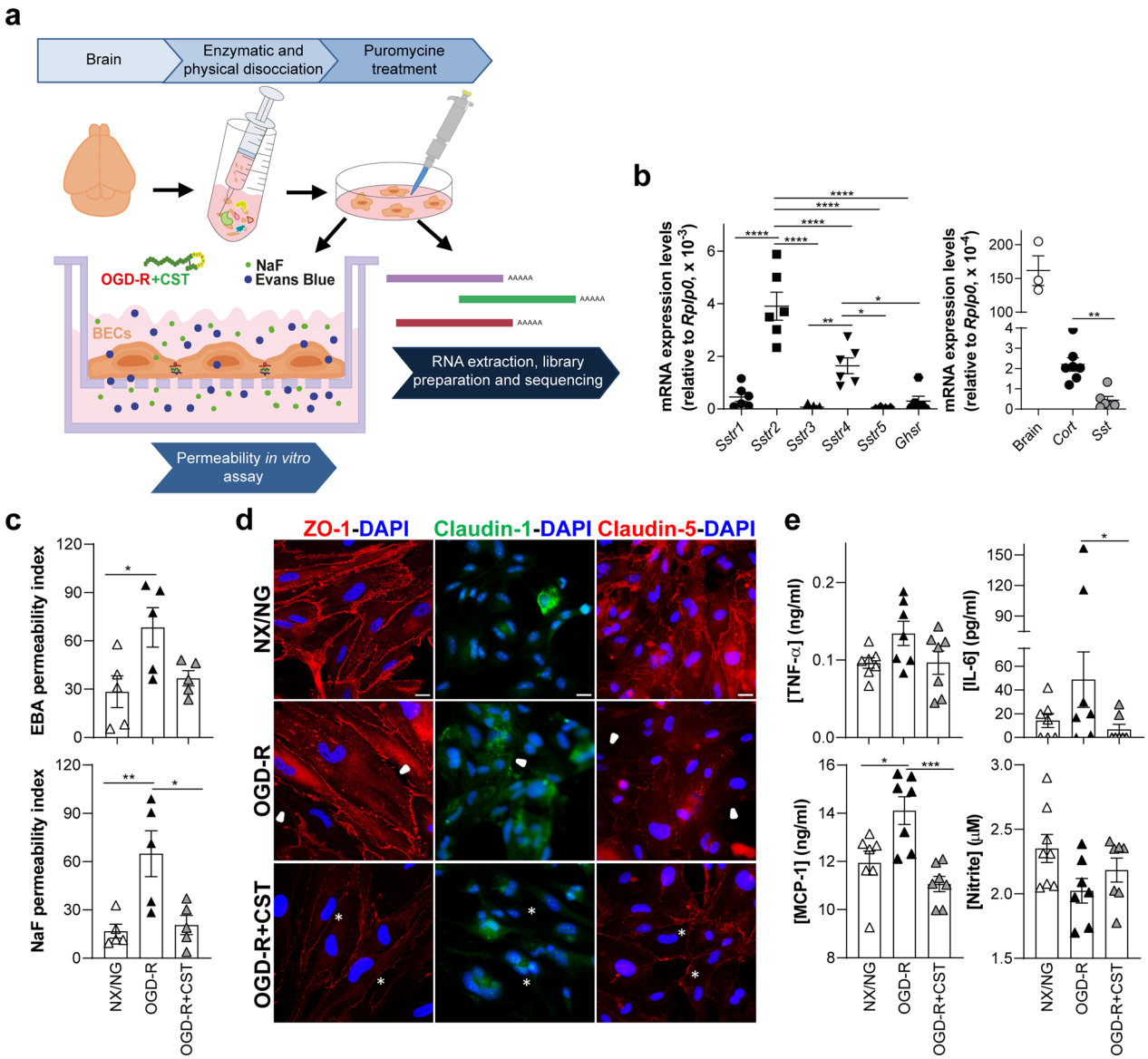

Fig. 2 Cortistatin reverses murine brain endothelium disruption after ischemic-like conditions. **a** Graphical illustration of the experimental design. Primary brain endothelial cells (BECs) were isolated from 8-week-old *Cort*$^{+/+}$ mice and enriched after 60 h puromycin treatment. One week later, cells were plated in collagen/fibronectin-coated transwells as described before. BECs were exposed to OGD-R with or without cortistatin (CST, 100 nM) and gene profile expression analysis or permeability assays were performed. **b** mRNA expression levels of cortistatin system receptors (left, *Sstr* and *Ghsr1a*) and ligands (right, somatostatin, *Sst* and cortistatin, *Cort*) in the brain endothelium under NX/NG. Data represent the mean of mRNA expression levels quantified by real-time qPCR analyses and normalized to *Rplp0*. $N = 5–7$ cultures/group. Mouse brain ($n = 3$) was used as an internal reference for endogenous *Cort* expression. **c** Endothelium barrier functionality was assessed by evaluating permeability to EBA and NaF and tight-junctions integrity. Index (%) of the tracer permeability vs an empty-coated insert. $N = 5$ cultures/group. **d** Representative immunofluorescence images of the cellular distribution of ZO-1 (red), claudin-1 (green) and claudin-5 (red) in BECs after OGD-R in the absence or presence of cortistatin. Arrowheads indicate ZO-1 and claudin-5 disruption throughout the cell membrane and augmented cytosolic expression of claudin-1. After cortistatin treatment, asterisks point out the recovery of ZO-1 and claudin-5 continuous pattern in the membrane and the reduced claudin-1 intracellular location. Scale bar: 20 μm. **e** Levels of immune factors were determined in culture supernatants after OGD-R in the presence or absence of cortistatin. N = 7 cultures/group. Data are the mean ± SEM with dots representing individual values of independent cultures. Cells for each culture derived from 4 pooled brains. $*p \leq 0.05$, $**p \leq 0.01$, $***p \leq 0.001$, $****p \leq 0.0001$

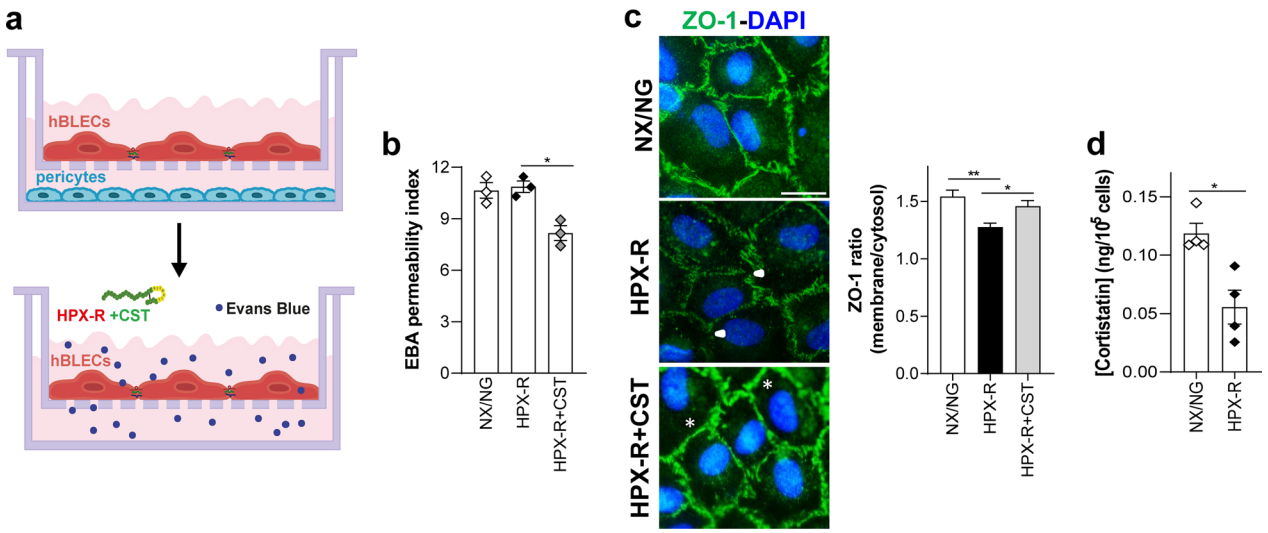

Fig. 3 Role of cortistatin in the human brain endothelium. **a** Human brain-like endothelial cells (hBLECs) were obtained after 1 week of co-culture of CD34+-derived endothelial cells with pericytes. hBLECs were incubated 4 h under hypoxia followed by 20 h of reoxygenation (HPX-R) in the absence or presence of cortistatin (HPX-R + CST, 100 nM). **b** Endothelium integrity was evaluated and represented as the index (%) of EBA permeability vs an empty-coated insert. $N = 3$ cultures/group. Data are the mean ± SEM with dots representing individual values of independent cultures. **c** *Left*, expression of ZO-1 (green) was evaluated by immunofluorescence. Arrowheads indicate reduced and disrupted expression of ZO-1 after HPX-R. Cortistatin treatment protected the membrane from breakdown and recovered the tight pattern of intercellular ZO-1 (asterisks). *Right*, delocalization of ZO-1 was evaluated through the ratio of ZO-1 staining intensity in the membrane vs the cytosol. 25–50 selected ROIs in 4 independent fields were analysed. $N = 6$ cultures/group. **d** Cortistatin protein levels were quantified in hBLECs supernatants 20 h after exposure to NX/NG and HPX-R, as described. Results are normalized in ng protein/10^5 cells. $N = 4$ cultures/group. *$p \leq 0.05$, **$p \leq 0.01$. Scale bar: 20 µm

Of note, production of cortistatin was regulated upon ischemic and reoxygenation damage, as the endogenous secretion of the neuropeptide was significantly reduced (Fig. 3d; Additional file 1: Fig. S5d).

Altogether, these data suggest that cortistatin-system (and not somatostatin) could play a crucial role in regulating brain endothelium integrity at different levels after several brain injury-like conditions.

Deficiency in cortistatin exacerbates a dysfunctional brain endothelium response

Previous studies demonstrated the regulatory properties of cortistatin in the peripheral vascular system, including exacerbated responses to vascular lesions in cortistatin-deficient mice [13–15]. In addition, our findings demonstrate that cortistatin modulates the dynamics of the brain endothelium and that both murine and human brain ECs respond to pathological conditions by modifying the expression of cortistatin (Figs. 1, 2, 3). To further investigate whether endogenous cortistatin plays a role in the control of brain endothelium functionality, we characterized the phenotype and dynamics of BECs isolated from the brain microvasculature of wild-type ($Cort^{+/+}$) and cortistatin-deficient mice ($Cort^{+/-}$ and $Cort^{-/-}$) under basal (NX/NG) and pathological (OGD-R) environments (Fig. 2a). Compared to wild-type BECs, cortistatin-deficient cultures showed a significant increase in endothelial permeability, not only after the insult but also when receiving a continuous supply of oxygen and nutrients (Fig. 4a; Additional file 1: Fig. S6a). Our data showed that the enhanced permeability observed with partial/complete absence of cortistatin was correlated with a greater delocalization, disruption and dysfunctional assembly of the TJ/AJ in both ischemic and normal environments (Fig. 4b–d). Specifically, by determining the ratio between the location of ZO-1 in the membrane vs the cytosol, we demonstrated that, under both conditions (NX/NG and OGD-R), a dramatic disintegration and redistribution of this protein occurred in the absence of cortistatin (Fig. 4b). Moreover, claudin-1 was overexpressed in BECs cultures without cortistatin (Fig. 4b). Similar to ZO-1, the breakdown of claudin-5 and the AJ VE-cadherin showed junctional discontinuity and a significant reduction in the expression in cortistatin-deficient BECs compared to control cells (Fig. 4b, c).

In addition, to address the important role of the cytoskeleton-junctional proteins assembly in the modulation of BBB leakage, we performed a rhodamine–phalloidin labelling (Fig. 4d). While F-actin was distributed in random fibers throughout the cytosol in NX/NG wild-type BECs, it was drastically reorganized into thick stress bundles in all genotypes after injury. Interestingly, the absence of cortistatin also promoted a significant accumulation of stress fibers in physiological conditions

(Fig. 4d). Notably, all these changes affecting TJ/AJ architecture were mostly appreciated in BECs with complete lack of the neuropeptide. The hyperpermeability observed in BECs without cortistatin was also accompanied by an altered inflammatory phenotype (Fig. 4e). Notably, we found a downregulated production of nitrite not only after the insult but also under normal conditions in the absence of cortistatin (Fig. 4e).

Next, we checked the regulation of the components of the cortistatin system in the absence of the neuropeptide (Additional file 1: Fig. S6b). Although the expression levels of the receptors showed no changes when comparing BECs isolated from cortistatin-deficient mice to the expression levels in wild-type cells under NX/NG, we found a partial non-significant decrease in the physiological levels of *Sstr1, Sstr5* and *Sst* that was still reduced in the OGD-R environment. Importantly, only *Sstr4* was significantly and oppositely modulated after injury in wild type and cells lacking cortistatin (Additional file 1: Fig. S6b). Interestingly, endogenous levels of cortistatin in healthy heterozygous BECs were similar to those secreted by wild-type cells under hypoxic–reoxygenation conditions (Additional file 1: Fig. S6c).

Taken together, these findings indicate that the brain ECs from mice lacking cortistatin exhibit a leaky and inflammatory-like endothelium already under physiological conditions, being exacerbated under damage. Our results suggest that the system conformed by endogenous cortistatin (and probably, by *Sstr4/Sstr2/Sstr5*) might be crucial in the regulation of the brain endothelium dynamics during physiology and pathology, which could be determinant for BBB integrity.

Cortistatin-deficient brain endothelium shows a dysfunctional phenotype with dysregulated physiological pathways

To further investigate the molecular profile that could be linked to the cerebral vascular endothelium behaviour in the absence of cortistatin, we compared the transcriptomes of $Cort^{+/+}$ and $Cort^{-/-}$ BECs under NX/NG or OGD-R obtained by next-generation RNA-seq. First, we confirmed that our samples showed strong enrichment of BECs-specific markers (such as *Cldn5, Pecam1/*CD31 or *Tjp1/*ZO-1), while cells expressing markers of pericytes (*Cspg4, Kcnj8, Vtn*), astrocytes (*Gfap, Aqp4, Gli1*), neurons (*Nefl, Gabra1, Reln*), oligodendrocytes (*Olig1, Mog, Mbp*), or microglia (*Ptprc, Itgam, Tnf*) were barely detectable (Additional file 1: Fig. S7a).

In brain endothelium from cortistatin-deficient mice, we identified 613 genes (139 upregulated and 474 downregulated) with significant differential expression (FDR < 0.05) compared to wild type in an NX/NG environment (Fig. 5a; Additional file 2: Table S3).

On the other hand, we observed that 407 genes (111 upregulated and 296 downregulated) were differentially expressed between $Cort^{-/-}$ and $Cort^{+/+}$ BECs after OGD-R exposure (Fig. 5d; Additional file 2: Table S4). The unsupervised hierarchical clustering analysis revealed two distinct groups with minimal overlap under both experimental conditions (Fig. 5b, e). Next, we validated by qPCR the expression of key genes up and downregulated, showing a high degree of correlation with the RNA-seq quantification (Additional file 1: Fig. S7b, c). Notably, in cortistatin-deficient BECs, we observed that 226 DEGs (more than half out of the total) were shared between NX/NG and OGD-R when comparing $Cort^{+/+}$ vs $Cort^{-/-}$ BECs. Through GO terms overrepresentation analysis corresponding to biological processes (BP), molecular functions (MF) and cellular components (CC), we showed that most DEGs were associated with downregulated functional networks (Fig. 5c, f; Additional file 1: Fig. S8, Additional file 2: Tables S5, S6).

In fact, these gene clusters, i.e., cell matrix remodelling, brain endothelium dynamics, immune response, regulation of gene expression (through MAPK, Wnt, VEGF, and Erk1/2 pathways), growth factors activity (BMP, IGF-II,

(See figure on next page.)

Fig. 4 Cortistatin-deficient brain endothelial cells (BECs) show increased leakage and exacerbated immune activation. **a** BECs were isolated from wild type ($Cort^{+/+}$) and cortistatin-deficient (partial: $Cort^{+/-}$; complete: $Cort^{-/-}$) mice and exposed to 4 h oxygen–glucose deprivation followed by 20 h of reoxygenation (OGD-R). Barrier integrity was evaluated and represented as the index (%) of EBA permeability vs an empty-coated insert. $N = 5$–8 cultures/group. **b–d** Representative immunofluorescence images of cellular junctions distribution in BECs incubated in basal conditions (NX/NG) and after OGD-R. **b** Immunofluorescence of tight-junctions ZO-1 and claudin-5 (both in red, arrowheads point out membrane disruption) and claudin-1 (green, arrowheads indicate augmented cytosolic expression). Delocalization of ZO-1 was evaluated through the ratio of ZO-1 staining intensity in the membrane vs the cytosol. Claudin-1 and claudin-5 cellular expression was quantified by fluorescence intensity as described below. **c, d** Adherens-junction protein VE-cadherin (**c**, green, arrowheads show discontinuous expression) and stress fibers (**d**, red rhodamine–phalloidin F-actin labelling, arrowheads reveal cytosolic reorganization of F-actin thick bundles) were analysed by quantifying fluorescence intensity. 25–50 selected ROIs in 4 independent fields were analysed (expressed as arbitrary units, a.u). $N = 6$ cultures/group. Scale bar: 20 µm. **e** Levels of inflammatory factors were determined in culture supernatants after OGD-R. $N = 5$–10 cultures/group. Data are the mean ± SEM with dots representing individual values of independent cultures. Cells for each culture were derived from 4 pooled brains. *vs $Cort^{+/+}$ either in NX/NG and OGD-R; &vs corresponding genotype ($Cort^{+/+}$, $Cort^{+/-}$, $Cort^{-/-}$) in NX/NG. $^{*/\&}p \le 0.05$, $^{**/\&\&}p \le 0.01$, $^{***/\&\&\&}p \le 0.001$, $^{****/\&\&\&\&}p \le 0.0001$

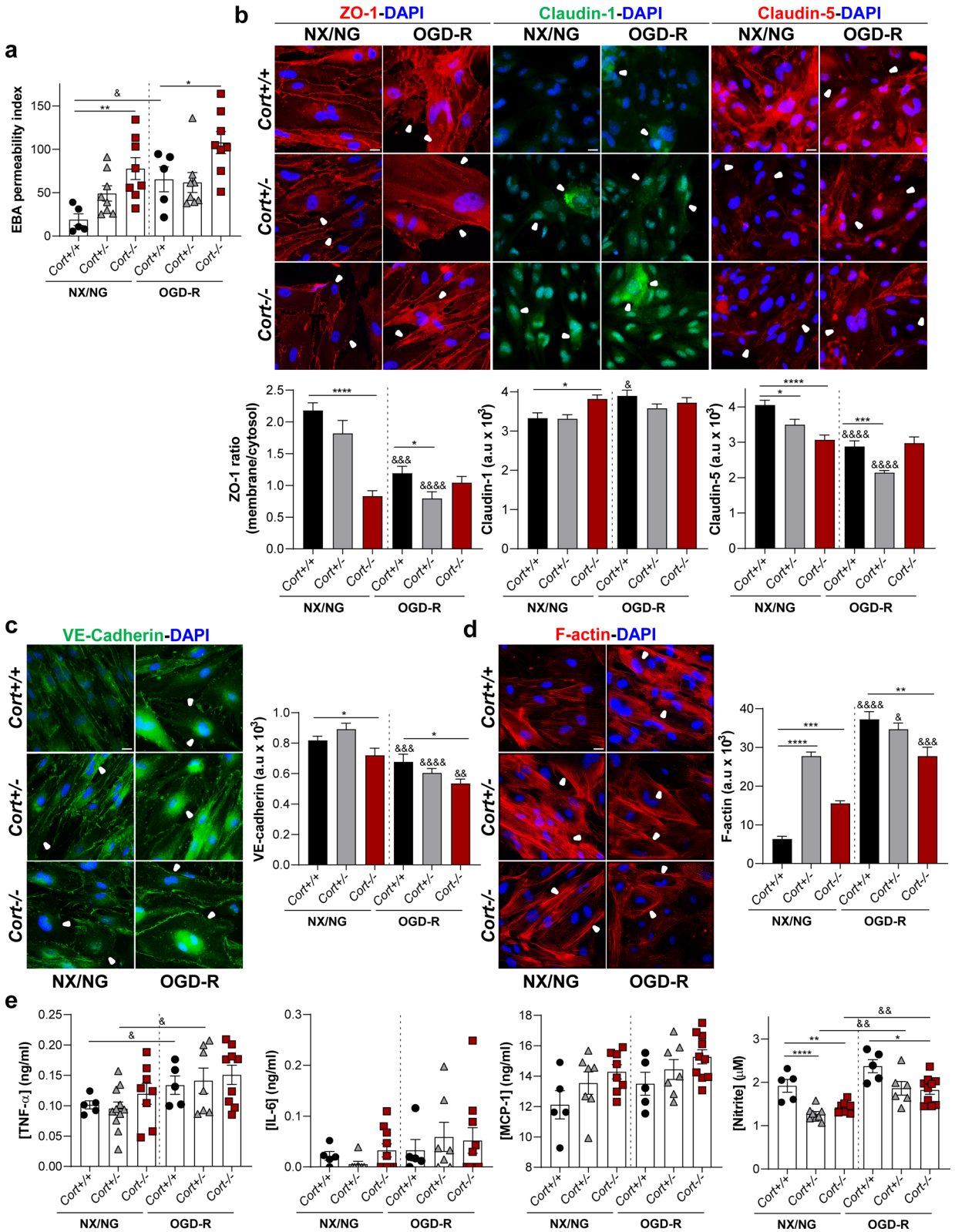

Fig. 4 (See legend on previous page.)

VEGF and TGF-β, among others), endothelial cell fate commitment, and endothelium-dependent cell adhesion and migration, were similarly affected by both conditions (Fig. 5c, f; Additional file 1: Fig. S8, Additional file 2: Tables S5, S6). These results indicate that the lack of cortistatin seems to induce downregulated pathways affecting both normal brain endothelium processes and injured-endothelium responses. To investigate the possible dysfunctional phenotype of brain endothelium from mice with cortistatin deficiency under physiological conditions, we compared the transcriptional programs associated with the progression from a healthy (NX/NG) to an injured state followed by reoxygenation (OGD-R), for both $Cort^{+/+}$ and $Cort^{-/-}$ BECs. Our results revealed that 83 genes (48 upregulated and 35 downregulated) were differentially expressed in wild-type cells when driving the transition from NX/NG to OGD-R (Fig. 6a, b; Additional file 2: Table S7).

Noteworthy, resulting GO terms revealed that upregulated DEGs found in $Cort^{+/+}$ BECs under OGD-R were positively associated with gene networks modulating endothelial injury responses (Fig. 6c; Additional file 1: Fig. S9a, Additional file 2: Table S9). Remarkably, these pathways were not only related to the deleterious response to damage, but also to several processes aimed at a later balanced repair response, such as the immune regulation of leukocyte migration, the response to immune mediators, the remodelling of the extracellular matrix and cytoskeleton, the regulation of angiogenesis and wound healing processes, and the activation of protective stress responses (Fig. 6c; Additional file 1: Fig. S9a). Surprisingly, in the dynamics of $Cort^{-/-}$ BECs from NX/NG to OGD-R, only 20 differentially expressed genes (3 upregulated and 17 downregulated) were identified in the transition from a healthy state to an ischemic and reperfusion context (Fig. 6d, e; Additional file 2: Table S8). In this case, the genes were predominantly involved in downregulated networks associated with the response to damage (Fig. 6f; Additional file 1: Fig. S9b, Additional file 2: Table S10).

Next, we performed a more detailed examination of the DEGs conforming these pathways based on their $\log_2$ fold change and their biological relevance to brain endothelial function (Additional file 2: Table S11). Analysis of the extracellular matrix (ECM) remodelling cluster (Fig. 7a), revealed that most of the genes encoding collagens and other ECM components, metalloproteinases inhibitors, metallopeptidases as well as genes regulating actin cytoskeleton dynamics, among others, were downregulated in the basal (NX/NG) and injured (OGD-R) brain endothelium when cortistatin was absent.

Notably, additional genes related to ECM remodelling, i.e., *Col1a2, Col6a3, Lama2, Mmp2, Mmp19, Timp2*, *Carmil1,* and *Cracd,* and to cytoskeleton disassembly, *Arhgap28* and *Cobl* were downregulated and upregulated, respectively, in cortistatin-deficient BECs only under NX/NG (Fig. 7a). On the contrary, the matrix components *Col5a3, Col15a1* and *Has2* (hyaluronic acid), the metalloproteinases *Mmp3, Mmp10* or *Mmp28* and the metalloproteinase inhibitor *Timp1* were upregulated in $Cort^{+/+}$ cells under OGD-R conditions, following the canonical response to damage and recovery (Fig. 7a). However, in $Cort^{-/-}$ cells during the progression from NX/NG to OGD-R, none of these or related genes demonstrated differential expression. In addition, several genes involved in cell adhesion/migration, as well as some integrins, were downregulated during NX/NG and OGD-R in cortistatin-deficient cells compared to wild-type endothelium (Fig. 7b). Of note, *Itga3* and *Itga4*, involved in the chemoattraction and activation of immune cells, were upregulated in the absence of cortistatin (Fig. 7b).

Furthermore, we observed that genes linked to BBB dynamics were affected. We found that many master regulators of angiogenesis vascular remodelling pathways, as well as genes involved in vasoregulation, were already downregulated in $Cort^{-/-}$ BECs under NX/NG and some

(See figure on next page.)

Fig. 5 Cortistatin-deficient brain endothelium shows deregulated gene pathways. Comparison of gene expression profiles from BECs isolated from $Cort^{+/+}$ vs $Cort^{-/-}$ mice cultured as described in Fig. 2a. Each biological replicate (Rep) was pooled from 3 mice per genotype. **a, d** Volcano plots illustrate differentially expressed genes (DEGs) from $Cort^{-/-}$ vs $Cort^{+/+}$ BECs incubated under NX/NG for 24 h (**a**) or under 4 h oxygen–glucose deprivation followed by 20 h reoxygenation (OGD-R) (**d**). Each dot represents one gene. Grey dots represent not significantly altered genes. The number of enriched (up, red) and decreased (down, blue) genes (with false discovery rate, FDR, $p < 0.05$) for cortistatin-deficient BECs is shown in the legend. Full description of DEGs is in Additional file 2: Tables S3 and S4. **b, e** Heatmaps and unsupervised hierarchical clustering of 613 DEGs (**b**) and 407 DEGs (**e**) in $Cort^{-/-}$ vs $Cort^{+/+}$ BECs exposed to NX/NG and OGD-R, respectively. The expression values are represented in shades of red and blue, indicating expression above and below the median value across all samples. **c, f** Gene ontology (GO) terms for biological processes significantly overrepresented in $Cort^{-/-}$ vs $Cort^{+/+}$ BECs incubated under NX/NG (**c**) or OGD-R (**f**). Data were grouped into similar gene sets and manually annotated into several networks, such as immune response, cellular matrix and remodelling, cell signalling and transcription, cell fate, brain endothelium dynamics, cell adhesion and migration, and cell metabolism. Red and blue bar-segments correspond to the numbers of upregulated and downregulated DEGs, respectively. All DEGs for each GO term are listed in Additional file 2: Tables S5 and S6. TGF-β, transforming growth factor beta; ECM, extracellular matrix; MAPK, mitogen-activated protein kinase; ERK, extracellular-signal-regulated kinase; VEGF, vascular endothelial growth factor; PDGFRβ, platelet-derived growth factor receptor beta; EMT, epithelial to mesenchymal transition

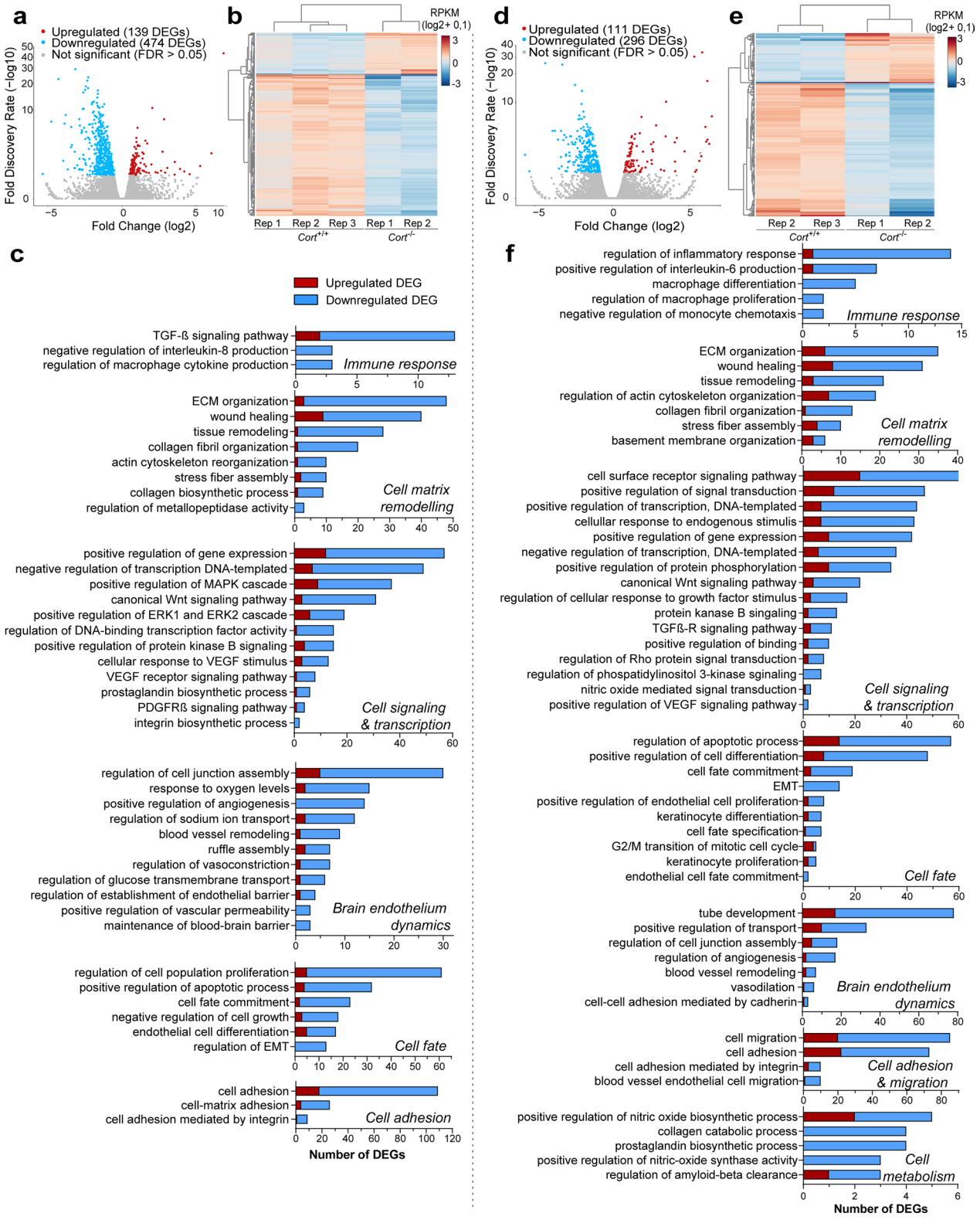

Fig. 5 (See legend on previous page.)

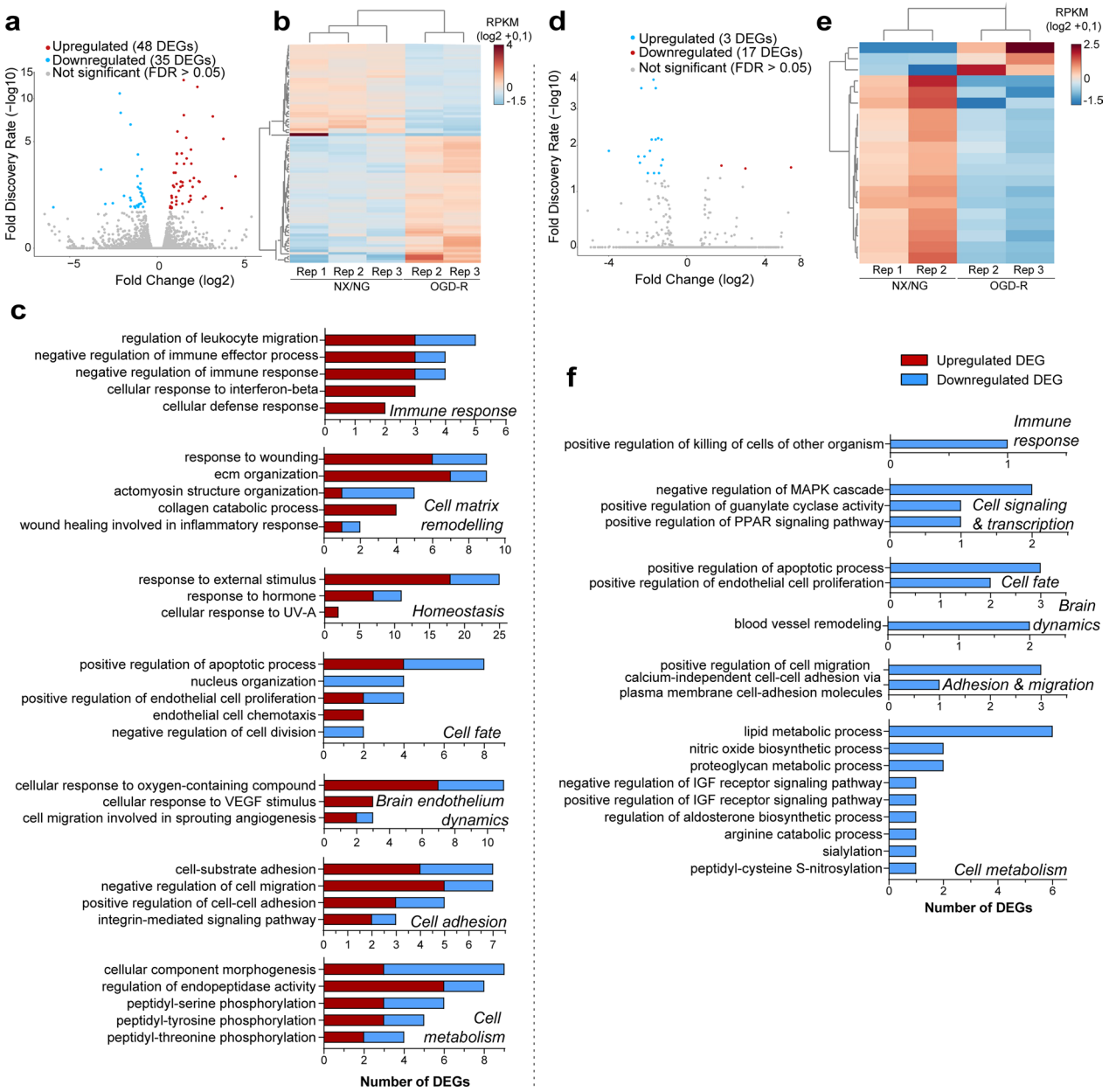

Fig. 6 Gene networks regulating brain endothelium dynamics are affected by the lack of cortistatin. Comparison of gene expression profiles in the dynamics from the basal (NX/NG) to ischemic and repairing (OGD-R) states in *Cort*$^{+/+}$ and *Cort*$^{-/-}$ BECs. Each biological replicate (Rep) was pooled from 3 mice per genotype. **a**, **d** Volcano plots illustrating DEGs between BECs incubated under NX/NG for 24 h and BECs exposed to 4 h oxygen–glucose deprivation and 20 h reoxygenation (OGD-R) from *Cort*$^{+/+}$ (**a**) or *Cort*$^{-/-}$ (**d**). Each dot represents one gene. Grey dots represent not significantly altered genes. The number of enriched (up, red) and decreased (down, blue) genes (FDR, $p < 0.05$) for OGD-R-derived BECs is shown in the legend. Full description of DEGs is in Additional file 2: Tables S7 and S8. **b, e** Heatmaps and unsupervised hierarchical clustering of 83 DEGs (**b**) and 20 DEGs (**e**) in BECs exposure to NX/NG vs OGD-R in *Cort*$^{+/+}$ and *Cort*$^{-/-}$, respectively. Expression values are represented in shades of red and blue, indicating expression above and below the median value across all samples. **c, f** GO terms for biological processes significantly overrepresented in BECs incubated under NX/NG vs OGD-R from *Cort*$^{+/+}$ (**c**) and *Cort*$^{-/-}$ (**f**) mice. Data were grouped into similar gene sets and manually annotated into several networks, such as immune response, cellular matrix and remodelling, homeostasis, cell signalling and transcription, cell fate, brain endothelium dynamics, cell adhesion and migration, and cell metabolism. Red and blue bar-segments correspond to the numbers of upregulated and downregulated DEGs, respectively. All DEGs for each GO term are listed in Additional file 2: Tables S9 and S10. *VEGF* vascular endothelial growth factor, *ECM* extracellular matrix, *MAPK* mitogen-activated protein kinase, *PPAR* peroxisome proliferator-activated receptor

also reduced after OGD-R (Fig. 7b, c). Moreover, some genes related to the integrity of the BBB were downregulated in *Cort*$^{-/-}$ BECs under NX/NG, OGD-R or both conditions (Fig. 7c). On the contrary, only a few pro-angiogenic genes such as *Srpx2, Stab1* or Notch-dependent *Pcdh12* were upregulated. Interestingly, genes linked to BBB breakdown and TJ destruction [27, 32, 33] were upregulated during OGD-R (*Cldn4, Cldn6*, *Cldn9*, *Cdh1*, *Mylk*, and *Myh14*) or even in the physiological state of the cortistatin-deficient brain endothelium (*Cldn1* and *F11r*) (Fig. 7c, h).

In addition, we observed that the absence of cortistatin induced a marked downregulation of factors that affect endothelial proliferation and differentiation, as well as those associated with apoptosis and the promotion of cell survival (Fig. 7d). Furthermore, genes related to DNA damage were upregulated. Interestingly, some genes linked to cell cycle such as *Chmp4c* and *Ticrr* were also upregulated (Fig. 7d).

Some of these genes, required to the response to damage (*Casp12, Egr1, Fos* and *Nr4a1*) [34], were upregulated in the dynamic transition from NX/NG to OGD-R for *Cort*$^{+/+}$ BECs, whereas none of them showed changes in the same process in endothelium lacking cortistatin (Fig. 7d, g).

Moreover, we detected that the network involving BBB transporters, crucial for metabolic and ionic endothelial homeostasis, was downregulated in the absence of cortistatin in both, control and injury conditions (Fig. 7e). On the contrary, *Slco4a1* and *Atp8a1*, detrimental to brain connectivity when elevated [35, 36], were upregulated in *Cort*$^{-/-}$ BECs in basal and injured states (Fig. 7e).

Regarding genes involved in immune pathways, our results revealed that factors linked to an anti-inflammatory, immunoregulatory and protective response, were downregulated in *Cort*$^{-/-}$ cells in NX/NG, OGD-R or both (Fig. 7f). On the contrary, upregulated genes in both physiological and injured *Cort*$^{-/-}$ cells included *Ccl9*, *Il16*, *Lcp1*, *Cd93*, *Itga3* and *Itga4* integrins, and *Ulbp1*, all related to activation and chemoattraction of immune cells (Fig. 7f). However, genes required for the inflammatory-driven repair response, such as *Il33*, *Egr1*, *Gbp2, Gbp3* and *Il11,* were only upregulated in *Cort*$^{+/+}$ cells after OGD-R conditions (Fig. 7f). None of these DEGs affecting immune pathways showed significant expression differences in *Cort*$^{-/-}$ BECs during the progression from physiological to OGD-R states.

Notably, some hypoxia-dependent responsive genes with neuroprotective roles (such as *Egr1, Nr4a1, Fos, Gbp2, Mmp3, Spp1*, and *Nr1d1*) [34] were only upregulated in wild-type endothelium after ischemia and reperfusion (Fig. 7d, f, g). Instead, some of them (*Egr1, Nr4a1* and *Spp1*) were downregulated not only after OGD-R but also under NX/NG conditions in the absence of cortistatin (Fig. 7f, g). Similarly, genes whose expression regulates radical oxygen species formation were downregulated in *Cort*$^{-/-}$ BECs even under NX/NG (Fig. 7g). Except for *Nos2* downregulation, none of these genes showed differential expression in *Cort*$^{-/-}$ BECs dynamics from the healthy to the injured state. Intriguingly, we observed gene markers for epithelial cells (*Epcam*) and the keratinization process (Fig. 7h) among the top 25 upregulated DEGs in cortistatin-deficient brain endothelium incubated under OGD-R.

According to all these results, we observed that many components of crucial signalling networks involved in regulating endothelial cell biology were downregulated in the absence of cortistatin under physiological conditions (i.e., genes involved in the regulation of Wnt, MAPK, TGF-β and Notch pathways) (Fig. 7i). In addition, various growth and transcription agents relevant for endothelium homeostasis were also downregulated in *Cort*$^{-/-}$ BECs in NX/NG environment (Fig. 7h, i). Moreover, some kinases (*Mapk6, Ntrk3, Ddr2*) and phosphatases (*Ptprk*) were dysregulated in the absence of cortistatin. Conversely, some factors (*Igf1, Sox17, Pdgfb, Pdgfra*) were upregulated in physiological *Cort*$^{-/-}$ cells, probably as a compensatory effect. Although some of the above-mentioned genes were also reduced in *Cort*$^{-/-}$ BECs under OGD-R (Fig. 7i), none of them showed differences in the transition from a basal to an injured state neither in wild type nor in cortistatin-deficient cells.

Together, these results indicate that the lack of cortistatin induced downregulated gene networks not only in damaged but also in uninjured cells isolated from cortistatin-deficient mice. Besides, while *Cort*$^{+/+}$ BECs

(See figure on next page.)

Fig. 7 Transcriptional alterations in cortistatin-deficient brain endothelium. Gene sets for *Cort*$^{+/+}$ and *Cort*$^{-/-}$ BECs displayed in Figs. 5 and 6 were manually annotated into gene modules relevant for key BBB features and functions: **a** extracellular matrix components; **b** cell–cell contact mediators; **c** BBB dynamics; **d** cell fate agents; **e** endothelial transporters; **f** immune response; **g** response to oxygen; **h** others, (genes with the highest fold change from different categories); and **i** signalling pathways. Differential expression patterns of selected DEGs modulated by the lack of cortistatin are represented in each module based on criteria defined in the legend box. Genes that do not have significant expression changes are displayed by a white box. Relative fold change expression (log_2FC) in each experimental group is shown by shades of red (upregulated) and blue (downregulated). *MMPs* matrix metalloproteinases, *TFs* transcription factors, *Aa* amino acids, *LDL* low density lipoprotein, *MAPKs* mitogen-activated protein kinases

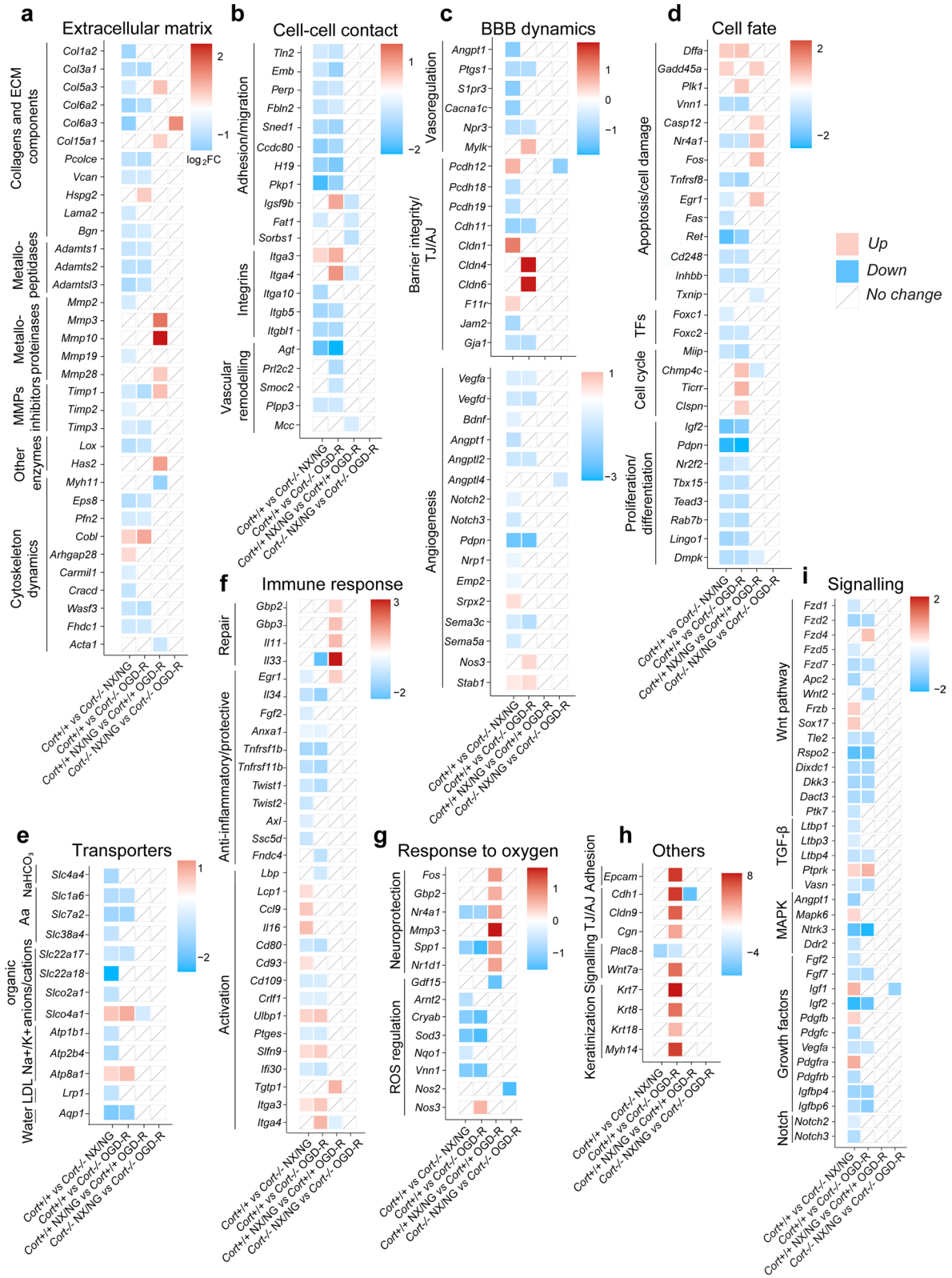

Fig. 7 (See legend on previous page.)

appeared to achieve a canonical balanced response to damage upregulating genes linked to a further recovery response, these pathways were impaired in *Cort*$^{-/-}$ BECs.

Treatment with cortistatin protects brain endothelium integrity, regulates junction assembly and reverses immune activation

To confirm the role of cortistatin as a controller of brain endothelium dynamics, we next investigated its effect in wild-type and cortistatin-deficient BECs. We showed that the addition of exogenous cortistatin after OGD and simultaneously to reoxygenation, in both control and cells with partial or complete absence of cortistatin, induced significant reduction in damage-derived endothelial permeability (Fig. 8a; Additional file 1: Fig. S10) that was coupled to the recovery of barrier permeability and of the functional intercellular architecture of the endothelium (Fig. 8b, c). This was demonstrated by the induction of the uniform and settled location of ZO-1 and claudin-5 in the peripheral membrane, the increased and solid expression of VE-cadherin, the decreased presence of cytosolic claudin-1, and the physiological reduced and randomised distribution of stress fibers (Fig. 8b, c). Moreover, the dysregulated immune response exerted by the injured endothelium was reversed to homeostatic state by cortistatin treatment (Fig. 8d). Specifically, TNF-α and MCP-1 levels were significantly reduced in *Cort*$^{+/+}$, *Cort*$^{+/-}$ and *Cort*$^{-/-}$ BECs compared to the cytokine levels found in injured cells (Fig. 8d). Interestingly, exogenous cortistatin added to cortistatin-deficient endothelium significantly increased the reduced levels of nitrite after injury (Fig. 8d). Regarding the interaction between disrupted permeability, inflammatory endothelium, and cell migration, we next evaluated whether cortistatin could regulate immune trafficking throughout the wild-type and cortistatin-deficient brain endothelium (Fig. 8e). While transendothelial migration was enhanced in the absence of cortistatin, our results showed that incubation with cortistatin significantly modulated macrophages and T-cell displacement through activated brain endothelium (Fig. 8e).

Despite endothelial cells being the main component of the neurovascular unit, astrocyte end-feet, microglia, pericytes, and other surrounding cells must also play important role in maintaining BBB homeostasis [1]. Following the data shown above, we analysed the potential role of cortistatin in the whole BBB structure. We found that systemic injection of cortistatin reversed the exacerbated leakage observed in wild-type and cortistatin-deficient mice subjected to mild neuroinflammation (Fig. 9). Notably, the lack of cortistatin resulted in enhanced permeability even in the absence of damage.

Altogether, these results suggest that endogenous cortistatin is critical for a healthy brain endothelial barrier and revealed the potential of this anti-inflammatory neuropeptide as a pleiotropic modulator of BBB dynamics.

Discussion

A tightly controlled BBB is essential for a fine-tuned microenvironment in the CNS, and its breakdown has been involved in several brain diseases. Therefore, research based on identifying BBB-related stabilizing factors focused on ECs, as the main BBB component, should be prioritized. To our knowledge, this is the first report to demonstrate the critical role of cortistatin as an endogenous factor in maintaining the integrity and functionality of the brain endothelium. We found that, even at low levels, cortistatin is produced by healthy murine and human brain endothelial cells, undergoing modulation after injury. Specifically, our findings demonstrated that the lack of cortistatin predisposes to endothelium disruption under basal

(See figure on next page.)

Fig. 8 Cortistatin recovers the integrity and function of brain endothelial cells after ischemic-like conditions. **a** Endothelial permeability to EBA was represented as the tracer permeability fold change vs the permeability in OGD-R wild-type BECs (set at 1). *N* = 5–8 cultures/group. **b** Immunofluorescence analysis of cellular distribution for tight/adherens-junctions and stress fibers in wild-type and cortistatin-deficient BECs after OGD-R incubated with cortistatin. Asterisks indicate continuous membrane expression of ZO-1 (red), claudin-5 (red), and VE-cadherin (green), reduced intracellular claudin-1 (green), and random cytosolic F-actin organization (red), when compared to BECs exposed to OGD-R without cortistatin addition (as shown in Fig. 4b–d; schematic images with injury hallmarks represented in the top: Ref-BECs). Scale bar: 20 µm. **c** Quantification of location (ZO-1) and expression (claudin-1, claudin-5, VE-cadherin, F-actin) by fluorescence intensity analysed from 25–50 ROIs in 4 independent fields. *N* = 6 cultures/group. **d** Levels of inflammatory mediators determined in culture supernatants. *N* = 8 cultures/group. **e** *Top*, representation of transendothelial migration assay. Wild-type mice immune cells were incubated for 24 h at the top of *Cort*$^{+/+}$, *Cort*$^{+/-}$, and *Cort*$^{-/-}$ BECs covered inserts, previously activated with TNF-α (10 ng/ml, 24 h). The migration assay was performed using MCP-1 (50 µg/ml) or IP-10 (50 µg/ml), as macrophages and T-cell chemoattractants, respectively. CST (100 nM) was applied when indicated. *Bottom*, data represented the percentage of migrated immune cells vs the control (empty-coated insert). *N* = 4–6 cultures/group. For data in c, d, FC represents fold change vs reference values based on OGD-R wild-type BECs quantification (set at 1). *Cort*$^{+/+}$ BECs in NX/NG are also used as a basal condition reference (dashed line). Data are the mean ± SEM with dots representing individual values of independent cultures. Cells in each culture were derived from 4 pooled brains. *vs *Cort*$^{+/+}$ BECs exposure to OGD-R + CST; $^{\#}$vs BECs of corresponding genotype (*Cort*$^{+/+}$, *Cort*$^{+/-}$, *Cort*$^{-/-}$) exposure to OGD-R.$^{*/\#}p \le 0.05$, $^{**/\#\#}p \le 0.01$, $^{***/\#\#\#}p \le 0.001$, $^{****/\#\#\#\#}p \le 0.0001$

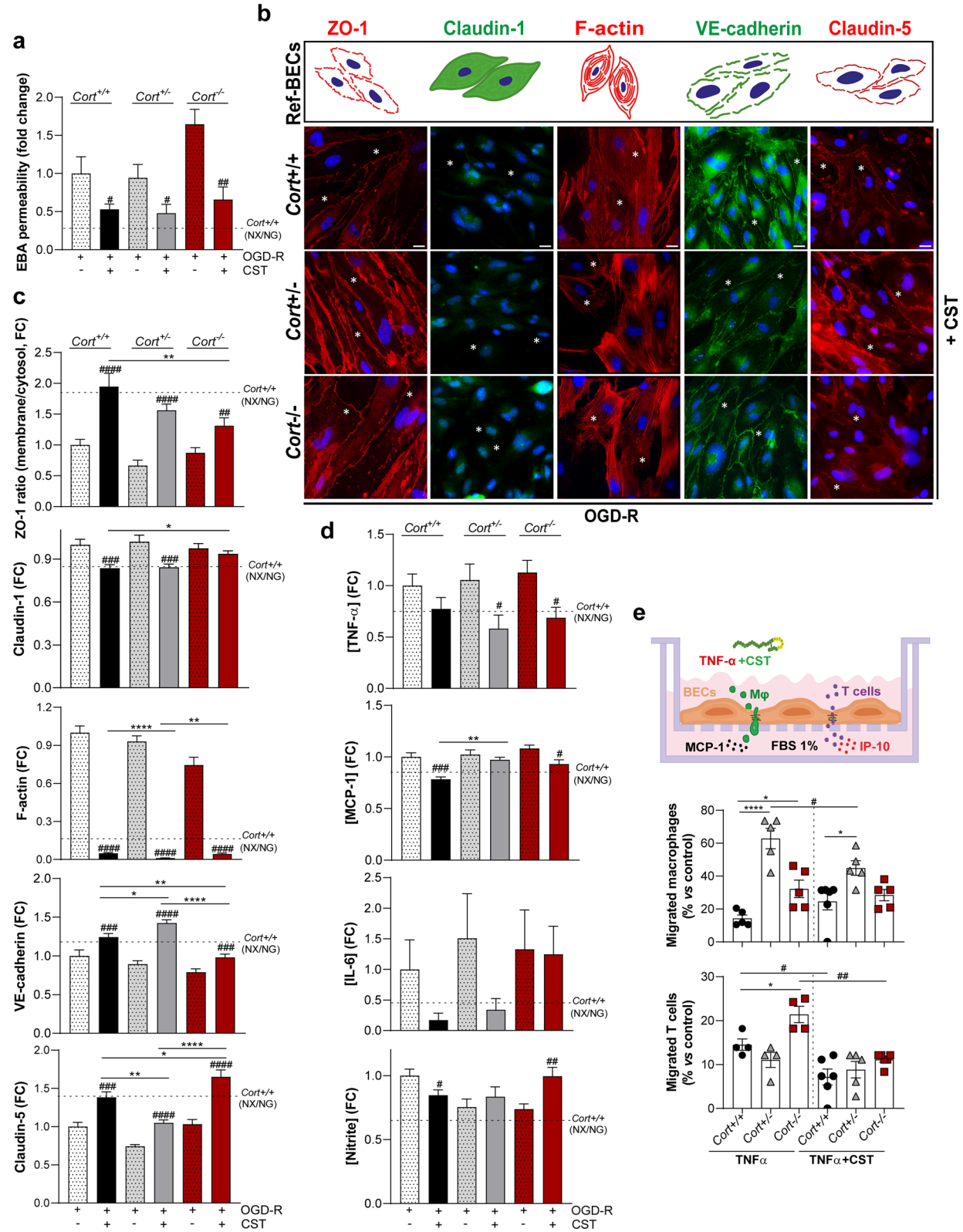

Fig. 8 (See legend on previous page.)

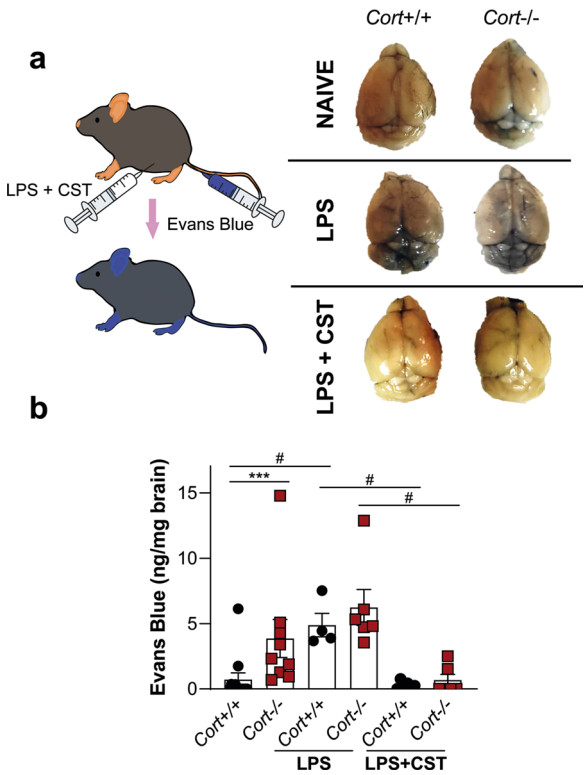

Fig. 9 Administration of cortistatin reduces exacerbated murine brain endothelial barrier breakdown. **a** *Left*, wild-type and cortistatin-deficient mice (1 year) were injected intraperitoneally with LPS (6 mg/kg) for 6 h. Evans-Blue (2% in PBS) was injected through the tail vein 1 h before sacrifice. Cortistatin (1 nmol, in PBS) was intraperitoneally administered immediately after LPS. Control mice were injected with PBS as vehicle. *Right*, representative images show EB brain extravasation. **b** Brains were collected and minced in *N*,*N*-dimethylformamide at 55 ºC for 24 h. Supernatants were collected and EB content (ng/mg brain) was measured on a spectrophotometer at 620 nm. Data are the mean ± SEM with dots representing individual mice ($n = 4$–8/group). $^{*}p \leq 0.05$, $^{**}p \leq 0.01$

conditions (Fig. 10). Notably, we observed that brain ECs isolated from heterozygous cortistatin mice, which secrete significant lower levels of cortistatin, exhibited phenotypic changes resembling those observed in wild-type endothelium after damage, where the levels of endogenous cortistatin are diminished. In addition, the breakdown of the brain endothelium from cortistatin-deficient mice was exacerbated after exposure to an ischemic-like context. Interestingly, the exogenous addition of cortistatin reversed hallmark features of the disturbed endothelium, such as intercellular junction instability, increased paracellular and transendothelial permeability, and dysregulated endothelial immune activity (Fig. 10). Based on these findings, we propose the involvement of various non-excluding and complementary mechanisms that could explain the role of cortistatin in BBB stability.

Regarding brain barrier integrity, numerous studies have demonstrated that disturbances in the content, cellular distribution, and/or post-translational modifications of TJs and AJs in ECs, increase BBB abnormalities and initiate neurodegenerative diseases [1, 37]. Recently, in addition to the well-known roles of TJs and AJs in organizing cell architecture, polarity, and cell–cell contacts, other non-canonical functions, including cell proliferation, differentiation, participation in angiogenesis and inflammatory processes, and regulation of gene expression, have also been demonstrated [4, 38]. Accordingly, we found an induction of hyperpermeability in the endothelium lacking cortistatin, which was probably accompanied by the alteration of both barrier and non-barrier roles of the TJ/AJs. In particular, the expression of some TJ/AJ genes (*Jam2, Gja1, Pcdh18, Pcdh19, Cdh11*) crucial for connecting adjacent ECs [3, 39], was down-regulated. On the contrary, levels of *Cldn1, Cldn4, Cldn6, Cldn9, Cgn, F11r,* and *Cdh1*, associated with exacerbated inflammation, perturbation of the TJ assembly [27, 40], and even with mesenchymal transformation or tumour progression [41, 42], were overexpressed. Importantly, cortistatin deficiency altered protein levels and cell distribution of ZO-1, claudin-1, claudin-5, and VE-cadherin, without significantly affecting their transcript levels. In fact, different studies have shown that while different insults may not impact TJ expression, they can affect their cellular redistribution and functional organization. For instance, ZO-1 translocation from the membrane out to the cytosol, without alterations in its expression, affected barrier integrity and resulted in TJ disorganization [43].

On the other hand, although controversial findings about the role of claudin-1 have been reported [40, 44, 45], several studies indicate that claudin-1 increases in the disrupted endothelium, affects claudin-5 assembly, and its cytosolic accumulation has been correlated with TJ arrangement deficits and limited full recovery of the barrier [27, 46]. In addition, emerging evidence suggests that claudin proteins can localize to sites outside of the tight-junction complex. Indeed, claudin-1 seems to be representative of claudins that shuttle between the cytoplasm and nucleus, acquiring non-canonical functions, including cell proliferation, differentiation, participation in angiogenesis and inflammatory processes, and regulation of gene expression [38, 47]. In fact, reducing claudin-1 was beneficial for modulating BBB permeability and endothelial inflammatory phenotype [27]. Therefore, the disruptive expression of ZO-1, VE-cadherin, and claudin-5, along with the cytosolic overexpression of ZO-1 and claudin-1 in cortistatin-deficient ECs

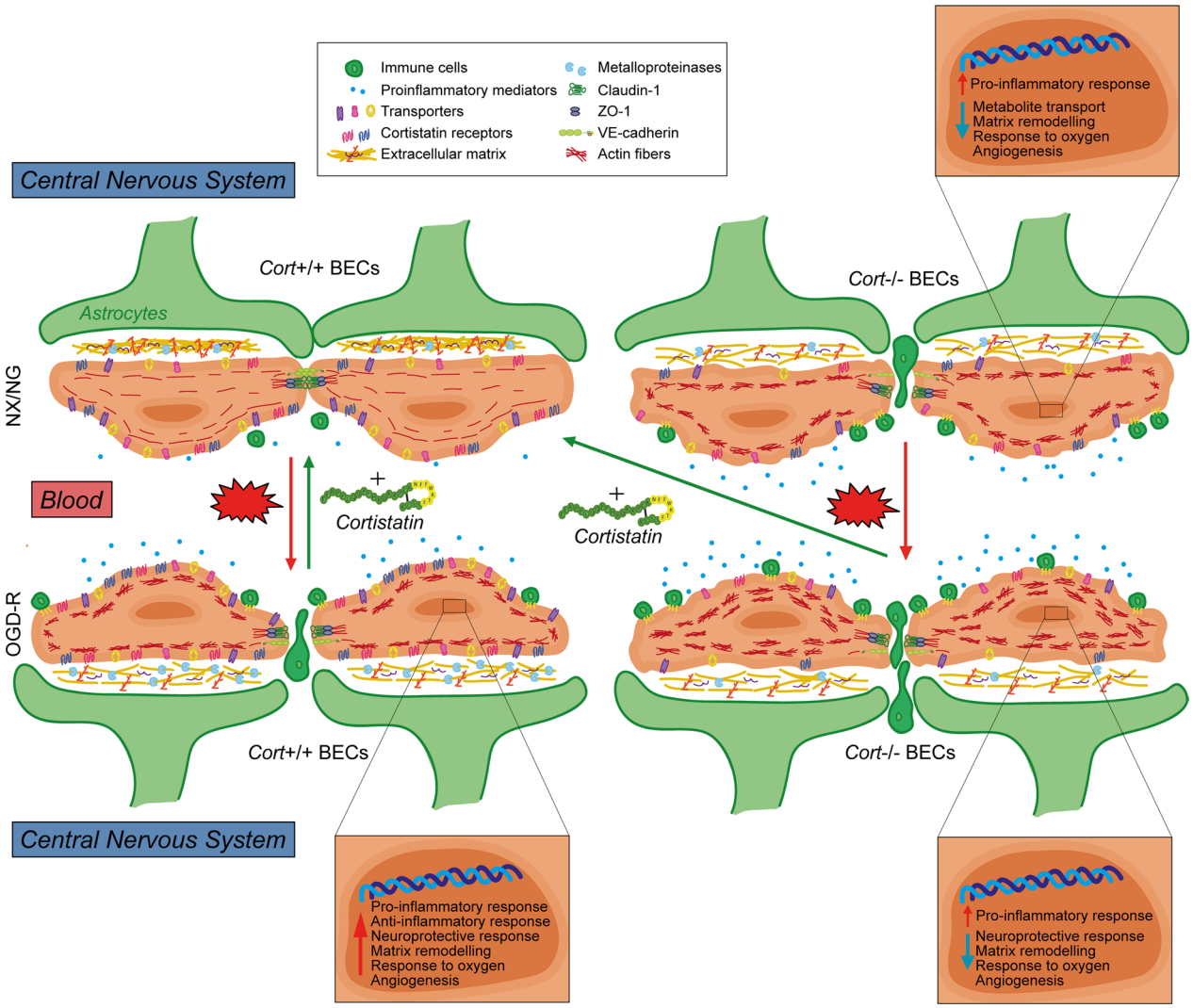

Fig. 10 Schematic illustration of the proposed role of cortistatin in regulating physiology and pathology of brain endothelium. *Top left, Cort*$^{+/+}$ BECs under normoxia/normoglycemia (NX/NG) conditions showing homeostatic endothelial barrier integrity. *Bottom left,* after oxygen–glucose deprivation and reoxygenation (OGD-R) to mimic ischemic damage (red arrow), *Cort*$^{+/+}$ BECs suffered a canonical response (i.e., tight-junctions disruption, immune cell infiltration, proinflammatory mediators release, reorganization of actin in stress fibers, and ECM remodelling), combined with upregulation of protective and reparative transcriptional mechanisms (e.g., anti-inflammatory response or angiogenesis) (zoom for details). Remarkably, these changes were reversed with cortistatin treatment (green arrow). *Top right, Cort*$^{-/-}$ BECs in NX/NG conditions presented similar phenotypic changes to *Cort*$^{+/+}$ BECs in OGD-R (except for a decrease in the number of transporters and cortistatin receptors), but a different genetic programming (i.e., exacerbated immune response, deregulated ECM remodelling, and downregulation of angiogenesis and protective pathways related to the response to damage) (zoom for details). *Bottom right,* after exposing *Cort*$^{-/-}$ BECs to OGD-R (red arrow), almost no significant transcriptional changes were observed when compared to *Cort*$^{-/-}$ BECs in NX/NG. However, downregulation of metabolites transporters, exacerbated stress fiber formation, and increased immune activity was found. Cortistatin reverted these changes up to physiological conditions (*top left*, green arrow)

(Fig. 10), in both injury and physiological conditions, emphasizes the relevance of this neuropeptide in maintaining a properly sealed and healthy barrier. In addition, TJs also regulate the distribution of enzymes and receptors in the luminal and abluminal membrane domains [39, 48]. Indeed, the disruption of junctional proteins in the absence of cortistatin was accompanied by the loss of cell polarity and downregulation of several transporters involved in endothelial metabolic support (Fig. 10), which can also have a negative impact on BBB permeability [1].

Furthermore, TJs are connected to actin cytoskeleton through intracellular proteins, providing a dynamic organization of actin filaments, crucial for BBB integrity.

In this sense, the reorganization of actin filaments into stress fibers is often associated with TJ instability, endothelial barrier dysfunction, and hyperpermeability [49]. In addition to TJ disruption, endothelium from cortistatin-deficient mice also exhibited an increase in F-actin stress fiber formation, which was correlated with a marked cytoskeletal disassembly in both uninjured and injured conditions (Fig. 10). In this context, both hyperpermeability and cytoskeleton disorganization in the absence of cortistatin may be linked to some dysregulated pathways involving kinases/phosphatases (such as *Mapk6, Dmpk, Ntrk3* and *Ptprk*), which have been described as crucial regulators of TJ/AJs organization/dissociation [50].

Moreover, ECM plays a key role in maintaining BBB dynamics. Alterations in ECM can result in BBB leakage, as evidenced by the decreased expression of certain ECM components, such as collagens and laminins, in aged mice [2]. Besides, mutations in genes related to collagens have been associated with leaky vessels that predispose to haemorrhage in humans [51]. Notably, we observed that the majority of genes involved in ECM composition were downregulated in cortistatin-deficient endothelium. Besides its physical and mechanical properties, ECM is crucial for matrix-cell and cell–cell signalling, with integrins complexes acting as the main receptors. An unbalanced ratio of ECM components and/or dysfunction of integrins can lead to BBB abnormalities as multiple endothelial functions are affected (survival, migration, differentiation, and cell adhesion) [52]. Alternatively, ECM components undergo alterations and modifications driven by matrix metalloproteinases (MMPs) and metallopeptidases, which are necessary to induce angiogenesis and vascular remodelling after injury [53, 54]. In this regard, while wild-type endothelial cells exhibited a canonical balanced response to damage by upregulating the pathways linked to recovery (including ECM reorganization, angiogenesis, cell fate determination, and response to hypoxia), these responses were impaired in $Cort^{-/-}$ BECs (Fig. 10).

Unexpectedly, we found high expression of the epithelial markers *Krt7, Krt8*, *Krt18*, *Cdh1,* and *Epcam* in cortistatin-deficient BECs. These are signature genes for choroid plexus epithelial cells [55], which can contaminate primary isolates of brain microvascular ECs. However, differentially increased expression of these factors was only identified in the cortistatin-deficient injured endothelium. This finding suggests that endogenous cortistatin may play a role in promoting endothelial cell determination over an epithelial-like fate. Indeed, regulatory factors of endothelial cell fate specification were downregulated in the endothelium lacking cortistatin. Confirming this, recent data also demonstrated an endogenous role for cortistatin as a controller of tissue-specific cell commitment in fibrogenic responses [56].

On the other side, it has been described the participation of IL-6, TNF-α, and MCP-1 in the loss of BBB integrity, stress fiber formation, TJ remodelling, and immune cell infiltration (reviewed in [57, 58]). Our data revealed a dysregulated immune response in the brain endothelium lacking cortistatin, characterized by the production of inflammatory factors, enhanced immune cell migration, inhibited immunoregulatory and restorative pathways, and upregulated integrin signalling. Despite other studies found high levels of peripheral glucocorticoids in cortistatin-deficient mice [7, 11], suggesting an immune suppressive phenotype in these animals, in this study the inflammatory phenotype of CST-deficient cells suggests that none of the protective effects associated with glucocorticoids are observed in this context. In fact, *Anxa1*, a glucocorticoid-induced endothelial factor correlated with BBB disruption [59], was downregulated in the absence of cortistatin.

Surprisingly, we observed reduced nitrite levels in $Cort^{-/-}$ BECs. Nitric oxide has been associated with both protective and deleterious effects, but recent reports have confirmed that insufficient availability of endothelial nitric oxide leads to endothelial dysfunction [60]. Importantly, the balance between the activities Nos2 and Nos3, along with the scavenging function of the superoxide anion, can regulate nitric oxide levels [60]. Future studies will address whether these pathways can be cooperating to reduce nitric oxide when cortistatin is absent.

Besides this, from a molecular perspective, our study revealed the downregulation of several gene networks involved in matrix remodelling, cytoskeleton architecture, junctions assembly, endothelial commitment, and immune activity (reviewed in [4]) in cortistatin-deficient mice (Fig. 10). Among the affected pathways, we identified VEGF-VEGFR2-Nrp1, TGF-β-Nrp1 and Notch signalling (all essential for angiogenesis), Wnt pathway (critical for BBB maturation and barriergenesis), Ang1/Tie2 interaction (essential for stabilizing TJs), and semaphorins signalling (key in cerebral vasculature growth and BBB functions). Although further research is needed to investigate the specific contribution of cortistatin in each network, our results provide support for the key role of endogenous cortistatin in the fine regulation of these interconnected pathways. Moreover, we found that several markers of neurodegeneration and aging (*Capn11, Eno1b, Cmpk2, Galnt3,* and *Ubiad1*, among others) were upregulated in cortistatin-deficient endothelium. Recently, the impact of normal ageing on BBB integrity and plasticity has been demonstrated [61]. Beyond ageing, other biological processes, such as sleep behaviour, can influence BBB functions [62, 63]. In this sense,

cortistatin has been identified as a crucial regulator of sleep homeostasis through activity-dependent BDNF [64, 65]. Interestingly, we found a decreased expression of *Bdnf* in cortistatin-deficient brain endothelium, supporting a link between BDNF, cortistatin and sleep physiology.

Finally, from a therapeutic point of view, our results suggest that the beneficial role of cortistatin could be exerted on brain endothelial cells in an autocrine/paracrine manner. While protective effects of somatostatin, ghrelin, and receptors-agonists in the endothelium have been reported [24, 26, 66], controversial findings regarding the pro- and anti-angiogenic properties of ghrelin [24, 67] and somatostatin-induced hyperpermeability have been observed [68]. However, similar studies have never been conducted with cortistatin. As previously described, cortistatin can exert many different physiological roles compared to somatostatin and ghrelin [7, 8, 69]. The activation of somatostatin/ghrelin receptors can trigger diverse signalling pathways [70–72]. Probably, the potential capability of cortistatin to synergistically signal through somatostatin/ghrelin receptors (in addition to a yet unknown-specific receptor) could imply an advantage vs the individual regulation of the BBB by somatostatin/ghrelin. Specifically, while somatostatin inhibits cAMP accumulation, cortistatin has been reported to stimulate it [73]. Interestingly, increased levels of cAMP are associated with greater endothelial TJ integrity [74], cytoskeleton and actin filaments stabilization, reinforcement of cell–matrix interactions [75], and anti-inflammatory actions [8, 76]. Besides, evidence supports that cortistatin promotes peripheral protective vascular responses after injury via somatostatin/ghrelin receptors, by inducing cAMP and inhibiting calcium rise [15]. In addition, it was described that the combined activation of SSTR5 and ghrelin receptor greatly increased cAMP accumulation, suggesting intracellular signal convergence and/or receptors interaction [77]. In our study, we found that *Sstr4* and *Sstr2* were differentially regulated comparing wild-type and cortistatin-deficient cells in physiological and pathological conditions. While future experiments would be necessary to characterize cortistatin-induced intracellular pathways, we advocate that the binding of cortistatin to these receptors might be regulating brain endothelium integrity. Alternatively, since somatostatin and ghrelin receptors are involved in the immunoregulatory activity of cortistatin [5], we cannot discard that the anti-inflammatory properties of cortistatin can be contributing to the protection of barrier integrity. Altogether, our results showing the efficient recovery of endothelium integrity after cortistatin treatment, support the capacity of this neuropeptide to directly limit injured ischemic-like responses. However, considering the in vivo protective effects of cortistatin on BBB leakage, and the expression of cortistatin and its receptors [11] in other BBB components (i.e., astrocytes, pericytes, and microglia), we can hypothesize that cortistatin might also influence brain endothelium dynamics through other glial cells. Moreover, we cannot discard that BBB-penetrating peripheral factors from cortistatin-deficient mice and/or surrounding cells lacking cortistatin could have influenced and determined endothelial cell phenotype.

In conclusion, our study contributes to the evolving understanding of the BBB as a highly dynamic and plastic structure that allows communication between the blood and the CNS, rather than being the traditionally considered impermeable wall [78]. We recognize that neurodegenerative/neuroinflammatory disorders, such as stroke, multiple sclerosis, or Alzheimer´s disease, often present acute, subacute, and chronic phases with different grades of BBB permeability. Therefore, it is crucial to consider approaches that finely modulate permeability alterations beyond simplistic categorizations of BBB opening or closing as solely "good" or "bad". In this sense, our models not only focus on the pathological and acute event of ischemia but also considered subsequent responses leading to repair and recovery during reoxygenation. In this regard, our study has several implications. From a physiological point of view, we uncovered a new role for endogenous cortistatin in maintaining BBB physiological functions and in recovering integrity after injury. Moreover, our findings emphasize the essential interplay between signals from the CNS and the periphery, exemplified by endogenous modulation of cortistatin levels, for maintaining a healthy BBB. We have shown for the first time that BBB is markedly impaired in the brains of cortistatin-deficient mice, which makes them susceptible to further disruptive changes. Indeed, lack of cortistatin confers the endothelium a pre-existing dysregulated phenotype, which could lead to a deactivated and/or quiescent non-responding behaviour upon further damage. Alternatively, from a treatment perspective, our findings support the beneficial effect of exogenous cortistatin by rescuing defects in BBB function. Given the scarce number of therapeutic agents available to restore BBB function in neurodegeneration [79, 80], the use of multifactorial agents that target at the same time components of the TJ complex, modulate endothelial permeability at different grades, and control immune dysregulation, looks promising for the treatment and prevention of neuroinflammatory/neurodegenerative disorders. Furthermore, restoring BBB disruption would also address the everlasting challenge of drug delivery to the injured brain, since vascular changes and accumulation of blood-derived toxics often restrict the transport of drugs to the brain [4].

In summary, the data presented in this study underscore the key role of cortistatin as a pleiotropic agent that mediates anti-inflammatory endothelial functions and exerts BBB reparative properties, through organizing endothelial junction proteins and reducing immune exacerbated responses (Fig. 10). Our findings also highlight the brain endothelium as an important but neglected source of molecular targets that should be particularly investigated. Overall, understanding the role of cortistatin in the physiology of the cerebral microvasculature has broader implications for gaining insights into the involvement of BBB disruption in various CNS disorders. The knowledge obtained from this study may contribute to the development of novel therapeutic strategies aimed at preserving BBB integrity and ameliorating CNS pathologies associated with BBB dysfunction.

Abbreviations

AJ	Adherens-junctions
BBB	Blood–brain barrier
BECs	Brain endothelial cells
CNS	Central nervous system
CST	Cortistatin
DEGs	Differential-expressed genes
EBA	Evans blue-albumin
ECs	Endothelial cells
GD	Glucose deprivation
hBLECs	Human brain-like endothelial cells
HPX	Hypoxia
HPX-R	Hypoxia-reoxygenation
IL-6	Interleukin-6
LPS	Lipopolysaccharide inflammation
MCP-1	Monocyte chemoattractant protein-1
NaF	Sodium fluorescein
NX/NG	Normoxia–normoglycemia
OGD-R	Oxygen–glucose deprivation and reoxygenation
SST	Somatostatin
TJ	Tight-junctions
TNF-α	Tumor necrosis factor-alpha
ZO-1	Zonula occludens-1

Supplementary Information

The online version contains supplementary material available at https://doi.org/10.1186/s12974-023-02908-5.

Additional file 1: Extended methods for animals, b.End5 and BECs cells, human BBB model, endothelial permeability assay, immunocytochemistry, determination of inflammatory factors, transendothelial migration assay, in vivo BBB permeability assay, RNA extraction and determination of gene expression, next-generation transcriptome sequencing. **Table S1**. Sequence of primers used for qPCR dynamic array. **Table S2**. Sequence of primers used for real-time PCR quantifications. **Figure S1**. Principal coordinates analysis (PCoA) and unsupervised hierarchical clustering of normalized RNA-Seq data. **Figure S2**. Expression profile of the components of the cortistatin pathway in b.End5 cells. **Figure S3**. Cortistatin modulates the immune function of activated b.End5 cells. **Figure S4**. Expression profile of the components of the cortistatin pathway in murine brain endothelial cells. **Figure S5**. Characterization of cortistatin in human brain endothelium **Figure S6**. Lack of barrier integrity and altered expression profile in cortistatin-deficient cells. **Figure S7**. Analysis of specific markers in BECs and validation of gene expression. **Figure S8**. Characterization of gene pathways in wild type vs cortistatin-deficient brain endothelium. **Figure S9**. Characterization of gene pathways in the dynamics of brain endothelium. **Figure S10**. Cortistatin restores the integrity of injured brain endothelial cells.

Additional file 2: **Table S3**. Differentially expressed genes (DEGs) in $Cort^{-/-}$ BECs in NX/NG compared to $Cort^{+/+}$ BECs. **Table S4**. Differentially expressed genes (DEGs) in $Cort^{-/-}$ BECs in OGD-R compared to $Cort^{+/+}$ BECs. **Table S5**. DEGs for NX/NG-incubated $Cort^{-/-}$ vs $Cort^{+/+}$ BECs included in Gene Ontology (GO) terms. **Table S6**. DEGs for OGD-R-incubated $Cort^{-/-}$ vs $Cort^{+/+}$ BECs included in Gene Ontology (GO) terms. **Table S7**. Differentially expressed genes (DEGs) in the dynamics of $Cort^{+/+}$ BECs from NX/NG to OGD-R. **Table S8**. Differentially expressed genes (DEGs) in the dynamics of $Cort^{-/-}$ BECs from NX/NG to OGD-R. **Table S9**. DEGs for $Cort^{+/+}$ BECs from NX/NG to OGD-R included in Gene Ontology (GO) terms. **Table S10**. DEGs for $Cort^{-/-}$ BECs from NX/NG to OGD-R included in Gene Ontology (GO) terms. **Table S11**. Comparative values between log2FC and RPKM for differentially expressed genes (DEGs) depicted in Fig. 7.

Acknowledgements
The authors would like to thank Dr. Mario Delgado for critical reading and discussion of the manuscript and Dr. Francisco Javier Oliver for the advice and technical support with the hypoxic experiments. We would also like to thank Animal Care Unit and Microscopy Service Unit staff from IPBLN for the technical support.

Author contributions
EG-R conceived, design and supervised the whole study. JC-G and EG-R outlined the experiments and analysed all the data. JC-G, AU-R, IF-L, IS-M, MC, JLR, AB-T, EA-L, JMP-G, RML and MS-N performed the experiments, interpreted the data, and discussed the results. JC-G, EG-R, JLR, RML and MS-N wrote and/or revised the manuscript. All authors have read and agreed to the published version of the manuscript.

Funding
This work was supported by grants from the Spanish Ministry of Economy and Competitiveness (SAF2017-85602-R to E.G-R), Spanish Ministry of Science and Innovation (PID2020-119638RB-I00 to E.G-R and PID2019-105564EB-I00 to RM.L)/AEI/ 10.13039/501100011033, FPU-program FPU17/02616 and FPU18/06009 to J.C-G and JM.P-G, respectively, and FPI-program PRE2018-084824 to I.S-M. M.S.-N. held a Ramón y Cajal contract (RYC2018-024759-I) from the Ministry of Science, Innovation and Universities. JL.R was supported by a contract (P20-01255) and EA-L by a postdoctoral fellowship (2020_DOC_00541), both from regional Andalusian Government.

Availability of data and materials
RNA-seq data sets generated during the current study are available in the GEO repository under accession number GSE207405, https://www.ncbi.nlm.nih.gov/geo/query/acc.cgi?acc=GSE207405.

Declarations

Ethics approval and consent to participate
All animal procedures were approved by the Animal Care and Use Board and the Ethical Committee of the Spanish National Research Council and were conducted according to the European guidelines for animal use in research.

Consent for publication
Not applicable.

Competing interests
The authors declare that they have no competing interest.

Author details
[1]Institute of Parasitology and Biomedicine Lopez-Neyra (IPBLN), CSIC, PT Salud, 18016 Granada, Spain. [2]Maimonides Biomedical Research Institute of Cordoba (IMIBIC), 14004 Cordoba, Spain. [3]Department of Cell Biology, Physiology, and Immunology, University of Cordoba, 14004 Cordoba, Spain. [4]Reina Sofia

University Hospital (HURS), 14004 Cordoba, Spain. [5]CIBER Physiopathology of Obesity and Nutrition (CIBERobn), 14004 Cordoba, Spain.

Received: 3 April 2023 Accepted: 26 September 2023
Published: 4 October 2023

References

1. Keaney J, Campbell M. The dynamic blood–brain barrier. FEBS J. 2015;282:4067–79.
2. Reed MJ, Damodarasamy M, Banks WA. The extracellular matrix of the blood–brain barrier: structural and functional roles in health, aging, and Alzheimer's disease. Tissue Barriers. 2019;7:1651157.
3. Cong X, Kong W. Endothelial tight junctions and their regulatory signaling pathways in vascular homeostasis and disease. Cell Signal. 2020;66: 109485.
4. Sweeney MD, Zhao Z, Montagne A, Nelson AR, Zlokovic BV. Blood–brain barrier: from physiology to disease and back. Physiol Rev. 2019;99:21–78.
5. Delgado M, Gonzalez-Rey E. Role of cortistatin in the stressed immune system. In: Savino W, Guaraldi F, editors. Frontiers of hormone research. 2017; p. 110–20. Available from: https://www.karger.com/Article/FullText/452910.
6. de Lecea L, Criado JR, Prospero-Garcia O, Gautvik KM, Schweitzer P, Danielson PE, et al. A cortical neuropeptide with neuronal depressant and sleep-modulating properties. Nature. 1996;381:242–5.
7. Córdoba-Chacón J, Gahete MD, Pozo-Salas AI, Martínez-Fuentes AJ, de Lecea L, Gracia-Navarro F, et al. Cortistatin is not a somatostatin analogue but stimulates prolactin release and inhibits GH and ACTH in a gender-dependent fashion: potential role of ghrelin. Endocrinology. 2011;152:4800–12.
8. Deghenghi R, Papotti M, Ghigo E, Muccioli G. Cortistatin, but not somatostatin, binds to growth hormone secretagogue (GHS) receptors of human pituitary gland. J Endocrinol Invest. 2001;24:1-RC3.
9. Braun H, Schulz S, Becker A, Schröder H, Höllt V. Protective effects of cortistatin (CST-14) against kainate-induced neurotoxicity in rat brain. Brain Res. 1998;803:54–60.
10. Chiu C-T, Wen L-L, Pao H-P, Wang J-Y. Cortistatin is induced in brain tissue and exerts neuroprotection in a rat model of bacterial meningoencephalitis. J Infect Dis. 2011;204:1563–72.
11. Souza-Moreira L, Morell M, Delgado-Maroto V, Pedreño M, Martinez-Escudero L, Caro M, et al. Paradoxical effect of cortistatin treatment and its deficiency on experimental autoimmune encephalomyelitis. J Immunol. 2013;191:2144–54.
12. Falo CP, Benitez R, Caro M, Morell M, Forte-Lago I, Hernandez-Cortes P, et al. The neuropeptide cortistatin alleviates neuropathic pain in experimental models of peripheral nerve injury. Pharmaceutics. 2021;13:947.
13. Delgado-Maroto V, Benitez R, Forte-Lago I, Morell M, Maganto-Garcia E, Souza-Moreira L, et al. Cortistatin reduces atherosclerosis in hyperlipidemic ApoE-deficient mice and the formation of foam cells. Sci Rep. 2017;7:46444.
14. Delgado-Maroto V, Falo CP, Forte-Lago I, Adan N, Morell M, Maganto-Garcia E, et al. The neuropeptide cortistatin attenuates experimental autoimmune myocarditis via inhibition of cardiomyogenic T cell-driven inflammatory responses. Br J Pharmacol. 2017;174:267–80.
15. Duran-Prado M, Morell M, Delgado-Maroto V, Castaño JP, Aneiros-Fernandez J, de Lecea L, et al. Cortistatin inhibits migration and proliferation of human vascular smooth muscle cells and decreases neointimal formation on carotid artery ligation. Circ Res. 2013;112:1444–55.
16. Yang T, Roder KE, Abbruscato TJ. Evaluation of bEnd5 cell line as an in vitro model for the blood–brain barrier under normal and hypoxic/aglycemic conditions. J Pharm Sci. 2007;96:3196–213.
17. Welser-Alves JV, Boroujerdi A, Milner R. Isolation and culture of primary mouse brain endothelial cells. In: Milner R, editor. Cerebral angiogenesis: methods and protocols. Springer: New York; 2014. p. 345–56. https://doi.org/10.1007/978-1-4939-0320-7_28.
18. Cecchelli R, Aday S, Sevin E, Almeida C, Culot M, Dehouck L, et al. A stable and reproducible human blood–brain barrier model derived from hematopoietic stem cells. PLoS ONE. 2014;9: e99733.
19. Takata F, Dohgu S, Yamauchi A, Matsumoto J, Machida T, Fujishita K, et al. In vitro blood–brain barrier models using brain capillary endothelial cells isolated from neonatal and adult rats retain age-related barrier properties. PLoS ONE. 2013;8:e55166.
20. Jangula A, Murphy EJ. Lipopolysaccharide-induced blood brain barrier permeability is enhanced by alpha-synuclein expression. Neurosci Lett. 2013;551:23–7.
21. Fuentes-Fayos AC, Vázquez-Borrego MC, Jiménez-Vacas JM, Bejarano L, Pedraza-Arévalo S, López LF, et al. Splicing machinery dysregulation drives glioblastoma development/aggressiveness: oncogenic role of SRSF3. Brain. 2020;143:3273–93.
22. Ruiz JL, Terrón-Camero LC, Castillo-González J, Fernández-Rengel I, Delgado M, Gonzalez-Rey E, et al. reanalyzerGSE: tackling the everlasting lack of reproducibility and reanalyses in transcriptomics. bioRxiv. 2023. https://doi.org/10.1101/2023.07.12.548663.
23. Andrés-León E, Rojas AM. miARma-Seq, a comprehensive pipeline for the simultaneous study and integration of miRNA and mRNA expression data. Methods. 2019;152:31–40.
24. Li R, Yao G, Zhou L, Zhang M, Yan J. The ghrelin-GHSR-1a pathway inhibits high glucose-induced retinal angiogenesis in vitro by alleviating endoplasmic reticulum stress. Eye Vis. 2022;9:20.
25. Yan S, Li M, Chai H, Yang H, Lin PH, Yao Q, et al. TNF-α decreases expression of somatostatin, somatostatin receptors, and cortistatin in human coronary endothelial cells. J Surg Res. 2005;123:294–301.
26. Basivireddy J, Somvanshi RK, Romero IA, Weksler BB, Couraud P-O, Oger J, et al. Somatostatin preserved blood brain barrier against cytokine induced alterations: possible role in multiple sclerosis. Biochem Pharmacol. 2013;86:497–507.
27. Sladojevic N, Stamatovic SM, Johnson AM, Choi J, Hu A, Dithmer S, et al. Claudin-1-dependent destabilization of the blood–brain barrier in chronic stroke. J Neurosci. 2019;39:743–57.
28. Coisne C, Dehouck L, Faveeuw C, Delplace Y, Miller F, Landry C, et al. Mouse syngenic in vitro blood–brain barrier model: a new tool to examine inflammatory events in cerebral endothelium. Lab Invest. 2005;85:734–46.
29. Kuntz M, Mysiorek C, Pétrault O, Boucau M-C, Aijjou R, Uzbekov R, et al. Transient oxygen–glucose deprivation sensitizes brain capillary endothelial cells to rtPA at 4h of reoxygenation. Microvasc Res. 2014;91:44–57.
30. Gerhartl A, Pracser N, Vladetic A, Hendrikx S, Friedl H-P, Neuhaus W. The pivotal role of micro-environmental cells in a human blood–brain barrier in vitro model of cerebral ischemia: functional and transcriptomic analysis. Fluids Barriers CNS. 2020;17:19.
31. Gray KM, Jung JW, Inglut CT, Huang H-C, Stroka KM. Quantitatively relating brain endothelial cell–cell junction phenotype to global and local barrier properties under varied culture conditions via the Junction Analyzer Program. Fluids Barriers CNS. 2020;17:16.
32. Babinska A, Kedees MH, Athar H, Ahmed T, Batuman O, Ehrlich YH, et al. F11-receptor (F11R/JAM) mediates platelet adhesion to endothelial cells: role in inflammatory thrombosis. Thromb Haemost. 2002;88:843–50.
33. Beard RS, Haines RJ, Wu KY, Reynolds JJ, Davis SM, Elliott JE, et al. Non-muscle Mlck is required for β-catenin- and FoxO1-dependent downregulation of Cldn5 in IL-1β-mediated barrier dysfunction in brain endothelial cells. J Cell Sci. 2014;127:1840–53.
34. Sperandio S, Fortin J, Sasik R, Robitaille L, Corbeil J, de Belle I. The transcription factor Egr1 regulates the HIF-1α gene during hypoxia. Mol Carcinog. 2009;48:38–44.
35. Kerr DJ, Marsillo A, Guariglia SR, Budylin T, Sadek R, Menkes S, et al. Aberrant hippocampal Atp8a1 levels are associated with altered synaptic strength, electrical activity, and autistic-like behavior. Biochim Biophys Acta BBA Mol Basis Dis. 2016;1862:1755–65.
36. Zhao Z, Nelson AR, Betsholtz C, Zlokovic BV. Establishment and dysfunction of the blood–brain barrier. Cell. 2015;163:1064–78.
37. Zlokovic BV. The blood–brain barrier in health and chronic neurodegenerative disorders. Neuron. 2008;57:178–201.
38. Hagen SJ. Non-canonical functions of claudin proteins: beyond the regulation of cell–cell adhesions. Tissue Barriers. 2017;5: e1327839.
39. Tietz S, Engelhardt B. Brain barriers: crosstalk between complex tight junctions and adherens junctions. J Cell Biol. 2015;209:493–506.
40. Schlingmann B, Overgaard CE, Molina SA, Lynn KS, Mitchell LA, Dorsainvil White S, et al. Regulation of claudin/zonula occludens-1 complexes by hetero-claudin interactions. Nat Commun. 2016;7:12276.
41. Yan T, Tan Y, Deng G, Sun Z, Liu B, Wang Y, et al. TGF-β induces GBM mesenchymal transition through upregulation of CLDN4 and nuclear

translocation to activate TNF-α/NF-κB signal pathway. Cell Death Dis. 2022;13:1–11.
42. Zavala-Zendejas VE, Torres-Martinez AC, Salas-Morales B, Fortoul TI, Montaño LF, Rendon-Huerta EP. Claudin-6, 7, or 9 overexpression in the human gastric adenocarcinoma cell line AGS increases its invasiveness, migration, and proliferation rate. Cancer Invest. 2011;29:1–11.
43. Sajja RK, Prasad S, Cucullo L. Impact of altered glycaemia on blood–brain barrier endothelium: an in vitro study using the hCMEC/D3 cell line. Fluids Barriers CNS. 2014;11:8.
44. Liebner S, Fischmann A, Rascher G, Duffner F, Grote E-H, Kalbacher H, et al. Claudin-1 and claudin-5 expression and tight junction morphology are altered in blood vessels of human glioblastoma multiforme. Acta Neuropathol. 2000;100:323–31.
45. Pfeiffer F, Schäfer J, Lyck R, Makrides V, Brunner S, Schaeren-Wiemers N, et al. Claudin-1 induced sealing of blood–brain barrier tight junctions ameliorates chronic experimental autoimmune encephalomyelitis. Acta Neuropathol. 2011;122:601–14.
46. Gonçalves A, Ambrósio AF, Fernandes R. Regulation of claudins in blood–tissue barriers under physiological and pathological states. Tissue Barriers. 2013;1: e24782.
47. Alshbool Fatima Z, Mohan S. Emerging multifunctional roles of claudin tight junction proteins in bone. Endocrinology. 2014;155:2363–76.
48. Haseloff RF, Dithmer S, Winkler L, Wolburg H, Blasig IE. Transmembrane proteins of the tight junctions at the blood–brain barrier: structural and functional aspects. Semin Cell Dev Biol. 2015;38:16–25.
49. Lai C-H, Kuo K-H, Leo JM. Critical role of actin in modulating BBB permeability. Brain Res Rev. 2005;50:7–13.
50. Rao RK, Basuroy S, Rao VU, Karnaky KJ Jr, Gupta A. Tyrosine phosphorylation and dissociation of occludin–ZO-1 and E-cadherin–β-catenin complexes from the cytoskeleton by oxidative stress. Biochem J. 2002;368:471–81.
51. Gould DB, Phalan FC, van Mil SE, Sundberg JP, Vahedi K, Massin P, et al. Role of COL4A1 in small-vessel disease and hemorrhagic stroke. N Engl J Med. 2006;354:1489–96.
52. Baeten KM, Akassoglou K. Extracellular matrix and matrix receptors in blood–brain barrier formation and stroke. Dev Neurobiol. 2011;71:1018–39.
53. Bauer AT, Bürgers HF, Rabie T, Marti HH. Matrix metalloproteinase-9 mediates hypoxia-induced vascular leakage in the brain via tight junction rearrangement. J Cereb Blood Flow Metab. 2010;30:837–48.
54. Ma Z, Mao C, Jia Y, Fu Y, Kong W. Extracellular matrix dynamics in vascular remodeling. Am J Physiol Cell Physiol. 2020;319:C481–99.
55. Ghersi-Egea J-F, Strazielle N, Catala M, Silva-Vargas V, Doetsch F, Engelhardt B. Molecular anatomy and functions of the choroidal blood–cerebrospinal fluid barrier in health and disease. Acta Neuropathol. 2018;135:337–61.
56. Benitez R, Caro M, Andres-Leon E, O'Valle F, Delgado M. Cortistatin regulates fibrosis and myofibroblast activation in experimental hepatotoxic- and cholestatic-induced liver injury. Br J Pharmacol. 2022;179:2275–96.
57. Sonar SA, Lal G. Blood–brain barrier and its function during inflammation and autoimmunity. J Leukoc Biol. 2018;103:839–53.
58. de Vries HE, Blom-Roosemalen MCM, van Oosten M, de Boer AG, van Berkel TJC, Breimer DD, et al. The influence of cytokines on the integrity of the blood-brain barrier in vitro. J Neuroimmunol. 1996;64:37–43.
59. Cristante E, McArthur S, Mauro C, Maggioli E, Romero IA, Wylezinska-Arridge M, et al. Identification of an essential endogenous regulator of blood–brain barrier integrity, and its pathological and therapeutic implications. Proc Natl Acad Sci USA. 2013;110:832–41.
60. Pacher P, Beckman JS, Liaudet L. Nitric oxide and peroxynitrite in health and disease. Physiol Rev. 2007;87:315–424.
61. Farrall AJ, Wardlaw JM. Blood–brain barrier: ageing and microvascular disease—systematic review and meta-analysis. Neurobiol Aging. 2009;30:337–52.
62. He J, Hsuchou H, He Y, Kastin AJ, Wang Y, Pan W. Sleep restriction impairs blood–brain barrier function. J Neurosci. 2014;34:14697–706.
63. Sun J, Wu J, Hua F, Chen Y, Zhan F, Xu G. Sleep Deprivation Induces Cognitive Impairment by Increasing Blood-Brain Barrier Permeability via CD44. Front Neurol. 2020. https://doi.org/10.3389/fneur.2020.563916.
64. Bourgin P, Fabre V, Huitrón-Reséndiz S, Henriksen SJ, Prospero-Garcia O, Criado JR, et al. Cortistatin promotes and negatively correlates with slow-wave sleep. Eur J Neurosci. 2007;26:729–38.
65. Faraguna U, Vyazovskiy VV, Nelson AB, Tononi G, Cirelli C. A causal role for brain-derived neurotrophic factor in the homeostatic regulation of sleep. J Neurosci. 2008;28:4088–95.
66. Monte MD, Cammalleri M, Martini D, Casini G, Bagnoli P. Antiangiogenic role of somatostatin receptor 2 in a model of hypoxia-induced neovascularization in the retina: results from transgenic mice. Invest Ophthalmol Vis Sci. 2007;48:3480–9.
67. Zaniolo K, Sapieha P, Shao Z, Stahl A, Zhu T, Tremblay S, et al. Ghrelin modulates physiologic and pathologic retinal angiogenesis through GHSR-1a. Invest Ophthalmol Vis Sci. 2011;52:5376–86.
68. Aslam M, Idrees H, Ferdinandy P, Helyes Z, Hamm C, Schulz R. Somatostatin primes endothelial cells for agonist-induced hyperpermeability and angiogenesis in vitro. Int J Mol Sci. 2022;23:3098.
69. Spier AD, de Lecea L. Cortistatin: a member of the somatostatin neuropeptide family with distinct physiological functions. Brain Res Rev. 2000;33:228–41.
70. Córdoba-Chacón J, Gahete MD, Duran-Prado M, Pozo-Salas AI, Malagón MM, Gracia-Navarro F, et al. Identification and characterization of new functional truncated variants of somatostatin receptor subtype 5 in rodents. Cell Mol Life Sci. 2010;67:1147–63.
71. Durán-Prado M, Malagón MM, Gracia-Navarro F, Castaño JP. Dimerization of G protein-coupled receptors: new avenues for somatostatin receptor signalling, control and functioning. Mol Cell Endocrinol. 2008;286:63–8.
72. Jiang H, Smith R. Modification of ghrelin and somatostatin signaling by formation of GHSR-1a/SSTR5 heterodimers. The Endocrine Society's 89th Annual Meeting. 2007;P9: 299.
73. Sánchez-Alavez M, Gómez-Chavarin M, Navarro L, Jiménez-Anguiano A, Murillo-Rodríguez E, Prado-Alcalá RA, et al. Cortistatin modulates memory processes in rats. Brain Res. 2000;858:78–83.
74. Hurst RD, Clark JB. Alterations in transendothelial electrical resistance by vasoactive agonists and cyclic AMP in a blood–brain barrier model system. Neurochem Res. 1998;23:149–54.
75. Lampugnani MG, Giorgi M, Gaboli M, Dejana E, Marchisio PC. Endothelial cell motility, integrin receptor clustering, and microfilament organization are inhibited by agents that increase intracellular cAMP. Lab Invest. 1990;63:521–31.
76. Dixit VD, Schaffer EM, Pyle RS, Collins GD, Sakthivel SK, Palaniappan R, et al. Ghrelin inhibits leptin- and activation-induced proinflammatory cytokine expression by human monocytes and T cells. J Clin Invest. 2004;114:57–66.
77. Córdoba-Chacón J, Gahete MD, Culler MD, Castaño JP, Kineman RD, Luque RM. Somatostatin dramatically stimulates growth hormone release from primate somatotrophs acting at low doses via somatostatin receptor 5 and cyclic AMP. J Neuroendocrinol. 2012;24:453–63.
78. Benz F, Liebner S. Structure and function of the blood–brain barrier (BBB). In: Cader Z, Neuhaus W, editors. Physiology, pharmacology and pathology of the blood–brain barrier. Cham: Springer International Publishing; 2022. p. 3–31. https://doi.org/10.1007/164_2020_404.
79. Montagne A, Zhao Z, Zlokovic BV. Alzheimer's disease: a matter of blood–brain barrier dysfunction? J Exp Med. 2017;214:3151–69.
80. Zlokovic BV, Griffin JH. Cytoprotective protein C pathways and implications for stroke and neurological disorders. Trends Neurosci. 2011;34:198–209.

Publisher's Note